

**NASA TECHNICAL
MEMORANDUM**



NASA TM X-3364

NASA TM X-3364

**REPORTS OF ACCOMPLISHMENTS
OF PLANETOLOGY PROGRAMS, 1975-1976**

*Office of Space Science
NASA Headquarters
Washington, D.C. 20546*



NATIONAL AERONAUTICS AND SPACE ADMINISTRATION • WASHINGTON, D. C. • MARCH 1976

1. Report No. NASA TM X-3364		2. Government Accession No.		3. Recipient's Catalog No.	
4. Title and Subtitle Reports of Accomplishments of Planetology Programs, 1975-1976				5. Report Date March 1976	
				6. Performing Organization Code	
7. Author(s)				8. Performing Organization Report No.	
9. Performing Organization Name and Address Office of Space Science Lunar and Planetary Programs Planetology Program				10. Work Unit No.	
				11. Contract or Grant No.	
12. Sponsoring Agency Name and Address National Aeronautics and Space Administration				13. Type of Report and Period Covered	
				14. Sponsoring Agency Code	
15. Supplementary Notes					
16. Abstract A compilation of abstracts of reports which summarizes work conducted by Planetology Program Principal Investigators. Full reports of selected abstracts were presented to the annual meeting of Planetology Program Principal Investigators at the Center for Astrogeology, U.S. Geological Survey, Flagstaff, Arizona, March 8, 9, 10, 1976.					
17. Key Words (Selected by Author(s)) Planetary Geology Solar System Evolution Mars and Mercury Geological Mapping Planetological Instrument Development				18. Distribution Statement Unclassified—Unlimited STAR Cat. 91	
19. Security Classif. (of this report) Unclassified		20. Security Classif. (of this page) Unclassified		21. No. of Pages 282	
				22. Price \$8.75	

For sale by the National Technical Information Service, Springfield, Virginia 22161

FOREWORD

This is a compilation of abstracts of reports from Principal Investigators of NASA's Office of Space Science, Division of Lunar and Planetary Programs, Planetology Program.

The purpose is to provide a document which succinctly summarizes work conducted in this program. Each report reflects significant accomplishments within the area of the author's funded grant or contract.

No attempt has been made to introduce editorial or stylistic uniformity; on the contrary, the style of each report is that of the Principal Investigator and may best portray his research. Bibliography information will be included in a separately published document.

Full reports of selected abstracts were presented to the annual meeting of Planetology Program Principal Investigators at the Center for Astrogeology, U.S. Geological Survey, Flagstaff, Arizona. March 8, 9, 10, 1976.

S. E. Dwornik
Chief, Planetology Program

R. Wahmann
Staff Scientist, Planetology Program

CONTENTS

	<i>Page</i>
Foreword	iii
 SOLAR SYSTEMS, COMETS, AND ASTEROIDS	
Conclusions About the Origin of the Solar System From Planetology Research . . . <i>Hannes Alfvén and Gustaf Arrhenius</i>	1
Theoretical Research in Planetary Physics <i>A. G. W. Cameron and W. R. Ward</i>	4
Asteroid Fragmentational Processes <i>Clark R. Chapman</i>	8
Planetology Studies: Studies of Io and the Other Galilean Satellites <i>F. P. Fanale</i>	11
Orbital Resonances in the Solar System <i>S. J. Peale</i>	15
Systematic Search for Planet-Crossing Asteroids and the Estimation of Impact Rates on the Terrestrial Planets <i>E. M. Shoemaker and E. F. Helin</i>	18
A Speculation About Comets and the Earth <i>Fred L. Whipple</i>	23
The Reality of Comet Groups and Pairs <i>Fred L. Whipple</i>	27
Orbital Linkage of Comets of Intermediate Period <i>Brian G. Marsden</i>	31
Orbit Determination of Nearly-Parabolic Comets <i>Brian G. Marsden and Zdenek Sekanina</i>	34
Evolution of Jupiter, Saturn and Their Satellite Systems <i>James B. Pollack</i>	38
Statistics of Anomalous Tails of Comets <i>Zdenek Sekanina</i>	40
A Probability of Encounter With Interstellar Comets and the Likelihood of Their Existence <i>Zdenek Sekanina</i>	43

GEOPHYSICS

On the Extent of a Mercurian Liquid Core	46
<i>S. J. Peale</i>	
Tharsis: Implications for Evolution and Present State of the Martian Interior	48
<i>R. J. Phillips</i>	
Analysis of Compensated Regions of Mars	53
<i>R. S. Saunders</i>	
Temperatures in the Interiors of the Terrestrial Planets	57
<i>Gerald Schubert</i>	
Mixed Electrical and Accretional Heating and the "Zero Age" Lunar Thermal Profile	60
<i>C. P. Sonett, F. Herbert, and M. J. Wiskerchen</i>	

COMPARATIVE PLANETARY GEOLOGY

A Siberian Analog of Martian Permafrost Terrain	65
<i>Duwayne M. Anderson and Lawrence W. Gatto</i>	
Comparative Planetology and Modification of Martian Uplands	66
<i>R. E. Arvidson</i>	
Possible Earth Analogs for Some Martian Channel Features	68
<i>Jon C. Boothroyd, Elizabeth J. Simpson, and Dag Nummedal</i>	
Craters and Plains on Mercury, the Moon, and Mars	69
<i>V. R. Oberbeck</i>	
Comparison of Lunar and Planetary Imagery	73
<i>Peter H. Schultz</i>	
Role of Planetesimals in Comparative Planetology	76
<i>William K. Hartmann</i>	

TECHNIQUES AND INSTRUMENT DEVELOPMENT

Scientific Rationale and Feasibility of Developing a Planetary Sementa	78
<i>A. L. Albee, J. R. Anderson, and A. A. Chodos</i>	
The Control Net of Mercury	81
<i>Merton E. Davies</i>	
Alpha/X-Ray Analysis Using Solid-State Detectors	85
<i>Ernest J. Franzgrote</i>	

Radar Studies of Mars	87
<i>R. A. Simpson, G. L. Tyler, and H. T. Howard</i>	
Measurement of Small-Scale Terrain Roughness: A Bonus From Airborne or Spacecraft-Borne Side-Looking Imaging Radar Systems	89
<i>Gerald G. Schaber</i>	
Imaging Radar for Planetary Studies	91
<i>R. S. Saunders, M. I. Daily, and C. Elachi</i>	
An Alpha Particle Instrument With Alpha, Proton and X-Ray Modes for Planetary Chemical Analyses	94
<i>T. E. Economou and A. L. Turkevich</i>	
Revised Albedo Measurements of Mercury	99
<i>Daniel Dzurisin and G. Edward Danielson</i>	
Evolutionary Time Scales and Histories Recorded on the Terrestrial Planets	100
<i>Laurence Soberblom</i>	
EOLIAN PHENOMENON	
Wind Tunnel Studies of Aeolian Processes	102
<i>Ronald Greeley</i>	
Eolian Bedforms in Unidirectional Winds	105
<i>Alan D. Howard, Mohamed Gad-el-Hak, Jeffrey B. Morton, and Deborah Pierce</i>	
Planetary Surface Sediments	107
<i>Elbert A. King</i>	
Terrestrial Yardangs	110
<i>John F. McCauley and Maurice J. Grolier</i>	
Wind Trends in Peru and on Mars	115
<i>Maurice J. Grolier, A. Wesley Ward, and John F. McCauley</i>	
Terrestrial Analogs of the Hellespontus Dunes, Mars	117
<i>Carol S. Breed</i>	
Differentiating Eolian Deposits Using Grain Size Parameters	120
<i>Augustus S. Cotera and Camilla K. McCauley</i>	
Aeolian Field Studies at Amboy Crater	123
<i>Ronald Greeley</i>	
A Statistical Study of Crater Related Wind Streaks in the North Equatorial Zone of Mars	126
<i>K. Cook and J. Veverka</i>	

TECTONICS, GEOMORPHOLOGY, AND VOLCANOLOGY

Morphologic Classification of Scarps and Lineaments in Discovery Quadrangle	127
<i>Daniel Dzurisin</i>	
Influence of Tectonic Setting, Composition, and Erosion on Basaltic Landforms: New Mexico and Mars	129
<i>Wolfgang E. Elston, Jayne C. Aubele, Larry S. Crumpler, and Dean B. Eppler</i>	
Martian Knobby Terrain	133
<i>J. E. Guest, R. Greeley, and P. S. Butterworth</i>	
Volcanic Features and Fracture Sets of the South Central Snake River Plain, Idaho .	135
<i>John S. King and Ronald Greeley</i>	
The Dependence of Topography on Volcanic Processes Within the Eastern Snake River Plain, Idaho	138
<i>John F. Karlo and John S. King</i>	
The Canyonlands Graben; Subsurface Stresses and a Possible Explanation for Regular Spacing	141
<i>Albert W. Stromquist and George E. McGill</i>	
Studies of the Mercurian Surface	146
<i>Michael C. Malin</i>	
Structural Analysis of Mars	147
<i>Philippe Masson</i>	
Fourier Analysis of Landforms: A Comparison of Features in the Washington Scablands and Selected Erosional Forms on Mars	148
<i>Dag Nummedal and Jon C. Boothroyd</i>	
The Proctor Dune Field of Mars: Additional Observations	149
<i>James E. Peterson</i>	
Elevation of Martian Volcanoes as a Function of Age	152
<i>Michael H. Carr</i>	
Volcanic Studies in Planetology	154
<i>Ronald Greeley</i>	
Rates of Structural and Landform Evolution of Hawaiian Volcanoes: Role of Short-Lived and Catastrophic Processes	157
<i>Robert I. Tilling, Robin T. Holcomb, Peter W. Lipman, and John P. Lockwood</i>	
Floor-Fractured Craters on the Moon, Mars, and Mercury	159
<i>Peter H. Schultz</i>	

Effects of Surface Gravity on the Occurrence of Central Peaks in Martian, Lunar, and Mercurian Craters	161
<i>Eugene I. Smith</i>	

CHANNELS

Interdisciplinary Ramifications of Mars Channel Studies	164
<i>William K. Hartmann</i>	
Preliminary Investigations of the Physics of Martian Channels	166
<i>Carl Sagan</i>	
Martian Channels	169
<i>Harold Masursky</i>	
Studies of the Channeled Scabland of Washington State as a Terrestrial Analogue to the Channeled Terrain of Mars	172
<i>Earl Ingerson and Victor R. Baker</i>	

CRATERS

Crater Morphologies on Mars at Mariner 9 B-Frame Scales	175
<i>Clark R. Chapman</i>	
Crater Size-Distribution Studies and Dating of Planetary Surfaces	178
<i>Gerhard Neukum and Beate König (H. Fechtig)</i>	
Mercury Craters Morphology: Statistics on Selected Areas	182
<i>The Italian Consortium for Planetary Studies, University of Rome (M. Fulchignoni)</i>	
Caloris-Age Changes in Mercury's Crater Populations	183
<i>D. E. Gault, J. E. Guest, and P. H. Schultz</i>	
Craters on the Moon, Mars, and Mercury: A Comparison of Depth/Diameter Characteristics	186
<i>Mark J. Cintala, James W. Head, and Thomas A. Mutch</i>	
Characteristics of Fresh Martian Craters as a Function of Diameter: Comparison With the Moon and Mercury	188
<i>Mark J. Cintala, James W. Head, and Thomas A. Mutch</i>	
Comparative Planetological Analysis of Cratering and Geomorphological Processes .	191
<i>Clark R. Chapman</i>	
Populations of Impacting Bodies in the Inner Solar System	194
<i>R. G. Strom and E. A. Whitaker</i>	

Crater Saturation and Equilibrium: A Monte Carlo Simulation	197
<i>A. Woronow</i>	
Depth-Diameter Relation for Large Martian Craters Determined From Mariner 9 UVS Altimetry	199
<i>J. Burt, J. Veverka, and K. Cook</i>	
 SURFACE PROCESSES AND FEATURES	
Optical Properties of Outer Planet Ices	200
<i>L. A. Lebofsky and J. E. Conel</i>	
Surface Processes on Mars	201
<i>James A. J. Cutts</i>	
Planetology Studies: Martian Volatile Studies	203
<i>F. P. Fanale</i>	
Martian Source Craters	206
<i>Robert H. Stockman</i>	
Some Characteristic Erosional Forms of Martian Stratigraphic Units	210
<i>B. K. Lucchitta</i>	
Surfaces of Phobos and Deimos	213
<i>M. Noland and J. Veverka</i>	
Significance of Bright Spots Observed During 1971 Martian Dust Storm	214
<i>Richard E. D'Alli and Thomas A. Mutch</i>	
The Martian Scarp: Influence on the Wind Circulation	217
<i>R. E. Arvidson</i>	
 MARS GEOLOGIC MAPPING	
Geology of the Eridania Quadrangle, Mars	218
<i>René A. DeHon</i>	
Geology of Mars Quadrangle MC-6 (Cadius)	221
<i>R. Greeley and J. E. Guest</i>	
Geologic History of Thaumasia Quadrangle, Mars	224
<i>George E. McGill</i>	
The New Geologic Map of Mars (1:25 Million Scale)	229
<i>D. H. Scott and M. H. Carr</i>	
Geologic Setting of Viking Mars "B" Prime Landing Site Cydonia Region, Mare Acidalium Quadrangle	231
<i>James R. Underwood, Jr.</i>	

Geology of the Phaethontis Quadrangle, Mars <i>J. Hatten Howard III</i>	233
Geologic Summary of the Mars Quadrangle MC-12 (Arabia) <i>John S. King</i>	236
MERCURY GEOLOGIC MAPPING	
Mercury Geologic Mapping Program <i>H. E. Holt</i>	238
Mercury Mapping: Process in the Study of Quadrangle H12 <i>Karl R. Blasius</i>	239
Geologic Mapping of the South Polar Region of Mercury <i>Michael C. Malin</i>	240
Multiring Basins in the Kuiper Quadrangle, Mercury <i>René A. DeHon</i>	242
VENUS	
Photometric Analyses of Mariner 10 Images of Venus <i>Bruce Hapke</i>	245
The Surface of Venus: Radar Observations and Terrestrial Analogs <i>Michael C. Malin</i>	249
Erosion of Surface Rocks on Venus <i>Carl Sagan</i>	251
Interpretation of Venus Radar: Crater Statistics <i>R. S. Saunders</i>	254
Thoughts on the Geology of Venus <i>R. E. Arvidson</i>	257
UNCATEGORIZED	
Multispectral Capability of the Viking Lander Imagery System <i>R. E. Arvidson, F. Huck, S. Wall, and W. Patterson</i>	258
Calibration of Martian Surface Dynamics by Analysis of Cosmic Ray Effects in Returned Sample <i>R. E. Arvidson and C. Hohenberg</i>	260
A Mariner 10 Atlas of Mercury <i>Merton E. Davies</i>	261

Photometric Analyses of Mariner 10 Images of Mercury	263
<i>Bruce Hapke</i>	
Excitation and Relaxation of the Wobble, Precession and Libration of the Moon . .	267
<i>S. J. Peale</i>	
Longterm Evolution of the Martian Atmosphere and Climatic Change	268
<i>Carl Sagan</i>	
A Numerical Circulation Model With Topography for the Martian Southern Hemisphere	273
<i>Carl Sagan</i>	
Chemical Equilibria Relevant to the Construction of Planetary Models for Mars and Mercury	275
<i>M. Charles Gilbert</i>	
A Short Course in Planetary Geology	277
<i>Peter H. Schultz and Ronald Greeley</i>	
UV Contrast Reversal on Mars: A Study of the UV Reflectance Characteristics of Possible Martian Surface Materials	279
<i>J. Veverka, J. Burt, and J. Goguen</i>	
Author Index	281

CONCLUSIONS ABOUT THE ORIGIN OF THE SOLAR SYSTEM FROM PLANETOLOGY RESEARCH

Hannes Alfvén and Gustaf Arrhenius
University of California, San Diego

Applicable sections of the NASA Special Publication 345, "Evolution of the Solar System" (Alfvén and Arrhenius, 1976) are reviewed.

It is especially stressed that although a comparison among the different planets is important, it is even more important to include the satellites in the comparison. Observing that the highly regular systems of Jupiter, Saturn and Uranus are in essential respects similar to the planetary system, the aim of planetological research should be a general theory of the formation of secondary bodies around a primary body. In certain respects the satellite systems provide even more significant information about evolutionary processes than does the planetary system, partly because of the uncertainty about the state of the early Sun. By requiring that a satisfactory theory of the formation of our solar system include the formation of the satellite systems, the choice of acceptable theories can be narrowed down considerably.

The theoretical assumptions made about the state of the solar nebula and the earliest formative stages of the solar system determine which courses of development are possible for the accretion and orbital evolution of satellites and planets. To be realistic, and thus acceptable as a basis for subsequent evolution, any theory describing the early state of the solar system must

satisfy the laws which now govern the behavior of matter in space and, under similar, controlled conditions, in the laboratory. A hydromagnetic treatment of the dynamic aspects of the problem is as important for such a theory as it is for the interpretation of space observations today.

A realistic discussion of the chemical conditions prevailing in the solar nebula must include the extreme thermodynamic conditions which characterize the formation of molecules and the condensation of solids in space. Such processes must have controlled the formation of the grains which now constitute comets and asteroids, and in a modified form, the satellites and planets.

Prerequisites for the formation of satellites and planets with the properties observed are, furthermore, that the source grains are given angular momentum and that they are placed in eccentric orbits. These allow focussing of the grains into jet streams where, at sufficiently low velocities, planetesimals can accrete to ultimately form the bodies observed today.

Applying these dynamic constraints in reconstruction of the earliest stages of the solar system, we find the course of accretion to be different for each of the planets. However, three main types of development can be defined. In the case of Mercury, Venus, Earth and Jupiter, their parent jet streams are exhausted catastrophically by the planetary embryo in an early state of its growth, for the Earth, at a size of about one-half its present radius. Another group is formed by Mars, Moon and Saturn, for which the catastrophic stage of accretion occurs near the end of the formation of the planet. Finally the growth of Uranus, Neptune, Triton and Pluto is characterized by a slow contraction of the parent jet stream.

The evolution of the planetary atmospheres and of the Earth's ocean were also strongly influenced by the course of accretion, and thus by the entire chain of assumptions concerning the preceding stages in the history of the solar system, including the process of formation of the solar nebula.

THEORETICAL RESEARCH IN PLANETARY PHYSICS

A. G. W. Cameron and W. R. Ward
Harvard College Observatory

Evolution of the primitive solar nebula

In previous work on modeling of the primitive solar nebula carried out by Cameron, it had been concluded that the characteristic times for cooling and angular momentum transport in the primitive solar nebula were substantially less than the time required for the gas to accrete into the primitive solar nebula from a fragment of a collapsing interstellar cloud. The dissipation times should be characteristically hundreds or thousands of years, whereas the infall and accretion time is more likely to be in the range 10^4 to 10^5 years. This means that one should do an evolutionary calculation, involving a sequence of models, in which dissipation is taken into account simultaneously with the accretion.

During the course of the summer it became apparent that the meridional circulation current, with a velocity approaching sound speed in the models which have been calculated, should induce large-scale violent turbulence in every part of the primitive solar nebula, a system having a high Reynolds number. It was shown by Cowling in 1951 that certain nonaxisymmetric perturbations are neutrally stable in the presence of differential rotation, and it is these Cowling modes which can be excited and which will generate a field of turbulence isotropic on the smaller scales. In addition, F. Seguin, at the Center for Astrophysics, has shown that these Cowling modes can be driven by violent dynamical instabilities under conditions in which the vorticity achieves a local maximum, as when an axisymmetric perturbation forms a ring within the primitive solar nebula. The presence of turbulence validates the use of a theory of viscous accretion disks, published by Lynden-Bell and Pringle in 1974, with turbulent viscosity providing the friction. In this theory a viscous couple is calculated at a point in the disk; the transport of angular momentum and of energy, and the local dissipation of energy, depend upon the local value of the viscous couple; the rate of transport of matter depends upon the gradient of the viscous couple. In a typical disk the viscous couple rises with increasing radial distance to a maximum, and then declines towards zero at the outer rim of the disk. There is a corresponding inward flow of mass in the inner regions of the disk, and an outward flow of mass in the outer regions of the disk. The properties of these viscous accretion disk representations of the primitive solar nebula have been studied intensively since the summer.

The first exploration of the properties was carried out for steady-flow models. These are models in which the accreting matter is transported entirely to the center and to the outside, and it is required that the surface density of the disk everywhere has reached a steady state, so that it is no longer changing with time. For any model it is necessary to specify the central mass, the external gas accretion rate, and the total angular momentum of the collapsing interstellar cloud fragment. The effect on the models of variations in these three parameters were explored. In addition, it is necessary to specify some quantity within the disk which would make it of interest in relation to the formation of the solar system. It was specified that an object having the same specific angular momentum as Jupiter should occur at a temperature of 140 K within the gas.

In these steady flow disks, the run of temperature through the disk is closely related to the condensation temperatures of the appropriate materials entering into the composition of the planets in the solar system. For low values of the infalling angular momentum, about one-tenth of that expected, the fit to the temperature structure is particularly good. On the other hand, the resulting disks have a very small mass and there is no possibility to form comets within the context of the theory. If the angular momentum has more nearly its expected value, then the temperature at the position of Mercury is too small to account for the mean density of that planet in terms of condensed constituents, but it appears that comets may be formed. These results are not persuasive, one way or the other, since in fact, in the time-dependent evolutionary sequence of models the temperature changes with time at the position associated with any specific angular momentum.

It was noted that if the angular momentum is of the expected order or somewhat greater, then the radius of the disk lay in the range several hundred to a few thousand astronomical units. Such disks tended to have of the order of one solar mass of material, the great bulk of it beyond the orbit of Neptune. This suggests that the possibility of a new theory for the formation of comets. A body in circular orbit at the outer edge of the disk will have a period of the order of 10^4 years or considerably longer. If most of the mass of the disk could be lost on a time scale short compared to an orbital period, then bodies near the outer edge of the disk would become nearly unbound, and would move outwards to populate the Oort cloud of comets. Furthermore, the bodies formed near the outer edge of the disk should be large clusters of interstellar grains which will have precisely the right properties for comets. This motivated an examination of the rate at which mass would flow away from the heated corona formed above the surface of the disk at large distances, due to waves generated by turbulence in the gas. It was indeed found that the resulting rates of mass loss were sufficiently high (10^{-4} solar masses per year) to justify the short time scale assumption regarding the mass loss. As the disk disappears, the mass loss rate slows down, but it seems likely that the observed T Tauri mass loss phases of young stars represent the later stages in this process. The picture that emerges is that when the external accretion slows down enough for the hot corona to form, mass loss will subsequently dominate, and external accretion will be abruptly halted as the infalling matter is swept out into space again. This follow-on mass loss episode has been included in the evolutionary studies of the primitive solar nebula.

At the present time evolutionary sequences of solar nebula models are being computed. These are parameterized by a mass accretion rate and by an angular momentum for the infalling cloud of material. In the course of an evolutionary sequence, the temperature associated with the position of any given planetary specific angular momentum starts out very low, increases to a maximum value similar to those obtained in the steady flow models, and then slowly decreases through the mass loss regime. The radius of the disk increases to values consistent with the conclusions of the steady flow models but then steadily decreases during the mass loss era.

With a highly turbulent nebula, small particles are unable to settle toward mid-plane, and hence the short-range Goldreich-Ward gravitational instability mechanism cannot operate. This remark does not apply to the region of the outer edge of the disk, where this mechanism can operate as the disk recedes, allowing the formation of cometary bodies by the

Goldreich-Ward instability process. However, this is not a suitable way to form the main planetary bodies. However, it is possible that longer-range instability mechanisms can play a role here. The total amount of mass near the outer edge of the disk is always quite large, and there should be an instability there against the formation of axisymmetric perturbations, which would form ring condensations among the gas in the nebula. Some numerical experiments have been carried out on such rings within the context of the steady flow models. It was found that there was a band extending inward some distance from the center of the ring in which the pressure gradient reverses sign, so that gas-drag effects on the more sizeable bodies within the nebula will cause them to spiral outwards toward the center of the ring, where they will collect together with similar bodies spiralling inward toward the center of the ring. We have conjectured that the ring becomes stabilized against further growth by the onset of the dynamical instability. If this should happen, it is likely that the material would collect quickly from around the circle to form a major planetary body. This mechanism could also provide the basis for an understanding of Bode's law. However, our investigations of this interesting possible mechanism must become much more extensive before any firmer conclusions can be drawn.

Work has started in collaboration with Dr. Richard Epstein to use the entropy values of the material which accretes onto the central body for finding the structure of the central body which is thus formed, and also studying the way in which that central body will ignite its thermonuclear reactions. Until that should happen, it is unlikely that the central body will be able to generate a hot corona, and therefore it will not be able to participate in the mass loss process of the T Tauri solar wind at that early stage. Similarly, the disk evolution code will be used to study the evolution of the disk formed about the giant planets Jupiter and Saturn, and the entropy at the inner radius of the disk will be used by Mr. DeCampli to construct initial models of these planets.

Planetary dynamics

Ward has continued his study of spin-orbit coupling effects upon the past dynamical history of planetary bodies. Interesting results have been obtained for Venus, the Earth, and the Moon.

The past spin-state history of the Moon has been investigated. It was found that the tidal evolution of the lunar orbit has generated an unusual history of the lunar spin axis orientation. Early in the Earth-Moon system, tides raised on the Moon drove the spin-axis nearly parallel to the orbit normal into a special configuration designated a Cassini state. As the lunar orbit expanded due to tides raised on the Earth, the obliquity of the occupied Cassini state increased to $\sim 25^\circ$ until at an orbital distance ~ 34 earth radii, the occupied state became unstable and the spin axis began to circle a second Cassini state laying about $\sim 49^\circ$ from the orbit normal. During this reorientation episode, the lunar obliquity became as high as $\sim 77^\circ$. Tides eventually drove the spin axis to the new state, and further evolution of the orbit brought the Moon to its present configuration. A preliminary report of this work has appeared in Science and a more comprehensive paper is in preparation.

This paper will also include an analysis of the future of the Earth-Moon system. In particular, the Earth's obliquity will undergo radical changes when the lunar orbit has expanded another ~ 5 earth radii.

At the present tidal dissipation rate in the earth, this event is ~2 billion years away. (However, had the Earth's Q been equal to its present value throughout geological time, the Earth would have already entered this stage).

When the lunar obliquity was large, there was increased tidal dissipation in the Moon, since the tidal bulge librated over large latitudes. Possible effects of this on the lunar orbit and the lunar thermal history are also being considered.

A renewed interest in Venus has arisen because Mr. DeCampi, analyzing the results that he obtained on Venus working with Irwin Shapiro's planetary radar group, has determined that the spin axis of Venus lies at a significant angle with respect to the orbit normal. Ward has found the implication of this to be that Venus should have a very small mass quadrupole moment implying that the lithosphere of Venus is much weaker than those of the Earth, Moon and Mars.

In connection with the First International Mercury Colloquium, held at JPL on June 25-27, 1975, investigation of the origin of the large orbital eccentricity and inclination of Mercury was undertaken by Ward, Colombo and Franklin. It was found that the orbital parameters could have been produced by the passage of Mercury's orbit through two secular resonances with Venus, one involving the precession of the line of apsides, the other involving the regression of the ascending node. The orbit was pushed through these resonances by the decaying mass quadrupole moment of the sun during solar spin-down. We find that an initial rotation period < 5 hours and a characteristic spin-down time $\sim 10^6$ years could produce the observed orbit. In addition, this is an upper limit for the spin-down time, since a slower despinning produces a larger eccentricity and inclination. Such a rapid spin-down rate may have accompanied the T Tauri stage of the primordial sun.

Ward has also investigated the dynamical effects of the dissipation of the solar nebula. At present, the eigenfrequencies describing the nodal and apsidal line precession rates of the planets tend to increase from Mercury to Mars (as one approaches Jupiter). However, in the presence of a solar nebula, the equivalent mass quadrupole moment of the nebula would cause these eigenfrequencies to increase as one moves away from the sun. During the removal of the nebula, these rates must have inverted. This event could produce large secular changes in the eccentricities and inclinations of the planet similar to those described above for Mercury. The present values of these parameters can thus be used to set an upper limit for the time scale for nebula dissipation. Preliminary estimates indicate that the removal must have occurred over an interval short compared to a million years. A similar argument can be applied to Saturn's satellite system.

The latter application involves the orbit of Iapetus. An analytic solution has been found for the evolution of the inclination of the orbit of Iapetus under the assumption that it initially lay in the local Laplacian plane and that subsequent removal of a pre-satellite gaseous disk orbiting Saturn caused the plane to rotate from lying in the equator of Saturn to its present orientation, i.e. tilting by $\sim 14^\circ$ to the equator. The present orbit of Iapetus could be produced by the removal of a disk containing ~ 10 Titan masses in a few thousand years. This is in turn consistent with an estimate of the upper limit of the removal time scale implied by the eccentricity of Hyperion, under the assumption that this satellite was driven through a secular resonance with Titan when the gaseous disk dissipated.

ASTEROID FRAGMENTATIONAL PROCESSES

Clark R. Chapman
Planetary Science Institute

It has been recognized that the asteroids are probably composed predominantly of two very different kinds of geological materials -- those similar to carbonaceous chondrites with a probable crushing strength of only a few bars and those similar to stony-iron meteorites with strengths of many kilobars (Chapman, 1974). Further, it has been determined that asteroids are far larger than previously believed (Morrison, 1974; Zellner et al, 1974; Chapman, Morrison, and Zellner, 1975). Thus the collisional cross-sections are much larger and collisions occur much more frequently than previously believed. Indeed Chapman and Davis (1975) suggest that the present-day asteroids are only a small remnant of a vastly larger mass of asteroids that once existed in the belt.

There are some profound implications of these new results for the terrestrial planets. First, the mass loss from the belt has been chiefly due to radiation processes (e.g. Poynting-Robertson) acting on asteroidal dust. Such dust may have accumulated on the surfaces of Mars and other planets. The implications for the geochemistry and role of volatiles on Mars and other planets are of obvious significance.

Second, if the asteroids were once vastly more numerous than today, they are far more likely to have been dominantly responsible for the cratering of terrestrial planetary surfaces. Whether this cratering occurred in the traditional manner, or during a cataclysm perhaps caused by the catastrophic

collision (Chapman, 1976) or tidal-disruption (Wetherill, 1975) of a large Mars-crossing object, it is evident that a thorough understanding of the asteroid collisional processes will shed light on the whole question of planetary cratering. Since the fragmental distribution "maps itself" into a crater distribution, an understanding of asteroidal collisions, combined with the understanding of cratering physics developed chiefly in Gault's research group at Ames, provides the basis from which subsequent analyses of a geomorphological and geochronological nature can be done.

The first order modelling has already been completed. In a project initiated only one month prior to the time this abstract was written, Chapman has begun an extension of the collisional model to include the several different types of material now believed to exist in the belt. In addition to the carbonaceous and stony-iron objects, there is at least one differentiated asteroid (Vesta) and a number of "rocky" bodies. Appropriate analysis of collisional physics, employing appropriate values for the strengths of asteroidal materials, can yield a definitive picture of the compositional evolution of the asteroid belt in a collisional regime.

Particular attention is being given to:

- (1) the dissipation of energy as heat in asteroidal collisions;
- (2) the effects of erosion of asteroids (collisions involving bodies having a mass ratio too large to result in catastrophic fragmentation of the larger one);

- (3) the distribution of fragmental velocities (including comparison with the presently observed dispersion of Hirayama families and analysis of the efficiency of getting fragments into resonances from which they may be accelerated onto Earth-crossing orbits); and
- (4) the distribution of fragmental compositions from collisions involving geochemically differentiated objects (also including comparison with the compositions of Hirayama family members).

PLANETOLOGY STUDIES: STUDIES OF IO AND THE OTHER GALILEAN SATELLITES

F. P. Fanale
Jet Propulsion Laboratory

Last year, detailed models for 1) the composition and evolution of the surface of Io (1,2), 2) the mechanism of transfer of Na to its surrounding cloud or torus (3) and 3) excitation of the Na in the cloud (3) were presented and extensively tested. First, it was hypothesized that the surface of Io was relatively ice free, and was largely covered by Na and S-rich evaporite deposits formed as a residuum when H_2O which migrated to the surface of Io as the result of internal activity was subsequently lost to space. Second, it was hypothesized that the Na was transferred from Io's Na-rich surface to the surrounding cloud by sputtering by Jovian magnetospheric protons. Third, it was hypothesized that the main mechanism for excitation of the Na emission was resonant scattering of sunlight.

The above hypotheses (the evaporite hypotheses) are supported by 1) measurements of the UV, visible and near-infrared reflectance of Io's surface which reveal a very sharp absorption edge in the UV, a very high visible albedo, and a flat spectrum in the near infrared which does not exhibit detectable H_2O or NH_3 ice bands; 2) Quantitative models of the pre-accretion thermal history of the material which formed each of the Galilean satellites, based on studies of the early luminosity history of Jupiter by Grossman, Graboske, Pollack, Reynolds and Cameron. These studies suggest that Io probably formed as a virtually ice-free but bound water-rich object; 3) Quantitative modeling of the subsequent internal thermal history of Io which suggests that extensive devolatilization of the interior was probable relatively early in Io's history; 4) Studies of atmospheric loss mechanisms

which suggest that enough H_2O could have been lost from Io (but not Europa) to produce significant evaporite deposits; 5) Studies of meteorites by DuFresne, Anders and others which suggest that very extensive salt deposition occurred in carbonaceous chondritic meteorites (the best approximation to bulk Io material according to "2") and therefore, by implication, probably in a parent body smaller than Io. Peripherally, the evaporite hypothesis may also provide plausible explanations for 6.) (a.) Io's dark poles (because of greater unannealed radiation damage in "salt" lattices there, (b.) the sharp UV cutoff, because of production of S from sulfates by proton radiation and/or impact vaporization in a vacuum, and (c.) Io's surface polarization. In conjunction with the sputtering hypothesis, the evaporite hypothesis also allows sufficient absolute supply of neutral Na to the cloud ($\approx 1 \times 10^7$ at/cm²/sec) to compensate for steady state electron impact ionization whereas other surface materials (e.g. meteoritic materials) with only trace concentrations of Na will not.

Current studies are directed along two distinct fronts: First, supply of neutrals from Io's surface to the cloud, their orbital paths in the cloud and the mechanisms of their ionization is being carefully modeled. This is being done so that data on the spatial distribution and time variation in intensity of line emission from neutral species other than Na can be interpreted, first in terms of ratios of other neutrals to Na in the cloud and, second (insofar as this proves possible) in terms of the chemical composition of the surface. The latter is much more difficult than former since the former involves corrections for differences in oscillator strength, solar background continuum, trajectories leaving Io (a function of mass),

and so on -- all of which corrections are either small or straightforward. However, connection between cloud composition and surface composition is an exceedingly tenuous one since it involves the corrections listed above plus uncertainties concerning surface-atmosphere and atmosphere-cloud or (in the $\leq 10^{-10}$ atm. model) surface-cloud fractionation. It is difficult to model such fractionation, not only because it may involve several properties of Na and the other neutral atoms, but because it is necessary to fully model the competitive effect of regolith alteration by sputtering and regolith renewal by meteorite gardening. Despite the complexity, it now appears possible to place some constraints on the effectiveness of each of the above fractionation mechanisms so that some limits likewise can be placed on the composition of the surface. This may be done by combining the theoretical cloud and surface modeling as reported above, with data on the cloud distribution and intensity obtained at JPL's Table Mt. observatory, and with data on the intensity (or upper limits on the intensity) of lines obtained from Kitt Peak, Hale Observatories and elsewhere. From such sources, upper limits on Al, Ca, and Fe in the cloud, as well as a detection of K, are available. Data on Mg and S^+ appear to be in the offing. Using the data, together with the models described above, we are able to place some constraints on Io's surface compositions. So far, these are not sufficiently "tight" to allow characterization of the origin or composition of Io's surface material. However, the data thus far appear conformable with the evaporite hypothesis (albeit not uniquely), and unconformable with the possible global occurrence of any common igneous rocks or meteorite types on the surface of Io.

On another front, a detailed laboratory study of the spectral reflectance of mixtures of likely or possible Io surface materials is underway. Data on the spectral reflectance systematics of such mixtures is currently almost nonexistent. The mixtures consist primarily of elemental S with various salts (especially sulfates) and other Io surface candidate minerals. The effects of various proportions of candidate materials, grain size, packing, temperature, degree of vitrification, etc. on UV, visible, and near IR reflectance spectra are being measured along with the effects of proton irradiation on these spectra. These results are being used to interpret Io's surface reflectance in general and, in particular, differences between the spectra of Io's leading and trailing sides.

ORBITAL RESONANCES IN THE SOLAR SYSTEM

S. J. Peale

University of California, Santa Barbara

There are numerous examples of orbital resonances in the solar system, by which we shall mean any system of two satellites orbiting the same primary whose orbital mean motions are in the ratio of small whole numbers. The term "satellites" here includes the planets as satellites of the sun. Often an orbital resonance is characterized by the absence of objects in an otherwise crowded region of the solar system. The major gaps in the rings of Saturn occur at distances from Saturn corresponding to orbital periods near $1/2$ and $1/3$ the orbital period of the satellite Mimas. The Kirkwood gaps in the spatial distribution of the asteroids correspond to orbital periods which are integral fractions of Jupiter's period. At the same time there are some asteroids in these gaps whose orbit periods are commensurate with Jupiter's and others (Hilda group) that preferentially occupy resonant orbits. There are also several orbital resonances among the satellites of Jupiter and Saturn, the most renowned being the three body commensurability (the Laplace relation) among the inner three Galilean satellites of Jupiter. In this system $n_1 - 3n_2 + 2n_3 = 0$ to 9 significant figures, where n_i is the orbital mean motion of the i th Galilean satellite.

Our understanding of the origin and evolution of such orbital resonances has increased dramatically in the last few years and can be summarized as follows:

I. Large fluctuations in orbital eccentricity for bodies librating about a commensurate orbit can lead to collisions with objects in nearby, stable orbits and remove the librating object from the commensurability. Such an explanation can be invoked to explain the Kirkwood gaps and the gaps in Saturn's rings.

II. A resonance maximizes the distance of closest approach for the two resonant objects. Thus, conjunctions of Neptune and Pluto always occur near Pluto's aphelion. Conjunctions of Jupiter and the Hilda and Thule asteroids always occur near the perihelia of the asteroids. The Trojans asteroids librate about longitudes in Jupiter's orbit displaced $\pm 60^\circ$ from Jupiter's position. Pluto and the Hilda, Thule and Trojan asteroids owe their preservation in the solar system to their occupancy of a resonance. Otherwise close approaches with Neptune in the case of Pluto and with Jupiter in the case of the asteroids would eliminate these objects. The rapid elimination of all the objects in non-resonant orbits near the Hilda, Thule, and Trojan asteroids and near Pluto prevents the collisions which could have removed these objects from the resonances.

III. The origin, evolution and present state of the three two-body resonances among the satellites of Saturn are understood in terms of tidal transfer of angular momentum from Saturn to each satellite.

A. No other mechanism satisfactorily accounts for the existence of so many orbital resonances among the satellites of Saturn and Jupiter.

B. An analytical theory by Charles Yoder (formally supported by NASA grant NGR 05-010-062) allows one to follow the differential tidal evolution of an orbiting pair of satellites from a non-resonant through or into a resonant configuration in great detail.

1. Analytical probabilities of capture into a resonance have been determined.

2. Conditions for the stability of a resonance to further tidal evolution constrain models of dissipation in the primary.

3. Present amplitudes of libration and values of inclination and eccentricity are understood in terms of evolution within the resonance.

4. Many different types of resonances are handled with the same mathematical formalism.

5. The avoidance of resonances very near the one currently occupied is also understood either because the probability of capture was considerably less than 1 or because the currently occupied resonance was the first one encountered as the orbits were expanded by tidal friction.

C. The Titan-Hyperion commensurability may be due to a chance primordial configuration instead of tidal evolution unless the tidal dissipation in Saturn has the proper frequency and amplitude dependence. If Hyperion's spin is not synchronous with its orbital motion but has a value $3/2$ times the orbital motion, the primordial eccentricity of Hyperion's orbit would have to be large, which would have prevented tidal evolution into the resonance. A $3/2$ spin-orbit resonance would thus comprise an observational verification of primordial (non tidal) origin of the Titan-Hyperion orbital commensurability.

IV. The successful analysis of the two body commensurabilities has not been extended to the 3 body Laplace relation for the Galilean satellites of Jupiter. The explanation of the unmeasurably small amplitude of libration of this three body resonance remains the outstanding unsolved problem of orbital resonance theory.

SYSTEMATIC SEARCH FOR PLANET-CROSSING ASTEROIDS AND THE ESTIMATION OF IMPACT RATES ON THE TERRESTRIAL PLANETS

E. M. Shoemaker and E. F. Helin
California Institute of Technology

Knowledge of both the absolute and relative rates of impact cratering on the terrestrial planets is fundamental to deciphering their histories. The present cratering rates on each planet can be estimated, provided that sufficient information is available about the present populations of planet-crossing asteroids. A comparison of the present rates of impact with the histories of impact cratering on the Earth and the Moon then permits inferences to be drawn about the histories of impact on Mercury, Venus, and Mars.

At present, 18 Earth-crossing asteroids ($q \leq 1.017$) and about 100 Mars-crossing asteroids ($1.017 \leq q \leq 1.666$) are known that have been sufficiently well observed for orbits of useful precision to be determined. Half of the known Earth-crossing asteroids (Apollo asteroids) cross the orbit of Venus, and 3 cross the orbit of Mercury. Assessments of the circumstances of discovery of these objects by Öpik (1963), Whipple (1973), Wetherill (1975), and ourselves have led to the conclusion that the cumulative numbers of the planet-crossing asteroids to absolute magnitude 18 are from six to several hundred times greater than the numbers so far discovered. Closer estimates of the populations of planet-crossing asteroids can be obtained from the number of discoveries made in the course of systematic surveys of the sky, where the exact system of survey is known. Only a small fraction of the known objects have been discovered under these circumstances, however. Systematic surveys designed specifically for detection and identification of planet-crossing asteroids are needed, therefore, to determine the populations of these bodies with desired accuracy.

We began a survey for planet-crossing asteroids (hereafter called PCA) with the 18-inch Schmidt camera of the Hale observatories at Mt. Palomar in January, 1973. Objects with unusually high rates of motion near opposition were searched for and followed for orbit determination. The search scheme was designed to discover all planet-crossing objects in the search fields with apparent magnitudes equal to or less than 14^m . Objects were detected to 15^m , but the search is not complete at this level. Immediate scanning of the plates for fast-moving objects is essential in order to secure followup observations for orbit determination. The method of search has led to the discovery of several other asteroids, generally with orbits of high inclination or high eccentricity, in addition to planet-crossing objects.

In three years of observation, more than 600 independent fields covering about 30,000 square degrees of the sky were photographed and scanned for fast-moving objects. Each field was photographed twice for asteroid detection. To date, the survey has yielded 11 new asteroids, 7 of which are planet-crossers (Table 1). These results, when combined with discoveries, from the Palomar-National Geographic Sky Survey (PNGS) and the Lick Proper Motion Survey (LPM), both completed about 20 years ago, provide an observational basis for estimating the populations of planet-crossing asteroids.

A theory relating the probability of discovery of asteroids of a given orbital class to the conditions of search has been developed and briefly outlined by Shoemaker, Helin, and Gillett (1975). The magnitude-

frequency distribution of each class of planet-crossing objects is assumed to be of the following form,

$$N_g = K e^{bg}, \quad (1)$$

where N_g = cumulative number of asteroids equal in absolute magnitude to g or brighter,
 g = absolute magnitude,

and K and b are constants to be determined by observation. The magnitude-frequency distributions of both main-belt asteroids and inactive comet nuclei follow this simple exponential law closely; the size-frequency distributions of large craters on the Moon, Mars, and Mercury indicate that planet-crossing asteroids also have a magnitude distribution of this form. The coefficient in the exponent, b , is observed to be close to 1 for all classes of small bodies large enough to be observed at the telescope. The constant K is determined, by means of the formal theory, from the number of objects discovered in the systematic surveys. An empirical model of the photometric phase function and the observed statistical distributions of orbital elements of the known planet-crossing asteroids are employed in the solution for K .

On the basis of 5 Earth-crossing asteroids discovered in the PCA, PNGS, and LPM surveys and 6 Mars-crossing asteroids discovered in the PCA survey, our estimates of the total number of planet-crossing asteroids to absolute magnitude 18 are:

Earth-crossing asteroids. $N_{18} = 800 \pm 400$
Mars-crossing asteroids $N_{18} = 30,000 \pm 15,000$.

Only very preliminary orbits are available for two of the Mars-crossing asteroids discovered in the PCA survey (Table 1). If these two objects are discarded, then $N_{18} = 20,000 \pm 10,000$ is obtained as a lower bound for the population of Mars-crossers.

Approximate estimates for the rate of impact of planet-crossing asteroids with the planets can be obtained from the radial flux of asteroids in the vicinity of each planetary orbit. These estimates are useful for rough comparison of rates of impact on the different terrestrial planets. The radial flux of objects is given by

$$F_g = \frac{N_g}{\pi \bar{p}(Q_0^2 - q_0^2)} \int_{q_0}^{Q_0} \int_{i_m}^{\pi/2} \frac{c(r)h(i)}{r \sin i} di dr, \quad (2)$$

where F_g = mean two-way radial flux of planet-crossing objects to g ,
 \bar{p} = harmonic mean period of planet-crossing objects,
 Q_0 = aphelion of planet,
 q_0 = perihelion of planet,
 r = distance from barycenter of solar system,
 $N_g c(r)$ = cumulative number of planet-crossing objects to g at r ,
 i = inclination of orbits of planet-crossing objects relative to orbital plane of planet,
 $h(i)di$ = differential frequency of planet-crossing objects at i ,
 i_m = minimum inclination of planet-crossing objects.

It may be seen from (2) that the calculated flux depends strongly on the frequency distribution of i at small i . A sufficient number of Mars-crossing asteroids is known to estimate this distribution reasonably well, but not enough Earth-crossing asteroids are known to bound the modelling of $h(i)di$ for Earth-crossers very tightly. The plausible range of $h(i)di$ at small i for Earth-crossers contributes an uncertainty to F_g comparable to that contributed by the uncertainty in N_g . Discovery of many more Earth-crossing asteroids is needed in order to reduce this uncertainty.

Mars has a relatively highly eccentric orbit, and the number of Mars-crossing asteroids increases approximately as an exponential function of r . A fairly good estimate of the function $c(r)$, which is derived from the perihelion distribution of known Mars-crossers, is required to solve (2) for Mars.

Utilizing the osculating orbital elements of the known planet-crossing asteroids, to estimate \bar{p} , $c(r)$, and $h(i)$, and the osculating elements of the planets, to derive Q_0 and q_0 , our best estimates of the fluxes of planet-crossing asteroids to absolute magnitude 18 are:

At the orbit of Earth. $F_{18} \approx 2 \times 10^{-14} \text{ km}^{-2} \text{ yr}^{-1}$
 At the orbit of Mars $F_{18} \approx 8 \times 10^{-14} \text{ km}^{-2} \text{ yr}^{-1}$
 At the orbit of Mars (lower bound) . . . $F_{18} \approx 5 \times 10^{-14} \text{ km}^{-2} \text{ yr}^{-1}$

Considering all of the uncertainties, the difference between the calculated flux of asteroids at the orbit of Earth and that at the orbit of Mars may be just marginally significant. Very roughly, on the basis of the perihelion distribution of the known Earth-crossers, the fluxes at the orbit of Venus and at the orbit of Mercury are about the same as the flux at the orbit of Earth.

In order to calculate the rate of impact on the surface of a planet from the mean flux of objects in the vicinity of its orbit, the capture cross-section of a planet must be determined. The radius of the capture cross-section, σ , is given by

$$\sigma = R \sqrt{1 + \frac{2GR}{u^2}}, \quad (3)$$

where R = physical radius of planet,
 G = gravitational acceleration at surface of planet,
 u = encounter velocity of planet-crossing object prior to appreciable acceleration in gravitation field of the planet.

As shown by Opik (1951), u can be determined with good accuracy by

$$\left. \begin{aligned} U^2 &= 3 - \frac{1}{A} - 2\sqrt{A(1-e^2)} \cos i + \frac{4}{9}e_0^2, \\ U &= \frac{u}{v}, \quad A = \frac{a}{a_0}, \end{aligned} \right\} (4)$$

where v = mean orbital velocity of planet,
 a = semimajor axis of planet-crossing object,
 a_0 = semimajor axis of planet,
 e = eccentricity of planet-crossing object,
 e_0 = eccentricity of planet.

The rms value of u for the 18 known Earth-crossing asteroids is 21.6 km/sec., and the mean ratio of the capture cross-section to the physical cross-section is 1.44. The approximate rate of impact on Earth of planet-crossing asteroids to magnitude 18, given by $(1.44)(2 \times 10^{-14} \text{ km}^{-2} \text{ yr}^{-1})/4$, is $0.7 \times 10^{-14} \text{ km}^{-2} \text{ yr}^{-1}$.

A complete solution for the probability, P , of impact with a planet by planet-crossing object, which takes account of the relative motions of the two bodies, has been given by Öpik (1951). The rate of impact, I , on a planet can be estimated from

$$I = \frac{N_g}{4R^2\pi} \left(\frac{\sum_{j=1}^{j=n} P_j}{n} \right), \quad (5)$$

where P_j = probability of impact for known individual planet-crossing objects, calculated from Öpik's equations
 n = number of known planet-crossing objects.

Utilizing the osculating elements for the 18 known Earth-crossers and the osculating elements of the Earth for evaluation of (5), the impact rate on Earth of planet-crossing asteroids to magnitude 18 is found to be $(0.7 \pm 0.35) 10^{-14} \text{ km}^{-2} \text{ yr}^{-1}$. This estimate is nearly identical with that obtained from the radial flux. In both methods of estimation it is assumed that the longitudes of the node and longitudes of perihelion of the planet-crossing objects are randomly distributed.

The cratering rate on Earth can be found from the estimated impact rate of Earth-crossing asteroids, with aid of appropriate formulae for the relationship between crater diameter and the kinetic energy of the impacting objects. Knowledge of certain physical characteristics of the asteroids is required for this calculation. Polarimetric studies of two Earth-crossing asteroids indicate their geometric albedo is close to 0.2; the corresponding radius for an 18^m object is 0.5 km. Spectrophotometric studies of the same two asteroids suggests they are similar in composition to some of the more common classes of chondritic meteorites. It is reasonable, therefore, to assign bulk densities to these objects of about 3.3 gm/cm³. Assuming that these characteristics are representative of Earth-crossers, and employing the formula for crater-scaling on Earth given by Shoemaker, Hackman, and Eggleton (1963), the rate of production of craters 10 km in diameter and larger is found to be $(1.6 \pm 0.8) 10^{-14} \text{ km}^{-2} \text{ yr}^{-1}$.

From analysis of the size and distribution of impact structures in the central United States, we estimate that the average production rate of craters 10 km and larger over the last half billion years has been $(2.2 \pm 1.1) 10^{-14} \text{ km}^{-2} \text{ yr}^{-1}$. About 2/3 of these craters should have been formed by impact of Earth-crossing asteroids and 1/3 by still active comet nuclei. Thus the Phanerozoic record of impact cratering on Earth is consistent with the estimated present flux of Earth-crossing asteroids. We infer that the present flux of planet-crossing objects provides a reliable guide to the rate of cratering over the last half billion years on the other terrestrial planets, as well.

Table 1. Objects Discovered by Planet-crossing Asteroid Survey,
18-inch Schmidt Camera, Hale Observatories

Object	Discovery Date	Orbital Elements				Disc. mag.	g	Orbital Type
		a	e	i	q			
1973 NA	7/4/73	2.43	0.64	68°0	0.88	10 ^m	14.5	Apollo
1973 QA	8/27/73	1.95	0.04	23°8	1.87	15 ^m	13.5	Hungaria
1973 SA	9/25/73	2.2 ^{1/}	0.4 ^{1/}	5°1 [/]	1.3 ^{1/}	14 ^m	13.5	Mars-crossing?
1973 SB	9/25/73	2.7 ^{1/}	0.4 ^{1/}	16°1 [/]	1.5 ^{1/}	14 ^m	13	Mars-crossing?
1973 WB	11/29/73	2.78	0.42	33°	1.61	14 ^m	12.5	Mars-crossing
1974 KA	5/28/74	2.33	0.24	26°6	1.78	13 ^m .5	12.5	Phocaea
1974 UA	10/17/74	1.80	0.08	30°	1.65	13 ^m .5	13	Mars-crossing
1974 UB	10/17/74	2.12	0.36	36°	1.36	13 ^m	12.5	Mars-crossing
1975 TA	10/8/75	2.55	0.28	8°	1.84	14 ^m .5	13	Main-belt
1975 VA	11/4/75	2.53	0.37	8°	1.59	13 ^m .5	11.5	Mars-crossing
1975 VB	11/4/75	3.15	0.20	3°	2.52	12 ^m .5	9.5	Main-belt (Themis family)

^{1/} Very preliminary orbits

A SPECULATION ABOUT COMETS AND THE EARTH

Fred L. Whipple

Harvard College Observatory and Smithsonian Astrophysical Observatory

Presented first is a brief condensation of our knowledge about comet nuclei. Whether or not the comets we see today originally formed in the outer planetary system in the region of Uranus and Neptune, or whether they condensed directly from interstellar clouds associated with the forming solar system, I assume that the order of 100 earth masses of excess icy conglomerate material were formed in the Uranus-Neptune region, possibly to the Saturn region. Dispersal by perturbations could have transferred a large fraction of this material into Saturn- and Jupiter-crossing orbits with a total time constant for dissipation of the order of 10^7 - 10^8 yr, according to recent theoretical developments by Weidenschilling.

The T-Tauri phase of the Sun, accompanied by an extremely high intensity solar "gale," probably persisted for a shorter period of time, less than 10^8 yr according to Ezer and Cameron and the order of 10^7 yr according to Kuhl and Forbes. The solar gale would probably have eliminated the primitive solar nebula rather quickly and also the primitive atmospheres of the terrestrial planets. It would then have settled down to much its present

activity. Evidence is accumulating that the terrestrial planets and the Moon were all quite hot at some early period, so that the Earth may well have degassed itself with a loss not only of the light elements but of many volatile minerals (Turekian and Clark, Jr.). The life-giving elements of the Earth may well have been accumulated from comets and from asteroids.

The speculation of this paper concerns the possible formation of a "cometary nebula" within Jupiter's orbit and the accumulation of significant cometary material on the Earth. The cometary flux within Jupiter, I_m , may have attained a million times its present value for a period of 10-100 million years after the basic formation of the planets. The current flux on the Earth adds only about 10^{-7} - 10^{-8} earth masses in 4.6×10^9 years but the accretion rate does not scale directly with I_m but with the local density, ρ_m , of the cometary material being collisionally destroyed. Because the collision rate varies as ρ_m^2 , the characteristic time for destruction, T_m , which is now somewhat more than 10^4 yr, therefore varies as ρ_m^{-2} . Obviously $\rho_m \sim I_m T_m$, leading to the conclusion that $\rho_m \sim I_m^{1/3}$. Hence the accretion rate for an increase by only 10^2 times, still adds a trivial mass to the Earth.

The heart of the speculation thus centers on the possibility that for a considerable time the solar wind was unable to cope

with the high value of I_m so that a "pile up" of cometary debris occurred in the inner solar system, providing a cometary nebula with a density many orders of magnitude greater than the present value. If at any time the density of the cometary gas in the inner solar system reached about 10^2 times the present density of cometary solids, i.e. about 10^2 times 10^{-22} g/cm³, any new gas released from comets would be trapped in a cometary nebula. The cross-section for collisions of an escaping atom or molecule would exceed unity. The cometary nebula would increase in density until an equilibrium with loss by solar radiation pressure developed, at a much greater density than equilibrium with the solar wind of today's activity.

Several possible mechanisms could produce a "pile up" as required by the speculation: a) rapid disintegration of new porous comets, b) newly formed passing stars that perturbed an excessive number of comets into the inner region, c) passage through a relatively dense interstellar cloud, or d) a collision of a very large comet with the Moon or even the Earth.

Once the cometary nebula had developed, it would have persisted for millions of years and settled down to a quasi-stable configuration in which the flux of cometary gas and solids on the Earth could increase by several orders of magnitude, adding up to

a significant fraction of the Earth's present mass. The possibility provides a strong incentive for continued efforts to discover the degree to which the life-giving elements on the Earth were indeed contributed by comets or asteroids..

THE REALITY OF COMET GROUPS AND PAIRS

Fred L. Whipple

Harvard College Observatory and Smithsonian Astrophysical Observatory

The subject of comet families with common genetic origin was sparked by the recognition of the Kreutz sun-grazing family, which clearly originated from the tidal disruption of a truly giant comet several thousands of years ago. Subsequent splitting of some of the offspring may have occurred. The splitting of comets by forces other than tidal disruption is not uncommon, perhaps the most notable being the case of P/Biela. Splitting can occur for "new" as well as for "old" comets at orbital positions far from perihelion or from disturbing planets. Thus it seems natural to speculate that comets in similar orbits may have a common parent. Porter has listed a number of such groups. In this spirit, Öpik (1971) has made an exhaustive effort, intercomparing the orbits of all of the comets having aphelion beyond Saturn. Applying statistical methods he concludes that some 60% or more belong to families or groups, the largest groups containing six or seven members. This conclusion demands that many comets in orbits of extremely long periods (millions of years) belong to groups with large enough memberships that two or more representatives have

come to perihelion during the short span of time in which we have obtained good quality orbits. The implications with regard to the mode of origin of comets are startling and difficult to understand. Simple splitting with survival for both components is not adequate. In fact we know of no long-lived split pairs of comets except for the sun-grazing family.

The present paper explores the statistical reality of the comet groups and pairs, excluding the sun-grazing family and the comets that have been observed to split. The Monte-Carlo method as well as ordinary probability theory is employed and applied to the comet groups that Öpik has assembled. He deals with 472 comets, analyzing only the three angular elements: argument of perihelion, ω , longitude of the ascending node, Ω , and the inclination, i , all of these with respect to the ecliptic. He constructs 72 "boxes" consisting of comets with elements in 30° intervals of Ω and i ; within each box he finds clusters of values of ω that appear statistically improbable. His method of search is "opportunistic," the spread generally increasing with the number of members in the group and also being larger in boxes with sparse membership. Thus the rules of selection are not rigid and therefore not subject to precise probability calculations. Nevertheless, he concludes that the comets fall into 97 groups.

consisting of two to seven members with an overall probability of some 10^{-39} that the groups have occurred by chance.

I find that his method of calculating the probabilities is subject to three major criticisms: a) a factor of 2 to 4 error in the probability which he introduces correctly into the Bernoulli probability expression, b) an assumption that the existence of a "most important group" within a box reduces the effective original number in the box and thereby reduces the probability of successive less important groups that may be found within the box, c) an assumption that the extreme spread of i or Ω among members of a group within a box divided by the 30° width of the box represents a concentration factor equal to the probability of such an occurrence. Actually the average separation in i or Ω between members randomly chosen from a 30° box should be 10.0° .

I have simulated cometary orbital elements by random numbers and applied Öpik's opportunistic technique for identifying groups. For these groups and for Öpik's groups of real comet orbits, I have applied uniformly a slightly revised version of Öpik's probability theory based on Bernoulli's formulation. I have assumed that all groups within a box are derived statistically from the same initial number. I find that his groups with more than two members occur with the same frequency as one would expect

from a random distribution of orbital elements. In other words, groups containing more than two members occur no more frequently among the actual comets than among the comets with randomly derived elements. Also within these groups the average separation of i and of Ω occur statistically with the expected 10% value for a 30° box. There remain, however, a few close pairs that appear to occur somewhat more frequently than one might expect from a random assemblage. To date I have not been able to demonstrate that any of these pairs are of common genetic origin but the statistics, at least, suggest that a few may be physically real among the 472 comets having large orbits.

ORBITAL LINKAGE OF COMETS OF INTERMEDIATE PERIOD

Brian G. Marsden

Harvard College Observatory and Smithsonian Astrophysical Observatory

There are nine comets having periods in excess of 20 years that have been observed at more than one passage through perihelion. The best known of these is P/Halley, one of the five comets having periods between 60 and 80 years. We can expect that the motions of most, if not all, of these comets are affected by nongravitational forces, although almost all the work hitherto published on nongravitational forces [e.g., Astron. J. 74, 720-734 (1969); 75, 75-84 (1970); 76, 1135-1151 (1971); 78, 211-225 (1973); 79, 413-419 (1974)] refers to comets of much shorter period. It is of interest to try to extend the studies to these comets of longer period, for the results may shed some light, not only on the form adopted for the nongravitational forces in the equations of motion of a comet, but also on the nature of the forces.

Somewhat surprisingly, we have found that it is possible to link the 1873, 1928 and 1956 apparitions of P/Crommelin (period $P = 28$ years) without the inclusion of any nongravitational terms at all, and the observations in 1818 are really too uncertain to shed further light on the matter; it does appear that the supposed 1625 and 1457 observations do not in fact refer to this comet.

According to the computations by Schubart, there are noticeable nongravitational forces acting on the Leonid comet P/Tempel-Tuttle ($P = 33$ years), but there are only two modern apparitions of this comet (in 1866 and 1965). P/Stephan-Oterma ($P = 39$ years) was observed in 1867 and 1942-43, and an important series of observations by the 1942-43 discoverer has just come to light.

Our computations on P/Westphal ($P = 62$ years) show that it is impossible to link the two apparitions (1852, 1913) gravitationally; since this comet faded out before reaching perihelion in 1913 one can expect that its motion was rather substantially affected by nongravitational forces, and although attempts to allow for these forces have been made they cannot be regarded as successful; not surprisingly, this comet has not been observed at its return to perihelion in 1975/76. P/Olbers ($P = 69$ years) has recently been studied by Yeomans (private communication), who experienced no difficulty fitting two consecutive apparitions gravitationally, and with allowance for nongravitational forces in the way (giving radial and transverse components $A_1 = +0.2$ and $A_2 = +0.07$) we advocate he has obtained a tolerably good fit to all three apparitions. Trouble with the orbit of P/Pons-Brooks ($P = 71$ years) was reported some years ago by Musen and by Herget and Carr, and further work on this comet is therefore desirable. We have recently been trying to link the two apparitions of P/Brorsen-Metcalf ($P = 72$ years) but have run into the same difficulties experienced in the case of P/Westphal (although this comet did not fade out at its last return); Yeomans confirms these difficulties, and we plan to experiment further with solutions allowing for nongravitational forces. Yeomans has recently worked also on P/Halley, finding results ($A_1 = +0.2$, $A_2 = +0.02$) comparable to those for P/Olbers; he does not confirm the results previously

reported by Brady and notes that the perihelion time in 1986 will probably be 0.3 day later than predicted by Brady.

We have made an approximate linkage of the two apparitions of P/Herschel-Rigollet ($P = 155$ years), although the 1788 observations are very rough. Ex-P/Grigg-Mellish ($P \neq 164$ years) should also be mentioned in this connection, for we have proven that the 1742 and 1907 comets are not the same object. Finally, we can refer to our earlier work on the Perseid comet P/Swift-Tuttle [Astron. J. 78, 654-662 (1973)]: this comet has $P = 120$ years and has not definitely been seen before its discovery in 1862, although it is not completely impossible that it is identical with comet 1737 II, and we made a reasonably successful attempt to link these two apparitions with the inclusion of non-gravitational terms; if the identification is correct, the comet will return in 1992, although other indications are that it will in fact return a decade or more earlier.

P/Halley and P/Swift-Tuttle (curiously) have both been mentioned as the possible objectives of space missions, and the outcome of the calculations discussed here could well affect the success of such missions.

ORBIT DETERMINATION OF NEARLY-PARABOLIC COMETS

Brian G. Marsden and Zdenek Sekanina

Harvard College Observatory and Smithsonian Astrophysical Observatory

Having found that the original orbits of comets of perihelion distances exceeding 2.2 AU tend to pile up around a peak, corresponding to an aphelion distance of about 50 000 AU [Astron. J. 78, 1118-1124 (1973)], we undertook to extend our orbital calculations to comets with smaller perihelion distances.

Substantial progress in this project is now being reported. Table I, which gives improved orbits (most of them of high quality) for 70 comets between 1844 and 1974, contains a significant fraction of comets with very elongated orbits [original reciprocal barycentric semimajor axes $(1/a_b)_{\text{orig}} < 0.0007 \text{ AU}^{-1}$] and these are listed by perihelion distance q in Table II. A plot of $(1/a_b)_{\text{orig}}$ vs q [for comets with $(1/a_b)_{\text{orig}} \leq 0.0002 \text{ AU}^{-1}$] indicates a gradual increase in scatter as q decreases, which is interpreted as due to nongravitational forces.

A search for comets with directly detectable nongravitational effects in their positional residuals added three more cases to the previous list [Astron. J. 78, 211-225 (1973)], making a total of seven: 1915 II, 1954 X, 1957 III, 1960 II, 1970 II, 1971 V and 1974 III.

Recently calculated orbits of 70 long-period comets

COMET	T	Q	E	PERI.	NODE	INCL.	EPOCH
1844 III	44 DEC.	0.250537	0.999302	177.4980	119.8977	45.5689	44 DEC. 20
1851 IV	51 OCT.	0.142053	1.0	294.4418	45.7318	73.9821	
1889 I	89 JAN.	1.814916	1.001230	340.4625	358.2749	166.3777	89 FEB. 7
1892 II	92 MAY	1.970726	1.000371	129.3253	254.2404	89.6971	92 MAY 22
1895 IV	95 DEC.	0.191978	1.000051	272.6723	321.2614	141.6209	96 JAN. 2
1897 I	97 FEB.	1.062791	1.000983	172.3277	87.2233	146.1368	97 FEB. 5
1898 VII	98 SEPT.	1.701595	1.000934	233.2624	74.7125	69.9347	98 SEPT. 28
1900 I	00 APR.	1.331529	1.001058	24.4010	41.0886	146.4441	00 APR. 11
1903 IV	03 AUG.	0.330182	1.000406	127.2578	294.2109	85.0123	03 SEPT. 3
1904 II	04 NOV.	1.882049	1.000678	40.7453	219.0913	99.6036	04 NOV. 16
1907 I	07 MAR.	2.051703	1.001114	317.1088	97.7777	141.6609	07 APR. 15
1910 IV	10 SEPT.	1.948013	0.999797	50.9643	290.0849	121.0528	10 SEPT. 6
1914 II	14 JUNE	1.198527	1.000106	72.2321	199.4116	23.9197	14 MAY 28
1914 IV	14 AUG.	0.712756	0.998666	270.3460	0.8845	77.8295	14 AUG. 16
1915 II	15 JULY	1.005286	1.000151	247.7767	72.7588	54.7908	15 JULY 2
1917 III	17 JUNE	1.686446	0.999405	120.6239	183.7566	25.6656	17 JUNE 21
1919 V	19 DEC.	1.115291	1.000222	185.7461	121.4039	46.3862	19 NOV. 18
1921 II	21 MAY	1.008457	1.000357	64.4989	268.7468	132.1871	21 APR. 21
1924 I	24 MAR.	1.755695	0.998590	271.4341	114.3771	72.3306	24 FEB. 25
1925 I	25 APR.	1.109477	1.000605	36.1854	318.4118	100.0172	25 MAR. 31
1925 VII	25 OCT.	1.566243	1.000382	106.4021	334.9126	49.3246	25 OCT. 17
1927 IX	27 DEC.	0.176157	0.999840	47.1523	77.5456	85.1117	27 DEC. 26
1932 VII	32 SEPT.	1.647412	1.000602	69.7933	245.3898	78.3916	32 SEPT. 10
1937 IV	37 JUNE	1.733791	1.000137	107.7273	127.9151	41.5560	37 JULY 6
1937 V	37 AUG.	0.862744	0.999985	114.8260	58.7134	146.4127	37 AUG. 15
1941 I	41 JAN.	0.367751	1.000485	199.5763	295.8873	49.8909	41 JAN. 6
1941 II	41 JAN.	0.941864	0.981221	132.7383	329.0854	26.2697	
1946 I	46 APR.	1.724129	1.001169	54.3231	128.9679	72.8472	46 APR. 10
1946 II	46 MAY	1.018252	1.0	22.2617	301.3064	169.5580	
1946 VI	46 OCT.	1.136113	1.000776	320.4200	237.6333	56.9677	46 OCT. 27
1947 IV	47 MAY	0.559799	0.997427	303.7548	353.2111	39.2949	47 MAY 15
1947 V	47 MAY	1.402863	1.0	357.3948	232.3665	111.4129	
1948 I	48 FEB.	0.748125	1.000363	350.2248	270.7491	140.5674	48 FEB. 19
1948 II	48 FEB.	1.499557	1.001085	61.9268	198.6019	77.5391	48 FEB. 19
1948 V	48 MAY	2.107056	1.000787	66.9043	246.9543	92.9214	48 MAY 9

Table I (continued)

COMET	T	Q	E	PERI.	NODE	INCL.	EPOCH
1948 X	48 OCT.	1.273428	0.997499	274.2030	66.9702	87.6034	48 OCT. 16
1952 I	52 JAN.	0.740427	0.999739	269.6066	76.1833	152.5327	52 JAN. 29
1953 I	53 JAN.	1.664977	0.995910	191.6314	220.6904	59.1199	53 JAN. 23
1953 II	53 JAN.	0.777729	1.000343	253.8232	342.8832	97.1773	53 JAN. 23
1953 III	53 MAY	1.022132	0.997391	85.7464	275.1874	93.8561	53 MAY 23
1954 II	54 JAN.	0.072347	1.0	94.0537	114.5577	13.5761	
1954 VIII	54 JUNE	0.677461	1.000286	357.2544	122.1237	116.1581	54 MAY 18
1954 X	54 JULY	0.970116	1.000564	194.3817	2.3350	53.2224	54 JUNE 27
1955 III	55 JUNE	0.534419	0.989361	32.5090	48.2434	86.4978	55 JUNE 22
1955 V	55 AUG.	0.884616	1.000947	348.1948	338.7233	107.5159	55 AUG. 1
1958 III	58 APR.	1.322689	0.999943	16.4559	150.5054	15.7938	58 APR. 27
1959 I	59 MAR.	1.628199	0.999867	100.7396	323.0787	61.2520	59 FEB. 1
1959 IX	59 NOV.	1.253464	0.999748	84.6737	99.9396	19.6356	59 NOV. 8
1961 II	61 FEB.	1.061612	0.989900	136.6144	176.5797	150.9618	61 JAN. 21
1961 VIII	61 OCT.	0.681129	0.991812	126.5900	246.6704	155.7128	61 OCT. 28
1964 VIII	64 AUG.	0.821752	0.984643	290.8080	269.2965	171.9195	64 JULY 24
1966 II	66 APR.	2.018766	0.998183	136.1683	166.9923	28.7123	66 APR. 25
1967 II	67 JAN.	0.419225	1.000391	79.7433	75.0494	9.0787	67 JAN. 30
1968 VI	68 AUG.	1.160434	1.000665	88.7049	106.0404	143.2408	68 AUG. 12
1969 IX	69 DEC.	0.472638	0.999920	267.8274	100.9629	75.8196	69 DEC. 5
1970 III	70 MAR.	1.719088	0.999137	123.4737	301.0593	86.3089	70 APR. 4
1970 XV	70 OCT.	1.112539	1.000048	96.5799	21.0007	126.7141	70 OCT. 21
1971 I	71 JAN.	3.276561	0.996943	128.6899	24.0084	175.6103	71 JAN. 9
1972 VIII	72 OCT.	2.511124	1.000501	346.2352	175.1787	138.6348	72 OCT. 10
1972 IX	72 NOV.	4.275707	1.006288	56.6628	224.7868	79.3723	72 NOV. 19
1972 XII	72 DEC.	4.860748	0.999910	267.2089	314.1872	113.0852	72 DEC. 29
1973 II	73 FEB.	2.147032	1.001018	334.2980	42.4838	141.8510	73 FEB. 7
1973 III	73 MAR.	2.384384	0.972800	123.4850	57.1492	48.3239	
1973 VII	73 JUNE	1.382019	0.998723	74.8584	164.1185	121.6046	73 JUNE 7
1973 IX	73 AUG.	3.842738	1.0	221.2928	243.9008	108.0671	
1973 X	73 NOV.	4.812054	1.000036	72.5541	278.5454	137.4017	73 NOV. 14
1973 XII	73 DEC.	0.142425	1.000008	37.8238	257.7656	14.3051	73 DEC. 24
1974 III	74 MAR.	0.503191	0.999697	333.1302	143.0379	61.2898	74 MAR. 14
1974 VII	74 MAY	1.372826	0.978898	176.7406	165.0304	173.1648	
1974 XII	74 AUG.	6.019617	1.004022	151.8041	225.4025	60.8578	74 AUG. 21

Table II

Those comets in Table I that have $(1/a_b)_{\text{orig}} < 0.0007 \text{ AU}^{-1}$,
arranged in order of decreasing perihelion distance

Comet	q (AU)	$(1/a_b)_{\text{orig}}$ (10^{-6} AU^{-1})	Comet	q (AU)	$(1/a_b)_{\text{orig}}$ (10^{-6} AU^{-1})	Comet	q (AU)	$(1/a_b)_{\text{orig}}$ (10^{-6} AU^{-1})
1974 XII	6.02	- 2 \pm 54	1917 III	1.69	+ 18 \pm 3	1921 II	1.01	+ 19 \pm 11
1972 XII	4.86	+477 \pm 4	1932 VII	1.65	- 56 \pm 15	1915 II	1.01	+ 75 \pm 5*
1973 X	4.81	+539 \pm 19	1959 I	1.63	+ 77 \pm 6	1954 X	0.97	+ 71 \pm 25*
1972 IX	4.28	+ 72 \pm 7	1925 VII	1.57	+ 24 \pm 12	1955 V	0.88	-727 \pm 121
1972 VIII	2.51	+ 49 \pm 13	1948 II	1.50	+ 27 \pm 8	1937 V	0.86	+124 \pm 29
1973 II	2.15	+321 \pm 6	1900 I	1.33	+ 57 \pm 30	1953 II	0.78	-125 \pm 9
1948 V	2.11	+ 35 \pm 4	1958 III	1.32	+256 \pm 14	1948 I	0.75	+ 26 \pm 18
1907 I	2.05	+ 25 \pm 19	1959 IX	1.25	+ 70 \pm 14	1954 VIII	0.68	+ 51 \pm 40
1910 IV	1.95	+474 \pm 11	1914 II	1.20	+127 \pm 27	1974 III	0.50	+690 \pm 13*
1904 II	1.88	- 76 \pm 98	1968 VI	1.16	- 83 \pm 116	1969 IX	0.47	+507 \pm 4
1889 I	1.81	+ 49 \pm 3	1946 VI	1.14	+ 44 \pm 4	1967 II	0.42	+ 49 \pm 38
1937 IV	1.73	+ 63 \pm 8	1919 V	1.12	+ 21 \pm 33	1941 I	0.37	+ 1 \pm 10
1946 I	1.72	- 13 \pm 3	1970 XV	1.11	+283 \pm 2	1903 IV	0.33	+ 33 \pm 6
1970 III	1.72	+549 \pm 7	1925 I	1.11	+ 40 \pm 11	1895 IV	0.19	-168 \pm 8
1898 VII	1.70	+ 69 \pm 7	1897 I	1.06	+ 6 \pm 17	1973 XII	0.14	+ 20 \pm 3

*This value is from a gravitational solution, although the orbit in Table I is from a nongravitational solution.

EVOLUTION OF JUPITER, SATURN AND THEIR SATELLITE SYSTEMS

James B. Pollack
NASA Ames Research Center

We have three clues about the formation and evolution of Jupiter, Saturn, and their satellite systems. These are the observed amounts of energy that these giant planets radiate to space, which exceeds by a substantial fraction the amount of sunlight they absorb; the density of their satellites; and inferences that can be drawn from the planets' present observable quantities concerning the presence of a heavy element core. The first of these observations can be attributed to the release of gravitational potential energy, but it has been unclear as to what the relative contributions of past contraction, present contraction, and chemical separation due to immiscibility effects have been. We have studied these three clues by performing calculations of the gravitational contraction history of Jupiter and Saturn and by modeling their present structure.

The evolutionary calculations have been performed with a code used to study the evolution of low mass stars. As auxiliary data for these calculations, we have computed a grid of model atmospheres and a complete, detailed set of thermodynamic variables for the planetary interiors. Our model planets are homogeneous and have a solar composition. The calculations begin when the planets are much larger than their present dimensions and we follow their slow quasi-equilibrium contraction for 4.5 billion years, the approximate age of the solar system.

Both planets contract very quickly during the first million years of their evolutionary history and exhibit at this time a behavior analogous to that of a pre-main sequence, low mass star. After this period their centers exhibit partial electron degeneracy and resist further contraction, although their outer envelopes continue to contract. At times after 1 million years of evolution and continuing up until the present, their internal thermal energy, which was built up during the initial phases, steadily declines. This behavior can be likened to that of a degenerate white dwarf star.

After 4.5 billion years of evolution, the model Jupiter achieves a radius and excess luminosity very close to the observed values. The interior, even at present, is too warm for helium to become immiscible in metallic hydrogen. We find that most of the model's excess energy is due to the decay of the thermal energy built up during the early, rapid contraction phase, but that a non-negligible contribution also comes from its present contraction.

Our model Saturn is somewhat less successful. The model's radius and luminosity are 9% larger and a factor of 3 smaller than the observed values, respectively. These discrepancies are due to a combination of errors in the equation of state and a neglect of the possible presence of a heavy element core (such as a rocky core). Again a good portion of the excess energy is due to past contraction, but the temperatures in the later models become low enough that immiscibility effects might be important.

Both the Jupiter and Saturn models exhibit a luminosity in their early history that is many orders of magnitude larger than their present values. This result implies that the radiation from these planets may have been an important factor at the time their satellites were forming. We suggest that the systematic decrease in the density of the Galilean satellites with distance from Jupiter was due to the inability of water ice to condense in the region of the inner satellites as a result of Jupiter's high luminosity. To pursue this matter further we have used our evolutionary calculations to determine the time history of temperature conditions within region of the present satellites. We find that the observed density trend of the Galilean satellites can be understood if the incorporation of icy material into the satellites ceased about a million years from the start of our contraction calculations.

A similar analysis of Saturn's system of satellites shows that icy satellites could form closer to Saturn than Jupiter because Saturn's early luminosity was about an order of magnitude smaller than Jupiter's. This result is consistent with the low density of Saturn's inner satellites. With the same time scale for satellite formation as for Jupiter, we find that Titan is the innermost satellite at whose orbit methane containing ices can form and that temperatures may have been cold enough towards the end of the formation period for water ice to condense in the outer regions of the rings.

Finally, we find that with our present equation of state a rocky core of only about 0.03 Earth masses is needed to match Jupiter's observed mass and radius, but that a core of 20 Earth masses, i.e. 20% of the planet's total mass, is needed to match the corresponding quantities for Saturn. The Jupiter model has gravitational moments J_2 , and J_4 and an effective temperature that are in good agreement with the observed values. A somewhat less good but still adequate set of predicted values is exhibited by the Saturn model.

STATISTICS OF ANOMALOUS TAILS OF COMETS

Zdenek Sekanina

Harvard College Observatory and Smithsonian Astrophysical Observatory

The observability of an anomalous tail (antitail) of a comet can be rather straightforwardly predicted from the dynamical and projection conditions. The physical presence or absence of the antitail at a precalculated time is then a measure of the comet's production rate, at the relevant emission times, of relatively heavy dust particles (mostly of submillimeter size) that constitute such an antitail. Because the large grains are emitted from the nucleus at very low velocities (typically meters or tens of meters per second), an antitail is essentially a two-dimensional formation in the orbit plane of the comet and can be recognized best when projected edge-on, i.e., when the Earth crosses the nodal line of the comet's orbit. In general, however, this condition is not essential for the recognition of antitails (cf., e.g., Comet Kohoutek 1973 XII).

Since the emission rate of heavy dust particles is a potentially significant parameter for a physical classification of comets, we made use of the visibility conditions to list the comets that should have displayed a sunward tail around the time of the Earth's passages through the orbit plane. This type of the antitail observability will be termed the nodal appearance. A

computer program executing the conditions for a nodal appearance was applied to the Catalogue of Cometary Orbits (Marsden, 1975), starting with the comets of 1737, but excluding elongations over 135° and heliocentric distances larger than 2 AU.

The statistics of the nodal appearance of antitails of comets, whose conditions were satisfied within the period of observation show that about 20 to 30% of the nearly-parabolic comets that should have displayed an antitail at the node were actually observed to do so. The results are dramatically different for short-period comets. Although there were numerous opportunities for observing a nodal appearance of an antitail, we do not yet have a single clearly positive observation. The only promising case so far is that of P/Encke in 1964, for which Roemer secured a pair of plates only 2.5 days after the Earth's nodal passage, when the comet was 88 days after perihelion. A close inspection of the plates revealed two extensions emanating from the weak, nearly stellar image of the comet in the opposite directions, one of them pointing right toward the Sun. Although this sunward tail does not resemble the gas jets, frequently observed in P/Encke before perihelion, there is still no more than a 50% chance that it is a true antitail.

The general absence of antitails among the short-period comets appears to be incompatible with the existence of meteor streams known to be associated with many of these comets. Unfortunately, at their observed returns, the parent comets of the three spectacular-storm producing meteor streams — P/Biela, P/Giacobini-Zinner and P/Tempel-Tuttle — were never placed favorably enough for a nodal appearance of an antitail. And, of all the other comets known to be related to meteor streams, only two had such very favorable

apparitions: P/Encke in 1878, 1888 and 1964, and P/Pons-Winnecke in 1909, although P/Pons-Winnecke is not apparently associated with a permanent stream. The other comets with favorable conditions were P/Tempel 1 in 1867, P/Finlay in 1919, P/Kopff in 1945, P/Grigg-Skjellerup in 1947, and P/Schaumasse in 1952 and 1960. Streams that could be associated with P/Finlay or P/Grigg-Skjellerup have never been reported; the other comets have perihelia well beyond 1 AU.

With one doubtful and two negative results in the three nearly-ideal returns, P/Encke presents probably the most solid evidence to date against the positive correlation between the antitails and the meteor streams. In order to obtain more data on the occurrence of the antitails, their conditions of visibility in the future returns of the short-period comets will be investigated.

This work was supported in part by grant NSG 7082 from the National Aeronautics and Space Administration.

A PROBABILITY OF ENCOUNTER WITH INTERSTELLAR COMETS AND THE LIKELIHOOD OF THEIR EXISTENCE

Zdenek Sekanina

Harvard College Observatory and Smithsonian Astrophysical Observatory

The aim of this paper is to investigate the possibility of the existence of a cloud of interstellar comets in the Sun's neighborhood. Some work along these lines was done in the past, but the results seem to depend rather strongly on the starting assumptions. Our approach is formulated with a minimum of necessary restrictions, yet it is mathematically tractable with relative ease.

The presented probability theory of encounter of the Sun with interstellar comets at distances comparable with the Earth-Sun distance offers a set of general expressions establishing the relations among the influx rate of interstellar comets, the distribution of their semimajor axes, the range of perihelion distances, the space density of the comets, the dispersion coefficient of the spherical Maxwellian distribution of comet velocities in the interstellar cloud, and the cloud's systematic velocity relative to the Sun. The fact that no comet with a strongly hyperbolic orbit has so far been observed is used to determine an upper limit for the space density of interstellar comets. It is

concluded that the existence, in the solar neighborhood, of a cloud of interstellar comets with a space density of 6×10^{-4} solar masses per cubic parsec (4×10^{-26} g cm $^{-3}$) or higher is virtually ruled out, and that the existence of a comet cloud 10 times less dense is very unlikely. However, the probability of encounter with the Sun of a comet from a cloud whose space density does not exceed 10^{-5} solar masses per cubic parsec (less than 10^{-27} g cm $^{-3}$) is too low to exclude a priori the existence of interstellar comets altogether. For comparison, we note that Oort's estimates of the size and population of his model of a solar-bound comet cloud give a mean space density of only about 10^{-6} solar masses per cubic parsec ($\sim 10^{-28}$ g cm $^{-3}$), although Whipple has recently shown that the possible unobserved mass of comets in the solar system could be a not-insignificant fraction of the solar mass.

The hypothetical interstellar comets might have originated in situ or might have been, at birth, star-bound comets that were later ejected from circumstellar areas in a manner similar, perhaps, to the expulsion of a fraction of nearly parabolic comets from the solar system by planetary perturbations. In either case, the motions of such interstellar comets should show an appreciable systematic velocity relative to the Sun (more than 10 km sec $^{-1}$) and a dispersion in individual velocities of at least 5 km sec $^{-1}$, judging from analogy with other groups of galactic objects. While a distinct systematic motion of the cloud relative to the Sun implies the presence of a preferential direction in the distribution of cometary aphelia, which was detected by some in the motions of nearly parabolic comets, it also requires that an overabundance of strongly hyperbolic orbits be observed, which, of course, has never materialized.

On the other hand, the apparent absence of strongly hyperbolic orbits, together with the scarce occurrence of slightly hyperbolic orbits among the

observed comets, could only imply a cloud of comets traveling with the Sun (no systematic velocity and a very low dispersion), but the aphelion points would then have to be distributed essentially isotropically. Since an alternative and very plausible explanation (nongravitational effects) is at hand for the few slightly hyperbolic original orbits that are observed, we do not find it attractive to link any of the orbital properties of the actual comets with the hypothesis of interstellar comets.

The model considered here could, of course, be generalized even further by considering an ellipsoidal, rather than spherical, distribution of comet velocities in the cloud. In the light of present results, however, such a move — substantially complicating the mathematical treatment of the problem — does not appear to be worth the effort.

This research was supported by grant NSG 7082 from the National Aeronautics and Space Administration.

ON THE EXTENT OF A MERCURIAN LIQUID CORE

S. J. Peale

University of California, Santa Barbara

The discovery of an intrinsic magnetic field for the planet Mercury has increased speculation about the existence and properties of a liquid core thought necessary for a dynamo generation of the field. The observational verification of a liquid core would have far reaching implications for the theory of planetary interiors in general and dynamo generation of a magnetic field in particular. The dynamical effect of a large liquid core affords a straightforward, albeit expensive, observational test of the extent of such a fluid core.

Since a fluid core could not follow the forced physical librations of Mercury about its mean spin rate, the amplitude of these librations would be approximately $(B-A)/C_m$ where $A < B < C$ are the principal moments of inertia and C_m refers to the mantle alone. On the other hand the core would follow the mantle on the much longer time scale of the 250,000 year precession period. The occupancy by Mercury of a Cassini spin state means a measurement of the obliquity of Mercury's equator plane to its orbit plane is a measure of the response of the planet to the external torque causing the precession. This yields $(C-A)/C$ where C here refers to the entire planet. The two moment differences are separately evaluated by the determination by artificial satellite of the gravitational harmonics C_{20} and C_{22}

which together yield $(C-A)/MR^2$ and $(B-A)/MR^2$. Combination of these results yields C/MR^2 , which is a measure of the central condensation and C_m/C which determines the fraction of the interior which is decoupled from the mantle. The latter number determines the extent of the fluid core.

All that is required of the core properties for this determination is that the kinematic viscosity be within the bounds $8 \times 10^{-4} \lesssim \nu \lesssim 2 \times 10^9 \text{ cm}^2/\text{sec}$ which includes the extreme range of values estimated for the earth's core ($5 \times 10^{-3} \lesssim \nu_{\oplus} \lesssim 10^7 \text{ cm}^2/\text{sec}$). The expense of this determination is high, since the obliquity $\lesssim 1^\circ$ and the libration amplitude is the order of 20" of arc, so a surface instrument of some kind will be necessary for an accurate measurement.

THARSIS: IMPLICATIONS FOR EVOLUTION AND PRESENT STATE OF THE MARTIAN INTERIOR

R. J. Phillips
Jet Propulsion Laboratory

One of the outstanding geophysical problems for Mars regards the Tharsis uplift and associated gravity anomaly. The chief questions are: (1) What is the energy source of the uplift? (2) Is this energy source also related to the Tharsis volcanism? (3) How has the Tharsis gravity anomaly persisted for such a long period, by terrestrial comparison, of geologic time? (4) How can volcanic activity and large gravity anomalies co-exist, since they can imply thermally diverse regimes?

As summarized by Carr [1974], the Tharsis updoming appears to have been a single unique event in Martian history. Topographically and gravitationally, the doming is dominantly described by the second and third spherical harmonics and is therefore global in nature. The radial (and to a lesser extent concentric) tensional features associated with Tharsis, as well as the doming, suggest the dominance of vertical stress in formation. It has previously been argued [Phillips and Saunders, 1975] that the relationship of gravity and topography imply that uplift of Tharsis and the subsidence of the Chryse and Amazonis lowlands are contemporaneous. In particular, the Chryse trough is circumferential to the Tharsis dome, suggesting the trough is a concentric graben formed during the uplift.

It is suggested that the doming was caused by an upwelling of material in the upper mantle. This material would be of lower density than normal

mantle material. Tharsis is uplifted by both buoyant and viscous stresses. Densification due to cooling notwithstanding, the presently observed Bouguer gravity [Phillips et al., 1973] gives the maximum amount of buoyant stress available. This follows because any isostatic adjustment following the doming will only serve to increase buoyant stresses at the base of the crust. Evidence for adjustment is given by regional stress patterns [Wise, 1975; see also Artyushkov, 1973]. This present day maximum stress is not sufficient to cause the doming of Tharsis, because sufficient buoyancy would imply an isostatic condition, which is far from the case [Phillips and Saunders, 1975]. This implies a significant amount of viscous stress was imparted by the upwelling material. An approximate lower bound on this stress is the stress due to the uncompensated topography prior to the addition of the volcanics in the Tharsis region, roughly 100 bars.

Possibilities for the upwelling are various states of thermal convection and chemical differentiation in the mantle. Below it is argued that chemical differentiation at depth and subsequent diapirism is perhaps the most likely mechanism for the Tharsis doming. We are constrained by the present day observation of an abnormally thick region of low (relative to mantle) density beneath Tharsis, extending to depths no greater than about 150 km. Active thermal convection can provide doming and density deficiencies, as is observed with the Mid-Atlantic Ridge.

However, the abrupt cessation of doming about a billion years ago [Carr, 1974] would mark the termination of active thermal convection, with a gradual cooling to normal mantle densities. Material at 150 km depth would cool to half of its initial temperature in about 700 m.y. Given the

uncertainty in the age of the doming, it is possible that the present negative Bouguer anomaly is a still-cooling fossil convection cell. The small density contrast to be expected (say, less than $.05 \text{ gm/cm}^3$) places the depth extent of the anomalous region close to the maximum depth inferred from the analysis of Phillips and Saunders [1975].

That the Rayleigh number is sufficient for Martian mantle convection is discussed by Schubert et al. [1969]. Lingenfelter and Schubert [1972] argue that Tharsis is a region of convective downwelling, which in fact gives the wrong algebraic sign for doming by viscous stresses. Their argument is based on a thicker crust at Tharsis resulting from accumulation of chemically differentiated material from the descending portion of the convection cell. However, as discussed above, the density anomaly need not be interpreted in terms of a thicker crust.

The absence of any surficial or gravitational evidence for upwelling or downwelling diametrically opposite Tharsis and the episodic nature of the fracturing argue against steady-state convection, at least in the upper mantle, over at least the last billion years. Marginal convection in terms of a diapir would arise from a thermal (hence density) instability in the middle or lower mantle. Low density material would rise to the upper mantle but the Rayleigh number would be insufficient to achieve steady state.

A chemical diapir arising from a gravitational instability following deep differentiation is also a possibility and avoids the marginal difficulty of cooling and depth extent discussed above for purely thermal instabilities.

The radial normal viscous stress is given by:

$$\sigma_{rr} = 2\eta \frac{\partial V_r}{\partial r} \approx \frac{2\eta V_r}{d}$$

where η is the viscosity, V_r is the radial velocity, and d is the depth extent of fluid flow in the mantle. Terrestrial convection velocities are typically about 5 cm/year and diapiric (plume) velocities are thought to be upwards of 10 cm/yr. Using the lower value because of lower gravity in the Martian mantle and adopting a characteristic depth extent of 1000 km, then a 100 bar stress is realized with a viscosity of about 3×10^{22} poise. This value is typical of values in the terrestrial mid-mantle and does not preclude even a steady state convection in the ancient Martian mantle.

That the major fracturing stopped about a billion years ago implies cessation of viscous stress on the base of the crust. This does not preclude present day convection in the lower mantle.

The dominant uncompensated harmonics are the second and third; they both must be supported in the lower mantle, assuming the existence of a strengthless core [Dolginov, 1975]. This conclusion is independent of the presence of an upper mantle low rigidity zone. The fourth harmonic is strong topographically in the Tharsis region, but appears to be compensated. It must be supported at a depth of about 800 km. This suggests that the strength of the mantle increases with depth. This result is not surprising when rock strength is considered to be proportional to the difference between the actual temperature and the melting temperature, the latter increasing with increasing depth (pressure). The lower mantle strength required to support the uncompensated fraction of the dominant harmonic J_{22} is about 90 bars.

Using the thermal models of Johnston et al. [1974] and an analogy to terrestrial melting temperatures at pressures equivalent to those in the Martian lower mantle, it is found that a 90 bar strength is reasonable. No other mechanism is required to support the anisostasy.

The upwelling of mantle material to form the Tharsis dome is an obvious source for magma for subsequent volcanic activity. The role of viscous heating in magma generation during upwelling and subsequent isostatic adjustment is currently being investigated.

ANALYSIS OF COMPENSATED REGIONS OF MARS

R. S. Saunders
Jet Propulsion Laboratory

A new histogram of elevations on Mars (figure 1) has been constructed using the latest compilation of elevation data (Christensen, 1975) and extending the coverage to the poles using available Mariner 9 occultation points (Mutch et al., 1976). A previous histogram which did not include the higher latitudes shows a strong bimodality which was interpreted to indicate that the martian crust is differentiated into more- and less-silicic blocks (Hartmann, 1973). The new histogram is not strongly bimodal, but does contain three modes that correspond to distinct regions of the planet. The purpose of this paper is to discuss these regions in terms of crustal development.

It has previously been shown that the most elevated region of Mars, the Tharsis plateau, is not fully compensated, with the equivalent of 3 km or more of uncompensated topography (Phillips and Saunders, 1975). The lowlands that flank the Tharsis plateau are also uncompensated with a mass deficit of 1 km or more of topography. Except for these regions, the planet is regionally nearly in isostatic balance. The regions in isostatic balance, being areally more significant, may be outlined by topographic contours based on the three largest modes of the elevation histogram. The regions so identified form continuous "continental" scale areas of the planet.

The largest region, the cratered province, forms the mode between 2 and 3 km. The region that represents this mode lies between 1 and 5 km in elevation and includes all of the ancient cratered terrain of the planet. The uplifted Tharsis region within this province forms the tail of the

histogram in excess of 5 km in elevation and does not contribute to one of the major modes; the minor mode between 7 and 8 km represents the mean elevation of the Tharsis plateau. The Elysium plateau is included in the 1 to 5 km elevation province but it is more related to the Tharsis plateau in geologic setting. Hellas is included in the cratered province because it is an isostatically compensated basin within the cratered province. Hellas lies on the low elevation tail of the compensated ancient population much as the Thaumasia region occupies the high elevation tail.

A second province, the northern plains, includes two topographic modes. The northern plains lie below 1 km and are completely contained in the region north of the 1 km contour line as it meanders around the globe. The largest mode between 0 and 1 km represents the marginal zone between the cratered province and the lowest elevations of the northern plains. Geologically the region is characterized by discontinuous blocks that are remnants of the cratered terrain. These blocks become progressively smaller and more scattered toward the north. The second mode between -2 and -3 km represents a trough-like collar of lowland at 60° north latitude. Taken as a unit, the northern plains are a low lying region that has been resurfaced partly by tectonism, erosion, volcanism, and eolian deposits.

Since these broad regions on Mars are essentially in isostatic equilibrium and since the model that appears to best satisfy the gravity and topography data is one that features a low density crust no more than 100 km thick overlying a denser mantle, it may be presumed that, as on the Earth, regional variations in elevation correspond to regional variations in crustal thickness. Estimates of crustal thickness must clearly depend upon values chosen for density and mean crustal thickness. In a previous analysis,

Hartmann (1973) estimated the crustal thickness of 'continental' crust on Mars to be approximately 20 km. This value is much too low because of the fact that thicknesses represent a deviation from some unknown mean value. Without some additional constraint such as the gravity modeling (Phillips and Saunders, 1975) there remain two unknowns, mantle topography and mean crustal thickness, but only one known (except for the densities), the topography.

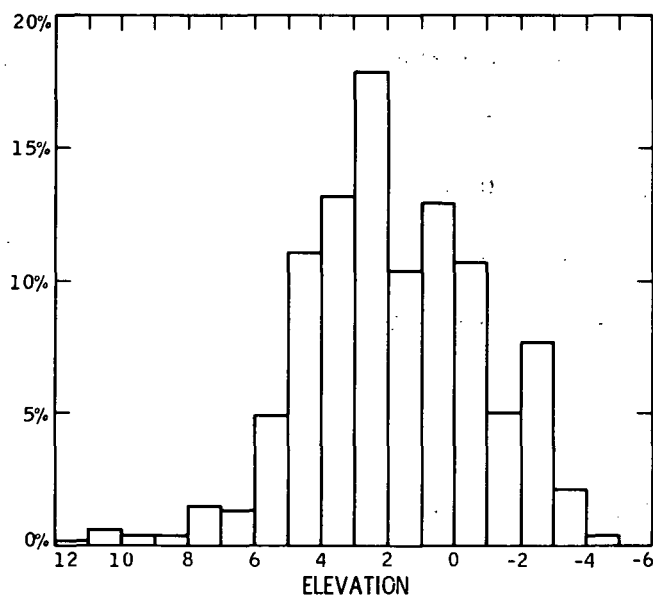
For the present analysis of variations in crustal thickness of the compensated regions a crustal density of 3.0 g/cm^3 and a mantle density of 3.4 g/cm^3 was chosen. The mean crustal thickness of 50 km for cratered terrain at elevations of 3 km was chosen to be consistent with the gravity models and yet not result in regions of "negative" crustal thickness with the above density values. Deviations from the mean crustal thickness are

$$\frac{\rho_m}{\Delta\rho} h,$$

where ρ_m is the mantle density, $\Delta\rho$ the density contrast, and h the topography. Using the above values, the mean crustal thickness beneath the Tharsis plateau is nearly 90 km, including the excess topography. The crustal thickness beneath the floor of the Hellas basin, the lowest elevation on the planet, thins to zero with the above parameters. The crustal thickness of the northern plains province varies from 30 km near the margin with the cratered province to 7 km or less in the lowest parts. The crustal thickness beneath the bulk of the cratered province varies between 30 and 70 km. The above values indicate the variations to be expected. The general trends are probably correct although the absolute values are probably not.

The observations described above provide additional data on the problem of genesis of the major terrain types of Mars. However, several fundamental questions remain. When did the northern topography form? How is the surface geology of the northern plains related to the crustal thickness? How much of the crustal thickness variation resulted from primary differentiation and how much may be attributed to other processes? What other process results in variations in crustal thickness.

MARS ELEVATION DISTRIBUTION



TEMPERATURES IN THE INTERIORS OF THE TERRESTRIAL PLANETS

Gerald Schubert

University of California, Los Angeles

Since the geological features on a planet's surface are largely manifestations of the thermal and mechanical states of its interior, an understanding of the surface geology requires knowledge of these states for at least the outer few hundred kilometers of a planet. Of course, if we hope to understand, for example, why planets such as Earth, Mercury and Mars apparently have global intrinsic magnetic fields while the Moon does not, we must know the thermal and mechanical structures of their deep interiors. Observational limitations on the sensing of temperatures and mechanical conditions inside a planet, underline the importance of modelling as a tool in studies of planetary interiors. Because geologic material creeps under conditions of high temperature and pressure it is important to include the possible substantial contribution of cooling by subsolidus convection when modelling the thermal regime inside a planet. We have modelled the temperatures inside Earth, Mars, Mercury and the Moon accounting for solid state convection as an important heat transfer mechanism. The major results of these studies are as follows:

Earth The mean core-mantle interface temperature is smaller than the melting temperature of pure iron when the viscosity of the mantle is less than 10^{24} cm²/sec (Schubert and Young, 1976). Thus subject to the assumptions of the model, in particular that the Earth's heat is largely produced by radiogenic sources uniformly distributed throughout the mantle, that the mantle can be characterized by a uniform Newtonian viscosity, and that the adiabatic temperature gradient does not strongly influence the nature of convection, 10^{24} cm²/sec is a lower bound to the kinematic viscosity of the deep mantle. These results must be reconciled with Cathles' (1975) conclusion from the study of glacial rebound that the Earth's mantle behaves as a Newtonian fluid with a uniform viscosity of 10^{22} poise.

Mercury If Mercury's magnetic field requires it to presently have at least a liquid outer core, then the necessity of maintaining the core molten for geologic time against the cooling tendencies of conductive, radiative and convective heat transport is a major constraint on models of the planet. Most importantly, differentiation of Mercury could not have resulted in the complete removal of heat sources from the mantle

into a crust near the planet's surface. A heat-source density at least comparable to the Earth's mantle-wide average must have been retained throughout Mercury's mantle (Cassen et al., 1976).

Mars If internal heating in the mantle of Mars is similar to that in the Earth, solid-state convection is the mechanism preventing large-scale melting of the Martian mantle. The lithosphere of Mars is probably several hundred kilometers thick, intermediate in size between that of the Earth and Moon. As in the case of Earth, convection is so efficient in transporting heat to the surface, that if the viscosity of the mantle were less than 10^{22} - 10^{23} cm²/sec, the core-mantle interface temperature would fall below the iron melting temperature (Young and Schubert, 1974).

Moon Lunar thermal models provide estimates of 1500-1600 K for the temperature, and 10^{21} - 10^{22} cm²/sec for the viscosity of the deep interior. These calculations differed from those for the other planets in that a constant Newtonian viscosity was not assumed a-priori. Rather, temperature-dependence of viscosity was accounted for in a semi-quantitative way so that temperature and viscosity were simultaneously and self-consistently determined (Schubert et al., 1976).

MIXED ELECTRICAL AND ACCRETIONAL HEATING AND THE "ZERO AGE" LUNAR THERMAL PROFILE

C. P. Sonett, F. Herbert, and M. J. Wiskerchen
University of Arizona

A persistent and major problem in early solar system physics was established with the recognition that most meteorites had been thermally processed at a very early time. The most spectacular examples are perhaps the irons and stony irons for which the subsequent cooling cycle appears to indicate a depth of burial of 100-200 km. The discovery of meteorite magnetization is likely connected with the thermal problem, but this is not certain. More recently, the petrological and mineralogical features of the Moon unveiled by Apollo strongly suggest an early melting episode resulting in the separation out of the anorthositic highlands. The mare chronology shows that internal heat sources were active in the Moon as early as 3.9 b.y. ago. Magnetization of lunar rocks is presently not understood but a persistent current view is that a fossil regenerative dynamo was active at least in the mare time period. These results show that some exotic source heat must have been present in the Moon soon after its time of formation; long lived radioactives are ruled out except as a means of reshaping the later thermal history. The even more recent discovery of a global magnetic field at Mercury together with the topographical evidence for contraction on a planetary scale as well as evidence of

early mare flows also suggests a very early sequence of thermal episodes for that planet.

The view that fossil nuclides could have existed in sufficient abundance in the primeval solar nebula, subsequently being incorporated into planetary matter thus providing an important source of heat, has been revived by Lee et al. They find a concentration of ^{26}Mg (^{26}Al daughter) of 10^{-4} gms/gm in a Ca-Al rich Allende inclusion; but this does not solve the problem if more than about three half lives ($\tau_{\frac{1}{2}} \approx 7 \times 10^5$ yrs) passed between the time of inclusion of the ^{26}Al into material similar to the Al-Ca inclusions of Allende and the time of incorporation into a planet such as the Moon.

Among other forms of early heating, a source seated in accretion has long been popular, but there is little basis for the required time scale of 10^3 - 10^4 yrs from considerations of celestial mechanics.

A recent alternate approach taken by Wetherill suggests heating following a 10^8 yr accumulation interval, but this hypothesis has not been thoroughly explored.

The work reported here is an extension of our earlier work and follows a different line of reasoning in attempting to describe a source of early thermal energy based upon electromagnetic induction from a T Tauri solar wind. We previously investigated this mechanism of heating by considering separately the interplanetary electric and magnetic fields. Those studies ignored melting during the heating cycle. Although the chronology is essentially still unknown, the additional possibility is present that planets accumulate while heating, though this would require formation from particles of sufficient mass so as not

to be blown away by the enhanced solar wind. We have now incorporated both pseudoconvection and accretion in the modified computer code. The former is similar to the procedure used by Fricker and Reynolds, but we pseudoconvect on the solidus rather than the liquidus as in their case. Major differences between our previous work and our new calculation are apparent. The most striking interaction is between accretion and transverse magnetic (TM) inductive heating.

The centroid of electrical heat accumulation moves radially outward as the accretion rate increases over a series of evolutionary models. Accretion rate differences also strongly influence transverse electric (TE) inductive heating, but significant heating by this mode tends to be delayed until after the accretional phase, corresponding to the development of a thermal spike near the surface as in earlier work. However, the thermal spike is suppressed upon reaching the solidus because of convection. The two electrical modes also display an interaction through the temperature dependent bulk electrical conductivity of the rock. As the planet grows, strong TE heating near the surface tends to quench heating of the core by the TM mode; core heating had been observed in earlier work where only the TM mode was present. Heat distribution by pseudoconvection tends to increase TM heating in general by reducing the variation of electrical conductivity with radius.

These results show that a startlingly varied zero age planetary thermal profile develops depending upon the accretion-electrical heating chronology as well as the particular solar parameters used for the primordial solar wind. In a particular model, the case of accretion proportional

to combined gravitational and geometric cross-section. during electrical heating yields an evolutionary picture of the Moon where the core melts in 2×10^5 yrs. Eventually as the Moon grows larger than 770 km the pressure dependence of the solidus ($1.2 \times 10^{-7} \text{ } ^\circ\text{C m}^2/\text{N}$) causes resolidification. Heating continues as the Moon accumulates, with a peak in the final temperature profile after accumulation is complete (1.4×10^6 yrs) at about 1000 km radius. After 3×10^6 yr the Moon is everywhere above $1000 \text{ } ^\circ\text{C}$ and above $1200 \text{ } ^\circ\text{C}$ interior to 1000 km. It would be expected that long lived radioactives would be swept towards the 770 km level by the melting process. The subsequent "coasting phase" where only long lived radioactives are thermally active has not been investigated but would be expected to yield a range of melting conditions within the first 0.5 by after formation of the Moon.

The particular scenario presented above corresponds to a T Tauri Sun losing $0.5 M_\odot$ in about 11 m.y., a solar wind speed of 200 km/sec, a solar spin period of 12 hours, and a turbulent interplanetary magnetic field with a dominant fundamental period of ~ 440 second. The circumstellar nebula obscuration temperature was 700°C . The bulk electrical conductivity used was the latest version of Duba and Nichols for a Bamle enstatite at 1 atm pressure. The pressure dependent solidus is extrapolated from Ringwood and Essene. The mean velocity at infinity of the infalling material was assumed to be 1 km/sec.

Results similar to those discussed could lead to sufficient early thermal activity in the Moon to yield the highland anorthosites, the later mare flows, and either an Fe or Fe/FeS core, though the detailed

parameterization remains to be completed. Application to the zero age profile (ZAP) for Mercury and other subjects remain to be carried out.

Acknowledgements

This work was supported by the Planetology Program Office of NASA under Grant NGR 02-002-370. We also wish to thank Dr. Leo Goldberg and the staff of the Kitt Peak National Observatory, and the National Center for Atmospheric Research for their generous aid in supplying computational time.

A SIBERIAN ANALOG OF MARTIAN PERMAFROST TERRAIN

Duwayne M. Anderson and Lawrence W. Gatto
U.S. Army Cold Regions Research and Engineering Laboratory

In earlier papers we have proposed several terrestrial analogs for permafrost terrain on Mars (Anderson, et al, 1972, 1973; Gatto and Anderson, 1975). Beacon Valley, Antarctica, is analogous in many respects to the Martian polar regions. The thermokarst topography formed on the permafrost terrain of the North Slope of the Brooks Range in Alaska is analogous in some respects to Martian Fretted Terrain. Thermokarst terrain results from the subsidence that follows the removal of ground ice by melting or sublimation. The depths of thermokarst depressions depend upon the relative amounts of ground ice, the extent of melting or sublimation and the degree to which subsequent terrain modification has progressed. On the North Slope of the Brooks Range, the depths of the thermokarst depressions are typically 5 to 8 meters, considerably less than the local relief of the Martian Fretted Terrain.

Much larger thermokarst depressions (up to 40m in depth and 5 to 10 km across) are found in the loess deposits of the arid Yakutian Lowland in eastern Siberia (Figure 1). The depressions there have formed by the melting of high ice-content permafrost in a very thick loess blanket. Locally the ice constitutes more than 80-90% by volume (Solovyev 1973; Czedek and Demek 1970). This permafrost complex has formed from successive deposits of loess and ice from the Neogene to the present. The source area for the still accumulating loess is the glaciated Verkoyansk Range to the north and east and the Aldan Mountains to the south. Removal of the melt water has been accomplished primarily by evaporation. This has resulted in a poorly developed, beaded drainage system. Where individual thermokarst depressions coalesce they form valleys that, except for scale, resemble some Martian channels (Nummedal 1975).

COMPARATIVE PLANETOLOGY AND MODIFICATION OF MARTIAN UPLANDS

R. E. Arvidson
Washington University

The oldest terrain on Mars is undoubtedly the uplands*. There is, on the average, about 3 times more craters >8 km in diameter on cratered terrain relative to the oldest plains. This probably does not mean that cratered terrain is three times as old. Rather, Martian uplands preserve a record of heavy bombardment, which on the moon seems to have ceased $\sim 4 \times 10^9$ years ago. Martian cratered terrain, like the lunar uplands far from basins and associated secondary craters, and like Mercurian uplands, is deficient in crater sizes $\lesssim 30$ km in diameter. Either some surface process common to all three bodies (i.e. volcanism) has obliterated smaller craters, or the deficiency is a reflection of an impacting body population that was deficient in small sizes.

On Mercury, intercrater areas are covered with numerous irregular craters $\lesssim 10$ km in diameter. This suggests to some that intercrater units are older than the craters ($\gtrsim 30$ km) surrounding them, since the small irregular craters are probably secondaries from the larger craters. However, agreement is not universal. Resolving the age of large Mercurian craters relative to intercrater areas is clearly of considerable importance for understanding Mercurian thermal evolution (volcanism through time) and for understanding the origin and dynamics of bodies impacting the inner planets during heavy bombardment.

Martian cratered terrain is generally smoother and more subdued than uplands on either the moon or Mercury, although the extent of crater obliteration is an open question. Numerous channels are cut into the Martian uplands; some of the smaller channels are associated in some way with large (>15 km) craters. The edge of much of the Martian uplands consists of a complex of erosional escarpments, fretted terrain. In addition, an extensive area of severely fretted uplands extends northward from the present cratered terrain edge for about 50° of arc near 180° w. long. Most of these features are probably related to a phenomena unique to Mars, as compared to Mercury or the moon: the presence of volatiles, both as ground ice and as an atmosphere. The questions then become: (a) When did most of the activity occur?; and (b) By what set of processes and to what extent has the presence of volatiles shaped Martian uplands?

The question of when most modification of cratered terrain occurred can partly be answered by noting that crater densities for craters classified as "fresh-looking" are similar on older plains and on uplands. In other words, craters ($\gtrsim 8$ km) began to be retained without significant modification, certainly by the time that oldest plains had formed. More evidence for timing comes from analysis of fretted terrain. Crater counts for craters superimposed on fretted terrain indicate that most fretted regions are as old, and in some cases, older than the most heavily cratered plains. Major fretting therefore probably occurred concurrent with, and immediately after, heavy

* uplands = cratered terrain

bombardment, putting the fretting process dominantly within the first 500 X 10^6 years of Martian history. Minor amounts of fretting have probably continued to the present: for instance, the edge of heavily cratered plains (Lunae Planum) is fretted.

The question of what set of processes shaped the Martian uplands is more difficult to answer. Perhaps the best that can be done at this point is to develop a "working hypothesis" of the early history of Martian cratered terrain:

- Formation of a primitive crust, with incorporation of volatiles (H_2O , CO_2) as ground ice. Atmospheric pressure is buffered by coldest point on the planet.
- Uplands volcanism dominates the southern hemisphere. Surface temperatures need not be high enough to make H_2O liquid stable on the surface. However, a more erosive atmosphere is needed, which presumably means a higher density atmosphere. This requirement implies somewhat warmer conditions than the present. Large-scale pyroclastic and phreatic activity cannot be ruled out, in contrast to the more refractory lunar case. Most of the channels form during this period by break-out of ground water; others form by ice melting during large impact events. Break-up of the northern hemisphere, tectonically induced leads to ground water break-out. Exposure of the ice-regolith mixture on slopes leads to scarp retreat, which seems to be an integral part of the fretting process. Enough aeolian activity occurs on uplands to smooth the topography.
- Volcanism decreases in intensity, the surface cools, and atmospheric pressure decreases. This seems to have happened at the end of heavy bombardment. Impact processes alone may be an alternative to volcanism as an agent for liberating volatiles. With a drastic decrease in impact rates, liberation rates would drastically decrease.
- Since then, little has happened to uplands, with the exception of redistribution of older aeolian debris by winds. Also, some sporadic volcanic activity and channel formation cannot be ruled out.

POSSIBLE EARTH ANALOGS FOR SOME MARTIAN CHANNEL FEATURES

Jon C. Boothroyd and Elizabeth J. Simpson
University of Rhode Island

and

Dag Nummedal
University of South Carolina

Field study of channel features in southern Iceland, northeast Gulf of Alaska, Death Valley and the channeled scablands of eastern Washington suggest possible Earth analogs for selected Martian channel features, specifically those in Mangala Vallis, Kasei Vallis, and in the Chryse channels. A classification scheme has been developed for the terrestrial features that embodies concepts from Sharp and Malin (1975) and Baker and Milton (1974).

We believe that most "bar-like" features visible on Mariner 9 imagery are erosional, not depositional, forms. These forms may be: 1) developed in resistant bedrock (example: basalt mesas in Grand Coulee, Washington); 2) formed by consequent erosion of a prior depositional surface (Death Valley alluvial-fan surfaces); or 3) erosional enhancement of depositional features (streamlined hills, Cheney-Palouse tract, Washington). This conclusion differs somewhat from that of Baker and Milton (1974). Most purely depositional features (various bar types) appear not to have enough bed relief to be within the resolution capability of the Mariner 9 imaging system.

The apparently smooth beds of channels such as those in the Chryse region also pose a resolution problem. Catastrophic flooding as suggested by Baker and Milton (1974) may leave an erosional scabland surface (Cheney-Palouse butte and basin topography), whereas flooding on a smaller scale gives rise to a depositional surface (Icelandic outwash plain) as suggested by Nummedal (1975). Regional gradient (2-6m/km) is similar in both examples but bed relief of the erosional topography is much greater (up to 30m). This variation in small-scale bed relief is important in the consideration of Viking landing sites.

CRATERS AND PLAINS ON MERCURY, THE MOON, AND MARS

V. R. Oberbeck
NASA Ames Research Center

Mercurian intercrater terrain is apparently older than heavily cratered terrain (Trask and Guest, 1975). Since intercrater terrain contains mostly small subdued secondary craters and heavily cratered terrain contains primary craters larger than about 30 to 40 km, Oberbeck, Quaide, Arvidson, and Aggarwal (1975) proposed that there was a deficiency in bodies necessary to produce craters smaller than 30 km during the late bombardment of Mercury. Trask (1975) has noted that secondaries less than 15 km in diameter from all craters larger than 100 km are still visible today and that they overlap intercrater terrain; therefore he concludes that if the observed fall-off of craters smaller than 40 km on Mercury is due to obliteration, then the oblitative event preceded formation of all craters larger than 100 km. This would require that there must have been a late episode of basin formation which followed production of craters smaller than 100 km. Trask (1975) favors the simpler alternative that there was a deficiency in production of bodies necessary to produce Mercurian craters smaller than 40 km. We agree with this conclusion.

Oberbeck, Quaide, Arvidson, and Aggarwal (1975) presented evidence to support the view that there was a deficiency in production

of small bodies during the late bombardment of the Moon, Mercury, and Mars. The deficiency is revealed on the Moon only in areas unaffected by basins. The deficiency is obscured in most places by widespread production of basin secondaries up to 30 km in diameter; for example, the rare lunar surface area pointed out by Trask and Guest (1975) to be Mercurian in appearance is, according to our findings, in an area deficient in basin ejecta. It is also deficient in irregular, clustered, and chained craters up to 40 km in diameter according to the map of Wilhelms and McCauley (1971). Based on our laboratory simulations and the structure of lunar craters of this type, we believe these may be basin secondary craters. The deficiency in production of Mercurian primary craters less than 40 km in diameter has been revealed in most places on Mercury because there were fewer larger Mercurian basins formed which were capable of producing large secondaries and because higher Mercurian gravity restricted production of large secondary cratering only to areas near the basins.

Extensive high-energy-saturated secondary cratering in a belt near and concentric to Caloris Basin caused the rest of Mercury to experience a lower production of large secondaries. It also contributed to production of extensive continuous belts of smooth plains near Caloris. Our measurements of smooth plains inside craters pre-existing Caloris and within the smooth plains belt around Caloris show that the most degraded craters contain the greatest amounts of plains, thus supporting the view that plains are at least in part erosional products of secondary cratering.

If there was a deficiency in production of lunar and Mercurian primary craters less than about 40 km, a similar observed deficiency in Martian craters also is most likely the result of a lack of crater production instead of being due to pronounced obliteration by wind and water. This implies much less extensive obliteration by wind and water of Martian craters than has been postulated previously. On the other hand, if Mercurian intercrater terrain is younger than heavily cratered terrain (contrary to accepted theory), the deficiency of small Mercurian craters was caused by an unusual style of obliteration by volcanic flows only between the large craters. In this event, Martian intercrater volcanic flows also are a possibility. This leads to the possibility that there may have been less obliteration of large Martian craters by wind and water. The implications of the relative age of intercrater and heavily cratered terrain are also discussed by Arvidson at this meeting.

A probable deficiency in production of small primary craters during the late bombardment of Mars, Mercury, and the Moon can be related to the processes responsible for production of bodies impacting the inner planets during late bombardment. Our results (Aggarwal and Oberbeck, 1975) show that there has been a non-random distribution of impact craters on the surface of Mars. For craters larger than 30 km in the equatorial belt $\pm 30^\circ$ latitude, there are, according to our measurements and probability calculations, more recognizable pairs of craters than can be accounted for by random single body impact.

In addition, those pairs having septa between craters typically have members of the same age and size, whereas those without septa have members of different age and member craters show more of a difference in size. Members of pairs have fewer craters with central peaks than do isolated craters. All of these results are compatible with the hypothesis that some Martian crater clusters could be the products of tidal disruption of very weak bodies before impact. The deficiency of small bodies is also compatible with the process of tidal disruption for production of fragments impacting the terrestrial planets during the late bombardment as given by Wetherill (1975) because failure under low stress produces fewer small bodies than failure under high stress.

COMPARISON OF LUNAR AND PLANETARY IMAGERY

Peter H. Schultz
University of Santa Clara

Comparative planetary geology currently relies on imaging data from four major planetary and lunar missions: Mariner 9 (Mars), Mariner 10 (Mercury), Lunar Orbiter (Moon) and Apollo (Moon). These missions revealed planetary surfaces under a variety of resolutions and lighting conditions and through two different imaging systems, vidicon and photography. With the current trend to intercompare features on different planets, it is appropriate to examine the effects of the different imaging conditions.

Keene (1965) systematically considered the effects of solar illumination (angle between the sun and zenith directions), phase angle (angle between sun and optical axis at the surface), obliquity (angle between imaging axis and surface normal), and resolution on the ability to discern and identify different geometric objects from photographic images. His results demonstrated the combined importance of resolution capability and phase angle. On photographic emulsions a feature *detected* at phase angle (PA) 85° must be approximately twice the diameter at phase angle 40° ; however, for *identification* of the geometric shape, this factor increases to six. The ratio between the identification limit and detection limit dimensions at PA = 85° is approximately 2 and at PA = 40° , approximately 8. Such results illustrate the well-known loss of resolving ability with increasing solar illumination.

The importance of these effects can be demonstrated by application of Keene's results to Mariner 6 imagery of Mars. The discernability in the oblique image M6N09, for example, varies by a factor of five within its borders and requires features at least three times larger than those in M6N21 (Schultz and Ingerson, 1973). Comparing Mariner 9 imagery to Mariner 6 imagery (A frames) of the same regions, we find that the increased resolution provided by the smaller slant ranges for Mariner 9 is offset by the typically small phase angles (nominally 45°). Specifically, the theoretical resolution for M9-FDS-6714718 is a factor of 1.9 better than M6N21, but the phase angle for the former is 48° and 70° for the latter. Keene's results suggest that such lighting conditions would require twice as large features for detection and three times as large for identification for Mariner 9. Consequently, the effective resolutions for these two frames are predicted to be similar (approximately 2 km/pixel).

Although visual comparisons confirm this result, Mariner 9 imagery retains a small advantage -- attributed, in part, to the computer enhancement techniques that decrease the gap between detection threshold and identification threshold. Contrast stretching of Mariner imagery transforms photometrically darker regions into pseudo-shadows that increase the ability for feature identification (see Cutts, 1974 for an excellent review). The similarity in effective resolution of Mariner 6 and 9 imagery, however, illustrates the possible importance of solar illumination despite image enhancement. This result is important for the comparison of Mariner 9 mapping sequences at different latitudes and for comparison of martian craters with mercurian and lunar craters.

Mariner 10 imagery of the Moon permits direct comparison between vidicon and photographic imaging systems (also see Sauders et al., 1975 for a general comparison). Preliminary results indicate that under nearly identical viewing conditions ($PA = 85^\circ$ to 65°), the vidicon system with image enhancement approaches the limiting resolution of 2.2 TV lines (Danielson et al., 1975) for crisp features in plains regions. However, irregular depressions near the resolution limit are transformed into circular craterforms, and subdued (nonshadowed) craters are either enhanced into crisp-appearing craters or lost in the noise, alternatives depending on the crater wall slope and solar illumination. Moreover, the following effects are observed:

1. Measured crater diameters from Mariner 10 imagery commonly exhibit a 25% increase over true diameters for crisp craters smaller than 5 pixels.
2. Diameters of bright-rayed and haloed craters are overestimated.
3. At pixel widths of 1 km, hummocky ejecta facies around craters smaller than 30 km cannot be discerned reliably; only a small percentage of secondary craters around large (100 km) craters can be recognized; and ejecta facies in hummocky terrains and highlands typically are lost.
4. Resolving craters depends not only on lighting conditions and scale, but also the terrain type in which they occur.
5. Linear features with widths 4 times smaller than the predicted resolution can be detected.
6. Relatively poor resolution (pixel widths 1.2 km), moderate phase angles, and image enhancement transform small slumpless but flat-floored craters into bowl-shaped craters and large slumped craters into slumpless flat-floored craters.

In analyzing vidicon imagery, most researchers generally deal with feature measurements greater than at least 5 pixels (twice the theoretical resolution). However, the effect of resolution and lighting conditions on comparative morphologic studies is more subtle. For

example, these preliminary results suggest that most Mariner 9 (A frame) imagery involving moderate illumination angles (45°) would not reveal secondary crater fields around 100 km craters. Further studies will be made to define more precisely the detection, identification, and classification limits characteristic of the different planetary missions.

ROLE OF PLANETESIMALS IN COMPARATIVE PLANETOLOGY

William K. Hartmann
Planetary Science Institute

Sub-planetary-scale particles in the early solar system played several roles in determining the general configurations of planets and their surfaces, and are thus an important area of study in comparative planetology. As is now well-known, all planetary and satellite surfaces in the inner solar system show craters caused by planetesimal collisions, and limits set on the relative or absolute crater production rates would set limits on relative or absolute chronologies. A paper now in preparation, partially supported by the Planetology office, shows that Wetherill/Gault-type calculations of final impact points for particles in various chosen starting orbits (asteroidal, cometary, etc.) offer real promise in limiting crater production rates on planets. This would in turn reduce current controversy on ages of planetary features.

A second area of work (Icarus, in press) involves compositional effects of episodes of cratering by planetesimals formed in the region of some planet (A) and deflected by planet A from its region to impact on a second planet (B). An example is found in the earth-moon system. Wetherill's data show that while the earth accretes most of the low-velocity planetesimals originating nearby, because of its large gravitational cross-section, the moon receives a larger proportion of the higher-velocity planetesimals deflected across earth's orbit from other planets. For example, 60% of the moon's late-accreted material could come from the region of Venus, according to a model

based on Wetherill's calculations. The deflection of material by other planets could be maximized at the end of accretion, when masses of other planets were near maximum values, so that large inputs of anomalous composition might arrive at the end of planet formation. Plausibly small reservoirs of residual material near other planets could be deflected onto earth-crossing orbits and substantially modify the density and composition of the moon without much modifying the earth.

A third area of work, reported in another paper in preparation, partially supported by the Planetology office, describes three techniques of inventorying sizes of planetesimals at three stages of solar system history: theoretical calculations of growth rates of different-sized particles; measurement of effects on planet obliquities and eccentricities; and direct counts of craters and basins on the cumulative total of cratered planetary surfaces. Results show that bodies of $D > 100$ km must have been common in late stages of cratering; bodies 10 times as large probably existed earlier, carrying significant momentum and energy. Statistics of small numbers controlled the mode of disposal of the 2nd-largest, 3rd-largest, ... body in each planetary region by prograde impact, retrograde impact, capture, nearby fragmentation, collision with a large satellite, ...etc. Such "catastrophist processes" may explain puzzling major differences among planets' present configurations (Venus' peculiar rotation; earth's large satellite; Mars' small satellites; Saturn rings) in a manner consistent with the otherwise "uniformitarian" evolution of the planetary system.

SCIENTIFIC RATIONALE AND FEASIBILITY OF DEVELOPING A PLANETARY SEMEDA

A. L. Albee, J. R. Anderson, and A. A. Chodos
California Institute of Technology

INTRODUCTION: The scanning electron microscope with an energy dispersive X-ray analyzer (SEM-EDA) is a powerful tool for studying the morphologic and chemical characteristics of complex particulate material such as that which constitutes a planetary regolith. Its power lies in its ability to provide images with a great magnification range, with a great depth of field, and with a variety of contrast mechanisms including characteristic X-rays. Preliminary studies indicate that development of a SEM-EDA as a flight instrument for unmanned space missions is feasible with current technology and that it can provide information otherwise obtainable only by a sample return mission.

SCIENTIFIC RATIONALE: The mineral composition and the nature of particles in a planetary regolith can provide substantial evidence on the origin of a planet, how it evolved to its present state, and its on-surface and near-surface processes. Bulk chemical composition can provide significant constraints, but the identification of particular mineral phases and assemblages of phases provide much more stringent constraints on the nature of the source rock, the P and T of origin, activity of volatile species, likely minor elements, mineral density, state of oxidation and hydration, etc. The identification of a single grain of a low abundance phase may have great genetic significance. Grain size distribution, shape, and surface features provide information on surface processes including impact phenomena and mechanical and chemical interaction with an atmosphere. The lunar regolith due to its impact origin, provides a good sampling of lithologic units in the vicinity of a landing site and its study permits important deductions regarding local and regional lunar geology.

Using the extensive studies on the lunar regolith as a guide we can outline the major types of information that we would wish to obtain from a particulate sample of a planetary regolith or a comet:

1. Distribution of size and shape of particles in the sample as a whole and among the various particulate species.
2. Identification and abundance of both major and minor particulate species.
3. Average and/or range of chemical composition of the various particle species.
4. Bulk chemical composition of the entire sample.
5. Identification and chemical composition of individual particulate grains of great genetic significance.
6. Study of special features such as coatings, glass splashes, microcraters, fracture surfaces, growth surfaces, microorganisms, etc.

SEM-EDA CAPABILITY: The SEM-EDA has demonstrated that it is capable of doing all these tasks and no other single instrument possesses this versatility. It is able to provide images with magnifications from 40X to 40,000X or more, with a great depth of field or stereoscopically, and with a variety of simultaneous contrast mechanisms including secondary electrons and characteristic X-rays. In addition, semi-quantitative or quantitative chemical analyses can be made of individual particles or portions of particles.

Most lunar studies using the SEM-EDA have been concerned with higher resolution investigations of special features such as microcraters, splashes and coatings on glass balls, unusual and rare minerals, etc. Bulk properties have generally been obtained by other methods such as sieving, optical microscopy or standard chemical methods. Some groups are beginning to measure bulk properties in the very fine fraction of lunar soil samples by measurement of size, shape, chemical composition, etc., on a statistical selection of grains but such measurements have been much better exploited in other fields such as in studies of industrial particulate pollution (Bayard, 1973; Troutman et al., 1974).

The scanning of the electron beam produces an x-y "image" with z values for each picture point corresponding to the intensity of characteristic X-rays, secondary electrons, etc. Many image analysis techniques have been developed which are applicable to planetary studies (Gibbard, 1974; Jones, 1974; Troutman et al., 1974). Such techniques use the x-y parameters to describe and discriminate each particle in terms of area, parameter, projections, etc., and use the various z values for species classification, mass determination, etc. Gancarz and Albee (1973), using an automated-point counting technique, measured the relative volume and average composition of each mineral phase and calculated the bulk chemical composition of lunar rocks.

Most quantitative chemical data on lunar particles has been obtained with the electron microprobe using correction methods, such as the Bence-Albee, which are applicable to polished surfaces of large grains. New modified techniques will allow quantitative analysis of small, non-polished grains. We have expanded the basic equation to permit ready calculation of Bence-Albee correction factors for a wide range of take-off angles. The upper surface of grains considerably larger than the X-ray excitation volume can be analyzed by determining the effective take-off angle from stereoscopic SEM image pairs. Geometric correction techniques (Armstrong and Buseck, 1975) can be used for particles with sizes close to the excitation volume, and ratio correction techniques (Eugster et al., 1972) can be used for smaller particles.

SAMPLE HANDLING: The amount of sample handling utilized in the lunar SEM studies would place a strong limitation on a flight SEM. Since the lunar studies have mainly involved higher resolution study of special features they have been characterized by very extensive sample handling involving disaggregation, removal of adhering fine particles, selection of individual particles, coating with a conducting film, careful manipulation of the particle's position in the SEM, etc. Work in other fields indicates that much useful data can be obtained without such extensive sample handling. We are systematically testing the trade-offs between data quality and complexity of sample handling. It had been hoped that a proper choice of operating conditions and the use of highly conducting substrates would eliminate the need for a conductive film on small mineral particles. However, all types of analysis except X-ray elemental mapping are seriously impaired by operating on uncoated particles. Hence, we conclude that the sample-handling design for a flight SEM must include provisions for coating the samples with a

conducting film such as carbon or gold.

Clearly valuable information could be obtained by detailed examination of one, well-dispersed particulate sample. However, different information is contained in different size ranges and such a sample might contain only a single coarse lithic fragment. It therefore seems highly desirable to use a combination sieve and splitter designed to deliver more nearly the same number of particles in each size range to the SEM-EDA as separate samples--possibly on a sectored-wheel sample holder. Ultrasonic vibration of the splitter-sieve might serve to clean off adhering fine particles. These alternative approaches are being tested on lunar samples.

DESIGN CONSIDERATIONS: In recent years the development of both the SEM and the EDA has expanded with remarkable rapidity. Most of the emphasis in SEM development has been directed to the attainment of higher resolution. However, several moderate-resolution SEM's intended for table-top use by non-experts have been developed and are being widely used. They are designed to be small, simple, and trouble-free, yet they have resolutions equal to that obtainable only by the best instruments just a few years ago. It is these instruments which form a logical prototype for a flight instrument.

Most components of such a SEM-EDA are parts of instruments on or proposed for other flight missions and development is actively proceeding on them. These include high voltage power supply, vacuum requirements, solid-state detectors, coolers for detectors, transmission for scanning information, etc. It appears technically feasible to develop a flight SEM-EDA by straightforward modification of existing instruments. There are a number of possible options, for example in filaments, lenses and detectors, that could offer distinct advantages in a flight instrument. Optimum conditions for SEM imaging and EDA analysis differ, but a reasonable compromise can be reached for the simplest instrument.

SUMMARY: Clearly a flight SEM-EDA could perform many important data gathering functions in studying a planetary regolith. The high magnification imaging and chemical microanalysis could not be performed by any other flight instrument. Such data could otherwise only be obtained from sample return missions. The present technology of SEM-EDA systems and associated data processing techniques such as chemical analysis correction procedures and image analysis are adequate to develop a working instrument. Bearing in mind the type of information desired about a planetary regolith, further studies should involve a detailed analysis of design criteria leading to the possible development of a prototype flight SEM-EDA.

THE CONTROL NET OF MERCURY

Merton E. Davies
The Rand Corporation

Shortly after the first high-resolution pictures of Mercury were returned to earth by Mariner 10, work was started on the photogrammetric determination of the control net. Points and pictures have been added continuously to the computations -- at this time the net contains 1774 points and incorporates measurements on 680 pictures. The Mercury 2 pictures are the most useful for this purpose because they give maximum continuous coverage. The Mercury 1 high-resolution pictures are interesting but their coverage is so limited that they do not contribute much to the strength of the control net. The Mercury 1 low-resolution pictures do have extensive coverage and about the same resolution as Mercury 2 pictures, so the two together offer very useful stereoscopic views of the topography. The Mercury 3 pictures do not contribute to the strength of the control net because the format is much smaller than the Mercury 1 and 2 pictures and they offer no new coverage.

The coordinate system used for the control computations assumes that Mercury's spin axis is normal to its orbital plane (0° obliquity) and that the 20° meridian passes through the center of the small crater Hun Kal to define the longitudes (Murray, et al., 1974). In the most recent control computation, this system of longitudes differed from the IAU (1970) longitudes by $0^\circ 04' 19''$; in last year's computations they differed by more than one-half degree. The IAU (1970) longitudes define the prime meridian as

containing the subsolar point at the first perihelion passage of 1950. A large coordinate shift in the control net occurred on March 28, 1975, when the JPL SEDR trajectory data were first used.

The methods used in performing the analytical triangulation and coordinates of the control points as of February 23, 1975 were presented in Davies and Batson (1975). The control net has been updated four times since that computation was made. The latest computer run solved 5588 normal equations and gave coordinates to 1774 points and orientation matrices to 680 pictures (185 inbound M-1, 190 outbound M-1, 300 M-2, 5 M-3). There were 16,148 observation equations.

A change in camera focal lengths was introduced on January 10, 1975 when an analysis of star pictures and two lunar frames (FDS 2264, 2275) gave focal lengths different from the measured preflight values (Davies and Batson, 1975). Recently it was possible to obtain Apollo coordinates of lunar points measured on Mariner 10 pictures from L. Schirmerman of DMA. These were used to compute the focal lengths from three A frames (FDS 2253, 2275, 2285) and four B frames (FDS 2156, 2254, 2264, 2274). It was discovered that consistent results were obtained when pixel measures of points were converted to millimeter measures in the focal plane by interpolation between three or four reseau points. (The JPL GEOM program gave inconsistent results.) The camera focal lengths determined at different times by different methods are given in Table 1.

Table 1

CAMERA FOCAL LENGTH MEASUREMENTS

<u>Date Introduced</u>	<u>A Camera</u>	<u>B Camera</u>	<u>Method</u>
	1495.76 mm	1503.77 mm	Preflight calibration
1/10/75	1501.0 mm	1496.1 mm	Stars & single lunar frames
12/20/75	1499.0 mm	1499.5 mm	Average of multiple lunar frames

After each new update of the control net, camera station coordinates and orientation matrices for each picture are given to IPL/JPL and USGS/Flagstaff. These are proving to be very valuable in programs of computer mosaics of the Mercury frames. Coordinates of the control points are supplied to USGS/Flagstaff and C. A. Cross/Northwich, England, for use in their mapping programs.

New points and pictures will continue to be incorporated in the control net, and the search for measurement errors will go on simultaneously. This search is aided by observing the recomputed residuals and checking any measurements whose residuals are over three pixels. The work is time consuming and tedious because of the large data set.

There will be an effort to compute photogrammetrically the planetary radii at some of the control points. As the radii and the camera orientation angles are highly correlated in the solution of the normal equations, it is preferred to extend photogrammetrically into new areas from points and regions where radii have been measured by other means.

An occultation measurement of the radius (2438.3 km) at 68°4N latitude and 101°2W longitude was made from the M-1 flyby. At these coordinates the

maximum stereo angle available is $6^{\circ}4$ (FDS 149, 529086), which is not large enough to permit photogrammetric radii measurements.

Radar profiles have been measured on a few areas of Mercury and when combined with an accurate ephemeris can give planetary radii; the difficulty, of course, is that the ephemeris must be very accurate due to the slow rotation rate of Mercury. A radar profile from 35° to 50° longitude at -3° to $-3^{\circ}5$ latitude was taken in 1972; in this region the stereo angle of $32^{\circ}7$ (FDS 27233, 166589) should give useful photogrammetric measurements. Another profile from longitude 160° to 173° at latitude $+11^{\circ}$ to $+11^{\circ}5$ is in an area where a stereo angle of $24^{\circ}1$ (FDS 226, 167021) is marginal for interesting photogrammetric measurements at the available resolution.

ALPHA/X-RAY ANALYSIS USING SOLID-STATE DETECTORS

Ernest J. Franzgrote
Jet Propulsion Laboratory

The alpha-scattering technique was used on the Surveyor missions to obtain the first elemental analyses of the lunar surface. Reported accuracies of those results have been verified by subsequent analyses of Apollo returned lunar samples. Further development of the alpha-scattering method for a Mars lander, both at the University of Chicago and at JPL, has resulted in improvements in accuracy beyond those of the Surveyor experiments. At JPL it has been demonstrated that addition of a high-resolution x-ray mode to the technique significantly improves the analysis of the heavier elements; work on the x-ray mode has been continued at the University of Chicago. This abstract describes recent work at JPL in support of the University of Chicago on development of the x-ray mode of analysis.

The x-ray mode takes advantage of recent developments in solid-state detectors that are an order of magnitude better in resolution than gas proportional counters. The silicon and germanium detectors which have been investigated to date require cooling to realize this advantage. Earlier work in this task on the development of a compact feasibility model employing a heat-sterilizable germanium detector cooled by a Joule-Thomson cryostat has been described in earlier status reports. This work is presently being written up for submission to the journal Nuclear Instruments and Methods. For the purpose of operating this system in the laboratory, an auxiliary high-pressure gas supply system has been assembled and tested. This system consists of a reservoir of high-purity argon or nitrogen gas at 6000 psi, a suitable pressure

regulator to reduce the pressure to below 3500 psi, a gas-purification system to remove most of the residual condensable impurities, and high-pressure lines to connect these systems to each other and to the Joule-Thomson cryostat. A new high-resolution germanium detector was installed in the feasibility model and this system was then cooled and tested using high-pressure nitrogen gas. The system was shown to operate reliably at resolutions of 250 eV or better for Fe^{55} (5.9 keV.)

This x-ray detector system, Joule-Thomson cryostat, and auxiliary gas-supply system have been delivered to the University of Chicago.

The system has been operated successfully there to supplement earlier studies in which a liquid-nitrogen cooled detector was employed. The system is being used together with the alpha-scattering and proton modes of the "Mini-Alpha" instrument.

On-going work at JPL on the Joule-Thomson cooled detectors includes a study to improve the efficiency of gas-usage and developments to meet the requirements and constraints (mass, volume, shock) of a Mars penetrator mission. A design study by Applied Detector Corporation has shown that the mass and the radiative, conductive and electrical heat loads of the Joule-Thomson cryostat can be significantly reduced below those of the feasibility model. This study shows that the gas consumption of the cryostat can be significantly reduced without affecting adversely the detector performance. For a penetrator mission, the walls of the penetrator are of sufficient strength that a section of it could be used to store the high-pressure gas. Shock environment is perhaps the most severe requirement on the cryostat; this will be investigated using demand-flow cryostats of standard configuration to determine if modifications are necessary.

Because of the severe constraints of a penetrator mission, advantages of detectors that can be operated at ambient temperatures have become more apparent. Recent developments of mercuric iodide and cadmium telluride detectors for room-temperature operation show promise in this area. A study initiated by JPL to improve the resolution of cadmium telluride detectors for low-energy x-rays is now underway.

RADAR STUDIES OF MARS

R. A. Simpson, G. L. Tyler, and H. T. Howard
Stanford University

Radar studies of Mars undertaken to characterize the properties of the Viking landing sites reveal the surface of the planet to be highly variegated. Data have been obtained from Haystack and Arecibo observatories, and Goldstone tracking station over a wavelength range of 3.8 to 70 cm. Observations provide quantitative indications of the statistical large-scale surface roughness over horizontal distances of 100-200 wavelengths, of the vertical compaction of the surface with depth on the order of a wavelength, and qualitative information on the presence and variability of wavelength size features such as rocks or sharp edges of material fragments on or very near the surface. Surface resolutions as fine as 6X100 km (E-W, N-S) have been achieved for the first two quantities above. The observations are limited to the equatorial region of Mars due to technical restrictions that arise from the rapid spin rate of the planet.

In the equatorial region, the data support the following conclusions:

- (1) The principal component of radio wave scattering of Mars is, at most, weakly wavelength dependent over the range of a few to a few tens of centimeters.
- (2) Surface reflectivity of the planet varies at least 5:1 over the surface, or alternately, there are extensive areas of extreme roughness with rms slope approximately $\gtrsim 10^\circ$ on a special set of

limited lateral scales. If the interpretation of low surface reflectivity is correct then surface densities on the order of 1 g-cm^{-3} are required. (3) The surface is extremely heterogeneous on large scales, values of rms slope vary between about 0.5° and 5° in adjacent regions. (4) On small lateral scales (approximately less than 100 meters) rms slopes are often 2° . (5) There is an indication of planet-wide approximately 10 cm scale roughness which may exceed that of the other terrestrial planets.

Over some areas of the planet surface properties as inferred from 1 km Mariner 9 images are consistent with those obtained for the smaller surface scales from the radar. Changes in radar properties often coincide with boundaries of mapped geologic units, but larger changes in radar properties are often observed within a mapped unit. The regions of anomalously low scattered power on Mars appears bland in 1 km resolution images and show little to distinguish them from other areas with radically different radar signatures.

The overall wide range in variation in radar scattering properties, the rapid change in radar signature with small changes in location on Mars (typ. 50 km), and the presence of the anomalous scattering regions clearly distinguish Mars from other terrestrial planets. Evidently, on the basis of differences between Mariner 9 images and radar results for some areas, there are marked changes in surface structure on lateral scales between about 100 and 1000 meters.

MEASUREMENT OF SMALL-SCALE TERRAIN ROUGHNESS: A BONUS FROM AIRBORNE OR SPACECRAFT-BORNE SIDE-LOOKING IMAGING RADAR SYSTEMS

Gerald G. Schaber
U.S. Geological Survey

Film density variations on 3 cm wavelength (X-Band) side-looking airborne radar (SLAR) images of the Cottonball Basin (Death Valley National Monument, California) correlate well with local saltpan geologic units and associated changes in small scale (0 cm to 70+ cm) surface roughness. The extreme flatness, near total absence of vegetation and extreme roughness variations on the Cottonball Basin permits calibration of SLAR image film density as a function of roughness alone. Film density values from a digitized 3 cm wavelength SLAR image, calibrated by hand measured surface height measurements, were used to produce color hypsometric maps of small-scale surface irregularities. Subsequent field surveys verified the accuracy of the SLAR image film density slicing technique for portraying surface roughness on flat, vegetation-free surfaces such as that characterized by the Cottonball Basin. Signal penetration or anomalous complex dielectric effects appear to have been minor because roughness of various surface units were alone found to account for nearly all of the observed backscatter data. The effects of signal polarization, antenna depression angle, film emulsion dynamic range, and other system parameters are discussed.

Although all of the experiments concerned with the development of scattering models have dealt with non-imaged radar backscatter data, the general conclusions resulting from all of these studies should qualitatively apply to a study of SLAR image interpretation. A SLAR image is essentially a two-dimensional plot of radar reflectivity and consisting of numerous resolution cells. Each cell represents a radar cross-section (σ) value for a specific portion of the imaged surface. The degree to which the image represents the true distribution of reflectance from the terrain depends upon: (1) the relationship between the image tone of each resolution element and corresponding actual σ value, and (2) the relative geometric position of each resolution element. Thus, the SLAR system records a statistical sampling of changing reflection signals.

The primary difficulty with using film emulsions to record radar return is the discrepancy between the dynamic range of image films (20 dB-25 dB) and the 60 dB dynamic range possible by gain switching on modern wide band radar receivers. If the greater portion of the available signal film or image film density is used to record differences between low intensity signals, high level, strong returns are compressed into a small density range. Conversely, if instrument

gain is set to discriminate between high level, strong returns; density separation at low levels is lost or clipped.

Taking all of the previous parameters into consideration, visually defined SLAR image tones should be related to radar cross-sections so that lighter tones generally represent higher decibel values of σ while darker tones represent lower σ values. These image tones are certainly qualitatively related to surface parameters and, with field calibration of the target area, it appears that semi-quantitative results can be obtained, if only for specific terrain types. The long range objective of the Death Valley radar project is to evaluate surface backscattering processes and to assess the general geologic potential of diverse wavelength SLAR images for utilization in future planetary radar investigations such as the Venus Orbiting Imaging Radar (VOIR) mission planned for the next decade.

IMAGING RADAR FOR PLANETARY STUDIES

R. S. Saunders, M. I. Daily, and C. Elachi
Jet Propulsion Laboratory

Spacecraft borne imaging radar systems under development will provide a new tool for the exploration of planetary bodies. In the next few years, the applicability of this instrument to problems of planetary geology will be tested by the SEASAT radar experiment and later a more advanced instrument may be operated on board the Space Shuttle. The first imaging radar instrument to be used in planetary studies was flown on Apollo 17. This experiment (Apollo Lunar Sounder Experiment) performed well and analysis of the enormous quantity of data continues to supply information about roughness, elevation profiles and subsurface layering on the Moon. Depending on the mode of operation, the imaging radar can be used to image, as a scatterometer or as a profiler. In many applications the instrument will yield unique information on the stratigraphic, structural, geodetic and geophysical properties of planets.

One of the most valuable attributes of radar is its ability to penetrate atmospheric aerosols and thus provide image information where conventional systems are unable to operate. The planet Venus offers the most obvious application for this mode. The planet Mars might also be studied in this manner since it appears that some low lying regions may be perpetually shrouded in dust, for example, the floor of Hellas.

Much information in addition to the photo-like image can be extracted from the radar imagery. Something about the nature of the surface materials may be deduced from the radar backscatter. Surface roughness, average

slope and dielectric properties of the surface are the major factors that determine the reflectance.

Field work confirms that radar can discriminate surface particle sizes ranging from sand to cobbles. Imagery from a variety of arid and semiarid areas in the southwestern United States demonstrates that there exist regional differences in the apparent surface grain size on alluvial aprons and valleys (Schaber and Brown, 1976). These differences may reflect contrasts in climate, age of the surface, or lithology (i.e., the characteristic weathered particle size). In areas having similar climate and rock types, a surface roughness map may serve as an indicator of relative ages of surfaces and may provide valuable information on the local tectonic histories.

The most useful classification schemes in field studies of desert sedimentology are based on grain size and surface roughness. Imagery from Death Valley, the Lake Mead area, Pisgah Crater, and elsewhere demonstrates radar's ability to identify incised desert pavements, distal sand facies, and active depositional surfaces (Daily, 1976).

Radar data are also applicable to engineering geologic studies. Surface particle size maps are a useful guide for sand and gravel prospecting. Such maps would be helpful in siting emergency landing fields on earth or spacecraft targets on other terrestrial planets. Knowledge of surface particle size would take on additional importance for return missions. Sample weights for most return spacecraft are only a few kilograms and few planned missions involve multi-site sampling. It is therefore of the greatest importance that the sample be chosen for optimum geochemical characteristics. Present geochemical techniques permit age-dating and detailed

chemical analyses of individual millimeter-sized particles. For the earliest return missions from a planet, the most useful sample would be a sand-sized deposit containing particles from a vast area of the planet's surface, presumably transported by wind or impact. Later, more detailed return missions would sample near bedrock where effects of shock or eolian winnowing and abrasion would be eliminated and where samples large enough for consortium study could be obtained. Radar offers the greatest potential for identifying safe lander targets that have optimum grain-size distributions.

AN ALPHA PARTICLE INSTRUMENT WITH ALPHA, PROTON AND X-RAY MODES FOR PLANETARY CHEMICAL ANALYSES

T. E. Economou and A. L. Turkevich
University of Chicago

Mini Alpha

An alpha particle instrument including alpha, proton and X-ray modes has been developed for rather complete in-situ chemical analyses of surfaces and thin atmospheres of extra-terrestrial bodies. It should identify and determine 99% of the atoms (other than H) present in rocks, and have a sensitivity down to the ppm range for some trace elements. The instrument should be suitable for soft landing missions to Mars, Mercury, asteroids, and the moons of all the planets. The classical Alpha Scattering Instrument has been improved and miniaturized (Mini-Alpha) to a volume of the sensor head less than one-tenth that of the Surveyor lunar instrument. Figure 1a shows the geometrical relationships of alpha sources and detecting systems to each other and to the sample in the Mini-Alpha instrument.

The backscattered alpha spectra in Mini-Alpha are obtained from front, thin ($\sim 35 \mu$), totally depleted detectors of two assemblies connected in parallel. Only signals not in coincidence with those from the detectors in back (proton detectors) are used for the alpha mode spectra. The proton spectra are obtained

by summing the signals in coincidence from the thin alpha detectors (dE/dx signals) and the thicker proton detectors (residual energy signals). This technique and the improved geometrical relationship of the proton detecting systems to the sources lead to higher accuracies for the proton producing elements nitrogen, fluorine, sodium, magnesium, aluminum and silicon than in previous models.

The alpha and proton modes give quantitative information on the most abundant light elements in rocks. Better resolution for the less abundant heavier chemical elements and more sensitivity for trace elements is obtainable by the addition of an X-ray mode. This uses a semi-conductor X-ray detector that has much higher resolution than the proportional counters being used on Viking. The excitation sources for the X rays are either the already present ^{242}Cm alpha sources, or special auxiliary sources.

Data have been obtained with a liquid N_2 cooled intrinsic germanium detector mated to Mini Alpha. Such a detector requires cooling only during the time of actual measurements (~20 min), and has been shown to be capable of surviving the sterilization requirements of a Martian mission. Both ^{242}Cm alpha sources and special radioactive sources have been used as excitation sources of the X rays both from typical rock samples and from synthetic mixtures containing known amounts of trace elements in order to evaluate the sensitivity and accuracy of the X-ray mode of an alpha particle instrument. An example of the X-ray spectra obtained

with the ^{242}Cm alpha sources from samples of basalt and granite are shown in Fig. 2a. In addition, an X-ray detecting unit (developed by E. Franzgrote of the Jet Propulsion Laboratory) that utilizes compressed gas Joule-Thomson cooling of an intrinsic Ge detector has been mated with Mini-Alpha, and data obtained under simulated space mission conditions. Cooling from ambient to operating temperatures takes less than 15 minutes. This system has a resolution of 150 eV at 5.9 keV with the cooling gas turned off (possible for up to 5 min), and 250 eV (due to residual microphonics) with the gas flowing. Fig. 2b shows part of a spectrum obtained with the Joule Thomson cooled detecting system. In addition, newly developed ambient temperature X-ray detectors (e.g. CdTe) are being studied as even simpler X-ray detecting devices for space missions.

Penetrator Mission Instrument

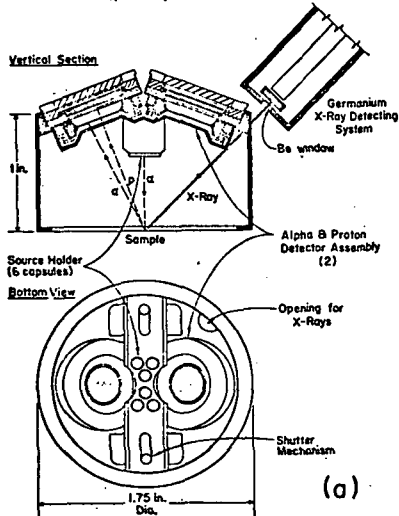
The Alpha Particle Instruments are also adaptable for semi-hard-landing missions on extraterrestrial bodies (penetrator missions). The physical dimensions of a penetrator (3" in diameter) requires a further miniaturization of the instrument. Fig. 1b shows a proposed tight geometrical arrangement of detectors, source, collimator and shutter in the sensor head (Micro-Alpha). In Micro-Alpha the alpha source is located in the back of the detectors and "sees" the sample through a hole in the center of the detectors. The sensor head could examine the material outside the penetrator through a small (1 cm^2) opening in the wall. Several sensor heads

using the same electronics could be placed along the penetrator length to obtain a stratigraphic information.

The high shock loads (~2000 g) anticipated on penetrator missions are a severe constraint on all instruments on board. In an Alpha Particle Instrument the solid state detectors are among the most fragile components. Two proton detectors with a hole in the center and two thin (~30 μ) detectors were shock tested at 700 g, 1500 g, 1950 g and 3500 g without any apparent mechanical or electrical damage. Thus, there is a good chance that the shocks will not present unsurmountable problems for the alpha and proton modes of the Alpha Particle Instrument on such missions.

In the case of the X-ray mode, work is underway currently to: a) harden the Joule-Thomson cryostat to withstand a shock of 2000 g deceleration (work at JPL) and b) evaluate the use of new semiconductor detectors made of materials such as CdTe or GaAs for detecting low energy X rays. These detectors operate at much higher temperatures so that cooling is easier or not necessary.

"Mini-Alpha" A Combined (α ,p,X-Ray) Alpha Particle Instrument



"MICRO-ALPHA" THE UNIVERSITY OF CHICAGO

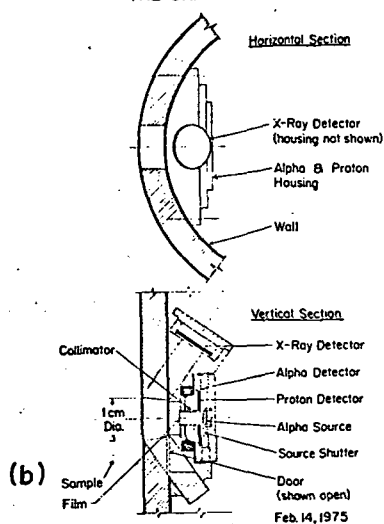


Fig.1

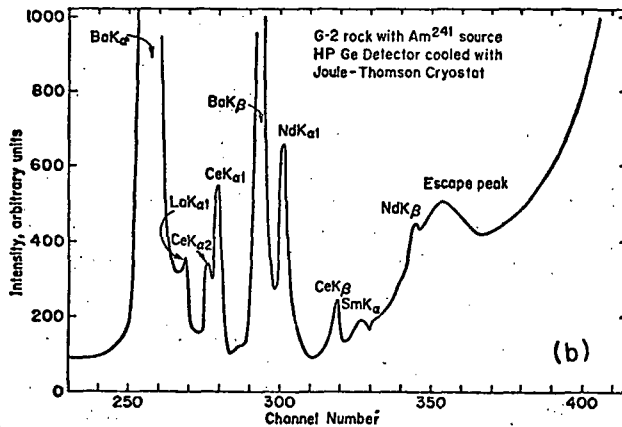
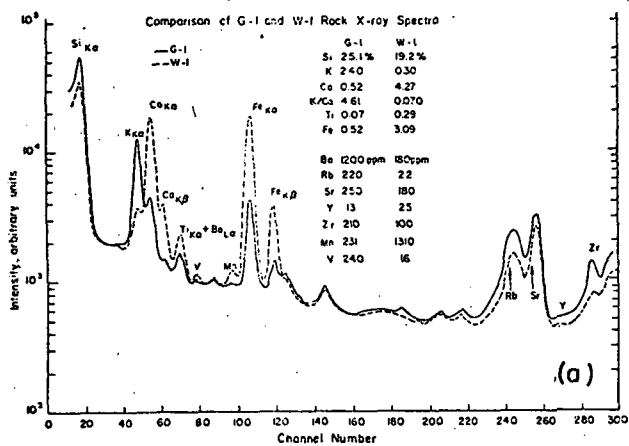


Fig.2

REVISED ALBEDO MEASUREMENTS OF MERCURY

Daniel Dzurisin and G. Edward Danielson
California Institute of Technology

Normal albedo measurements derived from Mariner 10 photometry of many small (50 km x 50 km) areas on Mercury, first reported by Hapke, et al., have been revised and expanded to include several new areas of geologic interest. In addition, a preliminary relative albedo map of Mercury at an average resolution of 5 km has been generated. To facilitate timely production of the map, a mean lunar photometric function was assumed. Although significant difficulties remain, initial results indicate that such a map can serve as a valuable tool for geologic interpretation.

In addition to distinguishing between light and dark smooth plains units, the preliminary map indicates that intercrater plains are in general essentially uniform in albedo. The possibility that normal albedos as high as 45% calculated for some very local areas may be in error owing to significant local departures from the mean lunar photometric function is being examined.

Analysis is continuing in an attempt to eliminate artifacts and verify the reliability of absolute albedo measurements. Computer techniques employed to generate the preliminary albedo map are applicable to color and color-ratio images as well.

EVOLUTIONARY TIME SCALES AND HISTORIES RECORDED ON THE TERRESTRIAL PLANETS

Laurence Soberblom
U.S. Geological Survey

Most attempts to unravel the evolutionary histories of the Moon, Mars, and Mercury have revolved on study of impact craters. The relative ages of different geologic provinces over a planet can be established on the basis of their crater densities. Until recently, crater density measurements for the Moon and Mars were available for only scattered isolated localities. Therefore, although the relative ages of these individual localities were known, little was known of the percentage of the planetary surfaces in different relative age intervals. Recent techniques developed by Boyce et al., 1975, for the Moon, and Soderblom, et al., 1974, for Mars, and in this paper, Mercury, provide continuous maps of planetwide crater density for those surfaces. Those data taken in concert with a knowledge of the lunar impact flux history can be used to derive the historical rates of surface evolution of the terrestrial planets. The derivation of those historical rates is the subject of this paper.

In analyzing the crater density distributions on Mercury and Mars, it would be inappropriate to use a flux history derived for the Moon. In fact, a number of previous studies have suggested that the flux histories on the three planets may be very different. Therefore, the model described here necessarily includes a technique for deriving a model impact flux history for a planet directly from its planetwide distribution of crater density, independent of the lunar impact flux rate.

Results show that the flux histories for the Moon, Mars and Mercury

have been very similar. Additionally, it is concluded that Mars has had a roughly continuous surface evolution throughout its history creating new surface at the rate of approximately 20% of the planet over a billion years. The moon had a less active surface evolution (about 15% per billion years) which ceased for the first 1.5 - 2 billion years of its history; and has remained quiescent. Mercury has a resurfacing history similar to the moon but apparently much shorter (less than 1 billion years). These results place important constraints on the initial thermal and chemical conditions in the inner solar system. The thermal models contain time-scales for early differentiation. The nature of the intercrater plains in the uplands of these bodies is consistent with these implied timescales.

WIND TUNNEL STUDIES OF AEOLIAN PROCESSES

Ronald Greeley
University of Santa Clara and NASA Ames Research Center

Wind tunnel analyses of several aspects of aeolian processes are currently in progress. During the previous year the following areas were investigated: 1) systematic analysis of flow-field patterns for craters, 2) low-pressure wind tunnel put in initial operation, 3) calculation of particle threshold speeds for Earth, Mars, Venus, and Titan, and 4) analyses of grain saltation under martian conditions.

Flow Field Patterns. This work was a follow-on of previous studies which were based on a *single* crater geometry. The current work involves a systematic qualitative survey of aeolian flow-fields for *fourteen* different crater geometries, to determine differences in erosional and depositional patterns as a function of crater geometry. For each model, four types of runs were made: 1) deposition under high speed (~ 600 cm/sec) winds, 2) erosion under high speed winds, 3) deposition under low speed (~ 300 cm/sec) winds, and 4) erosion under low speed winds. In the deposition cases, particles were introduced upstream, which then saltated across the model; in erosion cases, the supply of material was terminated. Time-lapse motion pictures and still frames taken at specified intervals allowed intercomparison of the different cases.

Two basic patterns resulted; the first, described previously (Greeley *et al.*, 1974a), appears to be applicable to all raised-rim craters regardless of variations in crater rim or floor configuration. Such variations do, however, cause second-order changes in the erosion-deposition pattern. In this pattern, two vortices are shed from the crater rim and cause zones of

preferential erosion in the crater wake. In the immediate lee of the rim, there are three distinctive zones of preferential deposition. The second general pattern results from non-raised rim craters and has the form of a general zone of erosion in the immediate wake of the crater, with no deposition occurring.

An erosion rate parameter was derived from the wind tunnel flow-field studies (Iversen et al., 1975) and is currently being applied to six different areas on Mars to determine the thickness of the active zone of particles (Greeley et al., in preparation).

Low Pressure Wind Tunnel. After two years from inception, a wind tunnel specially designed for martian studies has been constructed, instrumented, and is currently undergoing calibration and "debugging". The tunnel is an open circuit boundary layer facility with a 1.5 x 1.5 m cross section, 16 m long. It is placed in a space environment chamber of about 9000 m³ volume that can be evacuated to ~4 mb pressure.

The first series of experiments (planned to begin in February) will involve determination of threshold speeds for a wide range of particle densities and diameters over a series of atmospheric pressures down to 4 mb. The objective is to obtain threshold curves as a function of particle Reynolds numbers that will complement data previously obtained at one atmosphere (Greeley et al., 1974b) and that can be applied directly to Mars (Pollack et al., 1976).

Follow-on experiments include evaluation of roughness, interparticle forces, lift coefficients, particle shape, etc., on threshold conditions, studies of saltation trajectories, rates of erosion of various materials, and modelling studies, all under low pressure conditions.

Calculated Particle Threshold Speeds on Planets. Three planets (Earth, Mars, and Venus) and one satellite (Titan) have surface conditions in which aeolian processes are possible. Extrapolating from data acquired at one atmosphere (Greeley et al., 1974b), threshold speeds were calculated for these bodies. From Venus to Earth to Mars, atmospheric pressures range over about five orders of magnitude, and it is interesting to note that in the very dense venusian atmosphere, threshold speed ($\sqrt{2}$ cm/sec) is closer to that of water on Earth than that of air on Earth. Results from the Soviet Venera 9 and 10 spacecraft show wind velocities are well within the range of estimated threshold; thus, aeolian processes may operate on the venusian surface.

Calculations for Titan are highly speculative because of the uncertainties in the parameters. Threshold speeds, however, are within the general range of those for Mars.

These calculations are extrapolations from one atmosphere experiments and will undoubtedly change when experimental data are obtained at low pressure.

Estimated Grain Saltation in a Martian Atmosphere. Using experimental data at one atmosphere, numerical solutions for the equations of motion were obtained for particles under martian conditions (White et al., 1975). Calculations show that a lifting force is important on both Earth and Mars. It was found that saltating particles on Mars have longer trajectory paths, have a higher terminal grain velocity, and impact at a lower angle. These results suggest that erosion on Mars would be more effective on Earth for comparable saltating grains.

These studies are done in collaboration with J. Pollack (NASA-Ames), J. Iversen (Iowa State Univ.) and B. White (Univ. Calif., Davis).

EOLIAN BEDFORMS IN UNIDIRECTIONAL WINDS

Alan D. Howard, Mohamed Gad-el-Hak, Jeffrey B. Morton, and Deborah Pierce
University of Virginia

Dune complexes formed by unidirectional winds are composed of two simple forms, longitudinal dunes created by helicoidal flow and barchanoid dunes sculpted by a complex three-dimensional flow-transport interaction. Longitudinal dunes occur at two scales, 80-500 meter vegetated dunes and 1-3 km draas with superimposed transverse dunes. Proposed mechanisms for origin of longitudinal dunes either involve organized secondary flows or seasonal cross winds. Explanations of the second type do not account for dune scaling nor do they explain longitudinal dunes associated with topographic obstacles. Several mechanisms can possibly account for the origin of secondary flow, for example natural atmospheric instabilities, vorticity generated by upstream topographic obstacles, contrast in roughness or thermal properties between the dune and inter-dune flats, and the topography of the dune itself. The first two of these, although they may contribute to the secondary flow, do not explain the persistence of the circulation downwind or the spatial stability of the helicoidal vortex necessary to pile up sand ridges. A series of wind tunnel experiments is being conducted to determine the direction and strength of secondary circulation produced by lateral contrast in roughness and by longitudinal ridges.

The self-preservation of form during downwind migration of barchan dunes implies a simple relationship between the rate of erosion (or deposition) on the upwind slopes on one hand and the gradient and orientation or the slope on the other hand. Height and orientation of

the crest of the slip face are likewise related to the rate and direction of transport over the crest. The size and shape of barchan dunes are functionally related to the mean wind velocity, the size and grading of sediment in transport, the upwind velocity profile, the gravitational force, and atmospheric density. We are attempting to determine these relationships through a combination of empirical field and wind tunnel studies of air movement over barchans, theoretical modelling of airflow, and derivation of the relationship between rate of sand transport, surface slope, and the structure of near-surface winds. The approach is to budget the transport of sand (and hence forecast the pattern of erosion and deposition) as it flows over the dune, and to investigate effects of variation in wind direction, sand size, etc. upon this pattern. If successful, it would be possible to scale these processes to martian conditions.

PLANETARY SURFACE SEDIMENTS

Elbert A. King
University of Houston

The processes that shape a planet's surface also are responsible for many of the characteristics of particles that are transported across and deposited on that surface. The future return of a small Martian surface sample will offer an extremely interesting opportunity to learn a great amount about the planet and the dominant surface processes of Mars through the study of small volumes of fine surface particles.

We now have a semi-quantitative grasp of the origin and evolution of lunar particle types and the characteristics of small volumes of particles from the Moon (Butler and King, 1974). In the case of the Moon, we are dealing with ballistic sediments almost entirely. These particles owe their origins as particles and their current surface locations exclusively to impact processes. We now understand the relative importance of several processes that affect the characteristics of volumes of lunar fines. For example, comminution by meteoroids is the dominant process operative on the lunar surface regolith. Both agglutination of finer particles and addition of fresh coarse detritus are subordinate processes on the Moon. We may anticipate that particles from the regolith of Mercury will have many of the same characteristics and that volumes of fine particles may have many of the same properties. Shape, surface features, and grain size frequency distributions of particles from Mercury probably also will not show the effects of atmospheric wind or water.

Samples of particles from the surface of the Earth are very different from those of the Moon, reflecting the strikingly different sedimentary processes and particle histories. The almost ubiquitous presence of running water, ocean margins, rainfall and/or atmospheric wind has yielded a distinctly different suite of particle properties that has been documented in dozens of articles and texts. However, surface sediment from Mars may be of an intermediate nature between that of the Earth and the Moon.

Mars has had a large number of impact craters, but it also has a substantial atmosphere that is capable of transporting significant amounts of sediment. The transport of sediments on the Martian surface in the past by running water is still an open question. However, it is obvious that the Martian atmosphere is capable of transporting "fine" particles, as is shown by the frequent dust storms and the observations of "wind streaks", as well as surface dune fields. The exact size of the particles transported by the Martian atmosphere is speculative, but it is anticipated that at least some of the particles will be very fine. Therefore, a program to document and attempt to understand the properties of fine grained (especially wind-blown) terrestrial sediment is being initiated.

The literature is surprisingly bare of detailed studies of the properties of fine grained, especially wind-blown, sediment. A bibliographic search has yielded a substantial list of articles, but most of these deal only with coarser grain sizes or the gross properties of loess and wind-blown deposits. A few papers deal with the grain size and particle characteristics of loess, but these are rare (Swineford and Frye, 1944; Fisher, 1966).

Plots of older data in the literature have been recast to be comparable with recent lunar grain size data. Also, a number of new grain size analyses on terrestrial loess have been completed by exactly the same techniques as used for the lunar fines. Lunar fines are slightly bimodal, platykurtic, poorly to very poorly sorted, and nearly symmetrical. With slight exception, we expect that these characteristics will be those of ballistic sediments from virtually any planetary surface, especially those planetary bodies with no or only slight atmosphere. Terrestrial loess grain size frequency distributions in the same size interval tend to be unimodal, leptokurtic, well-sorted, and strongly positively skewed. Particle morphologies also show some interesting and diagnostic differences. For example, in the scanning electron microscope, terrestrial particles do not show the radiation damaged layer that has been found on so many lunar regolith grains. Also, there is no exact analog terrestrially to the lunar agglutinates. We anticipate that further systematic and interpretable differences in surface features and grain shapes can be documented as well.

Similar analyses of a very small sample of Martian surface regolith should be able to establish the relative importance of impact and aeolian processes in the vicinity of the landing site in the recent past. If individual layers from a Martian core tube or drive tube could be examined, we should be able to recognize layers that were deposited from predominantly ballistic and aeolian (and possibly other origins) sediments. We could thus build up a local stratigraphic chronology of Martian deposition and geologic history.

TERRESTRIAL YARDANGS

John F. McCauley and Maurice J. Grolier
U.S. Geological Survey

The existence of large fields of meter to kilometer scale wind-produced streamlined hills in certain terrestrial desert regions is not well known to American geologists but is recognized by most students of the deserts of the old world. In the southwestern United States many of the early workers overstated the role of the wind in landscape development, leaving a legacy of uncertainty about the effectiveness of the wind as an agent of surface sculpture. Wind is more rigorously limited than running water by the type of surface upon which it acts but given certain types of bedrock and little or no vegetation it can produce major erosional landforms called yardangs.

Yardangs were first described along the eastern edge of the Takla Makan desert of Chinese Turkestan by the explorer Sven Hedin in 1903. The term is considered by us as applicable to all aerodynamically shaped hills. (Yardang is the ablative form of the Turkestani word yar which means ridge or steep bank - the ablative in this case expressing a sense of removal - an appropriate connotation for wind erosion features). Wind sculptured hills have since been described, often under different names, in the desert regions of every continent except Australia. They are restricted to those parts of the deserts that are extremely arid where plant cover and soil development are minimal and strong unidirectional winds occur throughout much of the year. Among the better described examples are those of Jebel Dhalal in the Sinai Peninsula, the Dharan region of

Arabia, the El Kharga region of Egypt, the Lut Desert of Iran and the "cretes et couloirs" of the Tibesti region of northern Chad, Africa many of which are 20 kms or more in length. Doubtless there are other localities based on incomplete data from Libya, Afghanistan and the Namid desert of southern Africa. In the United States small yardangs have been described by Blackwelder on the northeast side of Rogers Lake, California.

Bosworth in 1922 described yardangs in the Talara region of northern Peru in an area of complexly folded and faulted, petroliferous Tertiary sediments. This region is subject to torrential heavy rains about every 20 years so that these windforms bear the imprint of episodic running water as do many of the African and Iranian examples. The coastal desert of central and southern Peru is essentially rainless (Less than 10 mm of precipitation reported at Pisco per year and this is in the form of condensate from the coastal fog). In the Ica Valley region of south central Peru there are thousands of small to large totally ungullied hills oriented parallel to one another. They occur in clusters with individual hills showing a high degree of streamlining in both plan and profile. These wind erosion forms occur in the upper Tertiary Pisco Formation which consists mostly of white to yellow diatomaceous sandstones interbedded with bentonites and thin layers of conglomerate. The Pisco Formation is being stripped off a paleozoic metamorphic complex of schists and gneiss over which it lies unconformably.

The Ica Valley is unusual among the large transverse valleys of the coastal desert that derive their water from the high Andes. It is

oriented in the direction of the prevailing southeasterly trade winds and is close to being at right angles to the coast so that the strong afternoon sea breeze and the trade winds can reinforce one another.

The yardangs occur on the flanks of the valley to a distance of about 120 kilometers inland. Those in the lower reaches of the valley are exceedingly well streamlined with many individual yardangs approaching the form of an overturned canoe. Little trace of any relief or ancestral drainage can be seen in the lower 50 km of the valley. Proceeding up valley towards Ocucaje the amount of erosion within the Pisco Formation diminishes. Traces of former water courses become more abundant and tend to dominate the topography in the upper reaches of the valley. In plan the shape of the yardangs also changes up valley - in the lower parts of the valley the yardangs are highly elongated with length to width ratios of about 10:1. In the upper parts of the Cerro Yesera region towards Ocucaje they are blunter and ratios are on the order of 3:1. Individual yardangs range from a hundred metres up to several kilometres in length - maximum heights are about 100 metres. The profiles of the yardangs are typically convex with their crests positioned towards their upwind ends. Long tapering downwind tails of bedrock and loose sand are also present. The upwind ends of many individual yardangs are blunt but many show the opposite relation and have a long tapering upwind end and a blunt terminus in the downwind direction. Many of the yardangs show benches that interrupt the symmetry of their profiles - others are perfectly smooth. The surfaces of some of the yardangs are swept clean of debris and show extensive evidence of wind scour. On the flanks of many of the yardangs dense networks of gypsum veinlets stand out in

bas relief. In the lower parts of the valley the very streamlined yardangs are covered with fine in situ detritus presumably derived by chemical and mechanical weathering of the bedrock.

Many authors have attributed yardangs to the effects of abrasion by sand in saltation and have emphasized the importance of the chutes or troughs between the yardangs that act as funnels to accelerate the flow of sand. Our experience in Peru and at the Rogers Lake, California along with a thorough review of the literature reveals that sandblasting effects are minimal and restricted to the prows and flanks of the yardangs up to a height of a few metres. We believe that yardangs that exhibit well developed streamlining, are primarily deflation features.

As granular material is loosened by either chemical or mechanical weathering it is picked up and carried away in suspension. A paramount factor that determine their evolution is rock type. Most of the early descriptions of yardangs are for small features on the order of a few meters in length formed in weakly consolidated lacustrine sediments. In Africa, however, there are yardangs that are kilometres to tens of kilometres in length and up to hundreds of metres high cut into the well consolidated Nubian Sandstone. The crystalline basement rocks below the Nubian does not show wind erosion effects. A similar situation prevails in the Ica Valley. The moderately well consolidated Pisco Formation is extensively wind sculptured - the underlying metamorphic complex is not and forms a temporary base level below which wind erosion proceeds at a negligible pace.

In general a well streamlined yardang can be thought of as a form of dynamic equilibrium. It is a form of least resistance that has adjusted itself to the local climatic regime. It is probable that the large yardangs of the Ica Valley and those of Africa and Iran are secondary landforms in that they represent "eolian takeover" of an earlier fluvial landscape. Since irregularly shaped hills of the type produced by fluvial activity offer more resistance to the wind than a streamlined body the wind will act by scouring and winnowing of loose detritus to produce the windform shape. In time more or less perfectly streamlined forms will be produced that are adapted to the local wind regime and individually offer minimum resistance to it. Once well streamlined the dimensions of the yardang will decrease with time but its overall shape will not change.

WIND TRENDS IN PERU AND ON MARS

Maurice J. Grolier, A. Wesley Ward, and John F. McCauley
U.S. Geological Survey

Directional trends of the major eolian erosional and depositional landforms of coastal Peru were mapped by M.J. Grolier in selected areas to determine how they deviate from known regional wind patterns. In this region, the dominant planetary winds are the southeasterly trade winds which undergo seasonal variations in intensity but are generally known for their constancy of direction. The forms mapped at the 1:1,000,000 scale include: 1) coastal sand streaks, 2) inland sand sheets, 3) longitudinal dunes, 4) transverse dunes, 5) wind fluted cliffs and 6) yardangs. The outstanding characteristic of the depositional forms is their gradual clockwise spiral rotation beginning at a distance of about 10 km from the coast. This spiraling effect is not due to the Coriolis Force because it is in the opposite direction from that expected in the southern hemisphere. Sand flow trends are also dramatically affected by the diurnal advective land-sea breeze that operates at essentially right angles to the coast. The afternoon onshore winds of the sea breeze provide most of the energy for sand transport. It is probable that the interaction of the sea breeze and the regional trade winds on the northwest trending coastline produce the spiral pattern. In addition, valley wind circulation and major coastal mountains cause deflections of the regional sand trends. Dramatic changes in the regional wind pattern due to Tibesti volcanic massif also have been reported in Chad, North Africa. The Ica Valley in central Peru is the only major transverse stream that is oriented directly into the prevailing southeasterly winds. This is a natural wind funnel that is the locale for some of the most perfect aerodynamically shaped hills or yardangs in the world. Thus, local conditions and the interplay between

planetary and local wind systems play an important role in determining the regional trends of windforms.

The sequential interplay between the wind and running water is also evident in coastal Peru. Wind has taken over as the dominant agent of land sculpture in the Ica Valley and has dismembered the ancestral tributary system of the Ica River. In the northeastern part of the Sechura Desert of northern Peru the alignment of the present stream gullies corresponds with the direction of the sea breeze. This particular region is considerably less arid than other parts of the coastal desert and experiences occasional tropical downpours. The bedrock is weakly consolidated eolian sand and loess. The parallel gullies are wind eroded furrows later utilized and modified by running water thus producing a hybrid topography where running water is now dominant.

This work in Peru was undertaken in order to better understand the eolian topography of Mars including the light and dark streaks and the widespread streamlining of what appears to be bedrock. A planet-wide plot of erosional windforms on Mars has been completed by A.W. Ward to supplement previous work by numerous investigators on the streaks alone. In the low-latitude regions the prevailing directions are east-west. The middle-latitude regions show trends that are generally at moderate angles to the local meridian, and the polar regions show an outward spiraling pattern. As in the Peruvian case, major topographic obstacles such as shields and basins produce diversions in these trends. The trends of the major erosion features on Mars and those of the light and dark streaks observed by Mariner 9 generally are not parallel. The light and dark streaks exhibit a more disordered pattern that is interpreted to result from redistribution of surficial material after the dust storm of 1971. As in Peru the interplay between local and regional winds is responsible for the final configuration of the surface.

TERRESTRIAL ANALOGS OF THE HELLESPONTUS DUNES, MARS

Carol S. Breed
U.S. Geological Survey

Close geomorphic similarities among features in the Hellespontus region, Mars, and dunes of the crescentic ridge type in numerous terrestrial sand seas are shown by dimensional analysis of dune lengths, widths, and wavelengths. Measurements are taken from sample areas of Landsat images, Skylab, and aerial photographs of sand seas in Africa, Asia, the Arabian peninsula, and North and South America, and on Mariner 9 photographs of Mars.

Ratios derived from measured mean dune widths, lengths, and wavelengths are similar in all sampled terrestrial sand seas, regardless of large differences in sizes of the dunes and in shapes and geographic locations of the dune fields. Mean dune width/length ratio for all sampled terrestrial crescentic dune ridges is 1.65, vs. 1.74 for the Hellespontus dunes. Mean width/wavelength ratio for the terrestrial dunes is 1.27, vs. 1.15 for the Hellespontus dunes. Mean wavelength/length ratio for the terrestrial dunes is 1.34, vs. 1.51 for the Hellespontus dunes. Thus the Hellespontus dunes are considered geomorphically similar, in planimetric aspect, to typical terrestrial dunes of a very common type.

Ratios of measured values in each terrestrial sand sea are compared with those of the Hellespontus dunes, to determine the closest terrestrial analogs by quantitative methods. Terrestrial dunes with scale ratios closest to those of the Hellespontus dunes are in the Karakum Desert of Turkmenia, USSR, along the Namib Desert coast, South West Africa, near the Persian Gulf in the southeastern Arabian peninsula, in the Taklamakan

and Alashan (Gobi) Deserts of northern China, and in the Algodones dunes of southern California, USA.

Distribution of terrestrial crescentic dune ridges is mainly in basins whose topographic boundaries determine the shapes of the sand seas. Variations in form and distribution of crescentic dunes are commonly observed around the margins of the sand seas, particularly near topographic boundaries to the movement of sand by surface winds. Forms and distribution of dunes in two terrestrial fields, the Algodones dunes, California, and the Badan-Jarang sand sea, China, are compared with forms and distribution of dunes in the Hellespontus field.

The Hellespontus dunes occupy a semi-circular field bounded by crater walls. Along the northeast margin, believed to be the downwind end of the field, large, sharp-crested crescentic ridges grade into smaller ridges and isolated features believed to include star dunes. The Algodones dunes, to which the Hellespontus field has previously been compared, occupy a narrow, elongate field along the axis of an intermontane valley. They are bounded on the southeast, downwind end not by topographic barriers but by irrigated fields of vegetation. Effective winds are from the northwest, parallel to the long dimension of the field. Crescentic dunes in the Algodones field grade southeastward from very small ridges to megabarchanoid ridges and megabarchans at the downwind end; no sharp-crested ridges or star dunes are seen.

The Badan-Jarang sand sea in the Alashan Desert, China, occupies a roughly equidimensional field on a gently sloping stony plain, bounded on the southern and eastern, downwind end by low mountain ranges.

Effective winds are dominantly from the northwest, but are variable. Very large megabarchanoid ridges with segments' averaging 2.7 km (1 2/3 miles) wide from horn to horn, in the center of the sand sea, grade southeastward into narrow, sharp-crested ridges interpreted as reversing dunes, and into star dunes around the perimeter of the field. Ratios of dune width, wavelength, and length in the center of the Badan-Jarang field, relative to those at the margin, are closely similar to ratios of measured values at the center and margin of the Hellespontus field. Dimensional analysis thus indicates that the Badan-Jarang dunes, rather than the Algodones dunes, are closer analogs in form and distribution to the Hellespontus dunes of Mars.

DIFFERENTIATING EOLIAN DEPOSITS USING GRAIN SIZE PARAMETERS

Augustus S. Cotera and Camilla K. McCauley
Northern Arizona University

Deposits of wind-blown sediment are amenable to grain size analysis in order to define distinguishing characteristics of source area, direction of transport and specific environment of deposition. In addition, different segments within an individual dune can be distinguished.

Four dune fields have provided data for this study:

- (1) Cameron--a small barchan dune field on the north side of a major intermittent wash draining the Ward Terrace and flowing into the Little Colorado River.
- (2) Moenkopi--a barchan-longitudinal dune complex on top of the Ward Terrace with no major fluvial source of sediments.
- (3) Tuba City--a barchan dune field situated in a deflation area and lying directly upon truncated eolian deposits of Triassic-Jurassic age.
- (4) Paiute Point--a climbing dune field moving eastward onto the Ward Terrace.

The first four moments of each grain size distribution were calculated for 68 samples from these four fields. Each of the four moments, mean grain size, sorting, skewness and kurtosis, are useful in estimating the distinguishing characteristics of the four dune fields.

1. Mean Grain Size: This first moment is of little value in distinguishing between segments of an individual dune or between dunes, there is however, a significant variation in grain size on a regional basis. For example in the Moenkopi Field, the generally finer grain size of the field is attributed to its elevated topographic position, about 200 feet above the wash from which the sediments are derived. The existing wind regime carries only finer size sand up onto the cliffs, leaving the coarser size fraction in the valley below. Once the sediments reach the edge of the terrace, the transportive capacity of the wind diminishes significantly as evidenced by the average finer grain size of the Moenkopi field and also by the still finer grain size of the farthest dune from the edge of the terrace.

The Tuba City Dune Field is in a deflation area and the grain size of these dunes is directly controlled by the size of the grains comprising the underlying Triassic-Jurassic rocks, whose average grain size is about 2.2 ϕ .

2. Sorting: Sorting shows parallel trends to grain size differences and is also useful only on a regional basis. As expected, there is a significant correlation ($r = 0.5636$, $p < .01^{**}$) between sorting and mean grain size: the finer the grain size, the better sorted the sample. Sorting differences between fields thus are attributable to the same reasons as those given above for mean grain size.

3. Skewness & Kurtosis: These two moments do not indicate consistent variation between dunes or between fields. Because these two parameters are extremely sensitive to minor variation within limited sedimentary environments, thus averaging several values tends to smooth out and compensate for individual variation. Precisely because of its sensitive nature, skewness is the only parameter which is amenable to defining the segments within a dune. Because of the similarity in geomorphic structure of the Cameron and Tuba City dune, the skewness values of the individual samples were averaged for each sample station, respectively. The Moenkopi dunes being geomorphologically different were averaged separately. Stations 1 and 2 are horn samples, stations 3, 4 and 5 are medial line samples. The results are as follows:

CAMERON & TUBA CITY				MOENKOPI			
Station	Surface		Subsurface	Station	Surface		Subsurface
1	0.37	0.42	0.21	1	0.10	0.17	0.06
2	0.48		0.13	2	0.23		0.14
3	0.19		0.09	3	-0.04		0.03
4	0.29	0.24	0.10	4	-0.13	-0.07	0.05
5	0.22		0.05	5	-0.04		0.08

It is self evident that horn samples, are consistently more positively skewed than medial line samples. Skewness measures the displacement of the median from the mean of the distribution, expressed as a fraction of the sorting or standard deviation. Stated in simple terms, a large positive skewness indicates an excess of fine size sediment. A normal distribution would have zero skewness.

The more positively skewed samples from the horns is attributed to the wind regime process by which the dune advances. The horns advance ahead of the main body of the dune and are areas of active avalanching. The crest of the dune is subject to the highest wind velocity and most of the finer sand size particles are blown off and away from the dune. In the horns, avalanching inhibits removal of the finer grains and thus retain them in the distribution, to a much greater extent than do the medial line crestal portions of the dune.

In the Paiute Point field, eight samples were obtained at increasingly higher elevations on the climbing dune on the face of the Ward Terrace. From the base of the dune to the uppermost top surface on the Terrace, the following differences are noted:

	bottom	top
Skewness	0.36 strongly fine skewed	0.01 symmetrical
Kurtosis	1.02 mesokurtic	1.16 leptokurtic
Sorting	0.57 moderately	0.41 well sorted

It is evident that as sand is blown up the face of the terrace, the sediment becomes better sorted and the distribution has a larger proportion

of the very fine sand size fraction. The leptokurtic values of kurtosis are significant and have not occurred in any samples from other dune fields. It is possible that because the uppermost terrace samples are unquestionably deposited only by wind with no possible input of water deposited sediment, kurtosis may be the most distinguishing parameter in differentiating dunes deposited from strictly eolian sources.

Present studies in the Paiute Point field are continuing in order to better define the size characteristics of the field. In addition, size studies are being augmented by analysis of the wind regime system using three portable weather stations and by time-lapse photography. Preliminary wind data indicates a bimodal prevailing wind direction, (NE and NW). However, the sand is moving in only a NE direction, thus additional data at different elevations, at different velocities and over several seasons is being obtained.

From these studies, it is expected to determine the precise size boundaries of the various eolian environments and to discriminate precisely the conditions of transport and grain size characteristics which controls dune morphology.

AEOLIAN FIELD STUDIES AT AMBOY CRATER

Ronald Greeley

University of Santa Clara and NASA Ames Research Center

This abstract gives the geological background and rationale for field studies conducted during January, 1976, at Amboy lava field in San Bernardino County, California. Preliminary results will be available in early February. The work has two primary objectives: (1) to determine the effect of surface roughness on the aeolian regime, and (2) to observe large scale flow patterns over various topographic landforms.

Surface Roughness

It is a well-known fact that surface roughness (the relief of a given surface and the spacing of roughness elements) affects the ability of a given wind to move particles because of the influence of roughness on the structure of the lower part of the planetary boundary layer. Surface roughness has been studied in boundary layer wind tunnels and in field experiments for agricultural applications, but full scale quantitative tests in geological environments are largely lacking. The evaluation of the roughness parameter is of first-order importance in determining aeolian erosion rates, zones of preferential erosion versus deposition, and in the general expressions for threshold speeds for particle movement.

In applications to Mars, roughness effects may account for the enigmatic pedestal craters where the aeolian regime may be altered as the wind blows across smooth plains, then encounters the rougher terrain of secondary craters and blocky ejecta near the crater.

Amboy Crater lava field ($\sim 70 \text{ km}^2$ of paheohoe basalt) offers the opportunity to study both the effects of roughness on the near-surface wind velocity profile and the aeolian flow pattern around a typical volcanic landform. A prevailing WNW wind has its fetch across a relatively flat, alluvial-fill valley, then abruptly encounters the rough, hummocky surface of the basalt lava flow. By concurrently measuring the wind profile over both the flat alluvial-fill surface and the lava surface for an extended period, it should be possible to assess the roughness parameter over a wide range of wind speeds.

Flow Patterns

An important factor in studies of aeolian processes is the relationship of flow pattern to landform shape. Flow pattern - the distribution of flow velocities and directions, and associated vortices and secondary flow fields - determines where and how aeolian erosion and deposition will occur as a function of wind and topographic form. For application to Mars the landform that has received most attention in terms of aeolian processes is the crater. Wind tunnel studies show a distinctive flow pattern that has been partly confirmed by preliminary analysis of full-scale structures. Much more work of full-scale features in geological environments is required for validation of the wind tunnel studies.

Although Amboy Crater is not an analog to an impact crater, it is a topographic landform that is common in some volcanic areas. Amboy Crater is a complex cinder cone about 76 m high and 460 m in diameter and contains an irregular summit crater about 200 m in diameter and 30 m deep. It is in the northeast quadrant of the lava field and has in its wake a dark aeolian streak extending more than 3 km downwind. Hypotheses for the origin of the streak

include: 1) that the cone-and-crater structure forms an obstruction that blocks particles from reaching the leeward area, 2) that the dark zone is composed of basaltic particles ablated from the cone and deposited downwind, or 3) that the cone-and-crater causes a vortical wind pattern in which the wind speed is effectively increased in the wake zone, creating an area of erosion which keeps the lava flow swept free of particles. Results from wind tunnel studies substantiate the last possibility. In addition, during a reconnaissance field trip by Greeley and Iversen in April, 1974, wind speeds close to the ground were measured in the wake zone and adjacent to the zone and a slightly higher wind speed was found in the wake. However, the measurements covered only a few hours and were made for only a single height above ground. More refined measurements are required to solve the problem.

Field Methods

Four, 50-foot meteorological towers, each having an array of cup anemometers and a wind vane, will be established and maintained for one month on site. This will permit the determination of the near surface wind velocity profile and resulting surface stress. Two towers will be used to determine roughness effects, and two will be used to study the flow field around Amboy Crater.

In addition, samples of wind-blown material will be collected over the field to assess the degree of sorting that occurs across the lava flow.

Lower priority tasks of the study include: 1) construction of 5-meter artificial craters, some with blocky rims, others without, to monitor differences in sand erosion and deposition, and 2) analysis of collapse depressions and other flow features on the pahoehoe basalt (non-aeolian study objective).

This work is done in collaboration with J. Iversen and J. Pollack.

A STATISTICAL STUDY OF CRATER RELATED WIND STREAKS IN THE NORTH EQUATORIAL ZONE OF MARS

K. Cook and J. Veverka
Cornell University

A statistical study of all crater related wind streaks visible on Mariner 9 A-camera frames in the latitude band 0° to 30°N has been completed. Of the 2325 streaks identified, 1914 (82%) are light tone streaks, 189 (8%) are dark tone, and the remaining 222 (10%) are of mixed tone. Ten physical parameters characterizing each streak and its associated crater were measured and intercorrelated. Due to the large number of light streaks in our sample our findings for this type of streak are most significant statistically:

1. Light tone streaks occur preferentially in Pc terrain (heavily cratered plains).
2. They are preferentially associated with fresh craters.
3. Craters 2 - 3km in diameter are significantly better at forming light streaks than larger craters.
4. No evidence for a separate dependence of the density of light tone streaks on altitude emerges.
5. A significant latitude effect does emerge: the density of light tone streaks peaks near 12°N , and drops off appreciably both towards the equator and towards higher latitudes.
6. The mean angular width of light streaks is about 20° ; long light streaks are significantly narrower than short ones.
7. The streak length/crater diameter ratio is typically <5 .
8. The light streak directions conform closely to the wind regime expected at the season of global dust storms (southern summer).

Generally speaking, the results for dark and mixed tone streaks in the northern equatorial zone, although statistically less significant, are similar. But the following possible exceptions exist:

9. Dark streaks may show a slight preference to form at higher altitudes.
10. Dark streaks may be slightly wider on average than light and mixed tone streaks.
11. Mixed tone streaks do not share the preference for fresh craters exhibited by light and dark streaks.
12. The pattern outlined by dark and mixed tone streaks does not conform to the general circulation pattern expected at the season of global dust storms.

MORPHOLOGIC CLASSIFICATION OF SCARPS AND LINEAMENTS IN DISCOVERY QUADRANGLE

Daniel Dzurisin
California Institute of Technology

A physiographic map of Discovery Quadrangle (H-11) is being prepared in support of a geologic mapping program undertaken in association with Dr. Newell J. Trask of USGS, Reston and Dr. James A. Dunne of the Jet Propulsion Laboratory. Preliminary morphologic description and classification of escarpments and other lineaments within the quadrangle is complete. Three morphologically distinct groups have been identified.

One group includes a series of linear features which define two prominent lineation directions and strongly influence the planimetric form of intersected crater rims and escarpments. Within intercrater plains, such features are often discontinuous and seldom display significant relief. There is no evidence of lateral offset associated with these features.

Major escarpments within intercrater plains (e.g. Discovery, Santa Maria) range from several hundred meters to more than a kilometer in local relief, and are generally arcuate and slightly lobate in planimetric configuration. Such escarpments occasionally disrupt the rims and floors of large craters, and in one such case some crater rim offset is indicated.

A third morphologic group consists of linear to arcuate escarpments which are generally several hundred meters high and confined to smooth plains within large craters.

The first group of surface lineations is tentatively identified as a regional jointing pattern responsible for strong structural control of crater rims and escarpments at scales ranging up to hundreds of kilometers. Major escarpments in intercrater plains and smooth plains within craters are most likely tectonic features,

although a volcanic origin for the latter cannot be excluded.

Finally, to support continuing morphologic studies as well as the Mercury Mapping Program, this work also included identification and pairing of all Mariner 10 frames which provide adequate stereoscopic viewing. Implications of crater depth/diameter relationships which bear on the early degradational history of Mercury have previously been reported (Malin, M.C. and D. Dzurisin, "Land-form Degradation on Mercury, the Moon, and Mars: Implications of Crater Depth/Diameter Relationships", J. Geophys. Res., in press).

INFLUENCE OF TECTONIC SETTING, COMPOSITION, AND EROSION ON BASALTIC LANDFORMS: NEW MEXICO AND MARS

Wolfgang E. Elston, Jayne C. Aubele, Larry S. Crumpler, and Dean B. Eppler
University of New Mexico

Composition of volcanic rocks reflects their tectonic environment and the chemistry of the planetary interior in which they originate. This is the first report of an attempt to analyze volcanic landforms of Mars in order to obtain information on the chemical composition of martian volcanoes. The project has three approaches: (1) the study of terrestrial basaltic landforms, (2) modelling experiments, and (3) study of imagery from Mariner 9 and Mariner Viking (when available). This paper deals with terrestrial landforms and extrapolates to Mars.

The Rio Grande rift of New Mexico, with as much as 8 km of structural relief, has been compared to an incipient oceanic spreading center, an interpretation not unlike that proposed for the Coprates-Marineris canyon system of Mars. Basaltic volcanism has been widespread within the Rio Grande rift and on its flanks. Within the rift (except at cross fractures), basalts tend to be tholeiitic and to differentiate along calc-alkalic trends. Outside the rift, basalts are more varied. Some fields are tholeiitic to calc-alkalic, others alkalic. Three areas of detailed study are: (1) the Taos Plateau within the Rio Grande rift, of tholeiitic and calc-alkalic rocks (Eppler), (2) the White Rock Canyon area near Los Alamos, where the rift undergoes 30 km of right-lateral displacement in an area of alkalic as well as tholeiitic to calc-alkalic volcanism (Aubele), and (3) the northern part of the Mount Taylor volcanic field, well outside the rift, with alkalic volcanism (Crumpler). There, representatives of the basanite-hawaiite-mugearite-benmorite-trachyte-phonolite suite have been found for the first time in North America.

The rocks of all three localities are between 1.4 and 4.3 m.y. old. The effects of degradation can be compared with basalts as young as 1,000 years (McCartys, Carrizozo, Bandera) and as old as 20-30 m.y. (Mogollon Plateau). In the semi-arid climate of New Mexico, basaltic rocks resist erosion.

The landforms and slope angles of volcanoes made up of lava flows (as opposed to cinder cones) depend on:

A. Viscosity - the more viscous the flow the steeper and more convex the slopes of volcanoes. Viscosity depends on:

(1) Composition

(a) Calc-alkalic lavas: viscosity and slope angles increase in the sequence tholeiite-andesite-latite-rhyolite (Taos field).

(b) Alkalic lavas: viscosity and slope angles increase in the sequence basanite-hawaiite-mugearite-benmorite-trachyte (Mount Taylor).

(2) Proportion of glass

(a) Glassy latite flows are thicker and more viscous than stony flows (Taos field).

(b) Glassy trachyte flows are less viscous than stony trachyte flows (Mt. Taylor).

(3) Temperature of flows

(a) Glassy trachyte flows have oligoclase phenocrysts; stony trachyte flows albite phenocrysts. Glassy flows were hotter, which explains their lower viscosity.

B. Degradation - zonation makes it possible to measure the rate of degradation of individual flows. Many fresh basalt flows have a glassy (tachylite) crust, about 2-3 mm thick, a frothy top, about 20 cm thick, a vesicular zone, about 30-60 cm thick, and a massive interior. The following degradational series can be observed (fig. 1):

(1) McCartys, Bandera, Carrizozo flows, age, 1,000-2,000 years: Glassy crust spalls off in chips 2-3 cm long. Depth of erosion about 2-3 mm.

(2) Flow beneath McCartys' flow and Jornada flow, south-central New Mexico, age about 10^4 years: Glassy crust gone, frothy flow tops broken into cobbles. Depth of erosion about 2-5 cm.

(3) Albuquerque volcanoes, age $190,000 \pm 50,000$ years: No cobbles of frothy material, flows worn down to the vesicular zone. Depth of erosion is about 20-30 cm.

- (4) Basalt of Cebolleta Mesa (Mt. Taylor) and Caja del Rio (Whiterock Canyon), about 2.5 m.y. old: Vesicular zone broken into irregular polygons or into local lag deposits. Depth of erosion 30-80 cm.
- (5) Servilleta Basalt (Taos field), age about 4 m.y.: Vesicular zone removed. Depth of erosion about 1 m.
- (6) Bearwallow Mountain Formation (Mogollon Plateau), age 21 m.y.: Vesicular zone and part of massive zone removed, depth of erosion erosion probably 1-3 m.

Erosion rates evidently decay exponentially. Lag deposits act as a protecting cap; in general there is little runoff on highly permeable basalt surfaces. Basaltic volcanoes, 20-30 m.y. old, of the Mogollon Plateau retain recognizable volcanic landforms; rhyolite lava domes of the same age do not. The stability of basaltic surfaces holds only for flat divides. Undercutting along retreating escarpments and channels causes rapid erosion. The Taos Plateau has been dissected by the Rio Grande gorge, more than 300 m deep; the northern Mount Taylor volcanic field caps a mesa 400 m high.

Positive features of solid basalt, such as pressure ridges, degrade about an order of magnitude faster than flow tops. The rate of degradation also decays exponentially. Pressure ridges, originally up to 10 m high, are distinctly subdued in the Albuquerque volcanoes (10^5 years) and are absent on Cebolleta Mesa (10^6 years). Cinder cones, once more than 100 m high, have lost tens of m on Cebolleta mesa and have worn down to stumps, 10-15 m high on the Mogollon Plateau.

Negative features, such as maar craters and collapse craters, last longer than positive features. The solid-rock parts of their rims degrade at the slow rate of lava flows. Infilling and ablation of wind-blown sand eventually reach a steady state.

In conclusion, the variety of slope angles of volcanoes on Mars suggests magmatic differentiation. The trend, calc-alkalic or alkalic, cannot be determined uniquely. On Earth, andesitic flow domes of the White Rock Canyon area and trachytic flow domes of the Mount Taylor field have similar morphologies, presumably because lavas had similar viscosities.

It is risky to extrapolate degradational processes from Earth to other planetary bodies, but it is reasonable to suppose that basalt is a resistant rock on Mars, in a climate even more arid than that of New Mexico. In the humid parts of Hawaii, basalt degrades about two orders

of magnitude faster than in New Mexico; it is not unreasonable to assume rates about an order of magnitude slower for Mars. The wealth of surface detail visible on Olympus Mons does not prove its youthful age and is not in contradiction to the high degree of erosion implied by the escarpment around its base.

With these considerations, it is possible to place constraints on the age of visible features on Mars, all of them larger than tens of meters, the minimum resolution of Mariner 9 B-frames. Using New Mexico erosion rates, flow levees and ramparts of Olympus Mons, tens of meters high, would degrade below resolution in 10^7 years. In tectonically stable areas, crater rims of solid basalt, hundreds of m (10^5 mm) high, would not erode below limits of resolution in the life of the solar system. If actual erosion rates are an order of magnitude slower, Olympus Mons could be as old as 10^8 years. Craters tens of m deep would be preserved since the end of the intense-bombardment stage of planetary history.

Basaltic surfaces are not the only ones protected from erosion by lag gravels. Ejecta blankets around impact craters have the same effect, as shown by pedestal craters. Quantitative scales for dating craters and other landforms of Mars by progressive degradation may be more nearly exponential than linear.

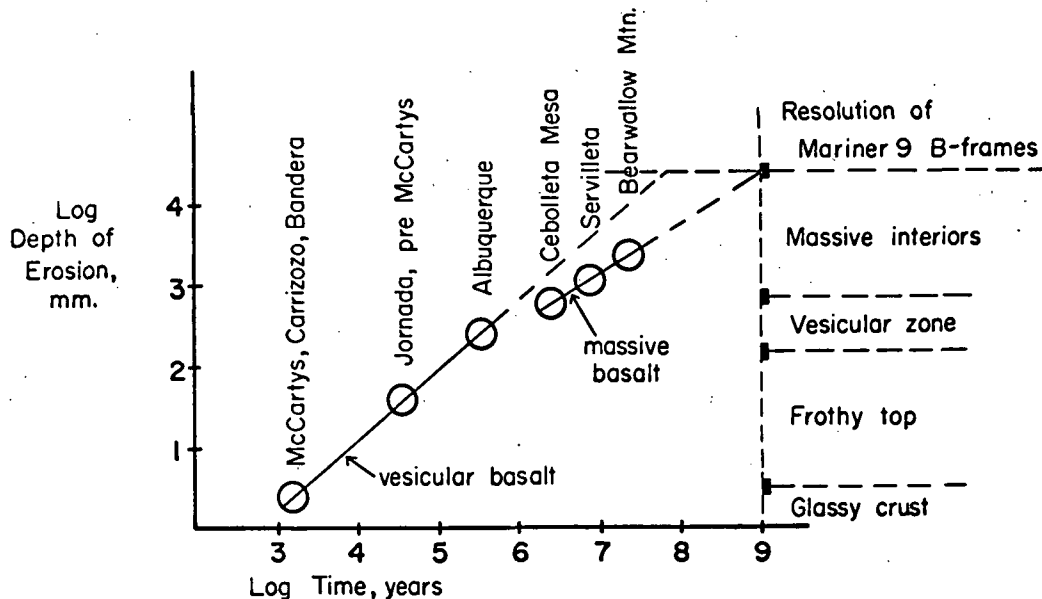


Fig.1 Erosion Rates of Basalt Flows, New Mexico

MARTIAN KNOBBY TERRAIN

J. E. Guest, R. Greeley, and P. S. Butterworth
University of London Observatory

Knobby terrain occurs in a number of regions on Mars and consists of swarms of hills, each hill being several kilometers long with an elliptical plan and of the order 1 km high. There is a close association of knobby terrain with scarps, particularly along the great circle boundary between the southern cratered highlands and the younger northern plains. It appears that knobby terrain is associated with scarp retreat and since the mechanism of scarp retreat on Mars is not yet fully understood the relationship between knobs and scarps may provide an important clue to the nature of both scarp retreat process and the three-dimensional structure of the units through which the scarps have retreated.

Our study is based on an examination of the Casius and Ismenius Lacus area together with preliminary studies elsewhere. In some other areas, knobs have different forms, often being less elliptical, and it should be emphasized that there may be more than one way to produce knobby terrain; thus, the arguments presented here may not be applicable planet-wide. In this paper we consider both aspects of knobby terrain: the origin of knob morphology and the origin of the material of which the knobs are composed.

Photogeological evidence suggests that knobs consist of more resistant material than the main rock unit affected by scarp retreat. Knobs are therefore considered as a separate rock unit that underlies the material making up

the main scarp; alternatively, they may be a more resistant facies within it, or younger volcanic extrusions or intrusions. Studies show that the original form of knobs as they appear in front of the scarp is structurally controlled; with increasing time of exposure they develop a form related to the present dominant wind directions.

VOLCANIC FEATURES AND FRACTURE SETS OF THE SOUTH CENTRAL SNAKE RIVER PLAIN, IDAHO

John S. King
State University of New York at Buffalo

and

Ronald Greeley
University of Santa Clara and NASA Ames Research Center

The Snake River Plain of Idaho has been described as a continental rift. It is a wide depression of low relief dominated in the central and eastern portion by a thick sequence of lava flows estimated to total in excess of 2000 m. Individual flows vary in thickness from 3-10 m and have originated dominantly from point source vents. The present plain is thus an accumulation of coalescing broad low shields which mark the most recent point sources. Youngest known ages of the lavas are about 2000 years B.P. and are associated with the King's Bowl Rift.

The south Central Plain is dominated by the Great Rift System otherwise known as the Idaho Rift System which is a northwest-southeast series of en echelon fractures extending from Craters of the Moon National Monument south for more than 100 km. Several rift zones or fracture sets have been designated among these tensional fractures. Most recently three subparallel fracture sets have been identified in the vicinity of the Crystal Ice Cave and have been designated from east to west as (1) the Inferno Chasm fracture set, (2) the Queen's Bowl fracture set, and (3) the King's Bowl fracture set. On the basis of geomorphology and superposition, these fracture sets appear to become younger to the west. This suggests that eruptive

activity shifted westward through time. This conclusion is at least in part reinforced by the degree of degradation and softening of features due to weathering in rocks exposed along the fractures in the Queen's Bowl fracture set as compared with those of the King's Bowl set. No comparison has as yet been made with the Inferno Chasm set.

Vents and collapse depressions are often aligned along these fracture sets and many of these show evidence of late stage lava lake activity. Several large depressions characterize the Inferno Chasm fracture set. Wildhorse Corral is a large, irregular depression 1 km long by 600 m wide and 50 m deep. Terraces on the crater wall which have resulted from slumping and lava lake subsidence coupled with vestiges of lava tubes and channels suggest a complex eruptive sequence. South of this on the same fracture set is located Cottrell's Blowout which is a narrow, elongate collapse depression 590 m long by 170 m wide and 40 m deep. Cottrell's Blowout surmounts a low shield and lava flows emanating from the Cottrell's source are of limited areal extent. Inferno Chasm itself is an irregularly circular vent some 175 m in diameter and about 20 m deep. A large lava channel narrows and becomes shallower as it curves generally to the west over a distance of some 1400 m. A sequence of flows exposed in section in the channel walls show a repeated use of the channel by flows through time. These three vents which align along the Inferno Chasm fracture set each indicate a sequence of eruptions from the point sources. As yet no indication has been established as to the length of time the vents were active nor has the eruptive

sequence between these vents been established. It is highly unlikely that they were simultaneously active however and a migration of activity has been recognized along the younger King's Bowl Rift to the west.

The southern end of the Great Rift System is marked by the young Wapi lava field which covers approximately 450 km². The Wapi field consists of a lava shield characterized by a hummocky pahoehoe surface containing well-developed pressure ridges, lava plateaus and collapse depressions. This lava shield makes up and dominates most of the Wapi field. In the northeastern portion of the field, a lava cone known as Pillar Butte marks the summit of the field. The cone is dominantly composed of aa with some associated pahoehoe.

THE DEPENDENCE OF TOPOGRAPHY ON VOLCANIC PROCESSES WITHIN THE EASTERN SNAKE RIVER PLAIN, IDAHO

John F. Karlo and John S. King
State University of New York at Buffalo

The Snake River Plain is a continental rift crossing southern Idaho. The geology of the province is dominated by basaltic volcanism with topographic modification dominantly the result of eolian processes. In an effort to better understand this province, the geology and the Bouguer gravity field of an area of approximately 700 square miles surrounding the Hell's Half Acre lava field southwest of Idaho Falls was mapped.

The Hell's Half Acre lava field is a young feature, on the order of 2000 years, which is surrounded by older basalts ranging in age from pre-Pinedale to just pre-Hell's Half Acre. The basalts vary petrographically from dark varieties with olivine phenocrysts to lighter porphyritic basalts highly charged with plagioclase phenocrysts. This variation is probably the result of discrete chemical differences resulting from subsurface differentiation. The non-porphyritic fine grained basalts are interpreted to be more primitive non-evolved basalts whereas the porphyritic basalts with plagioclase phenocrysts are interpreted to be chemically evolved. The basalts have been divided into about 40 flow units based on petrologic variation and flow morphology characteristics. A general chronology has been worked out on the basis of topographic changes accompanying gradual accumulation of loess on the flow surfaces.

A broad northeast-southwest trending fracture zone along which a concentration of vents occurs crosses the northern part of the study area. The vent concentration has produced a major topographic swell which has apparently existed over a very long period as evidenced by published subsurface data. The fracture zone is characterized by a distinct negative gravity anomaly and by chemically evolved basalts. Other vents not associated with the fracture zone occur along northwest-southeast trending lineaments and are characterized by more primitive basalts. The lack of gravity anomalies associated with these vents suggests that they may be relatively transitory features.

The filling of the Snake River Rift has often been described as progressing through a series of fissure eruptions such as those at the Craters of the Moon volcanic field. However this may be an oversimplification and overemphasis of a single feature. Although almost all vents within the study area can be correlated with some form of fracture control, all vents are points of eruption even where a number of vents lie along the same fracture. This suggests that true fissure eruptions in the area could only have occurred as minor early eruptive phases. The growth of this portion of the Plain has thus developed largely through coalescence of broad low basalt shields.

Basalt type, topographic style, vent morphology and the tectonic setting of the vents are all correlative. The relationship

between topography and basalt type is quite marked and probably relates to bulk viscosity differences. The wide range of both size and quantity of plagioclase phenocrysts in evolved basalts suggests an equally wide range in viscosity which would explain much of the observed topographic variation. The cones of the evolved basalts are in general larger and steeper and have large circular collapse craters at the vents. These craters are regular, have steep walls, and appear to be miniature caldera-like features. The cones of the primitive basalts by comparison are broad lava domes which commonly have irregular craters at the vent. These craters are characteristically elongate in the direction of the controlling fractures either through asymmetric growth and lava lake activity or later pit cratering along the fracture.

In summary, there are two general categories of volcanoes in the region. Those which are associated with the major structure in the area are large and steep owing to the high viscosities of their associated basalts and these have caldera-like craters at the vents. Those not associated with the major structure are low, broad and have minor vent craters produced through the action of a number of small scale events.

THE CANYONLANDS GRABEN; SUBSURFACE STRESSES AND A POSSIBLE EXPLANATION FOR REGULAR SPACING

Albert W. Stromquist and George E. McGill
University of Massachusetts

In previous papers (McGill and Stromquist, 1974, 1975; Stromquist and McGill, 1975; McGill, 1975; Stromquist, in press) we have developed a model for the evolution of the graben and valley anticlines of the Needles District, Canyonlands National Park, Utah using field data plus qualitative insights derived from scale-model experiments. Building on work by Harrison (1927) and Baker (1933), our earlier studies defined the geometry of the graben, the mechanism responsible for them, and the reasons for their curvature and lateral termination. This paper outlines an explanation for the regularity of graben spacing, and also presents estimates of stresses in the brittle rocks during faulting.

The Canyonlands graben occur in a plate of brittle rocks about 460 meters thick resting on rheologically weak evaporites. The entire system is inclined 4° towards the Colorado River which has eroded a valley (Cataract Canyon) entirely through the brittle plate. Thus the brittle plate has a free face on its downdip side, but is attached along its updip side.

The only vertical stress is due to gravity, and may be computed directly using the equation:

$$S_y = Rgy \quad (1)$$

where S_y is the normal stress in the y coordinate direction (perpendicular to bedding), R is mean rock density, and g is gravitational acceleration.

Compressive stresses are considered positive. There are two components of normal stress in the x coordinate direction (parallel to bedding and to the direction of dip). The first x-component is a compressive stress due to gravity, and is given by:

$$S_{x(1)} = \frac{N}{1-N} S_y \quad (2)$$

where N is Poisson's ratio. The second x-component is a result of the component of total weight directed down the 4° regional dip, and is tensile:

$$S_{x(2)} = - \frac{W \sin 4^\circ}{A} \quad (3)$$

where W is the weight of the brittle plate, and A is the cross-sectional area of attachment. The tendency for the plate to move downdip is counteracted by its attachment along the updip side (hence the tensile $S_{x(2)}$), and by a frictional shear stress along the base of the plate. If we now permit the evaporites below the brittle plate to flow towards the free face along Cataract Canyon, the basal shear stress resisting downdip motion of the brittle plate vanishes. In fact, a reverse shear acting to pull the brittle plate downdip is possible if the evaporites extrude. The existence of the Meander Anticline along Cataract Canyon suggests that some extrusion has occurred (Harrison, 1927; McGill, 1975). The following analysis assumes that evaporite flow is just sufficient to reduce the shear stress on the base of the brittle plate to 0; the possible effects of shear due to extrusion flow will be discussed later.

The evaporites nearest the Colorado River would be the first to flow, the zone of movement expanding updip with time. Thus, the frictional

resistance to sliding of the overlying brittle plate vanishes progressively updip until the total weight of unsupported rock exceeds the strength of the rock at some point. In the Canyonlands, a graben forms, propagating upward and along strike from its point of initiation. Once formed, the graben effectively detaches the downdip segment of the brittle slab from the intact rock updip, and this detached segment is free to creep downdip under the force of gravity. Expansion of evaporite flow continues under the intact rock farther updip, repeating the process. As long as the brittle plate remains homogeneous parallel to bedding and is without unique zones of weakness, graben spacing should be uniform.

This model may be visualized as a brittle block resting on an ideally frictionless 4° incline. The block is attached at its upper end. The total force tending to slide the block down the incline is simply $W \sin 4^\circ$. This force is resisted by the strength of the block. The total force increases as the downdip length of the block is increased, but because the cross-sectional area of attachment updip remains constant, the algebraic value of $S_{x(2)}$ decreases (its absolute magnitude increases), and thus the total stress parallel to x decreases. Hence the stress difference in the rock, $S_y - S_x$, is increased. Ultimately, the block must fail.

The block will fail either in tension or in shear. If the cohesive strength is small, the stress difference will cause shear failure; if it is large, S_x can decrease algebraically until the tensile strength is exceeded. Shear failure should produce fractures with dips of about 60° ; tensional failure should produce fractures with dips of 90° . The actual faults bounding the Canyonlands graben dip 90° to a depth of 100 meters, then dip $80-85^\circ$ inward until they join at the base of the brittle plate. The inward-dipping faults

seem to consist of segments with 90° dip alternating with segments with 60° dip, suggesting a combination of shear and tensional failure.

Some rough numbers may be generated if field relationships are used to place limits on the model. Noting that the graben in the north end of the Needles District tend to be about 1000 meters apart, $S_{x(2)}$ at the moment of graben formation may be calculated using equation (3) with 2.60 as an average rock density. The absence of open joints below 100 meters suggests that the tensile strength is sufficient to support the tensile stresses existing below that level. Combining $S_{x(2)}$ with $S_{x(1)}$ calculated for a range of Poisson's ratio of .17-.33 (Price, 1974, p. 492) yields an apparent tensile strength at 100 meters depth of -11 to -18 bars. This result assumes that the joints above 100 meters open early. Thus the lower 360 meters of the brittle date must support the total weight of the plate.

Experimentally determined cohesive strengths of sedimentary rocks (e.g., Handin, 1966) are generally on the order of 100-200 bars. At the base of the brittle plate, the stress difference, $S_y - S_x$, cannot possibly cause shear failure of rocks with cohesive strengths of this magnitude because the tensile strength will be exceeded long before the shear strength is exceeded. Nevertheless, the step-like geometry of the faults suggests that some beds did fail in shear. A shear stress superposed on the base of the brittle plate by extrusion flow of the underlying evaporites helps somewhat by increasing the stress difference. For rocks with small Poisson's ratios, a moderate increase in stress difference simply increases the probability of tensional failure. Large increases in stress difference resulting from large superposed shear stresses are possible for rocks with large Poisson's ratios, thus favoring shear failure in these rocks. However, a large superposed

shear stress requires a correspondingly large rotation of principal stresses with consequent loss of symmetry of the graben. The observed symmetry of the graben suggests either that this superposed shear stress is small, or that it dies out very rapidly upsection. Thus it seems that the true cohesive strength of the weaker rock layers must be about an order of magnitude less than the generally quoted laboratory determinations.

STUDIES OF THE MERCURIAN SURFACE

Michael C. Malin
Jet Propulsion Laboratory

Mariner 10 images have provided an exciting view of the planet Mercury. Recent and continuing studies by numerous investigators will produce geologic maps of the regions photographed during the three planetary encounters. The first task of this study is to complete the geologic map of the South Polar Quadrangle (H-15), as described elsewhere (Malin, 1976). This effort will require the reduction of stereo imagery and the synthesis of these data with terrain and structural maps already prepared.

The second task of this research program will be to extend studies of the intercrater plains reported previously (Malin, 1975a). In that work, a counter-proposal to the Murray et al (1975) episodic bombardment history suggested that intercrater plains were not uniform in age or properties and hence episodic planetary resurfacing was at least as likely. It is desirable to quantify the observational bases for this counter-proposal and relate them to similar phenomena on Mars (Malin, 1975b) and the Moon. Most of the surface of the most heavily cratered regions of Mars, Mercury, and the Moon consists of these plains which separate craters. They are clearly dominant surface forms and are potentially more important than craters to our understanding of the early histories of the terrestrial planets.

STRUCTURAL ANALYSIS OF MARS

Philippe Masson
Université Paris-Sud

Lineaments visible on Mars Mariner 9 A and B frames are studied from a tectonic point of view, using a stereoscope (when stereopairs are available) and an image laser beam analyzer (Fourier transform). Several types of structures are separated. Statistical analysis of trend orientations is done for each area studied (on polar diagrams). The several trend orientations are compared and related to the geologic units to define the correlations between the several tectonic events and the planet geologic history (relationships with volcanism, aeolian deposits). Comparison with terrestrial tectonic structures is attempted especially in the Eastern Mediterranean Basin where structural analysis of grabens and main regional features is done using Landsat imagery.

In 1974 a first study of Coprates Quad. (MC 18) has been done essentially at the Center of Astrogeology (USGS, Flagstaff, Ariz.): the structures were compared to the Ethiopian Rift. In 1975 the extension of Coprates structures (essentially in Phaeniceis Lacus Quad., MC 17) were studied in France and their study is still running. A comparison with the Dead Sea Rift started in October 1975.

In 1976, study of the all Dead Sea Rift using Landsat images, and tectonic interpretation of Valles Marineris extension to the eastern part of Mars, will be accomplished to get a general idea of this Martian equatorial structure. Techniques used will be the same as these described above.

FOURIER ANALYSIS OF LANDFORMS: A COMPARISON OF FEATURES IN THE WASHINGTON SCABLANDS AND SELECTED EROSIONAL FORMS ON MARS

Dag Nummedal
University of South Carolina

and

Jon C. Boothroyd
University of Rhode Island

Years of debate about the nature of erosion on Mars has not resolved the relative importance of surface water in the geologic history of that planet. Previous analyses have considered the morphologic assemblages within the large channels and found strong indications of fluvial action. These somewhat subjective morphological comparisons, however, made it impossible to evaluate the extent of modification of proposed fluvial forms by secondary processes.

This paper presents an exact method for characterization of the planimetric shape of any landform. The method is then applied to features in the Washington scablands and selected erosional forms on Mars in an objective assessment of the degree of fluvial erosion.

The landforms to be compared are traced from topographic maps, vertical airphotos and Mariner 9 imagery. Any scale of imagery can be used. The outline is digitized and the measured points on the periphery used to express the shape by a Fourier series in polar coordinates of the following form

$$R(\theta) = R_0 + \sum_{n=1}^{\infty} R_n \cos(n\theta - \phi_n)$$

where $R(\theta)$ is the radius from the center of gravity to a point on the periphery in direction θ , R_n is the amplitude and ϕ_n the phase angle of the n -th harmonic. All computations are carried out on an IBM 370 computer system.

Different shapes give different amplitudes and phase angles for the same harmonic number. In the simplest comparison of shapes the amplitude spectrum for each feature is plotted against the appropriate harmonic numbers. For more objective studies discriminant analysis is applied permitting the classification of given shapes into previously established "shape families".

The application of this technique to features in the Washington scablands and on Mars is presently in progress. Preliminary results indicate that hills eroded in basalt, streamlined hills in the Palouse loess and dry channels or coulees have parts of the harmonic amplitude spectrum in common indicating their fluvial origin. Higher order spectral differences exist which might provide criteria diagnostic of the materials being eroded.


THE PROCTOR DUNE FIELD OF MARS: ADDITIONAL OBSERVATIONS

James E. Peterson
University of Colorado

Three Mariner 9 B-frames (DAS 08548824, DAS 09807424, and DAS 09807494) show a Martian dark splotch to be a dune field. This dune field covers an oval about 35km by 60km and is located on the floor of Proctor, a 160km diameter crater in Hellespontus at 48°S , 330°W . It was discussed in detail by Cutts and Smith (1973). They examined the B-frames stereoscopically and concluded that the large sub-parallel ridges of the field are morphologically different from simple transverse dunes, many of them having rounded crests and similar slopes on both sides. Terrestrial dunes are commonly very complex in form, in many cases being transitional between two simple forms. Therefore I interpret the major ridges of the Proctor field to be transverse dunes, possibly modified by temporary reversals (or other shifts) of wind direction.

Cutts and Smith (1973) noted that dark splotches similar to the Proctor dune field that are located in other nearby craters commonly occur on the northeast edges of the crater floors. They concluded that the crater walls acted as barriers and caused sand to accumulate at their bases, and therefore speculated that the prevailing winds blow from the southwest. Arvidson (1974) reached a similar conclusion about crater walls acting as barriers, and cited the Great Sand Dunes of Colorado (which are trapped against the windward face of a mountain range) as a probable analog. However, the occurrence of dune fields on the northwest edges of crater floors can be explained in two other ways: (1) they may be spill-in dunes drifting over the windward walls of the craters, as at Wolf Creek Crater in Australia (McCall, 1965);

or (2) they may be dunes collected against crater walls by reverse airflow within the craters (Greeley, et al., 1973). The spill-in model is thought to be in effect in the case of Proctor, which does not have a high rim or sharp rimcrest. The reverse airflow model apparently requires a raised-rim crater.

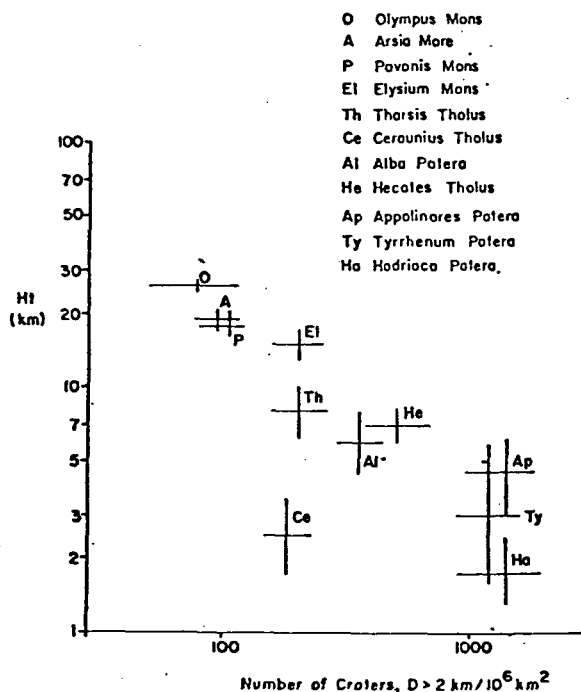
Although Cutts and Smith (1973) may be correct in their speculation about wind direction, there is evidence that they are not and that the prevailing winds responsible for the Proctor dune field (and probably for the splotches in nearby craters) blew from the northeast. The dune field itself provides most of this evidence. The northeast edge of the dune field appears to consist of one to two rows of barchans, followed by a few rows of small transverse dunes formed by gradationally coalesced barchans, followed in turn by transverse dunes which are increasingly larger in a southwesterly direction. If this interpretation is correct, the prevailing winds must be from the northeast. The small dunes along the edges of the field range in form from barchans to transverse to parabolic dunes. The typical size of the observed barchans and parabolic dunes is in the range of 400 to 700 meters wide, measured across the tips of the horns: . They are uncommonly large by terrestrial standards (though not ~~im~~possibly large--Simons (1956) reported an 800 meter wide barchan in Peru) but probably reasonable for Mars, where wind is a more important agent of erosion and particle transport than on the Earth. Individual transverse dunes in the field range up to 7km or more in length, with wavelengths of up to about 1600 meters between crests. The fact that the sizes of the transverse dunes and the wavelengths between dune crests both increase toward the southwest is further evidence of a northeasterly prevailing wind. This is typical of terrestrial dune fields, where dune sizes and wavelengths increase in the downwind direction (except at the margins of the fields, where dunes remain small in both terrestrial and Martian cases). Terrestrial examples include the Great Sand Dunes of Colorado and a North African coastal dune field shown by Smith (1963, figure 11).

Additional evidence for northeasterly prevailing winds in this area is the fact that no unambiguous wind direction indicators (streaks) within the Noachis Quadrangle result from winds with westerly components, while numerous streaks are definitely indicative of northeasterly winds.

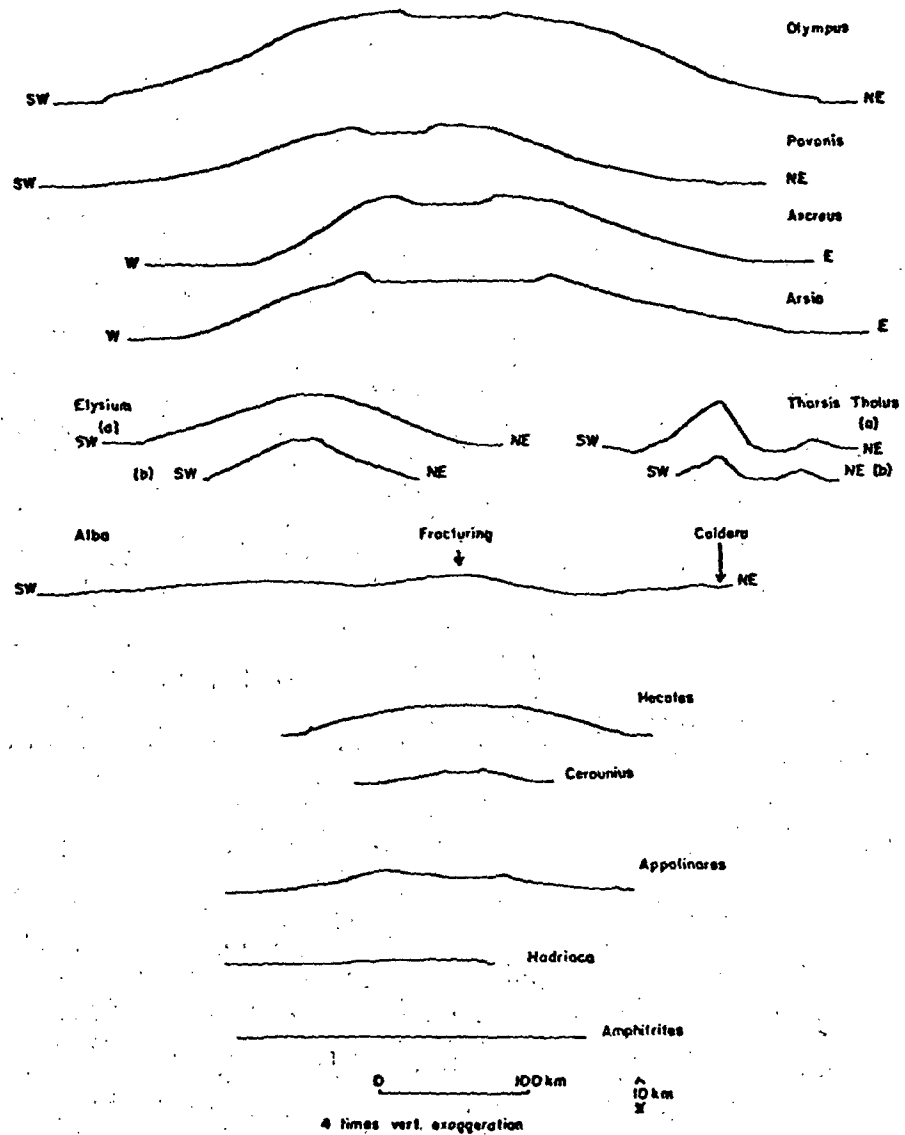
ELEVATION OF MARTIAN VOLCANOES AS A FUNCTION OF AGE

Michael H. Carr
U.S. Geological Survey

There appears to be an inverse relation between the height of Martian volcanoes and their relative age. The relatively young volcanoes of the Tharsis region, for example achieve elevations that are extremely high by terrestrial standards. In contrast the relatively old volcanoes in the Hellas region have barely any perceptible relief. From such a relationship inferences can be made concerning the history of the Martian lithosphere and viscosities of the Martian interior. Measurements of volcano heights were derived from several sources. Some were derived from published literature and maps; others were made specifically for this paper by photogrammetric and photometric techniques. Relative age was determined by crater counting. Some counts were taken from the literature but most are original. Considerable difficulty was encountered in making meaningful counts that could be used to directly compare ages. Problems arose because (1) volcanic craters cannot always be distinguished from impact craters, (2) some volcanoes are so young that statistics on even B frames is poor, (3) some volcanoes have no B frame coverage, (4) extrapolation of all counts had to be made to some reference diameter. From figure 1, which shows the results, we can see that for any particular age there appears to be a height limit to which volcanoes can grow. The younger the volcano the higher the limit. All volcanoes do not reach the height limit; several in Tharsis and Elysium fall far short of it. The height limit vs. time can be explained in several ways (1) the limit reflects the increasing thickness of the Mars lithosphere with time, (2) the older craters are isostatically compensated, (3) the composition of the lavas has changed with time, (4) the effect is statistical. The actual cause may be a combination of all these factors.



Profiles of Martian volcanoes



VOLCANIC STUDIES IN PLANETOLOGY

Ronald Greeley

University of Santa Clara and NASA Ames Research Center

Field studies of four major basaltic provinces have been underway for several years. The general objectives of these studies are to determine the criteria that permit the identification of basaltic landforms on lunar and planetary surfaces and to determine the significance that the presence of certain features has in terms of styles of volcanism and modes of lava emplacement. During the past year, field work was conducted on Mt. Etna and in the Snake River Plain, Idaho.

Mt. Etna

Work on Mt. Etna was focused on the examination of the 1614-1624 flow on the north flank of the volcano. This major flow displays large-scale terracing that in some respects is similar to terracing on the martian shield volcanoes. The objective of the study is to determine the mode of formation of the terraces and their relation to the construction of the volcano. Many of the terraces cover more than several km^2 and have relief of 100 m. In some cases the outer margins of the terraces are marked with domical structures.

Numerous lava tubes occur within the flow and it was suspected that the tubes played a significant role in the emplacement of the flow and the formation of the terraces. During the field season, one set of terraces and an associated lava tube (Grotto di Lamponi) were examined. From detailed mapping, the lava tube plunges rather deeply beneath the terrace and appears to have fed lavas to the developing terrace. Another set of lava tubes was discovered at a higher level than Grotto di Lamponi within the same terrace, but time did not permit its mapping.

Preliminary results from the work indicate that there was a highly complex interplay between tube-fed flows, hornitos, and sheet flows which built up the terraces. Some of the terrace sets are composed of imbricating terraces that appear to have been built from the bottom toward the top. Subsequent work will determine if this relation occurred throughout the flow.

A thorough study of the 1614-1624 geology and geomorphology will contribute not only to the understanding of Mt. Etna, but for shield volcanoes in general. Parts of the "upper story" of Olympus Mons display a similar small scale terracing that may have resulted from an analogous type of construction to Mt. Etna. High resolution Viking Orbiter pictures for the Martian shield volcanoes will be examined in light of these results.

Snake River Plain, Idaho

The Snake River Plain covers about 46,000 km² and consists of hundreds of small, low profile shields whose flanks coalesce. Individual lava flows (typically tube-fed) often occur between the flanks of adjacent shields. Current investigations are concentrated on field mapping and geomorphological studies in the south central part of the Plain where a series of rift systems, vents, lava tubes, and individual flows are well exposed (Greeley and King, 1975a,b). The following examples illustrate planetology applications of this work.

Small ring-moat structures (circular depressions) have been recognized in certain lunar maria regions (Schultz, 1972; Schultz et al., 1975). Three classes are identified: 1) depressed ring-moat (0.5 - 1.0 km-diameter), 2) moat (<0.5 km-diameter) encircling small dome, and 3) moat encircling dome (300 m - 400 m) with subdued summit depression. These features occur in the younger (Eratosthenian) mare basalts, typically in mare-flooded, subdued craters. Comparisons with features of similar morphology and size found in the

Snake River Plain suggest one or more modes of origin, involving in some cases multiple flows and in other cases single flows, as discussed by Greeley and Schultz (1975). Identification of specific modes of origin through comparisons of morphology provide clues to the style of volcanism involved in the emplacement of the mare lavas. For example, classification of ring-moat structures in Flamsteed and Letronne suggests that the youngest flows are probably less than 10 m thick and were erupted discontinuously.

Comparisons of the characteristics of flood basalts and shield-forming basalts with the Snake River Plain indicate that a third general type of basaltic province should be considered (Greeley, 1975), informally termed plains-forming basalts. Basaltic plains are typified by tube-fed flows (probably reflecting Hawaiian rates of eruption) erupted from point sources to produce small, low-profile shields. Vents, however, never remain fixed long enough to form large constructional features, but instead shift along rift zones to develop low relief plains on which flow features (e.g., lava tubes) are preserved. In contrast, flood basalts such as the Columbia River Plateau typically lack flow features, reflecting thick, ponded lava flows erupted at extremely high rates.

Thus, the presence or absence of certain basaltic features, such as lava tubes, provide clues to the style of volcanism involved in the emplacement of extraterrestrial basalts. For example, Mare Crisium lacks lava tubes and its basalts may have been emplaced by flood-type volcanism, while the younger lava flows in Oceanus Procellarum contain abundant lava tubes and small scale surface features typical of plains-type volcanism.

The work done on Mt. Etna is in collaboration with J. E. Guest and R. Romano; the Snake River Plain studies are in collaboration with J. S. King; the lunar mare comparisons are in collaboration with P. Schultz.

RATES OF STRUCTURAL AND LANDFORM EVOLUTION OF HAWAIIAN VOLCANOES: ROLE OF SHORT-LIVED AND CATASTROPHIC PROCESSES

Robert I. Tilling, Robin T. Holcomb, Peter W. Lipman, and John P. Lockwood
U.S. Geological Survey

The development of planetary surface features has been analyzed and interpreted largely by analogy with morphologically similar features on Earth. Most geologic features of the Earth have evolved over long time spans by gradual changes at slow rates, but some features have originated from abrupt or short-duration transformations at relatively infrequent intervals. Such contrast between essentially continuous, perhaps steady-state, processes and rapid or catastrophic changes is especially important in tracing the evolution of volcanic features, whether on the Earth or on extraterrestrial bodies.

Historic observations (ca. 1750 A.D. to present) of Kilauea and Mauna Loa, then volcanoes, indicate that major landform and structural changes do not occur gradually, but, rather, suddenly during short-lived, sporadic bursts of eruptive activity or catastrophic, seismo-volcanic events. Mapping and other geologic evidence suggest that short-duration phenomena were also important in prehistoric (pre-1750 A.D.) times: some prominent features have formed by abrupt processes at intervals too infrequent to have been observed directly.

Of the three principal processes in the development of volcanic terrane--volcanism, faulting, and erosion--only erosion may be considered as an essentially gradual, continuous, but relatively slow process. Faulting and volcanism in Hawaii are primarily catastrophic phenomena: some recent Kilauea eruptions, though long-lived by Hawaiian standards (i.e., lasting a year or longer), are virtually instantaneous within the context of geologic time. The effects of major earthquake and related catastrophic land movements are well illustrated by the events of November 29, 1975, when a 7.2-magnitude earthquake rocked the island of Hawaii. This quake, accompanied by a small tsunami, a Kilauea summit eruption, and massive subsidence and seaward movement of Kilauea's south flank, was the largest tectonic event since 1868, at which time similar events produced even greater changes. New faulting occurred along a 15 km-long zone, largely along pre-existing fault scarps. Kilauea's south flanks subsided as much as 3.5 m locally and shoreline configurations changed drastically. Preliminary geodetic measurements showed horizontal extensions of several meters across the south flank, whereas the cumulative extension for the previous 50 year interval totaled no more than 0.5 m. Moreover, following the earthquake and major subsidence, significant ground movement took place and is continuing at this writing (Jan. 1976) at rates

many times greater than those prior to the earthquake reflecting the continuing deformation.

Evolution of basaltic landforms is largely associated with short periods of peak or changing eruptive activity. For example, Mauna Ulu, the new 121 m-high satellitic volcanic shield at Kilauea, grew during a five-year eruptive interval (1969-74), long-lived in comparison to most recent Kilauean eruptions, but extremely brief relative to important geologic process. Presumably the other historic shields (Mauna Iki, 1919-1920; Heiheiiahulu, 1750?) and several prehistoric shields in Kilauea's risk zones also formed during comparably brief time intervals. The carapace of Kilauea volcano's summit region is mantled by basaltic ash deposit, mostly the products of the explosive eruption. Kilauea Caldera itself by catastrophic summit collapse may have been related to eruption of such ash deposit. However, the actual processes of caldera formation in Hawaii are poorly understood at present. That periods of ash formation and attendant drastic caldera modification were atypical events in Kilauea's recent and near-recent past is suggested by the virtual lack of similar ash layers in a 1262 m-deep drill hole about a mile south of Halemaumau. Although not known, the 1790? pyroclastic activity probably also modified the configuration and morphology of Kilauea Caldera. During the 1924 eruption, Halemaumau, the principal vent and pit crater of Kilauea Caldera, more than doubled in diameter, from about 400 m to nearly 1000 m. Large rockfalls, triggered by eruptive and/or seismic activity, can involve rim slices as great as 50 m wide and, hence, also result in abrupt enlargement of pit craters, whereas the average rim recession of Kilauean pit craters is only 0.3-0.7 m/yr under normal mass-wasting conditions.

On a more regional scale, the presently observed magma supply rate, about $0.1 \text{ km}^3/\text{yr}$ for Kilauea Volcano for the last 25 years, is an order of magnitude greater than the average supply rate (approximately $0.01 \text{ km}^3/\text{yr}$) calculated from the total volume of shield volcanoes that make up the Hawaiian chain and the known age span of volcanic propagation. This, and the smaller scale and shorter duration examples above, indicate that, while some structural and landform features of Hawaiian volcanoes are the products of nearly continuous slow processes, other major features developed as a result of poorly documented and understood short-lived or catastrophic processes that occur sporadically. Through refined photographic and geodetic documentation of active Hawaiian volcanoes, with their measurable, continuous as well as catastrophic changes, it will be possible to improve our understanding of the rates of processes that have shaped extinct volcanic terranes, including those on extraterrestrial bodies.

FLOOR-FRACTURED CRATERS ON THE MOON, MARS, AND MERCURY

Peter H. Schultz
University of Santa Clara

On the Moon, over 200 craters have been recognized that exhibit fracture systems on their floors. These craters typically are concentrated around the margins of the irregular maria and exhibit tectonic and volcanic modification. Interpretations of such craters include volcanically modified impact craters (Schultz, 1972, 1974; Young, 1972; Wood, 1974; and Brennan, 1975), rapid isostatic rebound (Masursky, 1964; Danes, 1965; Pike, 1968), and resurgent cauldrons (De Hon, 1971). Recent detailed studies (Schultz, 1976) have revealed seven different classes of floor-fractured craters. Owing to the wide range in both the diameters (10 km - over 100 km) and ages (pre-basin to Eratosthenian) of the affected craters, mare-related magmastatic adjustment of pre-mare impact craters is considered the dominant process for most -- but not all -- classes. Floor-fractured craters are believed to be important in: (1) the recognition of internal processes where other morphologic indicators (flow termini, volcanic constructs) are absent or poorly resolved; (2) the interpretation of the thermal history of the interior; (3) the emplacement sequence of the maria; and (4) understanding the style of crater modification.

Similar floor-fractured craters (total of 79) occur on Mars along the margins of the northern plains, near localized plains units, and surrounding the eastern extension of Valles Marineris (Schultz et al., 1973). An interpretation analogous to the lunar examples is proposed in which fractures generated by the impact later provide a path for magma related to extensive surface volcanism. On the Moon, one end result of floor modification is capping of the raised floor by mare basalts -- thereby producing a mare-flooded crater or ringed plain. Similarly, some smooth-floored martian craters are interpreted as lava-flooded craters rather than extensive filling by aeolian or fluvial processes.

Preliminary analysis of Mariner 10 imagery of Mercury has revealed four plausible floor-fractured craters. The paucity of examples is attributed primarily to sampling constrained by unfavorable lighting conditions and insufficient resolutions (0.5 km) over wide regions. Nevertheless, several comments can be made.

1. The region around the Caloris Basin does not exhibit floor-fractured craters. This observation is consistent with the general absence of such craters around the Imbrium and Orientale basins on the Moon owing to the destruction of most nearby pre-basin craters and mare-filling of post-basin, pre-mare craters (e.g., Archimedes, Plato). Archimedes-type craters within and around Caloris, however, are absent as noted by Strom et al. (1975).

2. A possible mercurian floor-fractured crater exhibits preserved ejecta facies and a dark floor unit that may be analogous to partly mare-flooded lunar craters. Color ratio data from Hapke et al. (1975) reveal that this crater is significantly redder than craters of similar size and preservation (nearby well-preserved craters also exhibit red floor patches and a red ejecta blanket). A similar relation exists for lunar floor-fractured craters as shown by the data of McCord et al. (1975).
3. Craters with floor-wall moats occur and lunar analogs suggest differential floor movement.
4. Ringed plains northeast of the Caloris Basin exhibit flat-topped rim profiles with inward and outward-facing scarps. Such profiles characterize heavily fractured lunar craters and mare-inundated ringed plains (Schultz, 1976).

These preliminary observations suggest that impact craters on Mercury, in addition to those on Mars and the Moon, provided paths for surface volcanism. Such an interpretation is consistent with Trask and Guest's (1975) and Strom's et al. (1975) proposal that some of the mercurian plains were internally derived. Moreover, the absence of both Archimedes-type mare-filled craters and floor-fractured craters within and around the Caloris Basin further supports the observation by Strom et al. (1975) that the time between basin formation and basin inundation was short. It is possible that the extensive plains units in this region represent a combination of molten material ejected from a molten interior and catastrophic volcanism triggered by the Caloris event.

EFFECTS OF SURFACE GRAVITY ON THE OCCURRENCE OF CENTRAL PEAKS IN MARTIAN, LUNAR, AND MERCURIAN CRATERS

Eugene I. Smith
University of Wisconsin-Parkside

A study of 193 relatively unmodified craters in the martian equatorial cratered terrain ($\pm 30^\circ$ latitude) reveals a large number of small (less than 30 km diameter) martian craters with central peaks. In fact, a comparison of these new central peak-crater size statistics with lunar central peak statistics (Smith and Sanchez, 1973), shows that below a crater diameter of 30 km a higher percentage of relatively unmodified martian craters have central peaks than do fresh lunar craters. For example, in the diameter range 10 to 20 km, 60% of studied martian craters have central peaks compared to 26% for the Moon. Previously, Gault et al. (1975) demonstrated that central peaks occur in smaller craters on Mercury than on the Moon, and that this effect is due to the different gravity fields in which the craters formed. Similar differences when comparing Mars and the Moon show that gravity has affected the diameter at which central peaks form on Mars. Erosion and other processes on Mars, therefore, do not completely mask differences in crater interior structure that are caused by differences in gravity. Above a diameter of 30 km, a greater

percentage of lunar craters have central peaks than do martian craters, and the martian and mercurian histograms begin to diverge (Fig. 1). These differences probably arise because of the erosion and/or obscuration of central peaks in martian craters above 30 km in diameter.

The central peak data for Mars contains a small percentage (15%) of central pits. Pits are usually centrally located on the crater floor, and characteristically have a diameter from 12 to 20% of the diameter of the enclosing crater. Central pits occur in craters from 10 to 60 km in diameter, and are most common in the diameter range 20 to 40 km. The conclusion regarding the effects of gravity on central peaks remains the same with or without the additional central pit data.

Other interior features of martian craters do not show effects of gravity. For example, there is a smaller percentage of less than 50 km diameter martian craters with distinguishable terraces than in lunar and mercurian craters in the same diameter range.

The data presented in this abstract suggests preferential destruction or obscuration of central peaks in martian craters above 30 km in diameter, and the preferential destruction or obscuration of terraces in craters below 50 km in diameter. This apparently contradictory observation is probably indicative of the complex nature of martian obliteration history.

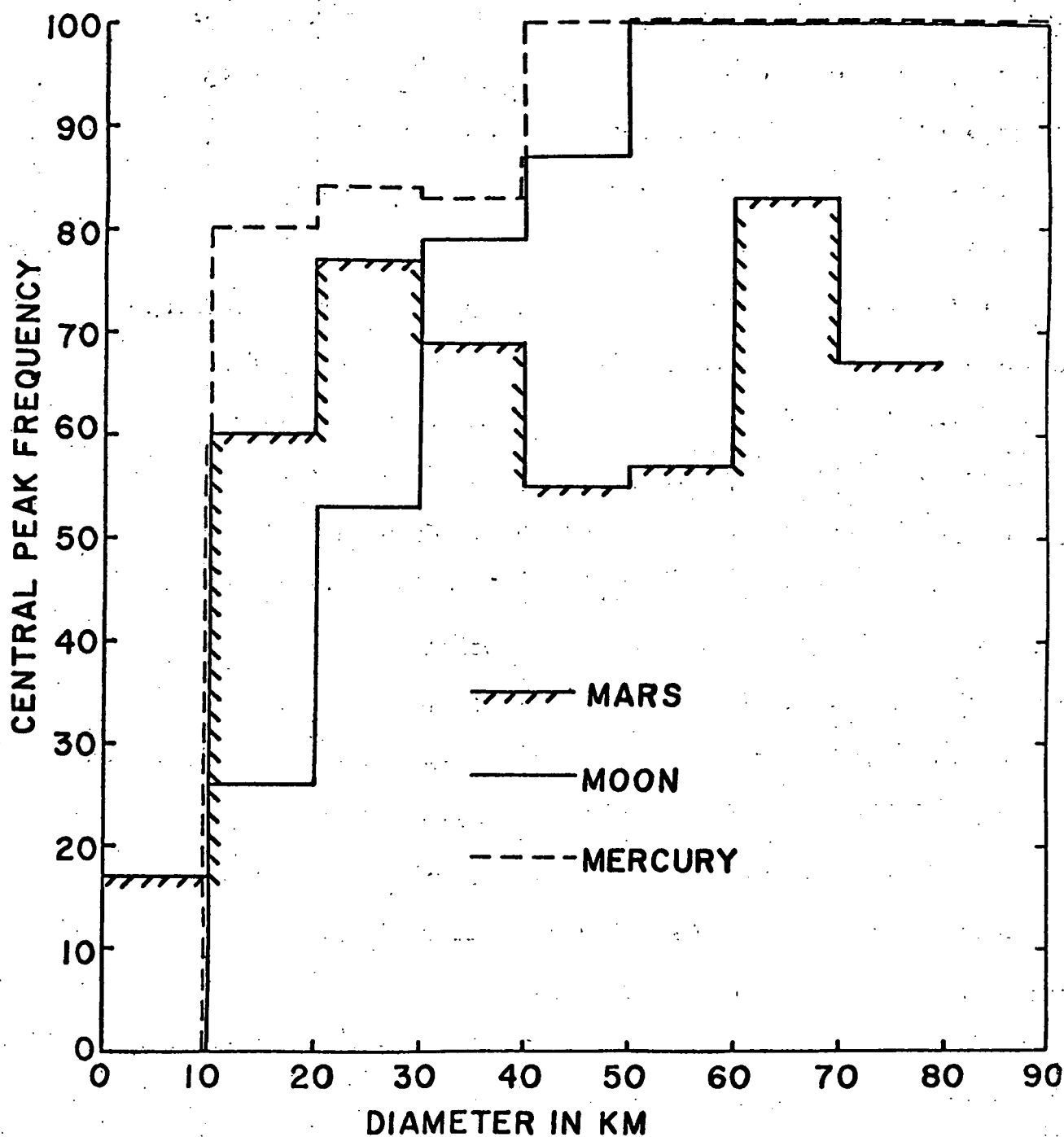


Figure 1. A comparison of central peak frequency-crater diameter histograms for Mars, Moon and Mercury. Mercury data is from Gault et al. (1975). Lunar data is from Smith and Sarchez (1973).

INTERDISCIPLINARY RAMIFICATIONS OF MARS CHANNEL STUDIES

William K. Hartmann
Planetary Science Institute

Studies of Martian channels by various Planetology Program investigators including the author have led most researchers to conclude that water flow took place on the Martian surface at some period. A massive primordial atmosphere may have been involved, but some evidence, including results found by the writer, suggest episodes of relatively recent flow, within the last half of geologic time. Other studies of crater morphology by several authors, including Arvidson, Chapman, Jones, Soderblom, and the writer have reported evidence for major surges or discontinuities in past Martian erosion rates. Chronologies based on plausible crater production rates suggest that the flow episodes and erosion events occurred on timescales equal to major changes in terrestrial climate, including apparent global warm periods such as that about 130 m.y. ago. New solar evidence suggests that models of the solar interior are inadequate, and raise the possibility of long-term and short-term variations in solar luminosity by a few percent (see review by Ulrich, Science 14 Nov., 1975). In addition, Sagan and Young and others have pointed to some astrophysical evidence of similar variations in luminosity among main-sequence stars like the sun. Four independent sources of observation, Martian, terrestrial, solar, and stellar, may thus point in the same direction. Models of the effects of solar luminosity changes on planetary climates are still in their infancy, though Sagan, Toon and Gierasch have identified theoretical runaway (non-grey-body) effects on Mars, and other

researchers have published increasing numbers of earth-models.

Therefore, researchers in comparative planetology should remain at least aware of, if not search for, possible effects of simultaneous warm and cold episodes, and attendant effects on rates of erosion and biological evolution, on planets, including the earth. Confirmation of such effects would not only clarify the climates and chronologies of other planets, but would be a major contribution of planetary exploration to terrestrial geology, meteorology, and biology.

PRELIMINARY INVESTIGATIONS OF THE PHYSICS OF MARTIAN CHANNELS

Carl Sagan
Cornell University

Evidence that Martian sinuous channels were produced by liquid water is reviewed and a distinction between channels produced by exogenous and endogenous water drawn. A comprehensive catalog of Martian channels by properties necessary to understand their physics is under construction. Under both present and past Martian climatic regimes the mean surface temperatures are likely to be well below the freezing point of water. Nevertheless liquid flow is possible both under present climatic conditions and under hypothesized more clement earlier conditions.

We find that liquid water, although it will boil or evaporate very rapidly at first under present Martian conditions, will quickly cover itself with a layer of ice due to evaporation. The ice will suppress boiling because of its weight if its pressure is above the triple point, and will greatly retard evaporation because its poor thermal conductivity prevents much of the heat from the liquid water below from reaching the top of the ice layer and increasing the sublimation rate. Under typical contemporary conditions, in a river or a body of water,

an equilibrium layer of ice nearly a meter thick will form, and the resulting evaporation rate will be about one meter per year, or somewhat more if the ice is dust-covered. Thus, under present conditions on Mars, large ice-choked rivers or bodies of water are possible, and stable over times of a year or more, and would generally resemble their counterparts in the arctic regions on Earth. The source of their water, however, would have to be eruptive in nature, such as from melting thermokarst or volcanic eruptions, since rainfall or water from melting snow is impossible under present Martian conditions. Calculations of aqueous flow in ice-choked rivers under previous high-pressure segments of Martian climatic cycling have also been carried out.

Studies on the origin of the Martian channels mainly involve comparisons with terrestrial analogues. The large braided channels resemble areas on the Earth which have been subjected to catastrophic flooding. Nirgal Vallis somewhat resembles terrestrial river valleys but was more likely fed by ground water than by rainfall. Neither of the above types of channels provide any evidence that the climate was any milder in the past on Mars, since volcanic action on buried ice has led to catastrophic floods on Earth, and a milder version could have led to the erosion of Nirgal Vallis. In fact, Nirgal Vallis

had a flow rate, which we crudely estimate from the meander wavelengths, equal to that of the contemporary Mississippi River. If the water was provided by rainfall, an absurdly large precipitation rate over the drainage basin would be required. The smaller channels, on the other hand, resemble terrestrial arroyos, produced by intermittent rainfall in arid land, and do suggest either a milder climate or localized rainstorms following volcanic eruptions.

MARTIAN CHANNELS

Harold Masursky
U.S. Geological Survey

Five types of Martian channels have been defined (Masursky, 1973). They are:

1. Broad channels that originate in areas of chaotic terrain. They vary from old to intermediate in age.
2. Medium size sinuous channels with many tributaries that arise in highland areas. They vary in age from old to young in age.
3. Small, commonly anastomosing channel networks that intertwine on the flanks of craters. They vary from very old to very young in age.
4. Intersecting arrays of rectilinear troughs modified by "fluvial" processes that occur along the northern continental margins. They vary from intermediate to young in age.
5. Distinctive channels that originate in volcanic centers. They vary from intermediate to young in age.

The first four classes show evidence of water erosion; their sinuous channels, branching tributaries, smoothly graded profiles, and braided channel floors all strongly imply formation by fluid processes. High resolution pictures show braided patterns on the channel floors that resemble terrestrial braid and bar patterns. In contrast, the fifth class of channels probably is formed by volcanic processes. Some emerge from volcanic craters (as do lunar rilles), some exhibit natural levees along the channel courses (as do terrestrial lava channels), some originate in lava fields and flow in sinuous channels without tributaries and braids. All except two of these seem unequivocally to be lava channels; the two exceptions exhibit features of both groups (water and lava) and may be composite in origin.

When the long profiles of the channels are plotted, the slopes for all except one channel appear smoothly graded without the irregular deviations that typify the lunar rilles; in one case an irregularity may be related to a later tectonic distortion of the channel. The slopes of the Mars channels are similar to terrestrial river systems.

Three techniques have been used for dating the channels. The first the standard "crater count" technique is statistically inconclusive for dating channels than for dating plains areas because so few craters are found along these linear features; therefore two new techniques have been devised. The first involves comparing the measurement of ragged edges of the channel with that of a smooth line drawn down the center of the channel. The ratio of edge to centerline measurement is the "Degradation Index": the greater the number of degradation features (such as small craters, slumps, and other mass wasting features) along the margin of the channel, the older the implied age of the channel. Degradation Index numbers for "A frames" (one kilometer resolution) and "B" frames" (100 meter resolution) of the same channel agree very closely. Very old channels are so degraded that they are barely visible; young channels have clean and pristine margins that show no degradation features.

The second new technique involves measuring the number of visible features on the channel floors. The floors of old channels are perfectly smooth; on young ones, many bars and braids are visible. The Roughness Index is a measurement of the number of features visible per unit width of channel floor. Both of these techniques are compared to age determinations of the adjacent plains regions made by the crater count method. The age of the oldest channels determined by cross-correlation of techniques is more than 2.5 billion years; the youngest are so young they cannot be dated by these techniques and are therefore considered to be recent in age.

Currently the ages of the volcanic rocks laid down at Arsia Mons and Olympus Mons are being determined by crater counting and roughness indices. These dates will be compared with ages from the standard crater flux curves and compared to channel erosion episodes. Preliminary results define at least three ages of erosion of volcanic deposits and channel erosional intervals.

One hypothesis implies that the Martian climate has alternated between the present cold or "glacial" climate and warm or "interglacial" episodes. The extensive preservation of the ancient cratered terrain, as remarked on by Murray, implies to me that most of Martian history has been dominated by the cold glacial climate, and that the total time and erosion during the interglacial periods has been small. No correlation is possible at present between martian glacial/interglacial cycles, and the earth glacial cycles that seem to occur about every 200 million years. We will continue searching for the possible 20 such episodes that may be recorded in the Mars record.

STUDIES OF THE CHanneled SCABLAND OF WASHINGTON STATE AS A TERRESTRIAL ANALOGUE TO THE CHanneled TERRAIN OF MARS

Earl Ingerson and Victor R. Baker
The University of Texas at Austin

Several recent studies have noted the morphologic similarity between certain of the exogenic Martian channels revealed by Mariner 9 and the Channeled Scabland of Washington state (Milton, 1973; Sharp and Malin, 1975; Baker and Milton, 1975). The present study extended previous work on the channeled scabland (Baker, 1973a, 1973b) to test this analogy further. Two months of field work in July and August, 1975, were used to map flood erosional and depositional features, especially in the Cheney-Palouse scabland tract that extends from Spokane, Washington, southwestward to the Snake River. For the past 4 months we have been analyzing the field data and comparing the results to Mariner 9 imagery of Martian channels.

Stratigraphy of the Cheney-Palouse flood deposits revealed at least two episodes of catastrophic Pleistocene flooding. An older flood gravel is everywhere capped by brown loess (Palouse Formation) on which is developed a 30-60 cm petrocalcic horizon. This gravel contains boulders of deep red loess of probable pre-Bull Lake age. At Marengo, Washington, this gravel is overlain by 3 loess units, each of which is capped by a calcic soil zone. These are then buried beneath flood gravel of the last catastrophic flood, dated at approximately 18,000 to 20,000 years B.P.

Flood erosion and deposition in the Cheney-Palouse scabland track were largely determined by the locations of residual loess "islands" within the main flood channel. Irregular "scabland" topography was produced by scour of the basalt bedrock in constricted reaches between the islands. Deposition, often as pendant bars

and giant current ripples, was favored at the channel expansions. The sizes of transported sediment ranges from house-sized boulders to granules and sand. Sizes decrease rapidly (1) downstream from resistant basalt ledges, (2) laterally toward the margins of a channel, and (3) in the lee of loess islands. The loess islands and occasional resistant knobs of basalt preserved a record of the flood load by forming long, streamlined "tails" of cobble- to granule-sized sediment on their downstream ends. Relatively smooth basalt surfaces with occasional basalt blocks occur below these depositional reaches.

Studies of boulder sizes deposited downstream from scabland constrictions revealed that blocks of basalt as large as 11 meters can be entrained by flood flows. Boulders larger than 0.5 meters were deposited over approximately 900 km² of the northern Quincy Basin below the Soap Lake constriction. Because the flood debris is a poorly sorted mixture of sizes, the boulders are concentrated on gravel bar surfaces only where scour has preferentially removed the finer sediment, leaving an armor of coarse particles. Flood sediment sizes decline from greater than 10 meters close to the constriction to sand and granule sizes at a distance of 35 km from the constriction.

The boulder relationships are particularly pertinent to planning the Viking A prime landing site in Chryse region of Mars. If scabland-like flooding was initiated at the chaotic terrain that occurs at the heads of Ares, Tiu, and Simud Valles (Milton, 1974; Baker and Milton, 1975), then the Chryse Planitia may be a zone of boulder deposition below the constricted Valles. These boulders would prove to be a grave hazard to the delicate Viking lander. In the channeled scabland boulder sizes decline rapidly downstream from a constriction. The precise rate of decline is related to the rate of velocity decline in the downstream expansion. The maximum distance of boulder transport encountered was 30-40 kilometers.

The streamlined loess hills of the Cheney-Palouse region are morphologically similar to streamlined features in the channels of the Lunae Palus and Oxia Palus Martian quadrangles. The ideal shape for formation by a fluid is with rounded blunt ends upstream and narrowing pointed ends downstream. The teardrop shaped islands on Mars all appear to have the proper flow orientation for floods emanating from areas of chaotic terrain. In the Chryse region, the smaller islands are long and thin, and many appear to trail downstream from bedrock projections that are 1 to 3 kilometers in diameter. Larger islands are shorter and wider. Some trail from craters 10 to 30 kilometers in diameter. Others appear to be eroded remnants of fretted terrain. Scabland analogues exist for each of these types. The scabland features appear to have required flood flow velocities of 10-15 m/sec for their formation. Some of the Martian "islands" show irregular scarps around their margins. These may have been altered by slope processes after their formation in a manner similar to the fretted terrain described by Sharp (1973).

In April, 1976, results of this project will be presented at the Cordilleran Section Meeting of the Geological Society of America, Pullman, Washington. An extensive journal article describing the research results is currently being prepared.

CRATER MORPHOLOGIES ON MARS AT MARINER 9 B-FRAME SCALES

Clark R. Chapman
Planetary Science Institute

Photogeological interpretation of Mariner 9 imagery since 1972 has led to interpretations of the evolution of different units that invoke episodes of a wide variety of geomorphological processes, some localized but others global in extent. An important technique of quantitative geomorphological analysis -- interpretation of diameter-frequency relations of different morphological classes of craters -- is here applied to analysis of small-crater populations in several different Martian units. Mariner 9 B-frames are the chief data source; some counts have been made from A-frames, supplemented by the large-crater morphology data in the Brown University catalog and earlier studies of Martian crater statistics.

Craters are classified into 4 classes representative of successive stages in degradation from "fresh" to "ghost". Frequencies are plotted in the standard incremental mode (saturation equilibrium has a -3 slope). Morphology definition is good only at diameters exceeding about 300 m, whereas B-frame counting statistics degrade at diameters of 1 to 2 km; supplementary A-frame data are most satisfactory in the 4 to 20 km diameter range.

Small-crater spatial densities are, in most cases, very low on all Martian units indicating that craters at B-frame scales have been obliterated one to two orders of magnitude more rapidly than they have been formed, on average. There are two chief exceptions to this generality: (1) secondary

crater fields, as indicated by crater morphologies and spatial relationships to nearby large craters, and (2) clusters of small, circular craters, perhaps representing nearly-simultaneous impact by swarms of bodies (comets or tidally disrupted asteroids?).

Nearly all units show a spectrum of crater morphologies at B-frame scales, implying that continuing processes are at work that degrade topography. These processes may be of a pseudo-continuous nature (e.g. aeolian deposition) at the very smallest scales, but a high degree of episodicity at the ≥ 100 -m depth scale is implied by the high proportion of fresh craters and the lack of a steady-state morphology spectrum of craters roughly 1 km in diameter. The episodic process in the pc and pm units is probably the lava flooding that produced these plains. In general, the qualitative aspects of Fig. 13 in Chapman's (1974) paper is confirmed at small crater diameters; if anything, crater degradation processes have been even less active than hypothesized by Chapman. Processes that obliterate craters 1 km in diameter or larger are active during only a tiny percentage of Martian cratering history.

The Ismenius Lacus area (Quad MC-5) displays many different terrain types indicating a variety of geomorphological processes. Cratered terrains to the south grade through dissected terrain to sparsely cratered plains to the north. Channelization is extensive. Diverse crater morphology distributions throughout this region reveal prominent local differences in both the relative efficacies of the degradational processes and in their temporal sequences.

There are preliminary indications in this area of episodic deposition, episodic cratering, and possible exhumation of craters by dissection. A very high spatial density of small, degraded craters exists south of Moreaux, and probably represents a field of secondaries from that crater.

Elucidation of the extremely complex geomorphology in several regions on Mars will require a synthesis of standard photogeological analysis with quantitative assessment of spatial and morphological parameters. The regional analyses performed in this small project exemplify the utility of the statistical analytical technique and point to the need for more systematic analysis of Mariner 9 B-frame imagery.

CRATER SIZE-DISTRIBUTION STUDIES AND DATING OF PLANETARY SURFACES

Gerhard Neukum and Beate König (H. Fechtig)
Max-Planck-Institut für Kernphysik

In dating planetary surfaces by crater statistics, it is necessary to relate frequencies of craters of different sizes to each other. This demands the exact knowledge of the distribution over a wide size range. It is further necessary to secure that the crater size distributions on the planets are comparable to that on the moon in order to apply lunar results directly in dating. We want to present some recent results on size-distribution studies and dating by crater statistics and point out unresolved problems.

1. LUNAR STUDIES

The lunar primary impact crater size-distribution was investigated in the size range between 10 meters and 500 meters. For this purpose, the superimposed craters on the young crater structures Tycho and Mösting were analysed. The distribution law is of the form $N \sim D^{-\alpha}$ (N cumulative crater frequency, D crater diameter) with α around -3 (whereas α is not constant for sizes $D > 500$ m (Neukum et al., 1975)). These measurements confirm former results (Shoemaker et al., 1970). The distribution curve seems to flatten towards 10 m crater diameter. This may be an observational effect. Comparison with mm-sized craters on lunar rocks in extrapolating the distribution from 10 meters to 1 mm yields crater frequencies several orders of magnitude too high. Therefore, we conclude that the primary production crater size-distribution actually flattens between 10 meters and 1 mm crater diameter. A slope close to -2 appears most likely.

These results together with our former ones (Neukum et al., 1975) can

be applied in dating younger structures like the Copernican and Eratosthenian craters. We analysed the crater populations on the ejecta blankets and/or in the floors of 20 of these craters. The crater classification is based on Wilhelms and McCauley's (1970) work. The results are displayed in Fig. 1. The cumulative crater frequency is plotted in reverse mode in order to produce a stratigraphical picture. The Copernican craters (C1 and C2) appear systematically younger than the Eratosthenian ones in accordance with Wilhelms and McCauley. There is, however, considerable overlap between Copernican C1 craters and Eratosthenian craters. Eratosthenian craters do not significantly differ in age from C1 craters. This relative dating that allows an absolute stratigraphical order not depending on ages of other units (like lava flows) suggests a new division of craters in only two classes: pre-Copernican and post-Copernican.

2. PLANETARY STUDIES

The impact crater size-distributions on Mars and Mercury were investigated in order to allow comparison with lunar data. The highest resolution pictures were chosen for being able to safely measure diameters as small as 800 m. The measurement areas were plains units.

RESULTS:

The Martian and Mercurian crater size-distributions are plotted in Figs 2 and 3. The lunar curve is inserted for comparison. The Mercurian distribution is as steep as the lunar one whereas the Martian distribution is flatter. This flattening appears to be real. Observational losses cannot be significant because of the sufficient picture quality. Erosion appears unlikely because of the sharpness of the craters observed.

The difference in the crater size-distributions could be due to a difference

in the distributions of the bodies responsible for cratering. This appears not so likely because the cratering on the terrestrial planets in the last 3-3.5 billion years seems to be largely due to Apollo and Amor asteroids. It is likely that these bodies with interchangeable members produce the same distribution on all terrestrial planets neglecting different impact conditions.

The effects of different impact conditions are discussed in the following. As displayed in Fig. 4, age differences or cross-section differences of Mars and Mercury with respect to the moon affect the crater size-distributions in a way different from velocity or target effects. Age or cross section differences result only in vertical shifts of the distribution curve. Velocity or target differences affect the crater sizes and result in a horizontal shift of the distribution curve. Since the distribution curve steepens close to $D = 1$ km (i.e. the exponent α in $N \sim D^\alpha$ varies), the effect on the cumulative crater frequency N is different at different crater sizes.

The average impact velocity on Mars is smaller than on the moon. Thus, for the same bodies smaller craters will be produced on Mars. This will result in a shift of the distribution to the left. When normalizing the Martian to the lunar curve at larger diameters ($D > 1$ km) the Martian curve will lie below the lunar one at smaller diameters ($D \lesssim 1$ km) because of the greater effect due to the variation of α in $N \sim D^\alpha$.

Since the impact velocity on Mercury is higher on the average than on the moon, we would have expected a steeper Mercurian distribution. The Mercury picture quality was not as high as to be safe that there could not be a deficiency of smaller craters due to observational losses. Further measurements are necessary for clarification.

The accurate knowledge of the crater size-distribution on the terrestrial

planets is necessary for application of lunar results in dating planetary surfaces. Because of the peculiar behavior of the time dependence of the impact rate observed on the Moon (e.g. Soderblom and Boyce, 1972; Neukum et al., 1975) in the last ≈ 3 billion years with little variation in cratering rate, factors of 2-3 can lead to errors in dating on the order of 1 billion years. We suggest further investigation of the crater size-distributions and the bodies (as e.g. done by Shoemaker et al., 1975) responsible for this cratering.

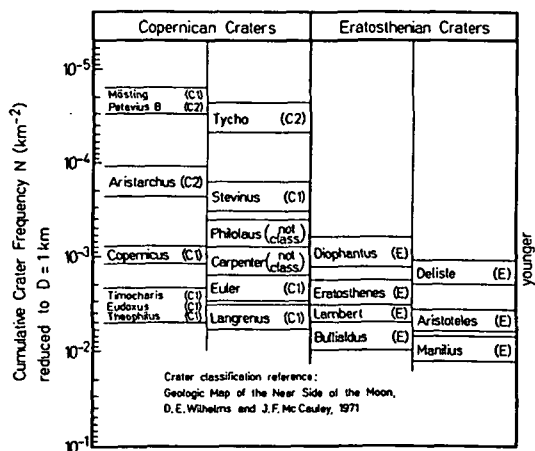


Fig. 1

Fig. 2

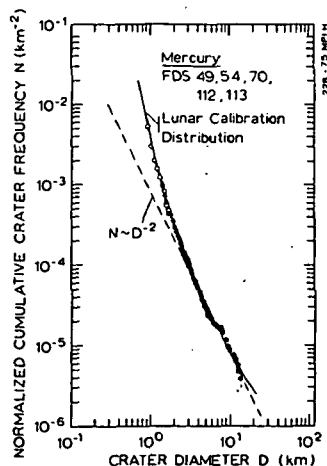
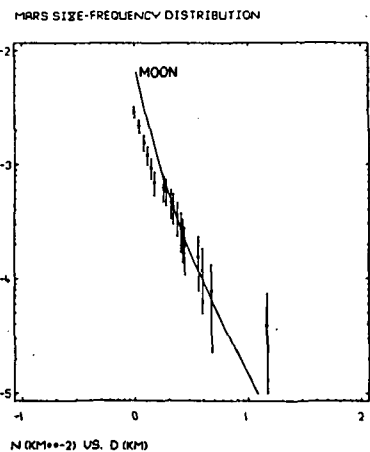
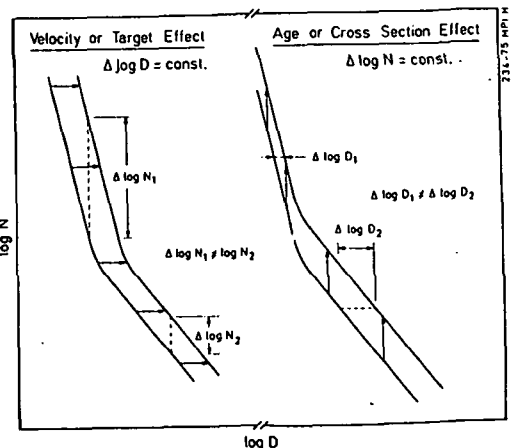


Fig. 3

Fig. 4



MERCURY CRATERS MORPHOLOGY: STATISTICS ON SELECTED AREAS

The Italian Consortium for Planetary Studies, University of Rome (M. Fulchignoni)

A morphological classification of about 5000 Mercury craters ($D > 20$ km) has been carried out. Craters have been morphologically identified and classified in several groups. The used classification criteria are based on the current literature.

Planet-wide distributions of each different class have been computed and compared with the general trends of planetary cratering.

A geological interpretation based on the above mentioned classification has been tempted in some selected regions.

Some evolutive implications have been speculated in comparison with the evolution of the terrestrial planets. Different modes of erosion are suggested.

CALORIS-AGE CHANGES IN MERCURY'S CRATER POPULATIONS

D. E. Gault, J. E. Guest, and P. H. Schultz
NASA Ames Research Center

Murray et al. (1974) have shown that on the younger plains units of Mercury there is a production population of craters larger than several kilometers that exhibit a slope of about -2 (log-log size-frequency distribution) at 1% saturation as defined by Gault (1970). Populations of craters on the older, more cratered, terrains, while displaying an approximately -2 slope over a short range of crater sizes at about a 10% saturation level, show a well defined kink or change in the size-frequency distribution near 50 km diameter indicating either a deficiency or loss of smaller craters with respect to the larger craters. Although this kink could be attributed to a loss of resolution resulting from the method used to rectify the Mariner 10 imagery for crater counting, the kink also can be attributed to some process(es) eliminating or reducing a family of craters prior to the formation of the younger (post-Caloris age) plains units.

In order to study Mercury's cratering history further, therefore, we have repeated the counts for craters larger than 5 km diameter in three of the same areas reported in Murray et al. (1974), and divided the craters into three morphological classes characterizing their state of degradation from fresh, sharp impact craters: Class 1, sharp-rimmed, fresh-appearing craters with readily identifiable continuous ejecta deposits and associated fields of secondary craters; Class 2, relatively sharp-rimmed craters but with no recognizable evidence for continuous ejecta deposits or secondary craters; Class 3, degraded craters with strongly modified rims, ranging from craters with many superposed craters to those craters that are barely discernible.

Counts and classifications were performed on three distinctly different mercurian terrains as mapped by Trask and Guest (1975): Unit 1, the cratered terrain on the geological units mapped as intercrater plains and heavily cratered terrain. These two (sub)units were combined for the purposes of counting because, even though they may represent different phases in the planet's history, it is difficult to separate the two units. The cratered terrain, at least in part, is a morphological unit and does not necessarily represent a given time period. Craters larger than 30 km were mapped by Trask and Guest as heavily cratered terrain, but smaller craters of the same age may also be present on the intercrater plains units. Both (sub)units, therefore, were included as one crater-counting unit that is older than the event that produced the Caloris Planitia. Unit 2, the plains units mapped as smooth plains and hummocky plains, the latter interpreted by Trask and Guest as ejecta from the Caloris impact event. The crater counts on these plains represent younger, post-Caloris population of craters. Unit 3, the hilly and lineated (weird) terrain which is antipodal to Caloris Planitia and has been

suggested to be genetically related to the Caloris event (Schultz and Gault, 1975).

Results from our new counts are in excellent agreement with the earlier results reported in Murray et al. (1974), and indicate that although two totally different counting procedures have been employed, neither data set contains any significant procedural or subjective bias. The total counts for the cratered terrain (Unit 1) show the same change in slope at about 50 km diameter indicated in the earlier results of Murray et al. Class 3 craters comprise 60-70% of the total crater population with Class 2 and Class 1 making up about 25% and 10%, respectively. Because the Class 3 craters are the major class, the slope change at 50 km stems primarily from these older populations of craters. In marked contrast, Class 3 craters comprise only 4% of the total counts on the plains (Unit 2); Class 2 craters are generally more numerous than the Class 1 craters, but the division between the two classes is poorly defined due to statistical limitations. The crater counts on hilly and lineated (weird) terrain (Unit 3) differ from both Units 1 and 2. Although the total counts are similar to Unit 1 and are also dominated by Class 3 craters, the population of Class 1 and 2 craters is the same as their counterparts on the plains (Unit 2).

Based on these results, the crater populations on the mercurian surface at the time of the Caloris event (or earlier) can be derived by subtracting the plains' populations from the cratered terrain populations (Unit 2 from Unit 1). Similarly, the crater populations in the hilly and lineated terrain that pre-date the age of the plains can be obtained by subtracting Unit 2 populations from Unit 3 populations. These derived crater populations reveal that all Class 1 and 2 craters smaller than 20-30 km are post-Caloris in age, and that the hilly and lineated terrain is younger than the cratered terrain.

Some process(es) or event(s) either prior to or contemporary with the formation of the Caloris Planitia eliminated a population of Class 1 and Class 2 craters on the cratered terrain and totally erased all Class 1 and 2 craters on the hilly and lineated terrain. The "lost" craters were either degraded into Class 3 craters or, possibly, the fresh structures were never formed, but the abrupt change in morphologic populations suggests that the change was not the normal crater degradation caused by a steady and continuous meteoritic bombardment. Many possible explanations can be advanced including: 1) a sudden change in the flux and/or size distribution of the impacting bodies; 2) volcanic and/or ancient aeolian processes removed or modified fresh craters to Class 3 structures; and 3) the Caloris per se, or perhaps in union with other major basin forming events, caused planet-wide degradation of craterforms. Although there are awkward points to explain for all possibilities and our observations cannot positively rule out or distinguish between the various explanations, we believe that the Caloris event (in conjunction with other basin forming events???) should be considered most seriously as the agent for degrading and removing the craters in the smaller size range. In this connection it is inter-

esting to note that the hypothesis of Schultz and Gault (1975) that the weird terrain resulted from seismic jostling caused by the Caloris impact event is consistent with these crater count data. Moreover, this origin for the modification of Class 1 and 2 craters to Class 3 (or their erasure) also explains how a co-existing population of Class 3 craters would be either totally eliminated or drastically reduced. Thus the loss of the Class 1 and 2 craters, and by inference their Class 3 companions, provides an explanation for the kink in the crater size-frequency distributions at 50 km diameter for the cratered terrain. The analogy between the Caloris and Imbrium basins implies parallel effects in lunar history.

CRATERS ON THE MOON, MARS, AND MERCURY: A COMPARISON OF DEPTH/ DIAMETER CHARACTERISTICS

Mark J. Cintala, James W. Head, and Thomas A. Mutch
Brown University

Analysis of the relationships of crater depths and crater diameters can provide important information on crater formation and modification on specific planetary bodies. In addition, a comparison of depth/diameter characteristics between planets may provide clues to the important variables in both cratering processes and modification processes (e.g. surface gravity, atmospheric effects, substrate variations). This paper examines the depth/diameter characteristics of lunar and mercurian craters and compares them with new information for martian craters.

Moon - The depth/diameter characteristics of fresh lunar craters are shown in Fig. 1. The distribution of craters smaller than about 10-15 km diameter is described by the expression $R_i = 0.196D_r^{1.010}$, where R_i is interior relief or depth, measured from rim crest to floor, and D_r is crater diameter measured from rim crest to rim crest. Craters over about 15 km diameter¹ are described by the expression $R_i = 1.044D_r^{0.301}$. The change in slope at about 15 km also corresponds to diameters at which changes in crater morphology are noted. This marks the approximate boundary between simple and complex craters. Changes in fresh crater morphology and morphometry between simple and complex craters have been attributed to 1) increased significance of modification stage above about 15 km with essentially no change in the cratering process (in this case, the depth/diameter ratio for small craters would scale up to larger craters, but modification in the terminal stages of the event would produce the observed depth/diameter relationship); 2) changes in the characteristics of the cratering process, followed by modification in the terminal stages of the event (in this case, the depth of the initial cavity does not grow at the same rate as smaller craters, causing the initial crater to be shallower; modification processes in the terminal stages of the event also add to the present configuration).

Degraded lunar craters show different depth/diameter characteristics (Fig. 1). Eratosthanian and Imbrian craters appear slightly shallower than Copernican craters but pre-Imbrian craters are significantly shallower. Pre-Imbrian craters are preferentially degraded by higher flux rates and multi-ringed basin erosion, both of which tend to decrease R_i by decreasing rim height and raising the floor by impact erosion and deposition.

Mercury - Data for depth/diameter relationships for 130 fresh mercurian craters greater than 1 km is shown in Fig. 1. Distinctive differences and similarities are seen with the lunar plot (1) including a distinctive kink in the curve, at 7-8 km. The lower diameters are essentially the same as the lunar depth/diameter curve, while above the kink, the line is parallel, but at depths approximately a factor of 2 shallower than lunar craters.

Mars - Depth/diameter data for martian craters comes from photoclinometric processing of Mariner IV data and from analysis of Mariner 9 UVS data (Fig. 1). Although the sample of 155 craters presented here includes degraded as well as fresh martian craters, the population lies at depths systematically shallower than either lunar or mercurian craters. Although an inflection point appears to exist at about 10-30 km diameter, its exact placement is difficult because of the small mixed population. However, evidence from fresh crater morphology supports a change in this range and suggests that it lies at about 13-15 km diameter.

Discussion - Differences in the depth/diameter relationships between fresh lunar and mercurian craters have been attributed to differences in surface gravity (Moon=0.16 Earth's; Mercury=0.37). If surface gravity were the dominant factor in the determination of depth/diameter for fresh craters, the martian data would be expected to closely parallel the mercurian data (Mercury=0.37; Mars=0.38). Fig. 1 shows considerable differences at all diameters. Although degraded craters are included in this sample, over 14 percent are fresh or only slightly modified. Therefore, shallowness of martian craters does not appear to be due to surface gravity or long-term modification processes alone. Possible additional factors include substrate differences, atmospheric effects, and impact velocity variations.

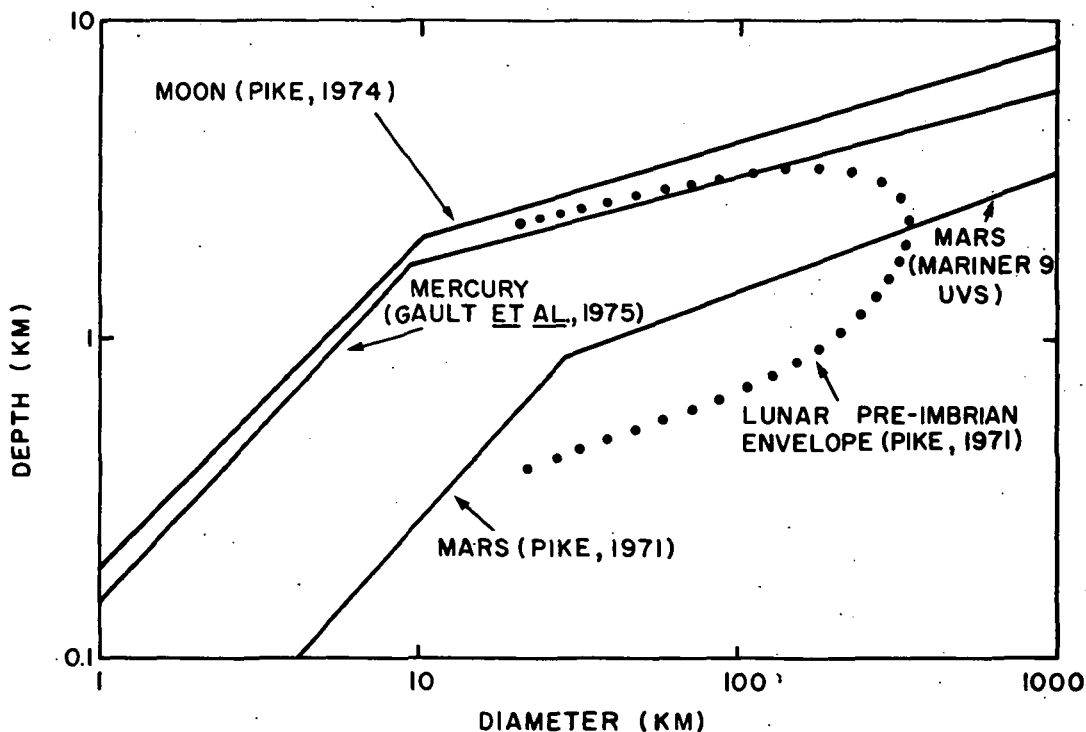


Figure 1. Depth/diameter relationships for craters on the Moon, Mars, and Mercury.

CHARACTERISTICS OF FRESH MARTIAN CRATERS AS A FUNCTION OF DIAMETER: COMPARISON WITH THE MOON AND MERCURY

Mark J. Cintala, James W. Head, and Thomas A. Mutch
Brown University

Martian craters defined as fresh on the basis of morphologic parameters stored in the Brown University Mars Crater File (Arvidson *et al.*, 1974) have been analyzed for the presence and abundance of various morphologic features as a function of size. Bowl-shaped craters dominate the fresh crater population below about 15 km (fig. 1a). The majority of fresh craters at larger diameters have flat floors (fig. 1b). The onset of central peaks occurs at about 5 km (fig. 1c). Many craters larger than 15 km have a combination of terraced walls (fig. 1d), central peaks, and hummocky floors (fig. 1e). Decreases in the relative abundance of hummocky floors and central peaks at large diameters (>50 km) may be due to small amounts of eolian infilling.

A comparison of the frequency of occurrence of terraces and central peaks as a function of diameter for Mars, Mercury, and the Moon is shown in figure 2. The onset of terraces occurs at about the same diameter on the Moon and Mars. However, the percentage of martian craters with terraces in each size class falls consistently below values for both the Moon and Mercury. A small percentage of central peaks are seen at diameters of less than 10 km on Mars, while on the Moon and Mercury, they do not occur below 10-20 km in diameter. However, martian central peaks show a slower rate of increase at higher diameters than do lunar and mercurian craters. This appears to be due to the difference in erosional processes on Mars, compared to the Moon and Mercury. Small amounts of eolian infilling may serve to obscure or bury the central peaks in many cases, while not changing the general fresh-crater appearance.

Previous investigators have attributed the differences in central peak and terrace frequencies between the Moon and Mars (Hartmann, 1972; 1973) and the Moon and Mercury (Gault *et al.*, 1975) to dissimilar gravitational field strengths. The Moon and Mercury differ in surface gravitational acceleration by over a factor of 2 (Moon, 0.16 relative to Earth=1; Mercury, 0.37). The gravitational acceleration at the surface of Mercury is approximately the same as that of Mars (0.38). Since Mars and Mercury have similar surface gravity, features such as terraces and central peaks which are thought to be gravity-controlled (Gault *et al.*, 1975) should appear at similar diameters if gravity is the dominant factor. However, central peaks appear at smaller diameters on Mars (fig. 2b) than on Mercury, and terraces appear at larger diameters than on Mercury (fig. 2a). These differences strongly suggest that, in addition to gravitational effects, other factors such as varying impact velocities at different distances from the Sun and dissimilar target and substrate characteristics may also be important.

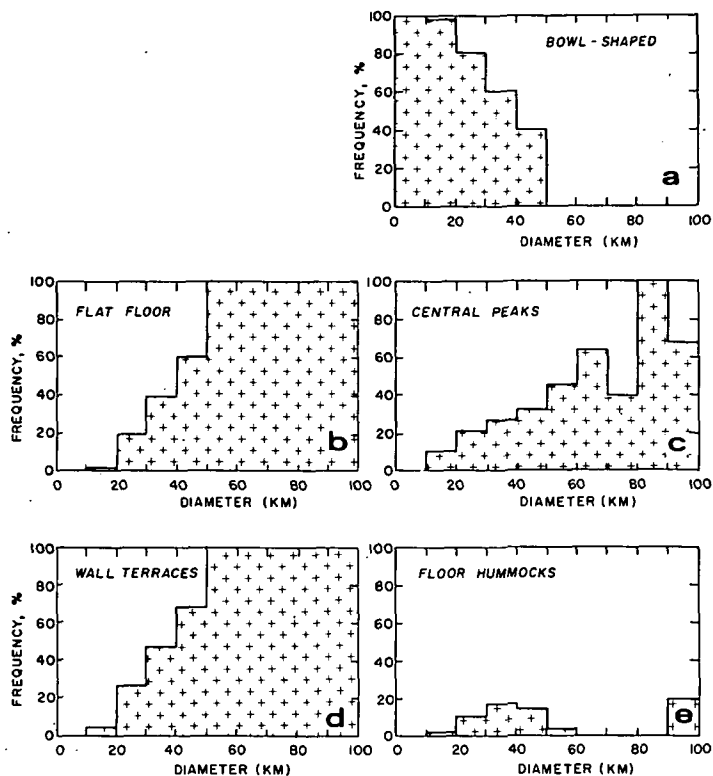


Figure 1. Morphologic characteristics of the fresh martian crater population as a function of diameter. Percentage of fresh craters with a particular feature is shown as a function of crater size (e.g., 98.5% of the fresh craters between 10-20 km diameter are bowl-shaped). a) bowl-shaped; b) flat-floored; c) central peaks; d) wall terraces; e) floor hummocks.

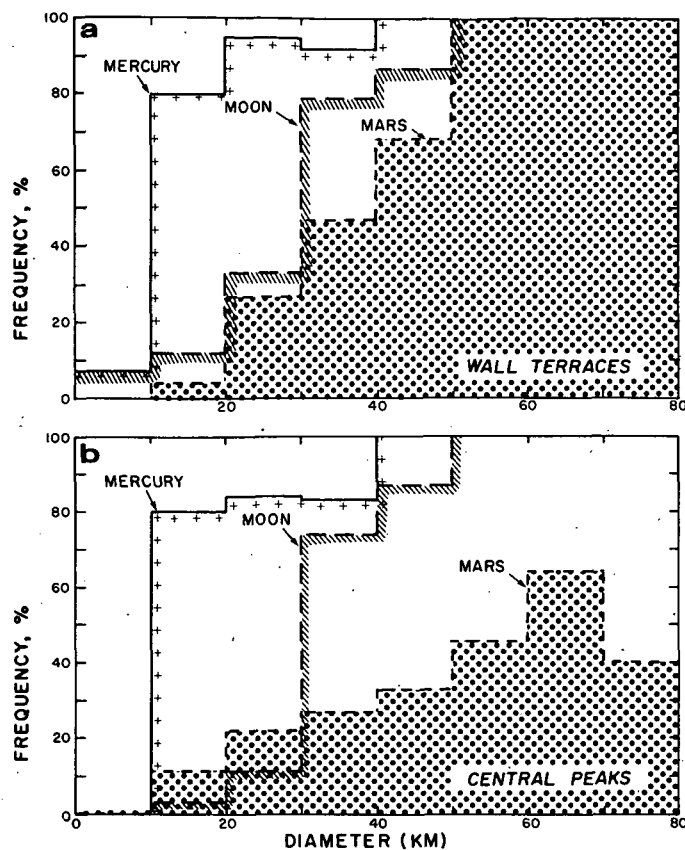


Figure 2. Comparison of Mars data with the Moon and Mercury for the frequency of occurrence of terraces (a) and central peaks (b) as a function of crater diameter (Mercury data from Gault *et al.*, 1975; lunar data from Smith and Sanchez, 1973, as modified by Gault *et al.*, 1975).

COMPARATIVE PLANETOLOGICAL ANALYSIS OF CRATERING AND GEOMORPHOLOGICAL PROCESSES

Clark R. Chapman
Planetary Science Institute

A project was initiated one month prior to the time this abstract was written to do comparative planetological studies of cratering, employing quantitative geomorphological techniques in order to understand geological processes on different units of several planets -- Mars, the moon, and, especially Mercury. This abstract describes the basis and background for the study, but few results are available at this writing since the project has only begun.

Statistical data on crater morphologies will be assembled from previously published work, from data banks (e.g. the Brown University catalog), and by new studies of spacecraft imagery. These data will be interpreted in the light of the following important comparative planetological questions:

(1) A fundamental question has been raised by Murray et al (1975) about the possibility of a distinct cratering episode on Mercury that may have been coincident with a similar event on other terrestrial planets. Although photogeological evidence cannot prove or disprove the possible occurrence of an episode in absolute time, quantitative geomorphological analysis can demonstrate whether or not an episode occurred in the ratio of the cratering/obliteration rates.

(2) The nature of the inter-crater plains on Mercury is not understood. If analogies to these units exist on the moon, then our concepts of saturation cratering must be revised. Perhaps this unit represents the primordial crust

of Mercury. Alternatively, it might post-date most of the larger Mercurian craters and be more analogous to regions on Mars created during the great erosive episode. Studies of the limits of this unit and of the nature and morphologies of the superimposed crater distributions should help to settle these questions. We may yet discover evidence of massive early endogenetic geomorphological processes (e.g. atmospheric activity) on Mercury which have been ruled out, prematurely in my opinion, by Murray et al (1975).

(3) There is renewed interest in explication of the diameter-frequency distributions of large craters on Mars, Mercury, and the moon. Recent work by Strom, Whitaker, Woronow, and others uncovers interesting observational similarities and differences among these populations. The observations have an important bearing on the interpretation of Wetherill's (1975) bombardment episode, on the interpretation of episodic oblitative histories on Mars by Chapman (1974), Jones (1974), and others, and on the topographical effects of the formation of lunar basins (Hartmann and Wood, 1971). But the interpretation of Strom et al depends on recent arguments by Woronow that (a) the production function of cratering debris in the solar system is not linear on a standard log-log frequency plot and (b) that crater-saturation plays a minor role in modifying this production function because the spatial densities of craters are too low. The first argument is inconsistent with a wide body of literature based on experiment, direct observation of the population of small bodies in the solar system, and sophisticated theoretical treatment of mutual

collisions among bodies. The second argument is based on a model that is too simplified to adequately model the complex physical reality; other theoretical models published in the literature, as well as experiments by Gault and coworkers among others, adequately demonstrate the plausibility that saturation conditions obtain in many areas on the moon, and more restricted areas on other planets, despite the fact that the cumulative crater area is much less than unity. Chapman intends to examine the new observational data in the light of the standard understanding of the production function and the manner in which various processes modify it.

POPULATIONS OF IMPACTING BODIES IN THE INNER SOLAR SYSTEM

R. G. Strom and E. A. Whitaker
University of Arizona

Lunar crater measurements, classifications, and background criteria for diameters from 7-150 km for 50% of the lunar surface, and for diameters >150 km for the entire surface, are used to generate various diameter-density curves. The much improved statistics permit the introduction of a new graphing technique which greatly facilitates both intercomparison and interpretation of the curves. In this method the graphs are normalized so that a traditional -2 slope (-3 for arithmetical bins) is a horizontal line and the ordinate ("crater density") is the fraction of any given area that is occupied by craters within the size-bin limits. This type of plot has the advantage over traditional diameter-frequency plots in that (1) departures from a -2 slope are easily detected, (2) "crater density" is a parameter readily related to such concepts as saturation and equilibrium, and (3) "crater density" values for each bin-size may be added together to obtain total crater areas from which the actual cratered and uncratered areas may be calculated.

In the diameter range used, the curves exhibit ordered variations which are not consistent with the long-held views that such variations can be fully explained through erosion and blanketing by the cratering process. Computer simulations of cratering by Woronow confirm that, with the crater densities and sequences observed, these processes produce only minor variances from the distributions of the cratering objects. Therefore, the graphs basically represent production curves and not saturation or equilibrium curves.

The structure of the diameter-density curves is consistent with two distinct populations of impacting bodies, here termed A and B. Population A

comprises two size groupings each with a -1 distribution function. Population B is characterized by a -2 distribution function. Class 3, 4, and 5 craters and probably the major basins were formed predominantly by Population A objects, while Class 1 craters (including post-mare craters) were produced primarily by Population B objects. Class 2 craters appear to be a mixture of the two populations. Based on improved counts in several areas of the Moon and their correlation with ages of dated events such as the Imbrium and Orientale impacts and the emplacement of mare basalts, it has been possible to estimate the flux of the two populations within fairly narrow limits. The Population A flux decreased from 180 impacting bodies per 10^6 years (for the crater size-range considered) to essentially zero near the beginning of mare flooding about 3.7 B.Y. ago. Population B rapidly reached a maximum flux of about 25 bodies per 10^6 years shortly after the Imbrium event (~4.0 B.Y. ago) falling to about 2 bodies per 10^6 years during the mare flooding epoch.

This identification of two separate populations is strongly supported by the notably different elemental abundances of the extra-lunar components found in lunar mare and highland soils and breccias by Morgan and others. The former are akin to primitive meteorites of dominantly carbonaceous chondritic composition and may be representative of Population B objects. The latter ancient component is found in highland breccias and soils more than 3.9 B.Y. old and does not match that of known meteorite classes. This ancient component is thought to be associated with the major basin-forming bodies and may be representative of population A objects. Thus two independent lines of evidence (geochemistry and crater statistics) support the view that two populations of bodies impacted the Moon. Furthermore, the geochemical evidence indicates these populations had different chemical compositions, as well as different size distributions, and therefore they probably had different origins.

Comparison with curves for Mercury and Mars strongly suggests that these planets have also undergone bombardment by the same two populations of bodies; possibly contemporaneously. The overall similarities between the curves for the Moon, Mars, and Mercury precludes the possibility that the deficit of smaller craters on Mars (7-50 km) is largely the result of atmospheric erosion processes.

The distribution function of Population B closely matches the present asteroidal size distribution which appears to be the result of mutual collisional breakup. This, together with the geochemical evidence previously mentioned, suggests that Population B objects may have originated from the asteroid belt. The origin of Population A is more ambiguous. One theoretical model by Hills predicts a -1 size distribution function for the larger planetoids formed during the rapid accretion in the inner Solar System, suggesting that Population B may have consisted of the remnants of these early accretionary bodies. Alternatively, Population A may represent bodies derived from the vicinity of Uranus and Neptune since, according to Wetherill, such bodies would combine the proper long life and near equality of flux on the Moon and terrestrial planets. One further possibility suggested by Woronow is that both Populations A and B represent one family of objects with a common origin, e.g., from the asteroid belt, which evolved with time from a -1 to -2 distribution function by collisional processes. However, the lunar geochemical evidence that suggests each population represents compositionally distinct objects tends to militate against this hypothesis.

CRATER SATURATION AND EQUILIBRIUM: A MONTE CARLO SIMULATION

A. Woronow
University of Arizona

Fundamental interpretations about crater formation and obliteration processes and about crater chronologies depend upon understanding the concepts of crater saturation and equilibrium; yet the literature concerning these two concepts is without consensus and is often confusing. Different authors commonly draw different "saturation" limits on their size-density plots and invoke the terms "saturation" and "equilibrium" to imply a multitude of different conditions. The literature contains definitions of saturation and equilibrium based on empirical observations of heavily cratered surfaces, on statistical models, and on physical experiments. Each of these approaches harbors its own difficulties. The empirical observations contain no a priori justification allowing the assertion that the specified surface represents either saturation or equilibrium conditions; the statistical models require considerable mathematical simplification by assumptions and approximations in order to arrive at a result; and the physical experiments suffer from difficulties in scaling and in realistically portraying the processes of cratering and ejecta blanketing.

This paper presents the results of an alternative approach to the problems of saturation and equilibrium; namely, a computerized Monte Carlo simulation. This study employs the following definitions of saturation and equilibrium:

When the function describing the crater size-density distribution on a surface no longer changes (either position or form) with the formation of any additional craters, and when the only crater destroying process is crater overlap, the surface will be said to have attained "saturation."

When the function describing the crater size-density distribution on a surface no longer changes (either position or form) with the formation of any additional craters, and when, in addition to crater overlap, crater destruction occurs by processes of erosion and filling, the surface will be said to have attained "equilibrium."

For this study, crater diameters are generated on a continuum according to the generating function $N=b \cdot D^{-a}$, where $-a$ is the generating function's "slope index."

Saturation Study: Histories for crater populations resulting from generating functions with slope indices of -3, -2, and -1.5 were examined. In each case the final size-density distribution of craters differs from that of the generating function.

The case where the generating function has a slope index of -3 probably schematically represents all cases with slope indices significantly less than -2. Examination of the printout from these runs reveals that at the 99% confidence level, beyond $T=7$ (i.e., 7 craters in the diameter range 4 to 32 km per 100 sq km), a slope index of -3 no longer represents the crater population. The hypothesis that the resultant population does not have a -2 slope index cannot be accepted at even a 90% confidence level. Of particular interest is the crater density at which saturation occurs. Ignoring transitory excursions, the area of all craters in each 2 diameter interval divided by the total surface area will not likely rise above 0.45, if the -2 slope index is maintained.

The case where the generating function has a slope index of -2 eventually results in a crater population with a slope index of -1.5. At the 99% confidence level, beyond $T=5$ a -2 slope index no longer adequately represents the size-density distribution. The position of this curve at saturation, relative to that from a generating function with a -3 slope index, shows a dearth of small craters and an excess of large craters.

The crater population resulting from a generating function with a slope index of -1.5 also increases its slope index with time. But in this case not until $T=17$, at a 99% confidence level, does the population no longer follow a -1.5 slope index. Again, with respect to results from a generating function with a slope index of -3, the final population has an excess of large craters and a dearth of small craters.

Equilibrium Study: The inclusion of the simple step function ejecta blanket has a predictable effect on the crater population. To a first approximation, the crater diameters, D , may be replaced by the product $E \cdot D$ in the equation $N=b \cdot D^{-a}$, where E is the ratio of the diameter of the crater plus ejecta blanket and the diameter of the crater alone. The size-density distribution thus becomes

$$N=b \cdot (E \cdot D)^{-a} = b' \cdot D^{-a}$$

That is, the size of the ejecta blanket affects only the density at which equilibrium is attained. The equation relating N_e , the number of craters attained at equilibrium within any size increment, to N_s the number at saturation, has been empirically determined as:

$$N_e = N_s \cdot \exp (1-E)$$

Implications: Even the most densely cratered surfaces observed, Phobos and Deimos, fall far short of having saturated surfaces. Indeed, on surfaces where ejecta blanketing is the only additional oblitative agent, one would need to assume that all portions of craters lying within six crater radii beyond a new crater's rim would be completely annihilated (an unlikely assumption) in order to claim that the observed surfaces are at equilibrium. Deposition from eolian activity has not been modeled; yet it seems unlikely that most Martian surfaces approach equilibrium conditions at crater diameters much above 10 km (although the Earth's surface may).

The manner in which a crater population curve, initially with a slope index less than -2, attains its final slope index of -2 is especially noteworthy. The most common assumption is that the generating function is directly imprinted on the surface until equilibrium is reached at a given diameter. Then the distribution is assumed to abruptly bend over and follow a -2 slope index. This study shows that the bending over occurs gradually. For the case of a -3 initial slope index, the bending initiates prior to $T=7$, becomes statistically significant at $T=7$, and is reasonably complete by approximately $T=18$. Generally, the bending occurs at densities beyond those observed on most surfaces (the lunar highlands have a model time, T , of less than 1 in the diameter range 4 to 32 km); therefore, except where sedimentation conditions increase the complexity of the problem, observed variations in the form of crater size-density distributions must result from complexities in the form of the generating functions.

DEPTH-DIAMETER RELATION FOR LARGE MARTIAN CRATERS DETERMINED FROM MARINER 9 UVS ALTIMETRY

J. Burt, J. Veverka, and K. Cook
Cornell University

We have determined the depth/diameter ratio for 87 craters on Mars using the Mariner 9 UVS altimetry of Barth et al (1974). Our sample includes craters 12 to 100 km in diameter, and 0.4 to 3.3 km in depth. The freshest appearing craters on Mars have depths similar to those of fresh craters on Mercury of comparable diameter, as expected in view of the almost identical gravitational acceleration on the two planets. However, more than half of our sample consists of craters which appear to be degraded and whose depths are significantly shallower than those of fresh craters on Mercury of similar diameter, confirming the interpretations of earlier photoanalysts (e.g. Hartmann, 1973, JGR, 78, 4096).

OPTICAL PROPERTIES OF OUTER PLANET ICES

L. A. Lebofsky and J. E. Conel
Jet Propulsion Laboratory

The visible and near-IR refractive indices of solid CH_4 and NH_3 are of importance in many applications relating to atmospheres of the outer planets and the surfaces of their satellites. We have devised methodology for determination of these constants from near-normal incidence reflectivity measurements on optically thick samples using the classical harmonic oscillator model. Recent advances in experimental procedure will be described, and results of the measurement program presented. Application of these results to interpretation of outer planet spectra will be described.

SURFACE PROCESSES ON MARS

James A. J. Cutts
Planetary Science Institute

This report contains science results based on data returned by Mariner 9, the first planetary orbiting spacecraft which was inserted into Mars orbit on November 14, 1971 and expired on October 27, 1972. The report is organized into three parts dealing with surface processes in the polar and equatorial regions of the planet Mars.

A common thread linking the three parts of the report is the issue of the eolian evolution of Mars and its relationship to the origin of the martian atmosphere and subsequent cyclic climatic change. The unexpected discovery of two impact craters with secondary crater fields reported in Part I places some important constraints on the time of creation of the Mars atmosphere and the subsequent formation of polar layered deposits. The recognition of a new type of polar landscape feature reported in Part 2 indicates that exogenic processes other than eolian and fluvial action have sculpted the landscape of Mars. This observation and a supporting analysis casts considerable doubt on the hypothesis that many martian morphological features originated during a warmer and wetter period of the planet's history.

In Part 3 of the report the nature and origin of a curious equatorial feature, which has been informally named the 'white rock', is examined. The conclusion of this examination is that the feature is a dune field composed of bright reddish sand. This is the first reasonable unequivocal indication that high albedo materials on Mars form dunes although there are several dunes of low albedo

materials and the mobility of bright materials in the form of suspended dust is well demonstrated.

This observation of a previously unrecognized type of surface material is relevant to a fundamental puzzle in the eolian evolution of Mars. On the one hand there is abundant morphological evidence for excavation of massive amounts of materials, transport to the poles and subsequent reerosion. On the other we have the very dynamic and visible effects of the shifting sediments on Mars. Yet, with few exceptions, there is no obvious relationship between the manifestations of shifting sediments as albedo markings and the net long term transport of material from place to place on Mars. What is the nature of this transport? From where do the shifting sediments originate and do they merely migrate to and fro across the surface or are they preferentially trapped in some locations? These are issues which must be seriously addressed in concert with the emerging plans for in situ compositional measurements on Mars and the orbital mapping of elemental abundances.

PLANETOLOGY STUDIES: MARTIAN VOLATILE STUDIES

F. P. Fanale
Jet Propulsion Laboratory

During the past year, an extensive study of the implications of currently available data on the martian atmosphere and regolith for martian volatile history and also the role of Viking measurements in elucidating that history has been completed.

Observations of Mars and cosmochemical considerations imply that the total inventory of degassed volatiles on Mars is 10^2 to 10^3 times that present in Mars atmosphere and polar caps. The degassed volatiles have been physically and chemically incorporated into a layer of unconsolidated surface rubble (a "megaregolith") up to 2 km thick. Tentative lines of evidence suggest a high concentration ($\sim 5 \text{ g/cm}^2$) of ^{40}Ar in the atmosphere of Mars. If correct, this would be consistent with a degassing model for Mars in which the martian "surface" volatile inventory is presumed identical to that of Earth but scaled to Mars' smaller mass and surface area. The implied inventory would be: $^{40}\text{Ar} = 4 \text{ g/cm}^2$; $\text{H}_2\text{O} = 1 \times 10^5 \text{ g/cm}^2$; $\text{CO}_2 = 7 \times 10^3 \text{ g/cm}^2$; $\text{N}_2 = 3 \times 10^2 \text{ g/cm}^2$; $\text{Cl} = 2 \times 10^3 \text{ g/cm}^2$; and $\text{S} = 2 \times 10^2 \text{ g/cm}^2$. Such a model is useful for testing, but differences in composition and planetary energy history may be anticipated between Mars and Earth on theoretical grounds. Also the model demands huge regolith sinks for the volatiles listed.

If the regolith were in physical equilibrium with the atmosphere, as much as 2×10^4 g/cm² of H₂O could be stored in it as hard-frozen permafrost, or 5×10^4 g/cm² if equilibrium with the atmosphere was inhibited. Spectral measurements of martian regolith material and laboratory measurement of weathering kinetics on simulated regolith material suggest large amounts of hydrated iron oxides and clay minerals exist in the regolith; the amount of chemically bound H₂O could be from 1×10^4 to 4×10^4 g/cm². In an Earth-analogous model, a 2 km mixed regolith must contain the following concentrations of other volatile-containing compounds by weight: carbonates = 1.5%, nitrates = 0.8%, chlorides = 0.6%, and sulfates = 0.1%. Such concentrations would be undetectable by current earth-based spectral reflectance measurements, and (except the nitrates) formation of the "required" amounts of these compounds could result from interaction of adsorbed H₂O and ice with primary silicates expected on Mars. Most of the CO₂ could be physically adsorbed on the regolith.

Thus, maximum amounts of H₂O and other volatiles which could be stored in the Mars regolith are marginally compatible with those required by an Earth-analogous model, although a lower atmospheric ⁴⁰Ar concentration and regolith volatile inventory would be easier to reconcile with observational constraints. Differences in the ratios of H₂O and other volatiles to ⁴⁰Ar between surface volatiles on the real Mars and on an Earth-analogous Mars could result from and reflect differences in bulk composition and time history of degassing between Mars and Earth. Models relating Viking-observable parameters, e.g. (⁴⁰Ar) and (³⁶Ar), to the time-history and overall intensity of Mars degassing are given.

Current efforts are largely concerned with obtaining new data on CO₂ and H₂O adsorption on likely martian regolith materials is in progress. An

experimental study of the problem (carried out entirely with the support of this task) was published in 1974. This study dealt with the inventories of CO_2 and H_2O anticipated to be adsorbed in the martian regolith and the effects of surface insolation variations on regolith-atmosphere CO_2 and H_2O exchange, thus the effect on atmospheric and near-surface conditions. Several workers have subsequently attempted to utilize this data to explain known atmospheric phenomena such as the seasonal variation in total pressure and the recently reported diurnal variations in atmospheric H_2O content. In particular, the regolith-atmosphere exchange of CO_2 consequent on seasonal insolation variations has been invoked by investigators to explain observed seasonal variations in the total atmospheric pressure that do not correlate in magnitude or phase with those expected as a consequence of cap advance and retreat alone. Also, the H_2O exchange results published were used by other investigators to explain quantitatively sharp diurnal variations in the atmospheric H_2O content that were poorly explained by models involving only surface frost condensation. Our current experimental studies are directed toward improving the validity with which adsorption data can be applied to such problems: 1) we are obtaining CO_2 adsorption isotherms on materials other than basalt (including hydrated iron oxides) and CO_2 isotherms on basalt and other materials at temperatures lower than those for which data is currently available, and comparable to temperatures in the season-latitude regime (near the edge of the polar caps) where most of the CO_2 exchange is thought to be taking place; 2) we are obtaining data on the interaction between CO_2 and H_2O adsorption (e.g. the effects of an adsorbed clathrate phase) so that CO_2 and H_2O adsorption may be modeled under completely realistic martian surface conditions.

MARTIAN SOURCE CRATERS

Robert H. Stockman
Brown University

A planet-wide survey of source craters defined herein as craters which have channels originating at the crater, breaching the crater rim, and extending a substantial distance from the crater has been accomplished by use of Mariner 9 A and B frames, U. S. Geological Survey photomosaics, and the Brown University Mars Crater File (Arvidson *et al.*, 1973). Statistical treatment of morphologic data emphasizes the uniqueness of source craters, and suggests the time and mode of their origin.

A total of 64 source craters has been identified. Channels of obvious volcanic or structural origin are excluded, although some channels, especially those issuing from craters along the border of the cratered highlands, may be controlled by the regional structure. Of the 64 craters identified, all but two are located in the cratered highlands. Some source craters occur in clusters, and are commonly found in association with other features interpreted to be fluvial in origin.

Statistics were compiled for source craters concerning the relative abundance of raised rims, breached rims, central peaks, hummocky floors, and superimposed craters in the population. Similar statistics were compiled for all Martian craters classified according to their wall type: smooth, terraced, hummocky, and furrowed/pitted. In general, the morphologic parameters are a measure of degradation. Raised rims, central peaks, and hummocky floors characterize youthful craters and are removed by progressive erosion and burial. Breached rims are another measure of the extent of degradation of a population. Superimposed craters should be a reliable measure of a population's age.

Figure 1 shows the distributions of various morphologic parameters for source craters and for craters with the four wall types. Terraced-, hummocky- and furrowed/pitted-walled craters show a predicted correlation of degradation with age (e.g., Decrease of percent with central peaks and hummocky floors is correlated with increase of percent with superimposed craters.) Smooth-walled craters have anomalously low percentages of central peaks and hummocky floors when plotted against superimposed craters. However, on a plot of central peaks versus hummocky floors (fig. 1c) the smooth walled craters fall along the same trend line defined by craters of other wall types. This suggests that smooth-walled craters may have experienced unusually rapid rates of degradation compared to the other types, perhaps due to eolian infilling in addition to erosion.

Source craters have a highly degraded appearance although their age, as determined by superimposed craters, is relatively recent. Figure 1c shows that source craters have an unusually large

percent of hummocky floors, relative to central peaks. Most degradational processes should destroy small hummocks before larger central peaks. Perhaps slumping within source craters, associated with release of subsurface water, could produce the observed floor roughness. Slumping may also explain the anomalously high percent of breached rims relative to raised rims (fig. 1d). Whatever interpretations are brought forward to explain the data of figure 1, it is clear that source craters have combinations of morphologic parameters which separate them from other Martian craters.

The relationship of source craters to regionally mapped geologic units has been examined. There is a good correlation between the age of a geologic unit, as determined by crater densities, and the percent of craters on the unit which have superimposed (younger) craters (fig. 2). Using this superimposed crater dating technique, source craters have the same age as cratered plains (pc) units. According to Jones (1974) the cratered plains were formed contemporaneously with a planet-wide degradational event. It is hypothesized that large amounts of water were transferred from the atmosphere to the regolith at that time. Impact events penetrated a ground ice cover and released large amounts of water trapped underneath. The pooled water commonly breached crater rims and formed the channels which characterize source craters.

Models which do not relate the formation of source craters to the impact event generally can be ruled out. If such models were correct, the average age for source craters should be similar to the average age for all craters. This is not the actual case.

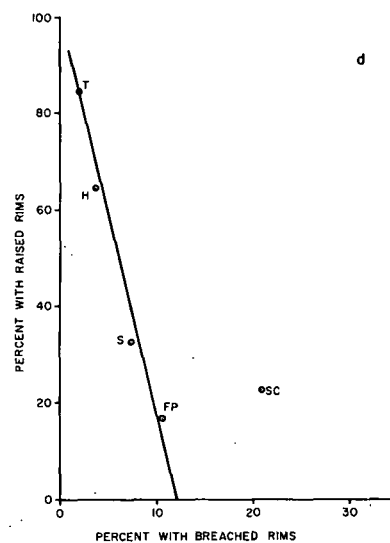
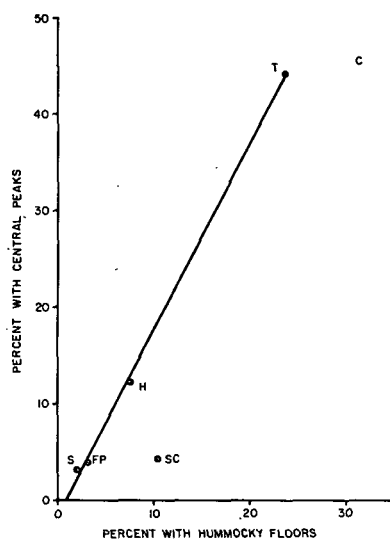
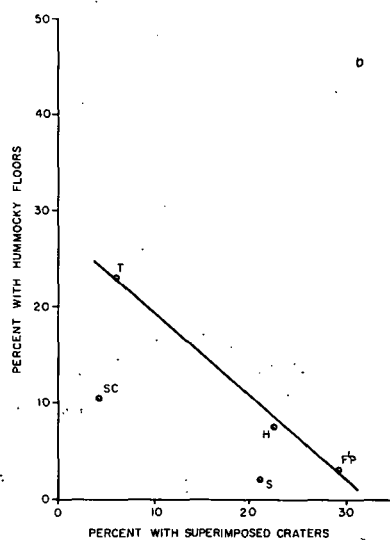
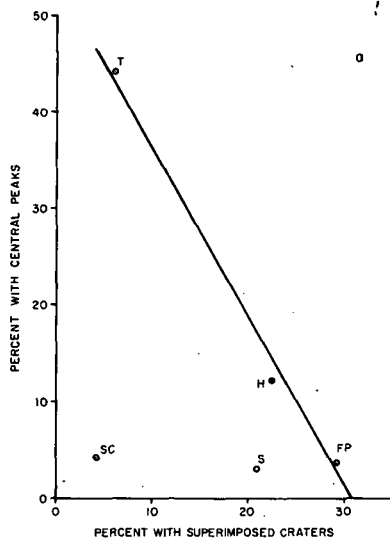


Fig. 1 - Variation in morphologic parameters for terraced (T), smooth-walled (S), hummocky walled (H), furrowed/pitted (FP) and Source Crater (SC) types.

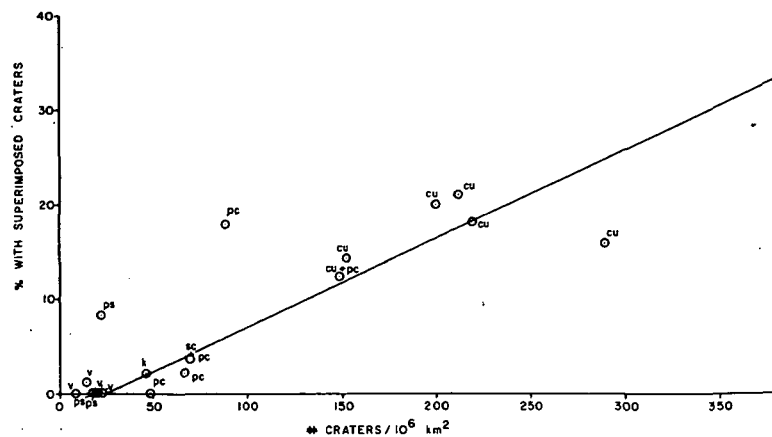


Fig. 2 - Crater density vs. superimposed craters for 18 regions of Mars. cu = cratered units, pc = cratered plains, ps = sparsely cratered plains, v = volcanic units, k = knobby terrain.

SOME CHARACTERISTIC EROSIONAL FORMS OF MARTIAN STRATIGRAPHIC UNITS

B. K. Lucchitta
U.S. Geological Survey

The major erosion and transport mechanisms on Mars appear to be wind, mass wasting under the influence of gravity, probably water at some time in the past, and perhaps ice. These processes, singly or in combination, created some characteristic erosional landforms.

Craters

Erosional forms of craters on Mars can be subdivided into craters superposed on their substrate, and those exhumed from total or partial burial. Small and intermediate-sized (approximately < 30 km) superposed craters usually retain a sharp crater rim, but the ejecta or rim deposits, where not totally removed are eroded into (1) pedestal forms with an irregular scarp around the outside of the ejecta, (2) a boxwork of hollows and ridges or (3) one or more sets of zig-zag ridges. Larger eroded craters may retain sets of curvilinear ridges on the rim, and have ejecta which forms arrays of rugged ridges and troughs in subparallel, angular or irregular arrangement. Basin deposits most characteristically remain as solitary massifs or mountain complexes. Exhumed small craters (less than about 5 km) form disks, and in some cases hummocks; many have continuous rims, and no visible ejecta. Exhumed craters larger than about 30 km consist of circles of knobs, with widely spaced knobs and hummocks both interior and exterior. Large rimless exhumed craters tend to form circular scarps.

Volcanic rocks

The surfaces of volcanic plateaus in many places show remarkably little obvious erosion, and graben walls and wrinkle ridges are generally fresh, attesting to highly resistant rock. Flow fronts on young volcanic terrain are largely uneroded, as are the surface flows on Mons Olympus. By contrast, the older shield Arsia Mons has an eroded surface of sharp and rugged shallow depressions. The grooved terrain around Mons Olympus may be an eroded shield, suggesting that erosion was more successful on formerly high shields than on level plateaus. Characteristic erosional forms exist where volcanic rock is breached, as in caldera and chasma walls: on the scarps the capping surface is lined by subparallel vertical rocky ribs and chutes underlain by smooth slopes, a characteristic landform of talus slopes developed on fairly massive rock. Chaotic landslide morphology and tureva-type slump blocks are a common feature on these scarps.

Debris mantles

Debris mantles are generally inferred to be present where plains are very smooth and uncratered, where topographic outlines are subdued, and where wind deposition features exist. Erosional forms on debris mantles appear to be characteristic: they consist of small, aligned and elongate knobs of yardang or drumlin shape, of densely grooved surfaces, and of scarps with yardang-shaped protrusions. These forms are common on valley floors and there most likely are wind eroded valley fill. However, in other areas these forms may also be developed on soft volcanic ash. Fine, intricate, and irregular hummocks, hollows, or depressions

in some areas of the smooth plains may also be eroded debris mantles, where the mantles are older or the wind direction has been more variable.

Debris mantles forming eroded sedimentary rocks of different color and resistance to erosion similar to those on earth apparently occur on Mars only in two areas: on the floor of Vallis Marineris, and on the polar layered terrain. This suggests that earthlike sequences of sedimentary rock are not common on Mars.

Conclusion

From the study of landforms on Mars it appears that characteristic erosional forms develop and that resistance to erosion varies: debris mantles and ejecta blankets are most readily modified by erosional process, crater rims are less readily modified, and volcanic flow materials least.

SURFACES OF PHOBOS AND DEIMOS

M. Noland and J. Veverka
Cornell University

We have completed our study of the surface layers of Phobos and Deimos using Mariner 9 photometry. The results are conveniently summarized in three categories:

1. Disc-integrated results: We have used the integrated brightnesses from Mariner 9 high-resolution photographs to determine the large phase angle (20° to 80°) phase curves of Phobos and Deimos. The derived phase coefficients are $\beta = 0.032 \pm 0.001$ mag/deg for Phobos and $\beta = 0.030 \pm 0.001$ mag/deg for Deimos, while the corresponding phase integrals are $q_{\text{Phobos}} = 0.52 \pm 0.03$ and $q_{\text{Deimos}} = 0.57 \pm 0.03$. The predicted intrinsic phase coefficients of the surface material are $\beta_1 = 0.019$ mag/deg and $\beta_1 = 0.017$ mag/deg for Phobos and Deimos, respectively. The phase curves, phase coefficients and phase integrals are typical of objects whose surface layers are dark and intricate in texture, and are consistent with the presence of a regolith on both satellites. The relative reflectance of Deimos to Phobos is 1.15 ± 0.10 . The presence of several bright patches on Deimos could account for this slight difference in average reflectance.

2. Study of Individual Areas on Deimos: To a good approximation the face of Deimos observed by Mariner 9 is covered uniformly by a dark, texturally complex material obeying a Hapke-Irvine scattering law. The intrinsic 20° to 80° phase coefficient of this material is $\beta_1 = 0.017 \pm 0.001$ mag/deg, corresponding to a disc-integrated value of $\beta = 0.030$ mag/deg. There is also evidence of a slightly brighter (by $\sim 30\%$) unit near some craters, which may have been produced by the cratering events. Its texture appears to be identical to that of the average material. No evidence of quasi-specular reflection has been found, suggesting that large-scale exposures of unpulverized rock are absent.

3. Study of Individual Areas on Phobos: At least three large areas on the surface of Phobos are covered by a dark material of complex texture which scatters light according to the Hapke-Irvine Law. The average intrinsic and disc-integrated phase coefficients of this surface material are $\beta_1 = 0.020 \pm 0.001$ mag/deg and $\beta = 0.033$ mag/deg, respectively. These values are slightly greater than the values found for Deimos. On the largest scale the surface of Phobos is rougher than the surface of Deimos, perhaps accounting for the slightly greater phase coefficients. Contrary to the situation on Deimos, no definite regions of intrinsically brighter material are apparent on Phobos. This difference could account for the slightly lower average reflectance of Phobos relative to Deimos. No evidence for large exposures of solid rock has been found in the three areas studied.

SIGNIFICANCE OF BRIGHT SPOTS OBSERVED DURING 1971 MARTIAN DUST STORM

Richard E. D'Alli and Thomas A. Mutch
Brown University

Initial television pictures of Mars acquired by the Mariner 9 spacecraft recorded a planet-wide dust storm. All surface details in lower latitude regions were obscured. However, contrast-enhanced versions of pictures taken early in the mission show many circular bright patches. It has been suggested that these bright spots indicate the presence of craters (Hartmann and Raper, 1974). This possibility has been evaluated by a detailed study of the Aeolis quadrangle.

Aeolis is a low-latitude, southern-hemisphere, cratered, upland region. Numerous bright and dark streaks are present, recording former aeolian activity. Numerous bright spots are present in A-frame pictures taken of this region during revolutions 8 and 10. The centers of 42 circular spots were located on unrectified photographs with respect to control points whose ground coordinates were known from spacecraft tracking data. A computer program was used to calculate surface coordinates of the spot centers. Circles with diameters scaled to those of the spots were drawn on a Mercator photomosaic of the Aeolis quadrangle. Every one of the 42 bright spots can be correlated with a crater (fig. 1). Diameters of bright spots agree well with diameters of associated craters (fig. 2).

The craters associated with bright spots range in diameter from 25 to 170 km. Associated depths are 1 to 3 km (Cintala et al., 1975). The craters display considerable morphologic variability. However, all of them have flat floors. Planet-wide, 94 percent of craters in the same size range have flat floors. Ninety percent of the bright-spot craters contain dark splotches in their interiors, more than three times the value which characterizes the total crater population. These findings suggest that generation of bright spots may depend not so much on crater topography as on the availability of a dust supply inside the crater. The confinement of dust to crater interiors suggests that the height of the dust layer is no greater than the depth of the crater, approximately 1 or 2 km.

Visibility of the bright spots depends on the bandpass filter used. Spots are most clearly delineated at longer wavelengths (i.e., with orange filter). This is consistent with the topographic evidence suggesting that the brightening occurs near the bottom of the dust-laden atmosphere, a region not penetrated by shorter wave-lengths (i.e., violet light). The same spots visible on revolutions 8 and 10 can be observed on a revolution 78-picture taken in violet light. This indicates, first, that the spots persist for substantial periods of time and, second, that the craters are the last regions of clearing.

It is likely that brightening over craters is entirely an atmospheric phenomenon, the result of multiple scattering from local concentrations of suspended dust. However, surface reflections may contribute to the effect. There may be intrinsic photometric differences in surface materials inside and outside craters. These may be emphasized during dust storms if intercrater bedrock areas are swept clear of a thin veneer of bright dust.

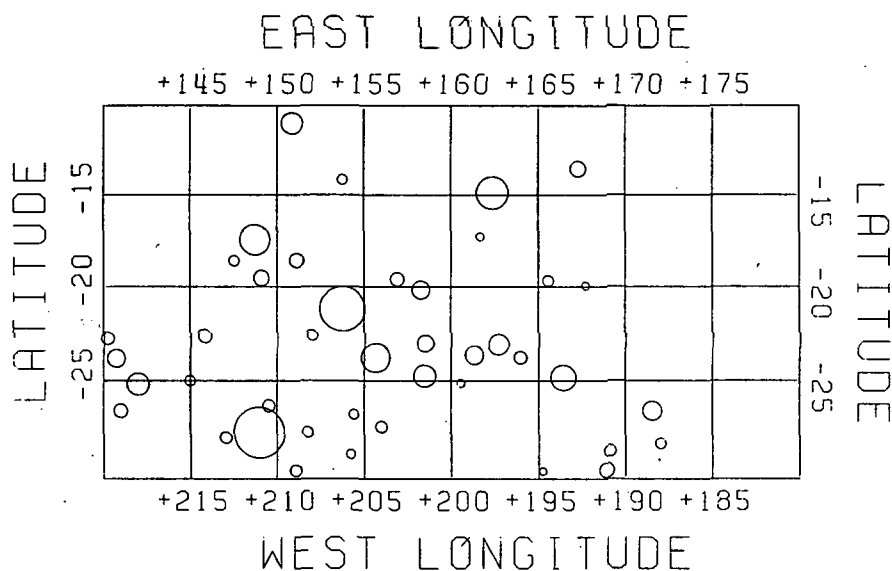


Figure 1. Calcomp plot of craters associated with bright spots in the Aeolis quadrangle.

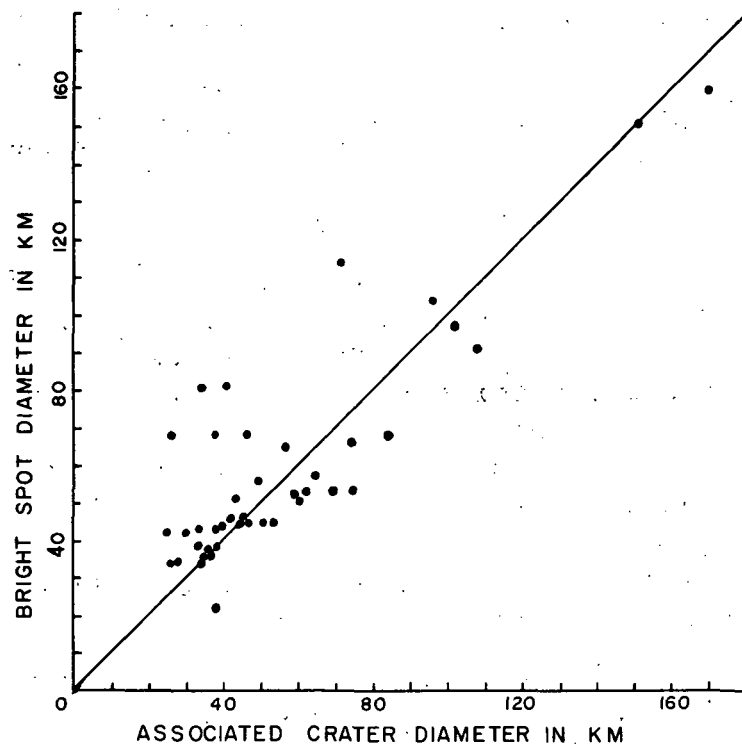


Figure 2. Plot of bright spot diameters measured on early mission photographs versus diameters of craters with which they correlate.

THE MARTIAN SCARP: INFLUENCE ON THE WIND CIRCULATION

R. E. Arvidson

Washington University and Italian Consortium for Planetary Studies, University of Rome

The contact between cratered terrain and plains in part consists of a complex erosional escarpment while in other regions the two terrains seem to meet more smoothly without large differences of elevation.

Craters counts have already shown that most regions have a peak in crater density in terrains lying between 250 km and 500 km from the contact with fretted terrain or plains. A Theoretical model of local wind circulation is used in this paper trying to demonstrate the validity of the hypothesis that relief differences between cratered terrains and fretted terrains lead to increased wind velocities on cratered terrain with consequent reshaping of fine-grained debris, that does not allow craters obliteration.

GEOLOGY OF THE ERIDANIA QUADRANGLE, MARS

René A. DeHon

University of Arkansas at Monticello

The Eridania Quadrangle is located within the density cratered terrain of the southern hemisphere of Mars, east of the Hellas Basin. The area contains three distinct physiographic provinces which divide the quadrangle into latitudinal belts. The northern belt is dominated by a cratered upland plateau, the central belt by plains, and the southern belt by mottled rugged terrain. Generally, the oldest geologic units occur in the upland terrains, and the youngest units occur in the central lowlands.

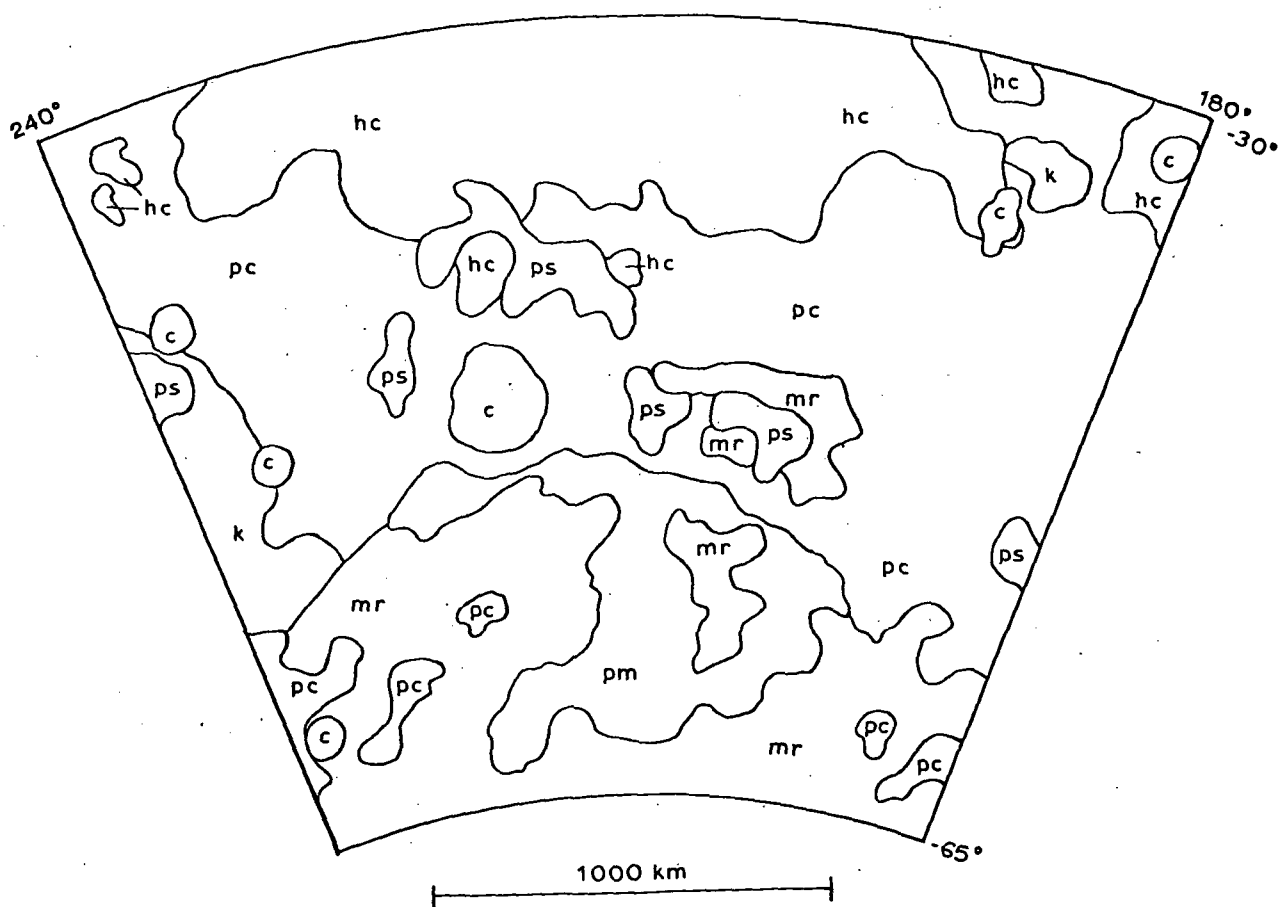
Relief forming materials, units that are higher and rougher than plains forming materials, occupy upland regions of high crater density. The oldest materials are probably the mottled rough terrain in the south which is characterized by dark mottling with sharp albedo boundaries and high density of large degraded craters. These materials may represent the late stages of planetary accretion. Dark mottling and the lack of young appearing craters suggest that these materials may be extensively altered by erosion and redeposition within the winter polar cap. The hilly and cratered terrain in the northern part of the quadrangle consist of densely to moderately cratered uplands associated with the near equatorial dark albedo band on Mars. Craters within the hilly and cratered terrain range from degraded to fresh, but there is a deficiency of small craters. Sinuous furrows or channels are locally abundant in areas of moderate regional slopes. Knobby terrains are present in limited areas of locally rugged relief which are probably formed at the expense of other terrains by faulting and erosional break-up of subjacent materials. Knobby terrain on the western edge of the quadrangle is peripheral to the Hellas Basin and is probably related to post-basin faulting.

Plains forming materials exhibit flat to rolling surfaces which are most extensive in the broad low area in the central part of the quadrangle. Rolling plains material is the most wide spread plains unit and the most cratered. Rolling plains material forms undulatory planar surface with moderate crater density and abundant lobate scarps. It is embayed by other plains units and, therefore, is probably the oldest. Mottled plains material in the south forms level to

rolling plains with low crater density and varying albedo. It mantles and subdues subjacent topography. Mottled plains appears to fill a topographic low in the southern rugged terrain belt. Smooth plains, occurring in topographically low areas, is relatively level and nearly featureless.

Due to the presence of atmosphere the surface of Mars is more actively weathered and eroded than that of the moon. A discontinuous surficial cover of weathered and transported materials is present throughout much of the region. Distinctive albedo mottling in the southern part of the quadrangle is, in part, related to compositional and thickness variations of the surficial cover. Some intercrater dark patches are dune fields, others may be lag gravels. Light and dark wind streaks are common downwind from some craters. Light streaks, in the northern part of the quadrangle, exhibit southeasterly trends. Dark streaks, in the north central part of the quadrangle, trend west to southwest along an apparent topographic trough.

The early history of the region was dominated by a high flux of meteoroids and impact cratering. The impact responsible for the Hellas Basin occurred during this late stage of planetary accretion. As the cratering rate decreased, volcanic flows were deposited across the central belt filling a regional depression with rolling plains material. As cratering by impact waned further, other plains materials of volcanic or eolian origin were deposited in lowlying basins. Erosion and redeposition have been continuous, though of variable intensity, in this region throughout Martian history.



GEOLOGIC UNITS

- c - Crater materials
- ps - Smooth plains materials
- pm - Mottled plains material
- pc - Cratered plains material
- k - Knobby materials
- hc - Hilly and cratered terrain material
- mr - Mottled rough terrain materials

GEOLOGIC SKETCH MAP OF THE ERIDANIA QUADRANGLE--MARS

GEOLOGY OF MARS QUADRANGLE MC-6 (CASIUS)

R. Greeley
University of Santa Clara and NASA Ames Research Center
and

J. E. Guest
University of London Observatory

Description

The Casius Quadrangle (30°N to 65°N lat.; 240°W to 300°W long.) is one of the northern tier of Lambert conformal sheets of the Mars Atlas. It consists of four distinctive physiographic regions: 1) part of the northern cratered plain which forms an incomplete annulus around the northern polar region of Mars, 2) smooth lowland plains of Utopia Planitia across the central and southeastern part of the map, 3) mountainous terrain, in the Nilosyrtris Mensal region south of the lowland plains, consisting of distinct mountains averaging 15 km across with intermediate hummocky surfaces, and 4) cratered plateau in the southwest part of the map forming the northern part of a large complex cratered region in the mid-latitudes of Mars. In the Casius Quadrangle, the cratered plateau is broken by a set of linear to curved parallel-sided canyons on its northern margin.

There are eight major geological units (some which are subdivided) in the Casius Quadrangle: 1) mottled cratered plains deposits, 2) plateau deposits, 3) lowland plains deposits, 4) variegated plains materials, 5) knobby deposits, 6) hill-forming deposits, 7) crater units (for craters larger than 20 km), and 8) surficial material.

The main structural elements occur in the southwest corner of the quadrangle. They consist of linear graben-like troughs generally trending WNW, with shorter troughs oriented approximately perpendicular to the main direction and trending NNE. Similar structures form sub-circular and radial patterns that are probably

controlled by buried craters below the mantle of cp.

These structures are part of a zone of faulting that borders the plateau material on its northern margin; to the west of Casius Quadrangle, the faults strike NW. The origin of the structures is unknown, but they may result from tension on the crest of a broad monoclinial downwarp into the basin to the north.

Erosional retreat of the scarp in cratered plains material has paralleled the fault trends. The age of the faulting is interpreted as post-plateau material and pre-hummocky material because the troughs are covered by hummocky material.

Historical Summary

The surface of Mars is divided roughly into two halves separated by a great circle which is slightly oblique to the equator. The southern half of the planet consists mostly of old and densely cratered terrain whereas there are more extensive plains units and younger volcanoes in the northern part. Superimposed on the northern plains are the polar caps which retreat and advance with the seasons.

The Casius Quadrangle lies across the boundary between the two geologically different hemispheres, and in its northern part, includes areas covered by winter frost. The densely cratered surface of the southern hemisphere is represented in the Casius Quadrangle by a cratered unit, whose remnants are now recognized as knobby material underlying the plateau material in the southwestern corner of the map. This surface is considered to represent a stage of the intense bombardment in the early history of the planet. At a later time this cratered surface was overlain by a thick unit of plains-forming material, possibly of aeolian and/or volcanic origin. The topography and structure

suggest that the densely cratered surface was down-warped towards the north into a basin of unknown size.

Following the emplacement of the plateau plains unit, faulting formed a series of graben roughly paralleling the present boundary between the older cratered terrain to the south and the northern plains in this area. Erosion of the plateau unit caused scarp retreat from the north towards the south, leaving behind a debris of hummocky material. This in turn was covered by the lowland plains material north of the scarp.

The time of emplacement of the mottled cratered plains material is not known but the density of cratering suggests that it is comparable in age with the base of the plateau unit.

It is likely that the surface of the lowland plains material is still being modified by aeolian processes deposited; the dark streaks and patches on its surface probably represent freshly modified surface. The variations in crater density over the surface of the lowland plains suggests that material is being added in localized areas.

GEOLOGIC HISTORY OF THAUMASIA QUADRANGLE, MARS

George E. McGill
University of Massachusetts

The Thaumasia quadrangle lies on the south flank of the Tharsis Dome, a very large bulge in the crust of Mars extending for more than 5000 km northward from the center of the quadrangle. Because of this major feature, the first-order topography is dominated by a generally southerly slope across the entire quadrangle. The other major topographic feature influencing the physiography of the quadrangle is the Argyre Basin to the east. Topography along the east-central border of the Thaumasia quadrangle exhibits curved scarps and lowlands concentric to Argyre.

Four geologic regions within the Thaumasia quadrangle may be defined on the basis of the dominant material unit exposed. Three of these regions (numbers 1, 3, 4 below) are expressed in arcuate patterns concentric with the south flank of the Tharsis Dome, the fourth is an arcuate region concentric with the Argyre Basin. The regions are listed in a sequence determined by the relative ages of the dominant material units defining them.

1. The southwestern and southern portions of the quadrangle are dominated by highly modified and partially buried cratered terrain that has been interpreted as primordial crust by Carr, et al. (1973). Although this terrain is underlain by ancient crater deposits, its surface appears young because of long-continued erosion, and because it is masked by a variable-thickness blanket of aeolian(?) smooth plains deposits.

2. Along the eastern border are deposits believed related to the formation of the Argyre Basin. These materials are younger than much of the ancient cratered terrain, but some large, ancient craters are clearly superposed on Argyre Basin deposits. Thus the Argyre Basin was formed during the time that the ancient cratered terrain formed.

3. The north-central portion of the quadrangle is dominantly underlain by materials of a cratered plains unit, probably of volcanic origin, and associated materials forming troughed and furrowed hills. The wreckage of a few large, ancient craters shows through the younger blanket of cratered plains. All these units are extensively faulted. This region occupies the most elevated portion of the quadrangle.

4. Extending from the northwest corner of the quadrangle southeastward to the center and then northeastward to the northeast corner is an annulus between the northern and southern provinces which is characterized by large areas underlain by either sparsely cratered, smooth plains-forming deposits or the older cratered plains materials. Although some faults extend southward into this province, most die out or are overlapped by smooth plains deposits.

Superposed on portions of regions 1, 2 and 3 are deposits radial to the double-ringed crater Lowell, one of the freshest large craters on Mars, and one of the few which preserves the concentric, hummocky and radial structures characteristic of large lunar craters. Isolated patches of smooth plains materials occur in all regions of the quadrangle. Almost without exception, areas that are obviously topographically lower than their immediate surroundings are underlain by smooth plains materials. In addition, gradational contacts with older units and the local gradual termination of crater rims and graben into areas underlain by smooth plains indicate that the plains materials

fill low areas to varying depths. These characteristics suggest that most of this material is of aeolian origin; wind-transported sediment deposited preferentially in low areas and overlapping onto all older units.

The earliest events in the Thaumasia quadrangle for which any record is preserved are related to the formation of the large craters whose degraded remains dominate the southern portion of the quadrangle. By analogy with lunar history, these craters probably date from the early history of the planet, on the order of 3-4 billion years ago (Hartmann, 1973; Soderblom et al., 1974). The Argyre Basin, and related deposits, were probably formed during this ancient cratering episode.

Overlying the ancient cratered terrain is a widespread series of deposits mapped as cratered plains. Associated with these plains on the south flank of the Tharsis Dome are materials forming distinctive furrowed hills and slopes. Both units are extensively cut by graben areally related to the Tharsis Dome. Because the hilly and furrowed terrain resembles some lunar basin deposits, and because it occurs in an arcuate belt, it is tempting to propose the existence of a gigantic (diameter roughly 3000 km), almost totally buried ancient basin. If one exists, then the pre-doming history of the Thaumasia area would involve formation of the basin, followed by almost complete burial of its rim by volcanics now preserved as cratered plains materials. Later doming and faulting would further obscure the old basin. Except for the faulting, such a scenario is similar to that suggested for the history of cryptic old basins on the moon (Wilhelms and Davis, 1971). Although most of the graben on the south flank of the Tharsis dome define a fan converging northward toward the Syria Planum region, in some areas there are other sets crosscutting the fanning graben. Unlike the situation in the Arcadia quadrangle to the north

(Wise, in press), clear evidence for relative ages of graben sets is rare in the Thaumasia quadrangle. Where evidence does exist, the graben can be divided into three subgroups on the basis of both relative age and orientation. The youngest graben are those of the set fanning from the Syria Planum region. Most graben are older than smooth plains materials, but a few cut even these deposits. Without exception, the graben cutting smooth plains deposits belong to the fanning set. Even with the sparse evidence in hand, it seems clear that faulting in this region has occurred over a long period of Martian history, so that any hypothesis attempting to explain the complex history of the Tharsis region as due to a single period of uplift and faulting is doomed to failure.

Both the age and the nature of the Tharsis Dome are of major concern to students of Martian history. A constructional origin seems untenable because the remains of faulted and nearly buried large craters showing through the younger materials suggest that the ancient cratered surface of the planet is not deeply buried. The graben, logically considered as somehow related to dome formation, date the structural movements as mostly post cratered plains, pre smooth plains. The conflicting age relationships between graben and craters in the 20-40 km diameter range, and the local faulting of smooth plains deposits by graben of the fanning set indicate a long history of faulting and, presumably, of related uplift as well.

Ejecta from the crater Lowell are superposed on all adjacent units except smooth plains materials. In addition, density of craters superposed on Lowell is very low, suggesting that the age of the crater is not much greater than the age of the smooth plains.

Since the formation of Lowell, low areas in the quadrangle have been filled with smooth plains deposits, most of which are of aeolian origin. It is very likely that these aeolian deposits have been deposited over a significant length of time. Indeed, there is no reason to eliminate the possibility that they are still being deposited today.

THE NEW GEOLOGIC MAP OF MARS (1:25 MILLION SCALE)

D. H. Scott and M. H. Carr
U.S. Geological Survey

A new geologic map of Mars at 1:25 million scale is being prepared which will synthesize much of the geology on the 1:5 million map series of the planet now being completed. Because of the large difference in scale as well as the individuality of the many authors expressed on the series maps, the present map has been generalized, partly revised, and some geologic units have been combined to provide planet-wide continuity of portrayal. Thus, the new map is not simply a reduced compilation of the larger scale maps, but reflects both the geologic concepts of its authors as well as the work of the Mars geologic mapping group.

Within the region bounded by 65°N-65°S latitude, the following major rock units of regional extent are recognized.

1. Smooth plains. Occurs in low regions and in local depressions. Generally featureless with a very low crater density. Believed to be largely aeolian in origin.
2. Ridged plains. Variable crater density, relatively high to moderate. Mare-ridge like features common. Occurs mainly in Lunae and Sinai Planum, Syrtis Major and Hesperia. Believed to be old volcanic plains.
3. Rolling plains. Plains with low indistinct ridges and scarps which are commonly emphasized by albedo differences. Crater density moderate, mostly intermediate between 1 and 2. Occurs around Elysium and Apollinaris Patera. Believed to be volcanic plains of intermediate age.

4. Plains, undifferentiated. Generally featureless except for superimposed impact craters. Crater density considerably higher than unit 1 but in most places less than unit 2. Gradational with both these units probably includes both volcanic and aeolian deposits.
5. Cratered plateau. Occurs chiefly in the cratered southern hemisphere. Refers to areas where intercrater plains are extensive and large craters are very subdued or very few in number.
6. Hilly and densely cratered materials. The most heavily cratered terrain where large craters are almost shoulder to shoulder. Intercrater areas rough, non-planar.

Other materials which make up volcanic constructs, knobby terrain, chaotic materials, channels, canyon flows and mountainous terrain are also mapped where they occur locally. Faults, mare ridges, and other structural features have also been mapped.

A preliminary map of the 65°S to 65°N area has been completed and is in the process of being extended to include the polar regions.

GEOLOGIC SETTING OF VIKING MARS "B" PRIME LANDING SITE CYDONIA REGION, MARE ACIDALIUM QUADRANGLE

James R. Underwood, Jr.
West Texas State University

Mare Acidalium Quadrangle is composed of four geologic provinces: (1) a cratered plateau province to the southeast, (2) a cratered and etched plateau province to the southwest, (3) an intervening province of younger, topographically subdued plains and dissected plateaus, and (4) a mottled plains province that covers most of the north half of the quadrangle.

The quadrangle contains no major volcanoes, although in places there are scattered small (less than 1 km diameter) hills, interpreted as volcanoes, that have convex upward flanks and small summit craters. Only a few faults, all of them normal, have been recognized; none of the large Martian channels originates in the quadrangle. Excepting occasional meteorite impact events, the principal geologic processes that characterize the quadrangle today are eolian erosion and deposition. Seasonal processes related to ground-ice decay also may occur.

Inasmuch as life on Earth depends on water, the search for life on Mars is being concentrated in those areas where the prospect of the existence of water is greatest. A mathematical model of the Martian atmosphere has suggested that pore spaces in the uppermost part of the regolith may contain free water in those areas in the 40 degree-50 degree north latitude belt where the planetary surface is sufficiently low to have atmospheric pressure in excess of the vapor pressure of water. Within that latitude belt, the Cydonia region is sufficiently low (approximately 1 km below the zero or 6.1 millibar datum), but more importantly an Iris data point at lat 44 degrees N long 10 degrees W indicated the highest water content reported on the planet. This was the determining factor in the selection of that site as the center of the landing ellipse for the second Viking landing late in the summer of 1976.

The landing site is centered with the east-northeast trending ellipse about 600 x 80 km that extends from the plains and dissected plateau province to the west-southwest across a limited area of plains material and onto the mottled plains province to the east-northeast. The site itself is on plains material. Three supposed impact craters (rim diameter 7-12 km) lie within a radius of 100 km of the landing site. Erosional remnants of an old, heavily cratered southward retreating plateau lie 85 km south. The landing site is covered only by wide-angle A-camera imagery (resolution 1 km), but the center of a narrow-angle B-camera image (resolution 0.1 km) lies within the landing ellipse 185 km east-northeast of the site. This high resolution image, probably typical of the landing site, reveals 19 craters (rim diameters equal to or less than 0.5 km); 2 of these may be volcanoes. Density of craters of all

types (rim diameters equal to or less than 0.5 km) is about one per 325 km². Many craters appear to be partly filled with eolian debris; this may be true at the landing site. High and low resolution images indicate that intercrater areas within the landing ellipse are flat to gently rolling plains. The plains material is interpreted to consist of an eolian blanket of varied thickness, possibly intermixed with fluvial deposits, overlying volcanic rocks. Although the intercrater areas appear to be smooth at the highest resolution of the available imagery, these areas still may be uneven enough to present a substantial hazard to the Viking spacecraft. Final selection of the landing site will be determined by: (1) orbital imagery obtained after the arrival of the spacecraft at Mars but prior to the descent to the surface, and (2) the results of the earlier Viking Mars "A" landing.

GEOLOGY OF THE PHAETHONTIS QUADRANGLE. MARS

J. Hatten Howard III
University of Georgia

Geologic terranes of the Phaethontis quadrangle range from heavily cratered uplands and very large craters, some of the oldest surfaces and features on Mars, to the sparsely cratered and relatively young equatorial plains materials of the Tharsis Ridge to the north. Numerous martian material units have been delineated: Four terra-forming units; five plains-material units; several crater-material units, defined on the basis of position relative to the crater and interpreted degradational modifications; and several localized, uniquely distinct, materials units.

The oldest units of the Phaethontis quadrangle are the heavily cratered uplands in the south and the more subdued, but highly cratered, plateau materials farther north. The density of large (>50 km diameter) craters of the plains which lie within and embay the southern uplands is comparable to that of these surrounding uplands; these plains probably result from modification of lower elevations of the upland by aeolian erosion and deposition.

Large impact craters (Newton, Copernicus), which range in diameter from 300 to 600 km, are small single-ring basins produced during final stages of early high-density cratering history of Mars, and the rim materials are thus some of the oldest materials now exposed on the planet's surface. The craters are filled and overlapped by younger plains-forming units, which may be of aeolian or volcanic origin.

The cratered plateau terrain in the northern part of the quadrangle contains younger plains in low portions of the plateau area, and the

youngest plains--which may be partially volcanic in origin--overlap and embay this same terrain from the region to the north.

Craters in the Phaethontis quadrangle larger than 20 km in diameter have been classified according to degree of modification, and the crater densities of these modified-crater populations were plotted and contoured. The degree of crater modification correlates with both the geologic unit in which the craters occur (suggesting either an age relationship or nature-of-material dependency) and geographic distribution, reflecting geographic variation in crater-modifying processes.

No features of certain volcanic origin have been identified in this quadrangle. Some features seen in a very few high-resolution frames of smooth plains in the northeastern part of the quadrangle might be interpreted as lobate flow fronts. Also, small branching furrows or channels in subdued (mantled?) uplands and adjacent low-lying plains may be lava channels or collapsed lava tubes.

The only tectonic features in the quadrangle are narrow grabens and escarpments (Sirenum Fossae) extending southwestward for 100's of kilometers from the Tharsis Ridge to the northeast.

Dark streaks and patches--aeolian features--associated with craters and in the lee of some uplands are locally prevalent throughout the quadrangle. At least some of the dark areas are dune fields, one of which is illustrated by a B frame. Erosion and/or some mantling process in the southern part of the Phaethontis quadrangle have obliterated small craters and the rims and rim materials around medium- to large-diameter craters of moderate depth.

Two interesting areas of bright, hilly terrain occur in the northwest part of the quadrangle. The distribution and geometry of these areas seems

to preclude an impact-associated origin. These areas are distinctly different from the surrounding materials and may represent localized material-forming events, such as volcanism or exposure of a distinct rock type by wind or solution erosion.

Impact cratering dominated the early history of the Phaethontis quadrangle. Successive plains-forming events during, and subsequent to, the last stages of the early cratering event, filled low areas of the heavily cratered surface. The plains were probably formed by aeolian and volcanic processes, although only the youngest, smooth plains in the northeast part of the quadrangle show possible volcanic flow features. Tectonism, forming the extension fractures, has been active throughout the later plains-forming events. Wind activity now predominates as the active geotopic agent.

GEOLOGIC SUMMARY OF THE MARS QUADRANGLE MC-12 (ARABIA)

John S. King
State University of New York at Buffalo

The Arabia quadrangle is a region of old cratered terrain located in the northern hemisphere of Mars. It extends 30° north from the equator and 45° east from the prime meridian. Crater density in the quadrangle is similar to the heavily cratered regions south of the equator owing to the inclination relative to the equator of the great circle division between heavily and less cratered Martian terrains.

Most craters in the Arabia quadrangle are of impact origin and are assigned to one of four general classes defined primarily on degree of rimcrest degradation and secondarily on presence or absence of central peaks and ejecta blankets. All of the largest craters (up to 430 km rimcrest diameter) are situated in the eastern portion of the quadrangle and belong to the oldest class. A single large (130 km x 40 km) irregular crater is located in the west and trends N 20° W. It is bounded by conspicuous linear scarps. This irregular crater is interpreted to be the result of faulting associated with collapse. Several small pedestal craters centered on irregular subcircular platforms which are bounded by steep scarps are located in the east central portion of the map. These pedestals may either be ejecta from impact at the central crater or alternatively may be small volcanic constructs composed dominantly of ash flow tuffs with some associated inter-

layered lava flows. Whatever the origin of the construct, the bounding scarps are interpreted to be the result of eolian erosion and slump and are now in retreat back toward the summit craters.

Seven different regional material units are defined in the quadrangle on the basis of texture, surface characteristics and albedo and are organized into a stratigraphic sequence based on relative age. Of these units the younger group is made up of one plateau unit and four plains units. The most extensive unit is the cratered plains unit which occurs in a broad east-west trending band which dominates the central portion of the map. The two older regional units include a hilly and cratered unit and a ridged and grooved unit. Both of these are characterized by rough, densely cratered surfaces of moderate relief. The ridged and grooved unit occurs in a wide zone peripheral to the degraded rimcrest of the Schiaparelli Basin centered in the Sabaeus Sinus quadrangle to the south. The surface of the ridged and grooved unit appears scaly due to the presence of an abundance of highly degraded intersecting and overlapping craters which may be of pre-basin origin.

No large scale or pervasive structures such as fault or fracture systems are obvious in the map area. There is a northwest structural trend definable at widely spaced locations by such things as channel alignments; alignment of some elongate central peaks; northwest trending polygonal rim segments of some craters; and the northwest trend of the long axis of the single large irregular crater. Wind plumes and streaks are conspicuous in the southwest portion of the Arabia quadrangle.

MERCURY GEOLOGIC MAPPING PROGRAM

H. E. Holt

U.S. Geological Survey

A systematic geologic mapping program of the Mercury surface at a scale of 1:5,000,000 was initiated during the summer of 1975. The program is a joint undertaking between the Planetology Program Office of NASA, the U.S. Geological Survey and NASA supported institutions. The objective of the Mercury Geologic Mapping Program (MGMP) is the publication of 1:5,000,000 scale Geologic Maps of Mercury to be produced from Mariner 10 data. Map authors were selected by the Mercury Geologic Mapping Committee, subject to approval by NASA, from among the qualified scientists who requested Mercury geologic mapping assignments. The committee, composed of representatives from the Planetology Program Office, university investigators, and the U.S. Geological Survey, was appointed by NASA to provide general program guidance, to adjudicate differences of scientific opinion, and to oversee program standards and schedules.

The planet Mercury is divided into 15 quadrangles at a scale of 1:5,000,000 and the Mariner 10 imagery extends over 9 quadrangles, varying from full coverage to as little as 40 percent coverage. Shaded relief maps and controlled photo-mosaics are being provided as base maps for compilation of stratigraphic units and geologic structures. In addition, 150 stereo-pairs have been rectified and scaled to aid the map author's interpretations of geologic features and processes.

The overall management responsibility for the Mercury program will reside with the Branch of Astrogeologic Studies, U.S. Geological Survey, and will include: 1) the refinement of planetary geologic mapping techniques, 2) the establishment of mapping stylistics and conventions, 3) map formats, 4) uniformity of portrayal, 5) the codification of Mercury stratigraphic nomenclature and symbology, and 6) final review and approval of all manuscript materials. Final drafting and actual publication will be carried out by the U.S. Geological Survey. Map compilation schedules by participants will be dependent upon the receipt times of final base maps, but all Mercury Geologic Quadrangle maps are planned to be final review stages by the end of fiscal year 1977.

MERCURY MAPPING: PROCESS IN THE STUDY OF QUADRANGLE H12

Karl R. Blasius
Planetary Science Institute

A general description of the major features of the H12 quadrangle will be presented along with first results of the systematic study of landforms using stereo images.

My investigation is part of the 1:5,000,000 scale Mercury Geologic Mapping Program. In cooperation with one or more scientists chosen by NASA, I shall study the geologic data and draw a map of the region designated quadrangle H12 extending between 70° and 20° south latitude and 72° and 144° west longitude.

Work on this project will begin about January 1, 1976, so no substantial progress can be reported at present.

In the coming year I shall study all the Mariner 9 images in my mapping region and prepare preliminary terrain maps. In conjunction with my map co-authors, geologic units will be defined and mapped. Progress of this project will be reported at periodic Mercury Mapper's meetings.

GEOLOGIC MAPPING OF THE SOUTH POLAR REGION OF MERCURY

Michael C. Malin
Jet Propulsion Laboratory

Using high resolution images of Mercury acquired by Mariner 10, a program to geologically map the south polar region is being pursued with co-mapper Robert Strom of the University of Arizona. The South Polar Quadrangle (H-15) includes the area poleward of 65°S latitude. Owing to illumination constraints, only half the polar region was photographed. Sun elevation angles range from 0° (terminator) to 15° ; thus the imagery is nearly ideal for photogeologic interpretation. Images taken during the first and second planetary encounters provide resolutions between 1 and 1.5 km and significant areas of stereo overlap.

Initial studies have centered on: 1) specifying terrain characteristics, 2) determining the distribution of terrain types, and 3) establishing a provisional chronology for the polar region. When stereo images are available, topographic relationships and detailed morphologic studies will allow a more definitive chronology to be formed. Combining knowledge of active processes (e.g. impact, volcanism, tectonism) with timescale, one can infer a time stratigraphy. By relating surface characteristics to material properties, it is possible to infer rock stratigraphic units, the end result portrayed as a geologic map.

The following are preliminary results of the initial studies:

- 1) As described by Strom et al (1975), the south polar region exhibits four main types of terrain - heavily cratered, intercrater plains, and two variants of smooth plains.
- 2) Intercrater plains exhibit superposition in at least one area, suggesting different ages.

- 3) Major escarpments appear more fully developed in smoother plains than in intercrater areas.
- 4) An isolated positive relief feature near 62°S , 153°W has been identified tentatively as a volcanic construct, and mapped to facilitate edge matching with the mercurian quadrangle H-12.

MULTIRING BASINS IN THE KUIPER QUADRANGLE, MERCURY

René A. DeHon

University of Arkansas at Monticello

Basins with multiple concentric ring structure are common features of the surface of Mercury. Several intermediate sized basins with two or three rings occur within the heavily cratered terrain of the Kuiper Quadrangle (25°N to 25°S; 0° to 72°W). Two basins with three rings exhibit decreased ring spacing outward (118, 226, 310 km and 134, 170, 194 km) in contrast to the ring spacing of lunar basins. Large craters are superposed on both basins, but radial features are preserved around at least part of the basins. Only one quarter of the ring diameter is preserved in the smaller southern basin. The center of arc for each ring segment is progressively offset to the west by about 15 km. The reconstructed ring structure is eccentric with all three rings coincident in the west. Four basins, ranging from 228 km to 140 km in diameter, exhibit a single inner ring. The largest basin has an incomplete inner ring, and the outer ring is broken into overlapping segments which might indicate incipient formation of a third ring. The other basins exhibit varying states of inner ring preservation and outer sharpness reflecting degradation in time. The ring spacing is a linear function of diameter. Figure 1 is a plot of the multiring basins in the Kuiper Quadrangle compared with the overall trend (determined by inspection) found elsewhere on Mercury. The overall trend is described by the function, $D \approx 1.56d + 58$, where D is the basin diameter (second ring) in km and d is the diameter of the inner ring in km.

Below approximately 125 km diameter internal ring structure is lacking, but some craters have multiple peaks arranged in a ring pattern. These central peak rings are analogous to the inner rings of larger basins and constitute a continuum in the linear function of ring diameters down to a lower limit of 55-60 km diameter (Fig. 1). Central peaks or clustered peaks occur in craters as large as 130 km diameter down to craters less than 25 km diameter (lower limit not determined). Craters as large as 160 km in diameter exist without central peaks or internal rings, but all such craters have very smooth floors and are presumably filled by later materials.

Smooth floor materials are found in all large craters and basins. Ghost rings of partially buried

craters on the floors of multiring basins indicate that the basins existed for a sufficient length of time to become cratered prior to the emplacement of the smooth floor material. The extent to which buried craters, internal rings, or shelf structure is obscured provides a rough indication of the thickness of the materials in each basin. The superposed crater density on the filling materials is low except when the secondary crater fields of nearby large fresh appearing craters is superposed on the smooth floor of the large basins. Hence, the basin filling material may be dated as post-basin and pre-secondary cratering (a sequence analogous to lunar mare materials). The nature of basin-filling material is undetermined but presumably volcanic in origin. The outer rim facies of the basins is degraded but the preservation of secondary craters; the lack of pooling of smooth materials in low areas; and the absence of an identifiable source suggest that the material is not a pervasive ejecta mantle.

TABLE I

MULTIRING BASINS

Location	Rim Crest* <u>Diameter(km)</u>	<u>Principle features</u>
-1.0;36.5	294	2 rings; incomplete or broken rings
-18.0;52.5	228	2 rings; both rings complete
+22.0;18.0	226	3 rings; discontinuous third ring
-14.5;63.0	204	2 rings; 15 km offset of ring centers
-16.0;14.5	170	3 rings; 30 km progressive offset of centers
+15.5;30.0	140	2 rings; faint inner ring

CRATERS WITH PEAK RINGS

-8.5;22.5	114	with central peak
+10.5;21.5	87	
+5.0;52.0	80	
+0.5;16.5	70	

*Diameter of ring believed to bound the crater proper.

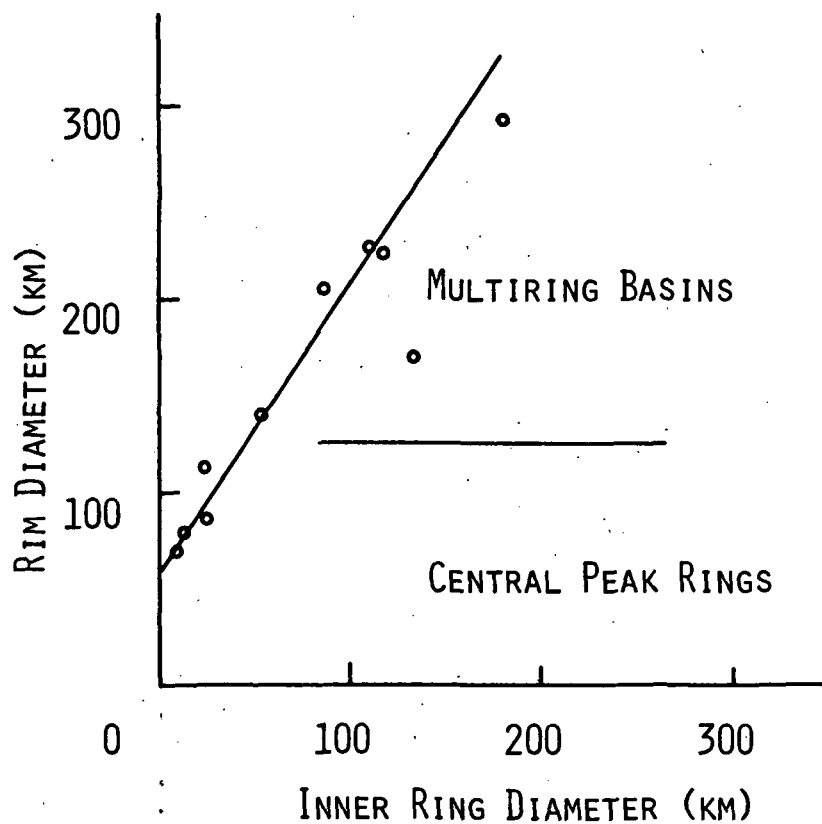


Figure 1. Rim diameter as a function of inner ring diameter. Trend line after Gault et al. (1975)

PHOTOMETRIC ANALYSES OF MARINER 10 IMAGES OF VENUS

Bruce Hapke
University of Pittsburgh

This abstract summarizes the work accomplished under NASA Grant NSG 7147 since the start of the grant, June 1, 1975.

The preliminary phase of the photometric analysis of Mariner 10 images of Venus has been completed and a paper has been submitted to the Journal of Atmospheric Sciences. The following is a summary of the results contained in this paper.

The elimination of the residual image problem in the Mariner 10 vidicons allowed photometry of moderately high accuracy to be carried out during the February 5, 1974 flyby of Venus. Due to the rapid rotation of the upper atmosphere the planet exhibits temporal brightness variations in the UV greater than 10% over a few hours. The observed terminator is 4° past the geometric terminator because of the detached haze layers at altitudes around 85 km. No indications of local cloud top elevation variations greater than a few hundred meters were found in the Mariner 10 data. The cloud tops are probably diffuse. The distribution of brightness across the planet at 23° phase angle is fit better by a cloud of isotropic scatters than by Mie spheres. In the UV the bright and dark regions both have low albedos at all scales, showing that the UV absorber is not just confined to the dark markings. Correlated contrasts can be seen on frames taken through the UV, blue and orange filters. The outlines of the UV markings are diffuse even at the highest resolution, with contrast gradients

of the order of 2%/10km. Regions which are brighter in the UV also have higher polarizations than darker areas. Several proposed models are discussed and are shown to be inconsistent with the polarimetric correlations. A cloud model which is consistent with the Mariner 10 observations has a third type of particle present in the clouds in addition to atmospheric gas molecules and sulfuric acid droplets. This particle is UV-absorbing, scatters nearly isotropically and is weakly polarizing; elemental sulfur has these properties. The UV absorbers are well-mixed vertically but incompletely mixed horizontally, thus causing the UV markings. The UV markings apparently represent stratospheric, rather than tropospheric, processes. There is little in the Mariner 10 pictures to suggest evaporation or condensation processes or strong horizontal shears of wind. The mixing between light and dark UV regions appears to be more diffusive than turbulent, with a stratospheric cloud particle mixing length of the order of 10 km.

More detailed analysis of the Mariner 10 images of Venus is currently in progress. The objective of the research is to ascertain what information exists in the Mariner 10 data concerning the cloud particle scattering properties and density distribution with altitude. Potential sources of such information are the high-resolution limb and terminator pictures of the planet. Since the scattering mean-free-path may be of the same order as the radius of the planet, it is necessary to develop and use solutions of the radiative transfer equation in a spherical atmosphere.

An approximate solution for scattering in a spherical atmosphere has been developed, subject to the following restrictions:

1. Scatterers have an exponential altitude distribution with

scale height H .

2. $H \ll R$ = the radius of the planet.

3. $\mu_0 \ll 1$, where $\mu_0 = \cos i$, i = angle of illumination.

4. μ is finite, where $\mu = \cos e$, e = angle of emergence.

5. Multiply-scattered radiation can be ignored. Then it can be shown that

$$\frac{1}{I} \frac{dI}{d\mu_0} = \left(\frac{H}{\mu R} + \sqrt{\frac{\pi}{2}} \frac{H}{R} - \mu_0 \right)^{-1}$$

where I is the reflected radiance.

This expression has been applied to high-resolution Mariner 10 images of the evening terminator of Venus in the North Polar Vortex to determine the scale height of the scatterers. The result is

$$H = 3.6 \pm 1 \text{ km.}$$

This value is in good agreement with $H = 3 \pm 1$ km derived by O'Leary from an independent analysis of the limb haze pictures taken at the subsolar meridian. The main source of error is the pointing uncertainty in the spacecraft.

It can be shown that multiply-scattered radiation will contribute of the order of 20% to the observed brightness in the terminator pictures, and considerably more to the subsolar limb images. Current work involves the development of an approximate theory for the multiply-scattered component in a spherical atmosphere using a two-stream approximation as a starting solution. A similar technique has been developed for a plane-parallel atmosphere and has yielded a photometric function which is accurate to better than 5% in most places, and which describes the

distribution of brightness on bodies as diverse as the moon and Venus.

This phase of the work is just beginning; when completed it will be applied to the limb and terminator images of Venus.

THE SURFACE OF VENUS: RADAR OBSERVATIONS AND TERRESTRIAL ANALOGS

Michael C. Malin
Jet Propulsion Laboratory

One year ago most planetary geologists considered the surface of Venus both inaccessible and of only marginal interest. Recent events have proved these scientists wrong. Radar observations (Goldstein, 1975; Goldstein and Rumsey, 1976) have shown numerous features at scales larger than 20 km. Many have been interpreted as craters (Schaber, 1975), but alternative explanations of several features have been proposed, based on detailed analysis of the radar data acquisition and reduction techniques (Malin, 1975; 1976). These alternatives include volcanoes, large rift-like valleys, continent-sized plateaus, mountain ranges, and fault zones. Visible images returned by the Soviet spacecraft Venera 9 and 10 provide two glimpses of an active planetary surface, with weathering and erosion strongly suggested.

The purpose of this study is threefold. First, continued investigation of earth-based radar images of Venus to determine the distribution of geologically recognizable features. To accomplish this task, radar data already acquired by Goldstein at the Jet Propulsion Laboratory's Goldstone Tracking Station (and possibly other data received at the Arecibo Observatory) will be processed and analyzed using image processing techniques developed at JPL by the Image Processing Laboratory.

The second task will be to assimilate the recent Soviet results, relate these to the radar observations if possible, and to quantify the geomorphologic environment revealed by these data. Image processing techniques will again play an important role in data interpretation.

The third, and perhaps most important task, will be to evaluate a potential terrestrial analog to the venusian surface, at least as identified by morphologic

character. The similarity in erosional regime between the surface of Venus and the floors of the terrestrial oceans is remarkable. Critical threshold velocity (u^*_t) for movement of particulate material and "current velocities" (wind and water) at "altitude" are strikingly analogous. Values for u^*_t for Venus and the oceans (water) are ~ 1 and ~ 1.5 cm/sec, respectively (R. Greeley, personal communication 1975). Values for "current velocities" of ~ 10 - 20 m/sec are indicated on both Venus (Ainsworth and Herman, 1975) and beneath the oceans (Heezen and Ewing, 1952). To explore this possible correlation, side-looking sonar images of the ocean floor at depths of ~ 1 km (near continental shelves and oceanic ridges) would be acquired, processed at IPL to enhance morphologic features, and interpreted within the framework of qualification of an alien environment. Comparison with side-looking radar of land surface forms would facilitate application to future radar missions to Venus. Studies of sea floor visible photographs could provide equivalent analogs to future lander imagery.

The remarkable photographs of the surface of Venus returned by the Venera 9 and 10 spacecraft have revealed the presence, in two different sites, of a variety of rocklike forms, some angular and some smooth. Press reports express surprise at the absence of very efficient erosional mechanisms. It may be useful to point out that, instead, it is the presence, not the absence, of erosional mechanisms on Venus which is surprising. The degree of erosion of surface rocks on Venus will, of course, be determined by an equilibrium between the rate of production and the rate of destruction of surface rocks. The principal causes of erosion of terrestrial rocks -- running water; diurnal and seasonal temperature changes, particularly in deserts; and aeolian abrasion -- are all absent on Venus. The surface temperature of 750 K is above the critical point temperature of water. Ground-based radioastronomical measurements; a comparison of the temperatures measured by Venera spacecraft at a variety of solar zenith angles; and the high heat capacity of the massive Venus atmosphere together clearly demonstrate that the diurnal temperature differences are a few

degrees K at most. The obliquity of the rotation axis of Venus is so small that there are effectively no seasons on the planet. The efficiency of aeolian abrasion on Venus depends on the velocity to a power ≥ 3 ; since both theory and observation show the velocities in the lower atmosphere of Venus to be about an order of magnitude less than at comparable regions in the Earth's atmosphere, it follows that sandblasting on Venus is at most 10^{-3} as efficient as on Earth.

The problem is to find a suitable source of erosion of surface rocks -- a problem somewhat similar to that caused by the radar discovery of large, presumably impact, basins which, in comparison to their lunar, martian and mercurian equivalents, are remarkably shallow. Two mechanisms for the erosion of crater ramparts on the surface of Venus can be suggested; I suggest that they also may be important for erosion of the rocks photographed by Venera 9 and 10. The atmosphere of Venus contains hydrochloric acid at mixing ratio of about 10^{-6} ; hydrofluoric acid at mixing ratio of about 10^{-8} ; and sulfuric acid at larger mixing ratios which, however, are as yet undetermined for the lower atmosphere of the planet. Chemical weathering by such a mixture of strong acids, even in very dilute concentrations, may, over sizeable periods of time, be quite adequate to erode angular projections of siliceous rocks.

A second possibility arises from the high surface temperature of Venus. While these temperatures are not so high as to melt silicates, they are high enough to bring many geochemically abundant materials near or to their melting points -- NaOH, KOH, HgS and KNO_2 to mention a few. If the rocks of Venus comprise such materials even in abundance of a few tenths of a percent, the rheological properties of their low melting point components may, over long periods of time, be adequate to soften the contours of surface rocks.

With typical terrestrial values of the subsurface temperature gradient, the high surface temperature of Venus implies that the melting points of silicates should be reached a few tens of km subsurface. The "granitic" values of the uranium/potassium/thorium radioisotope ratios, as determined by Venera 8 suggests that a terrestrial value to the subsurface temperature gradient may be a good first approximation. In this case, access of magmatic material from the interior of Venus to its surface should be considerably easier than on Earth and significant fractions of the surface may be frozen lava fields having reached thermal equilibrium at the low temperatures of 750 K.

Veneras 9 and 10 are the first spacecraft to obtain in situ photographs of the surface of another planet. The remarkable photographs which they have obtained open a new field of small scale planetary geology.

INTERPRETATION OF VENUS RADAR: CRATER STATISTICS

R. S. Saunders
Jet Propulsion Laboratory

Earth-based radar images of the surface of Venus obtained at Goldstone indicate that the surface of Venus has topographic features. The interpretation of these images is not as straightforward as is the interpretation of conventional planetary photographs.

The high resolution radar images of Venus presently cover 2% of the surface. The smallest features that can be identified are approximately 20 km across. The images each have a circular format that represents the sub-Earth point at the time the image was obtained. The regions are about 12° in diameter on Venus. The nature of the illumination geometry results in variations in the appearance of topographic features depending upon how they fall within the imaged region. In general, it appears that regional slope and the orientation of this slope in relation to the sub-Earth point has the greatest effect on the brightness of a point on the photograph. This is consistent with similar effects observed with terrestrial airborne radar. Less commonly, areas that are extremely rough or have contrasting dielectric constant may also be delineated in the radar image. The two images of the surface of Venus recently returned by the Soviets would be expected to be relatively bright in a radar image, although these spots may be typical of much of Venus.

The Goldstone radar images of Venus contain features that appear bright because of favorable slope orientation as well as regions that appear brighter because of roughness or higher dielectric constant. The

work described here concerns the recognition of topographic features. Since orientation can strongly influence radar return it is desirable to obtain overlapping coverage wherever possible such that each point is imaged from more than one sub-Earth point. The effect of more than one illumination direction is well illustrated by a shallow 200 km crater that occurs in two of the images. In one image the crater center is 4° from the sub-Earth point and occurs as a vague circular feature. In a second image the same crater lies 6° from the sub-Earth point and appears as two bright patches along a line radial to the sub-Earth point. The inner patch is the outer rim of the crater and the outer patch is the crater wall on the opposite side. These surfaces appear brighter because they are more favorably oriented and reflect more of the radar energy than do other parts of the crater.

Using the information so obtained on the effects of feature position relative to the sub-Earth point, it is possible to identify the more prominent craters that occur in the Goldstone images. The imaged region contains about 30 probable craters ranging in diameter from 40 to 350 km. Within the imaged regions there are clearly large areas that are not cratered and there are regions that contain many large craters. Venus shares this characteristic with Mercury, the Moon and Mars.

Detailed comparison of crater statistics of Venus with those of other planets is not yet possible. However, if one makes the assumption that all the craters observed on Venus are of impact origin, then the frequency of large craters on the most cratered region observed in the images is comparable to crater frequencies on the most cratered regions of Mercury,

the Moon, and Mars. The frequency of craters in this region of Venus declines sharply at diameters smaller than 80 km and none smaller than 40 km can be identified as craters.

Most of the venusian craters have gross morphology similar to impact craters on the other planets. The raised rim is relatively narrow in comparison to the diameter. Most volcanic calderas, however, are significantly smaller than the volcanic construct that they occupy. This suggests that the majority of venusian craters are of impact origin. The craters on Venus are apparently extremely shallow with floors at approximately the same elevation as the surrounding terrain. These craters and the terrain they occupy must be of approximately the same age as their counterparts on the Moon, Mercury and Mars and are therefore much older than any known terrestrial features. This does not indicate that the internal structure of Venus or the internal development must be different from that of the Earth. There may well be plate motions on Venus. The clear implication, however, would be that the integrated effect of erosion on Venus has been little more than that on Mars. If there is tectonic activity at the surface of Venus, it would be valuable to contrast its development to that of the Earth where in general erosion and deposition can keep pace with uplift and depression.

THOUGHTS ON THE GEOLOGY OF VENUS

R. E. Arvidson
Washington University

Because Venus is about the same size, mass, and assumed bulk chemistry as the Earth, thermal evolution models predict that, for much of its history the Venusian interior has been somewhat similar to the Earth's interior. Convection within a Venusian asthenosphere for much of geologic time cannot be ruled out. Radar imagery points to a number of large craters on the Venusian surface, including a ~1000 km diameter basin. Such a large feature is probably impact in origin and was probably produced during heavy bombardment, which for the moon ceased about 4 billion years ago. Preservation of such features severely limits the extent of modification by either surface processes or by tectonic activity. Without fluvial processes, rates of mass redistribution must be incredibly slow compared to terrestrial standards, where the continents would be eroded to sea level in 10^6 years with present sediment fluxes. If the lower atmosphere of Venus is in an isothermal state, so that high wind velocities and associated high aeolian erosion rates are rarities, then the surface may be surprisingly quiescent. In this context, the strewn block fields imaged by the Soviet Lander may indeed be ancient. Perhaps they are lag deposits left behind as finer-grained size fractions of an impact-produced regolith were removed by wind.

The style of tectonic activity expressed on the Venusian surface is of considerable interest, since a record of tectonism induced by convection over a long period of time may be recorded. In contrast to the Earth, that record would be without the added effects of massive accumulation, deformation, and partial melting of sedimentary debris in geosynclinal regions.

MULTISPECTRAL CAPABILITY OF THE VIKING LANDER IMAGERY SYSTEM

R. E. Arvidson
Washington University

F. Huck and S. Wall
NASA Langley Research Center

and

W. Patterson
Brown University

The two Viking spacecraft scheduled to land on Mars during the summer of 1976 will each use two facsimile cameras to spatially and radiometrically characterize the surface. The cameras contain a photosensor array with 12 silicon diodes, providing a variety of imaging modes, including 3 channels for color and 3 for near infrared imaging (Figure 1). The cameras will stand 1.3 m above the Martian surface. At this height the distance to the horizon, for a topographically smooth landing area, is nearly 3 km. Camera field of view in elevation ranges from 40° above to 60° below the horizon, and in azimuth the field of view is 342.5° . Angular resolving power for the color and IR channels is $.12^\circ$, which translates to 6 to 12 mm/lp for near-field and to ~ 12 m/lp for regions near the horizon.

Although the color and IR channels have large bandwidths and irregular transfer shapes, the broad electron transition absorption bands in pyroxenes and other minerals can be reproduced. On Mars, the channel $r_i(\lambda)$'s must first be calibrated by imaging reference test charts that are located on the spacecraft and that have known reflectance signatures. Ground truth can then be provided for the reflectance data by imaging areas that are to be and that have been sampled for the X-ray Fluorescence and Gas Chromatograph Mass Spectrometer analyses. The X-ray Fluorescence experiment provides elemental abundances for elements with atomic numbers greater than that of Na. The GCMS potentially can provide an indication of the extent of water of hydration. Multispectral imagery can then be used to survey much larger areas of the Martian surface, potentially providing significant information on the proportion and kinds of weathering materials and primary igneous products. In addition, two ground truth points will be provided for Earth-based observations and for future spacecraft multispectral observations.

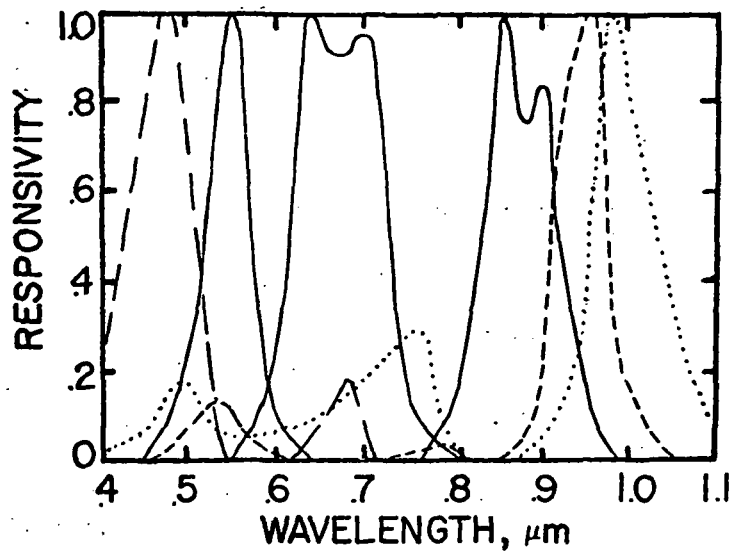


Figure 1: $\tau_i(\lambda)$'s for the 3 color and 3 infrared channels. The $\tau_i(\lambda)$'s are the normalized product of solar irradiance, estimated Martian atmospheric transmittance, camera optical through-put, and photosensor responsivity.

CALIBRATION OF MARTIAN SURFACE DYNAMICS BY ANALYSIS OF COSMIC RAY EFFECTS IN RETURNED SAMPLE

R. E. Arvidson and C. Hohenberg
Washington University

Measurements of cosmogenic nuclides and of nuclear particle tracks produced by cosmic rays in lunar soils and rocks have provided firm constraints on ages of lunar features and on rates of regolith turnover. On the moon, galactic cosmic ray iron group nuclei penetrate about 10 cm of rock or 15 cm of soil, while high-energy protons responsible for spallation reactions penetrate more than an order of magnitude more in depth. On Mars, the presence of a tenuous atmosphere should change the relationship between nuclear particle track production and effects due to high energy spallation reactions. The atmosphere produces about 10 gm/cm^2 of shielding, equivalent to about 3 cm of rock. Martian atmospheric shielding is negligible to the extent that cosmic ray protons can reach the surface unchanged. On the other hand, galactic cosmic ray iron group nuclei are more effectively shielded. Solar flares and solar wind particles, which are lower in energy, will be completely filtered-out with this level of shielding.

With ideal Martian samples, changes in atmospheric shielding as a function of time could be resolved, since a shielding change of a factor of 3 would eliminate iron group nuclei from reaching the surface. Further shielding would characteristically alter the pattern of cosmogenic nuclides in surface samples. Other types of samples could be used to calibrate rates of aeolian abrasion of rock surfaces. The most probable returned sample may very well be a scooped soil sample. Information as to surface dynamics could still be derived by, for instance, comparisons with lunar soils, which have been exposed to cosmic rays for known lengths of time and with no atmospheric shielding.

We are also examining, with terrestrial materials, ways to calibrate rates of sedimentary processes on Mars by utilizing nuclear effects not related to cosmic rays. Ages of some sedimentary rocks can be derived by analysis of fission tracks at the edges of uranium-poor mineral grains (quartz) that are embedded in uranium-rich matrices (shales). Such tracks occur by fission events in the matrix near the grain surfaces. In the best of cases, by knowing the uranium concentration of the matrix and the density of fission tracks at the grain surfaces, an age of deposition can be computed.

A MARINER 10 ATLAS OF MERCURY

Merton E. Davies
The Rand Corporation

An Atlas of Mercury is being prepared under the direction of an editorial board headed by Merton Davies; other members are Stephen Dwornik, Donald Gault, Bruce Murray, and Robert Strom. About 200 copies of the Atlas will be assembled with photographic illustrations. The page layouts will be made at Cal Tech and Rand; the format will probably be 10-1/2 x 13 inches.

Introductory material will discuss:

Mercury Before Mariner 10

Mariner 10 Spacecraft and Mission

History and Geography of Mercury

Nomenclature and Cartography

Following these sections will be a brief description of the organization of the Atlas. The surface of Mercury is divided into nine regions corresponding approximately to the 1:5,000,000 charts and a section on each will be prepared with pictures and data. Each section will contain a shaded relief map (USGS), a photo mosaic (JPL), and an index of the illustrations which follow. These illustrations will be individual high-resolution frames, mosaics, and stereograms selected from the hundreds of Mariner 10 pictures. There will probably be about 100 photographic pages of illustrations; there will also be an index, references, and a gazetteer.

The illustrations and their indices are being prepared by Jurrie Van Der Woude at Cal Tech. The members of the editorial board are selecting the content, preparing the written material, choosing the pictures for illustrations, etc. The entire board meets about once a month and progress reviews are held weekly. Jeanne Dunn of Rand is editing the written material and helping with the detailed organization. Rand is responsible for the reproduction and binding of the Atlas.

PHOTOMETRIC ANALYSES OF MARINER 10 IMAGES OF MERCURY

Bruce Hapke
University of Pittsburgh

This abstract summarizes the work on Mercury accomplished under NASA Grant NSG 7147 since the start of the grant, June 1, 1975.

The objectives of the research are to determine the differential photometric functions of the Mercurian surface and construct albedo and color ratio maps of Mercury from the Mariner 10 images. In order to construct the albedo maps several preliminary objectives must be met.

1. The photometric accuracy of the Mariner 10 cameras must be established, including temperature effects. The latter is especially important since the cameras were at a temperature of about -8°C on the second and third Mercury encounters, rather than at the design temperature of $+25^{\circ}\text{C}$.

2. The differential photometric function of various representative types of Mercurian terrain must be determined. The preliminary published values of the albedos assumed on average lunar photometric function, which at large phase angles conceivably could be in error by as much as 50%.

The first preliminary objective has been accomplished by measuring the brightnesses of a number of planetary objects viewed by Mariner 10 using pre-launch camera calibration data and comparing these values with those obtained from earth-based observations. Table I summarizes the results of measurements to date.

TABLE I.

<u>Object</u>	<u>Quantity Measured</u>	<u>Temperature</u>	<u>M-10 Value</u>	<u>Earth Value</u>
Moon	Geometric Albedo	Cold	.11	.115 ^a , .125 ^b
Moon	Normal Albedo of M. Crisium	Cold	.093	.085
Moon	Normal Albedo of M. Serenitatis	Cold	.093	.090
Moon	Normal Albedo of HL between M. Cr. and M. Ser.	Cold	.17	.14
Moon	Proclus	Cold	.25	.21
Moon	Tsiolkowski	Cold	.06	Not observed
Venus	Radiance of sub-solar point	Warm	310w/cm ² -ster	310w/cm ² -ster
Mercury	Geometric Albedo of Incoming Hemisphere	Warm	.11	Average = .115 ^a , .125 ^b
Mercury	Geometric Albedo of Outgoing Hemisphere	Warm	.086	
Jupiter	Geometric Albedo	Cold	.45	.45
<hr/>				
Moon	Weighted Average of Normal Albedos	Cold	.17	
Mercury	Weighted Average of Normal Albedos of Incoming Hemisphere	Warm	.18	
Mercury	Weighted Average of Normal Albedos of Outgoing Hemisphere	Warm	.12	

^aFrom absolute photometry^bFrom polarimetry

From the top part of Table I it can be seen that the accuracy of the radiance measured by the Mariner 10 cameras appears to be quite high, even when the cameras are cold. An additional indication that the low temperature had little effect on the photometric accuracy comes from mosaics constructed by combining Mercury I (warm) and Mercury II (cold) images which have been photometrically decalibrated. The boundaries between warm and cold images are virtually invisible on the mosaics.

The effect of temperature will be further investigated by direct comparison of the radiance from a number of areas photographed during the first and second Mercury encounters. However, the required images have not yet been processed by IPL/JPL.

The second objective, the photometric function, is presently being studied by measuring distribution of relative brightness on the crescents of the moon and Mercury. The results to date indicate that the accepted lunar photometric function is in need of some revision. The Mariner 10 lunar images, taken at phase angles around 83° , show pronounced polar darkening. The calculated equatorial normal albedos are about twice as bright as the albedos at latitude 70° . Since the full moon shows no polar darkening, this observation implies that the lunar differential photometric function is latitude-dependent, whereas it had previously been thought to be independent of latitude.

Normal albedos on the incoming side of Mercury, calculated using the average lunar photometric function, exhibit polar darkening of about 3:1. At present it is not clear whether this excess of polar darkening over the moon's is purely an effect of a different photometric function, or whether, there is a real dependence of albedo on latitude. If the polar

darkening is real on Mercury it would imply that the solar wind is more important to Mercurian and lunar surface darkening processes than meteorite impact effects.

The preliminary published albedos on Mercury, which were calculated using an average lunar photometric function, are substantially higher than those of morphologically similar lunar areas. However, the geometric albedo of Mercury, calculated using the measured integral Mercury photometric function is as low as the moon's. The geometric albedo of a planet is the weighted average of the normal albedos of the surface. For both Mercury and the moon the weighted averages of the normal albedos are considerably higher than the geometric albedos (see bottom part of Table I). This result implies that the differential photometric function used to deduce the albedos is incorrect. There are indications that on the moon the width of the backscatter peak for highlands is somewhat greater, and for maria, somewhat smaller, than the average lunar photometric function. If the same is true for Mercury, the effect would be to reduce the albedos of the bright intercrater plains and increase those of the dark smooth plains.

It is thus of great importance to resolve the question of the effect of photometric function since this problem has implications for both the geochemistry of the crust (a higher albedo implies a lower Fe-Ti content) and surface darkening processes. In future work the photometric function will be studied by measuring the variation of brightness of a number of representative areas on the second Mercury encounter, where the range of phase angles covered was much larger than on Mercury I or III. We are currently awaiting Mercury II images being processed by IPL/JPL.

EXCITATION AND RELAXATION OF THE WOBBLE, PRECESSION AND LIBRATION OF THE MOON

S. J. Peale

University of California, Santa Barbara

The rate of impact excitation of each of the free motions of the moon above a given amplitude is compared with the rate of damping from tidal and rotational distortion and from a possible core-mantle interaction. Criteria are developed in terms of the damping factor Q and the core kinematic viscosity ν for which each amplitude should be expected to be above the projected observational limit of 0.01° of arc determined by the laser ranging and VLBI experiments. Although observable amplitudes are compatible with reasonable values of Q and ν , it is also not unreasonable for the amplitudes to be below observability most of the time. Of the three free motions, the libration in longitude is the least likely to be observable in spite of its more frequent excitation, and amplitudes of this motion as high as 1.0° must be regarded as very unlikely. A tentatively identified liquid core of 270 km radius might keep some of the motions damped below observability if ν is well within the bounds estimated for the earth's core, but it probably could not keep all of them so damped. Within a given model, the uncertainty in the expectation of observable free motions rests on the uncertainty in the values of Q and ν , where the latter includes the possibility of no liquid core at all. Uncertainties in the various assumptions incorporated into the models themselves are discussed explicitly. The detection of any free motions may bound values of some of the parameters and thus yield information about the lunar interior.

LONGTERM EVOLUTION OF THE MARTIAN ATMOSPHERE AND CLIMATIC CHANGE

Carl Sagan
Cornell University

The most detailed present atmospheric models showing substantial climatic change on Mars (Sagan et al., 1973a; Gierasch and Toon, 1973) imply that for pure carbon dioxide polar caps there should be substantial variation of the total atmospheric pressure due to obliquity driving and polar albedo driving on timescales of 10^6 years or less. It is not excluded that small quantities of liquid water do indeed flow on such timescales on contemporary Mars -- perhaps down the centers of large existing channels. Indeed there is some Mariner 9 observational support for this idea which we intend to develop in the coming grant year. However, the old age implied by regional geology and cratering statistics for Martian channels implies that some conditions existed early in the history of Mars which no longer exist and which led to the cutting of channels. On all models channel formation must take substantial periods of time -- longer, say, than a century. On the assumption that the channels are cut by running water (Sagan et al., 1973a; Milton, 1973) we discuss four models of early channel formation:

In the first, volcanic outgassing is the driving function. For channels to form it is not enough simply to put water into a thin atmosphere because it will rapidly be transported by atmospheric motions to the pole where it condenses out. Instead a large increment

in the total atmospheric pressure is required. However, in a volcanic outburst the amount of hot water carried into the thin Martian atmosphere may be more than the carrying capacity of the atmosphere and for a timescale determined by the specific heat and latent heat of the atmospheric constituents the total pressure will remain large enough for liquid water to flow. However, this timescale is much less than the time for the cutting of the channels and much less than the time for the building of such volcanic constructs as Olympus Mons. (To an order of magnitude the total amount of water outgassed in the production of Olympus Mons buys no more than a few tens of times the characteristic equator to pole volatile transport time.)

The second possibility is impact vaporization in large crater-forming events. Here all impact producing craters larger than about a hundred kilometers will momentarily perturb the total Martian atmospheric pressure well above the triple point and permit liquid water to flow. However, the time constant problems are just the same as in the volcanic case. We integrate the total impact cratering flux of Mars over its early history to determine whether the steady state impact volatilization flux can overwhelm the atmospheric transport flux. In this view the preference of channel cutting for early Martian history is connected with the greater cratering flux. The Martian surface material is known to be approximately 1% physically and chemically bound water (Houck et al., 1973) and subsurface

permafrost represents an additional and substantial source of water which can be brought into the atmosphere either by volcanism or by impact cratering.

The third possibility is an early reducing atmosphere. A wide range of evidence suggests that the terrestrial planets began with more nearly typical cosmic composition than they exhibit today. Liquid water on primitive Mars is even more difficult to understand than liquid water on contemporary Mars because the solar luminosity has increased by about half a bolometric magnitude over the past 4×10^9 years. The existence of liquid water in the early history of the Earth seems explicable only in terms of a more efficient greenhouse effect due principally to small quantities of ammonia in the primitive reducing atmosphere of the Earth (Sagan and Mullen, 1972.) We are investigating more thoroughly the possibility of early Martian greenhouse models as outlined by Sagan and Mullen (1972), as well as the corresponding photochemical and Jeans escape problems. In this model the reason for preferential early channel formation is a massive early reducing atmosphere which has subsequently escaped to space.

In pursuing our fourth possibility, we note that the advective instability models of climatic change of Sagan, et al., (1973) assumed a pure carbon dioxide polar cap, the vapor pressure above which determines the atmospheric pressure on Mars. The composition and depth of the polar cap is a subject of some controversy. We

examine in particular the possibility that an early pure carbon dioxide polar cap gradually evolves into a CO₂/water clathrate polar cap; this has the implication in advective instability models of climatic change of decreasing the amplitude of climatic fluctuations while not affecting the period between episodes of flowing water on the planet.

The major difficulty with all the foregoing models is the difficulty in maintaining Martian polar temperatures above the freezing point of water. At lower temperatures the polar transport rate of water injected into the atmosphere will be so large as to make extensive epochs in which flowing liquid water is possible rather than dubious. With the solar luminosity less some billions of years ago this problem is made even more critical. The triple point of carbon dioxide however is 219°K, 5.1 bars. Since liquid CO₂ requires higher pressures than liquid water, it has been customary in the past to reject CO₂ as a possible channel-forming agent, although liquid CO₂ in the polar caps has been discussed (Sagan, 1973a.) However, there is some slightly non-marginal evidence that the Mars 5 entry probe has detected something like 35% of argon 40 in the Martian atmosphere (Istomin et al., 1975.) This may be consistent with recent high-resolution Fourier spectroscopy of the Martian atmosphere (Kaplan et al., 1975) and with other studies (Levine, 1975.) A crude scaling from terrestrial argon/carbon dioxide ratios would imply an early atmosphere with some tens of

bars carbon dioxide. Even if carbonates were formed readily, a period in which the CO_2 partial pressure was above 5.1 bars is not excluded. The total equivalent CO_2 contents on both the Earth and Venus are about 70 to 100^2 bars. The mechanisms we have been discussing are probably able to bring the Martian polar temperatures above 219°K , although they are very likely inadequate -- except for very massive early greenhouses -- to bring the polar temperatures above 273°K . (It is worth noting that from $^{16}\text{O}/^{18}\text{O}$ data, as well as from paleontological evidence, the terrestrial poles were at temperatures of about $+10^\circ\text{C}$ 10^8 years ago, implying something like a 30° fluctuation in the temperature of the Earth's poles in 10^8 years.) In this case channels would be cut preferentially early because only in the early history of the planet was the total pressure above the triple point pressure of CO_2 . The physics of channel cutting by liquid carbon dioxide and the question of the present sink for CO_2 -- polar caps or regolith -- will be discussed.

A NUMERICAL CIRCULATION MODEL WITH TOPOGRAPHY FOR THE MARTIAN SOUTHERN HEMISPHERE

Carl Sagan
Cornell University

A quasi-geostrophic numerical model, including friction, radiation, and the observed planetary topography, is applied to the general circulation of the Martian atmosphere in the southern hemisphere at latitudes south of about 35° . Near equilibrium weather systems developed after about 5 model days. To avoid violating the quasi-geostrophic approximation, only 0.8 of the already smoothed relief was employed. Weather systems and velocity fields are strikingly tied to topography. A 2mb middle latitude jet stream is found of remarkably terrestrial aspect. Highest surface velocities, both horizontal and vertical, are predicted in western Hellas Planitia and eastern Argyre Planitia, which are observed to be preferred sites of origin of major Martian dust storms. Mean horizontal velocities $> 30 \text{ m s}^{-1}$ and vertical velocities $> 0.2 \text{ m s}^{-1}$ are found just above the surface velocity boundary layer. When consideration is taken of scaling to full topography and the probable gustiness of Martian winds, it seems very likely that the general circulation is adequate, at certain times and places, to transport dust from

the surface of Mars, as observed. Certain sources and sinks of vertical dust streaming are suggested; the entire south circumpolar zone appears to be a dust sink in winter.

CHEMICAL EQUILIBRIA RELEVANT TO THE CONSTRUCTION OF PLANETARY MODELS FOR MARS AND MERCURY

M. Charles Gilbert

Virginia Polytechnic Institute and State University

No interpretation of physical data of the planets in terms of chemistry can be even approximately correct unless careful consideration is given 1) to the mineralogic and petrologic form the suggested bulk composition would yield, and 2) to the consequences of chemical differentiation which the model might imply. While our understanding of the Earth must, of necessity, represent the starting point for construction of models of other terrestrial planets, wholesale extrapolations are unwarranted. Chemistries of all the terrestrial planets are clearly different enough from each other that differences in mineralogy and petrology are required. Such differences when combined with likely physical boundary conditions simply mean that differentiation schemes found useful in interpreting the Earth may not be applicable on, for example, Mars. Experiences already gained from the study of the Moon support this point of view. The reasoning chains whereby planetary models are constructed must be cautiously and rigorously forged.

Review of data pertinent to the terrestrial planets gives the following as the most probably important chemical parameters for understanding planetary geochemical history: 1) volatile content, 2) Fe-Mg ratio, 3) alkali metal content, 4) Ni content, 5) oxidation state, and 6) sulfidation state. Whether one measures these parameters directly, or estimates them indirectly, values will be needed for constructing viable chemical models. Variations in each of these can cause significant changes in melting behavior and in mineralogy. Illustrative of the difficulties which can arise is the conflict between the picture of Mercury based on magnetic studies and that based on equilibrium chemical condensation models. The dipole magnetic field found for Mercury would appear to

require a molten core. To maintain a molten core some $4\frac{1}{2}$ billion years after Mercury's formation will require material with low melting temperatures in order to satisfy reasonable heat producing mechanisms. Such low melting temperatures in Fe-rich systems can be formed most readily in reaction with sulfur, the only element potentially abundant enough in the Solar System. This stands in contradiction to models wherein no sulfur-bearing species condense at Mercury's distance from the Sun. Clearly, an independent method of estimating the sulfur content of Mercury is necessary.

For Mars, arguments can be advanced which provide for relatively abundant Ni distributed in the crust and mantle. This may be the chief chemical difference between rocks of the Earth and of Mars. A predominance of oxidation over sulfidation effects is necessary to achieve this higher Ni concentration. The Viking Lander analysis of surficial material will therefore serve as an indication of the magnitude and importance of the oxidation-sulfidation effects.

A higher volatile content for Mars can also potentially provide explanations for different igneous fractionation sequences as compared with the Earth. A further consequence is the release of volatiles to the Martian surface through massive springs. Thus dating of stream deposits may date times of prominent igneous activity.

Selected experimental studies are needed to bolster application of the large amount of laboratory data generated for terrestrially important systems. Specifically, further studies are needed on 1) melting relations in Ni-bearing silicate systems, 2) Ni-Mg-Fe fractionation among coexisting oxides, sulfides, and silicates, 3) melt crystallization under conditions of high oxygen fugacity, and 4) effect of CO_2 on melting and crystallization behavior. A related laboratory study suggested by this analysis is the effect of composition and oxygen fugacity on viscosity of basaltic lava. Viscosity will determine directly the surface volcanic forms.

A SHORT COURSE IN PLANETARY GEOLOGY

Peter H. Schultz and Ronald Greeley
University of Santa Clara

Universities and four-year colleges generally have access to current results of the various planetary missions directly through principle investigators in the Planetology Program, current literature, or short courses (e.g., see Greeley and Schultz, 1974). High schools, however, have relatively limited access through popular journals and public relations documents, and teachers often relay this information through somewhat classical astronomy-oriented courses. With the extensive photo record of the inner planets, solar system astronomy for such objects has evolved into planetary geology, a multi-disciplinary field that relies on the fundamental principles of terrestrial geology.

Consequently, a three-day workshop-style short course in planetary geology will be offered this Spring to selected high-school teachers in the Fairfax County and Northern Virginia area. The primary goal is to provide these educators with the background, teaching ideas, and resources in planetary geology for incorporation into their earth-science curricula. An integral part of this course will be presentations by and interaction with researchers active in planetary research complemented by laboratory exercises. A tentative course outline is given below.

First Day: Introduction

- A. Registration
- B. Introductory Remarks
- C. Missions through the Solar System

Second Day: The Primordial Planets

- A. Origin of the Solar System
- B. Introduction to Planetary Surfaces
- C. Impact Cratering Exercise
- D. The Planetary Cratering Record
- E. The Primordial Earth

Third Day: The Evolving Planets

- A. Planetary Volcanism and Tectonism
- B. Photo-interpretation Exercise
- C. Comparative Geologic History of the Planets
- D. Geologic Mapping Exercise
- E. Teaching Methods

Fourth Day: The Planetary Atmospheres

- A. Planetary Climatology
- B. Atmospheric Circulation Exercise
- C. Gradational Processes
- D. Martian Aeolian Processes Exercise
- E. Planetary Geology: An Overview
- F. Closing Remarks

Our intent is not to create new planetary geologists but to illustrate geologic principles through the exposed history of other planetary surfaces.

UV CONTRAST REVERSAL ON MARS: A STUDY OF THE UV REFLECTANCE CHARACTERISTICS OF POSSIBLE MARTIAN SURFACE MATERIALS

J. Veverka, J. Burt, and J. Goguen
Cornell University

Evidence exists that some albedo markings on Mars show contrast reversal in the ultraviolet: in other words, an area which appears darker than its surroundings in the visible turns out to be brighter than its surroundings in the ultraviolet. To study this phenomenon we have obtained reflectance spectra between 2000 and 6000Å of 54 materials of various size fractions. These materials include an assortment of basalts, limonites, goethites, hematites, and montmorillonites, as well as olivine, pyroxene, quartz, red sandstone, rhyolite, etc. In most cases, particle size fractions measured range from samples containing particles less than 44µm in diameter, to those made up of particles between 250 and 420 µm. We are currently in the process of analyzing these spectra. A preliminary conclusion is that UV contrast reversal is not common for rocks and minerals in general, but is a characteristic of most iron oxide minerals. Thus, the phenomenon might be a useful diagnostic signature in locating iron oxide rich areas on Mars. Concurrently, we are in the processes of identifying locales of UV contrast reversal on Mars using Mariner 9 UVS data. Since until now there has been a scarcity of detailed UV spectra of possible Martian surface materials, our measurements should be generally useful to those investigators working with the Mariner 9 UVS data.

AUTHOR INDEX

- Albee, A. L., 78
 Alfvén, H., 1
 Anderson, D. M., 65
 Anderson, J. R., 78
 Arrhenius, G., 1
 Arvidson, R. E., 66, 217, 257, 258, 260
 Aubele, J. C., 129
 Baker, V. R., 172
 Blasius, K., 239
 Boothroyd, J. C., 68, 148
 Breed, C. S., 117
 Burt, J., 199, 279
 Butterworth, P. S., 133
 Cameron, A. G. W., 4
 Carr, M. H., 152, 229
 Chapman, C. R., 8, 175, 191
 Chodos, A. A., 78
 Cintala, M. J., 186, 188
 Conel, J. E., 200
 Cook, K., 126, 199
 Cotera, A. S., 120
 Crumpler, L. S., 129
 Cutts, J. A., 201
 Daily, M. I., 91
 D'Alli, R. E., 214
 Danielson, G. E., 99
 Davies, M. E., 81, 261
 DeHon, R., 218, 242
 Dzurisin, D., 99, 127
 Economou, T. E., 94
 Elachi, C., 91
 Elston, W. E., 129
 Eppler, D. B., 129
 Fanale, F. P., 11, 203
 Fechtig, H., 178
 Franzgrote, E. J., 85
 Fulchignoni, M., 182
 Gad-el-Hak, Mohamed, 105
 Gatto, L. W., 65
 Gault, D. E., 183
 Gilbert, M. C., 275
 Goguen, J., 279
 Greeley, R., 102, 123, 133, 135, 154, 221, 277
 Grolier, M. J., 110, 115
 Guest, J. E., 133, 183, 221
 Hapke, B., 245, 263
 Hartmann, W. K., 76, 164
 Head, J. W., 186, 188
 Helin, E. F., 18
 Herbert, F., 60
 Hohenberg, C., 260
 Holcomb, R. T., 157
 Holt, H. E., 238
 Howard, A. D., 105
 Howard, H. T., 87
 Howard, J. H., 233
 Huck, F., 258
 Ingerson, E., 172
 Karlo, J. F., 138
 King, E. A., 107
 King, J. S., 135, 138, 236
 König, B., 178
 Lebofsky, L. A., 200
 Lipman, P. W., 157
 Lockwood, J. P., 157
 Lucchitta, B. K., 210
 McCauley, C. K., 120
 McCauley, J. F., 110, 115
 McGill, G. E., 141, 224
 Malin, M. C., 146, 240, 249
 Marsden, B. G., 31, 34
 Masson, P., 147
 Masursky, H., 169
 Morton, J. B., 105
 Mutch, T. A., 186, 188, 214
 Neukum, G., 178
 Noland, M., 213
 Nummedal, D., 68, 148
 Oberbeck, V. R., 69
 Patterson, W., 258
 Peale, S. J., 15, 46, 267
 Peterson, J. E., 149
 Phillips, R. J., 48
 Pierce, D., 105
 Pollack, J. B., 38
 Sagan, C., 166, 251, 268, 273
 Saunders, R. S., 53, 91, 254
 Schaber, G. G., 89
 Schubert, G., 57
 Schultz, P. H., 73, 159, 183, 277
 Scott, D. H., 229
 Sekanina, Z., 34, 40, 43
 Shoemaker, E. M., 18
 Simpson, E. J., 68
 Simpson, R. A., 87
 Smith, E. I., 161
 Soderblom, L., 100
 Sonett, C. P., 60
 Stockman, R. H., 206
 Strom, R. G., 194
 Stromquist, A. W., 141

Tilling, R. I., 157
Turkevich, A. L., 94
Tyler, G. L., 87
Underwood, J. R., 231
Veverka, J., 126, 199, 213, 279
Wall, S., 258

Ward, A. W., 115
Ward, W. R., 4
Whipple, F. L., 23, 27
Whitaker, E. A., 194
Wiskerchen, M. J., 60
Woronow, A., 197



POSTMASTER: If Undeliverable (Section 158
Postal Manual) Do Not Return

"The aeronautical and space activities of the United States shall be conducted so as to contribute . . . to the expansion of human knowledge of phenomena in the atmosphere and space. The Administration shall provide for the widest practicable and appropriate dissemination of information concerning its activities and the results thereof."

—NATIONAL AERONAUTICS AND SPACE ACT OF 1958

NASA SCIENTIFIC AND TECHNICAL PUBLICATIONS

TECHNICAL REPORTS: Scientific and technical information considered important, complete, and a lasting contribution to existing knowledge.

TECHNICAL NOTES: Information less broad in scope but nevertheless of importance as a contribution to existing knowledge.

TECHNICAL MEMORANDUMS: Information receiving limited distribution because of preliminary data, security classification, or other reasons. Also includes conference proceedings with either limited or unlimited distribution.

CONTRACTOR REPORTS: Scientific and technical information generated under a NASA contract or grant and considered an important contribution to existing knowledge.

TECHNICAL TRANSLATIONS: Information published in a foreign language considered to merit NASA distribution in English.

SPECIAL PUBLICATIONS: Information derived from or of value to NASA activities. Publications include final reports of major projects, monographs, data compilations, handbooks, sourcebooks, and special bibliographies.

TECHNOLOGY UTILIZATION PUBLICATIONS: Information on technology used by NASA that may be of particular interest in commercial and other non-aerospace applications. Publications include Tech Briefs, Technology Utilization Reports and Technology Surveys.

Details on the availability of these publications may be obtained from:

SCIENTIFIC AND TECHNICAL INFORMATION OFFICE

NATIONAL AERONAUTICS AND SPACE ADMINISTRATION

Washington, D.C. 20546